

Characterization of amorphous solid dispersions

Kumulative Dissertation

zur Erlangung des
Doktorgrades der Naturwissenschaften (Dr. rer. nat.)

der

Naturwissenschaftlichen Fakultät I
– Biowissenschaften –

der Martin-Luther-Universität
Halle-Wittenberg,

vorgelegt

von Frau Carolin Auch

geb. am 15. Juli 1991 in Ludwigsburg

Gutachter/innen:

1. Prof. Dr. Karsten Mäder
2. Prof. Dr. Lea Ann Dailey
3. Prof. Dr. Karl Wagner

Tag der öffentlichen Verteidigung: 22. Juni 2020

An experiment is a question which science poses to nature and a measurement is the recording of nature's answer.

- Max Planck: Scientific Autobiography and Other Papers, 1949 -

Dedicated to my family and friends.

Contents

Preamble	iv
List of contents	v
List of figures	vii
List of tables	ix
Nomenclature	xi
1 Introduction	1
1.1 Poorly soluble drugs	1
1.2 Amorphous solid dispersions	4
1.2.1 The amorphous form	4
1.2.2 Functional principle of ASD	5
1.2.3 Translational drawbacks - status quo	8
1.3 Aim of work	14
2 Cumulative part	15
2.1 Overview of journals	15
2.2 Peer-reviewed publications	16
2.2.1 Melt-based screening method for polymer selection	19
2.2.2 Impact of polymer degradation in HME	21
2.2.3 Analysis of API-polymer interactions in ASD	23
2.2.4 Application of gastrointestinal transfer model for ASD	25
3 Results and discussion	27
4 Summary and outlook	45
4.1 Summary	45
4.2 Future perspectives	49
Bibliography	51
Acknowledgement	I
Appendix	A

List of Figures

1.1	Biopharmaceutical classification system	1
1.2	Drugs on the market and in the industrial pipelines according to their BCS classification	2
1.3	Schematic depiction of different states in which the API can occur in the GI tract	3
1.4	Schematic phase diagram for a two-component amorphous solid dispersion	6
1.5	Schematic dissolution profiles of crystalline API, neat amorphous API and ASD with spring and parachute effect	6
1.6	Publications in SciFinder database for the key word "amorphous solid dispersion"	8
1.7	FDA approved drugs marketed as solid dispersions	9
1.8	FDA approved amorphous drugs according to the manufacturing technique	11
1.9	Potential species being formed upon dissolution of a SDD	13
2.1	Graphical abstract to Auch et al. [74]	20
2.2	Graphical abstract to Auch et al. [36]	22
2.3	Graphical abstract to Auch et al. [75]	24
2.4	Graphical abstract to Auch et al. [75]	26
3.1	Chemical structure of model compound ketoconazole	28
3.2	Solvent screening for KTZ with various polymers and 40% DL	28
3.3	Non-sink dissolution testing of A) milled hot-melt extrudates and B) SDD powder	29
3.4	Exemplary results of A) DSC, B) PXRD and C) microscopy and PLM for HPMCAS with 40% DL KTZ	31
3.5	Overall comparison of concentration of drug dissolved with both screening tools (melt-based and solvent-based), SDD and HME with 40% DL KTZ	32
3.6	Relative viscosity increase between placebo and verum solutions with 50 mg/mL polymer each w/wo 40% DL	33
3.7	¹³ C ss-NMR spectra for neat PVP-VA64, HPMCAS and KTZ as references for peak assignment in Figure 3.8	34
3.8	T1ρ decay curves from ss-NMR relaxation time measurements of references and PM, HME and SDD formulations	35
3.9	Gel permeation chromatogram and molar mass plot of PVP-VA64 bulk powder	37

3.10	Molecular weight and PDI of unprocessed PVP-VA64 versus stress-samples . . .	38
3.11	¹ H NMR solution spectra of PVP-VA64 bulk powder, Ex 130, Ex 160 and Ex 180	38
3.12	Radius of gyration of the differently stressed PVP-VA64 extrudates versus unprocessed bulk powder	39
3.13	Concentration of KTZ dissolved of SDD produced with stressed versus unprocessed PVP-VA64	40
3.14	Non-sink dissolution testing versus transfer model with two different HPMCAS grades	41
3.15	Transfer model for SDD and PM of HPMCAS LF with 40% KTZ	42
3.16	Non-sink dissolution testing versus transfer model under hypochlorhydric conditions	43
3.17	Transfer model of ternary ASD with the polymers HPMCAS and E PO and 40% DL	44
4.1	Systematic formulation development of ASD	46

List of Tables

1.1	Nomenclature and classification of solid dispersions	5
1.2	Factors that influence performance and stability of ASD	7
2.1	Overview of journals where peer-reviewed articles were published	15
2.2	Declaration of contributions to the different publications	18
3.1	Summary of formulations developed and analyzed within PhD thesis	27

Nomenclature

Latin letters

Symbol	Name	Unit
M_w	Molecular weight	kDa
r_g	Radius of gyration	nm
$T_{1\rho}$	Spin-lattice relaxation time in the rotating frame	ms
T_{deg}	Degradation temperature	°C
T_g	Glass transition temperature	°C
T_m	Melting temperature	°C

List of abbreviations

Abbreviation	Name
API	Active pharmaceutical ingredient
APS	Amorphous-amorphous phase separation
ASD	Amorphous solid dispersion
BCS	Biopharmaceutical Classification System
CAP	Cellulose acetate phthalate
CCR	Critical cooling rate
CCVJ	9-(2-Carboxy-2-cyanovinyl)julolidine
DCS	Developability Classification System
DL	Drug load (w/w)
dRI	Differential refractive index
DSC	Differential scanning calorimetry
Ex	Extrudate
FaSSIF	Fasted-state simulated intestinal fluid
FeSSIF	Fed-state simulated intestinal fluid
FH	Flory-Huggins interaction parameter
FluViSc	Fluorescent viscosity screening
FTIR	Fourier-transform infrared spectroscopy
GFA	Glass forming ability
GI	Gastrointestinal
GPC	Gel permeation chromatography
GT	Gordon-Taylor equation
HME	Hot-melt extrusion
HPMCAS	Hydroxypropylmethylcellulose acetate succinate
HPMCP	Hydroxypropylmethylcellulose phthalate

ICH	International Conference on Harmonization
KTZ	Ketoconazole
LS	Light scattering signal
MALS	Multi-angle light scattering
NMR	Nuclear magnetic resonance
PDI	Polydispersity index
PLM	Polarized light microscopy
PM	Physical mixture
PVP	Polyvinylpyrrolidone
PVP-VA64	PVP-co-vinyl-acetate 60:40
PXRD	Powder X-Ray diffraction
r.h.	Relative humidity
rDCS	Refined DCS
RI	Refractive index
RP-HPLC	Reversed-phase high-performance liquid chromatography
SAXS	Small-angle X-Ray scattering
SD	Spray-drying
SDD	Spray-dried dispersion
SGF	Simulated gastric fluid
SIF	Simulated intestinal fluid
SPADS	Screening of Polymers for Amorphous Drug Stabilization
ss-NMR	Solid-state NMR
TGA	Thermogravimetric analysis

1 Introduction

1.1 Poorly soluble drugs

Poor aqueous solubility is one of the deficiencies of active pharmaceutical ingredients (API) in the current pipelines of the pharmaceutical industry. The biopharmaceutical classification system (BCS) was introduced by Amidon et al. [1] in 1995 to provide a regulatory framework for *in vitro-in vivo* correlations of immediate release oral dosage forms. It defines four classes of drugs according to their solubility and permeability in the gastrointestinal (GI) tract which is depicted in Figure 1.1.

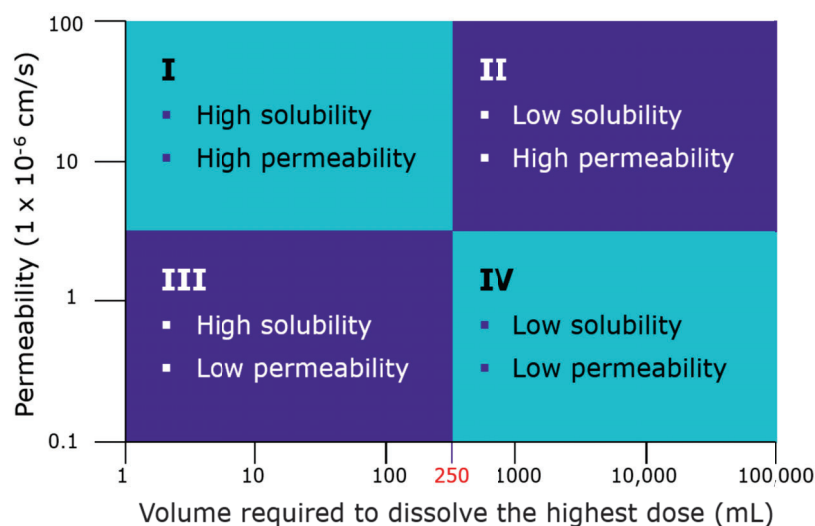


Figure 1.1: *Biopharmaceutical classification system as proposed by Amidon et al. [1]*

Accordingly, a drug has a low aqueous solubility if the highest single dose is not soluble in 250 mL aqueous media, referring to the volume that should be administered together with the medication for drug intake. The pH of this medium should be varied in the range from 1 until 6.8 at 37°C (according to the FDA Guideline on BCS [2]). These APIs are subsumed in BCS classes II and IV. Additionally, requirements on dissolution (at least 85% or more of dissolved drug within 30 min) have been set up. This is also of relevance for *in vivo* considering GI transit times. Although solubility and permeability are considered separately from each other in this classification system, the solubility-permeability interplay shall not be overlooked as pointed out by Dahan et al. [3]. A tradeoff between solubility increase and permeability decrease has been described e.g. for cyclodextrine complexation [4] where a decrease in the free fraction of the drug is only one out of several explanations for the paradoxical effect on the absorption.

In 2010, a modification of this classification system was proposed: the developability classification system (DCS) by Butler et al. [5]. As the BCS has a strong regulatory focus with regard to assurance of bioequivalence, it was designed conservatively in the context of protecting patients. The DCS aims at a classification of new drug molecules focusing on the parameters that in fact limit the extent of oral absorption. Therefore, it was proposed to consider the solubility of drugs under small intestinal conditions by using biorelevant media e.g. fasted-state simulated intestinal fluid (FaSSIF) with included bile salts instead of utilizing aqueous solubility and assuming higher fluid volumes in the GI tract (500 mL instead of 250 mL). Furthermore, BCS class II was divided into two subclasses: IIa (dissolution rate limited) and IIb (solubility limited).

Last, Butler et al. introduced the solubility limited absorbable dose considering that low solubility of class II drugs might be compensated by high permeability. In summary, this new classification was meant to improve guidance for formulation development [6]. In effect, particle size decrease with resulting higher surface areas and dissolution rates might lead to complete absorption of crystalline class IIa drugs. In contrast, class IIb compounds require improvement of the so-called "apparent solubility" which was the focus of this work.

The proposals by Butler et al. were further refined (rDCS) in 2018 with customized investigations e.g. on ionic drugs [7]. This classification outlines the additional factors that have to be taken into account for absorption of weak bases with high solubility at the acidic pH of the human stomach.

About 60-70% of pipeline drugs (Figure 1.2), which can be even up to 90% for certain indications [8, 9], need an increase in solubility to ensure sufficient bioavailability [10].

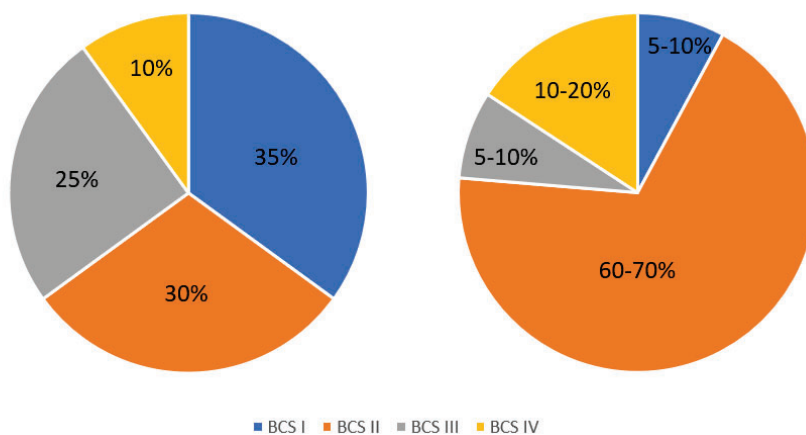


Figure 1.2: *Drugs on the market (left) and drugs in the industrial pipeline (right) according to their BCS classification, January 2018. Adapted from [11]*

Poor aqueous solubility can be derived from the API's lipophilicity or strong intermolecular forces within the crystal lattice. The increasing number of poorly soluble compounds in the current pipelines of the pharmaceutical industry (Figure 1.2) is related e.g. to results of the high throughput-screenings, combinatorial chemistry and computational drug design as the driving force for drug-receptor binding often is hydrophobicity [12].

Apart from chemical modifications like formation of salts or co-crystals, there are several possibilities for a formulation scientist to address the solubility issue [8]: particle size reduction (micronization, nanoization) and so-called "enabling formulation" approaches like solubilization with co-solvents or surfactants, amorphization, lipid-based drug-delivery formulations and cyclodextrine complexation to name a few. The physicochemical properties of newly developed drugs necessitate different formulation strategies to guarantee ease of administration, stability and a reproducible (and preferably food-independent) availability for uptake in the human body [13]. As the oral administration route is the most favored way in terms of compliance and adherence [14, 15, 16], many formulation strategies including this work are oriented towards this route of application.

The different forms in which a drug may occur upon dissolution and their corresponding permeabilities through the GI membrane are exemplarily depicted for enabling formulations in Figure 1.3.

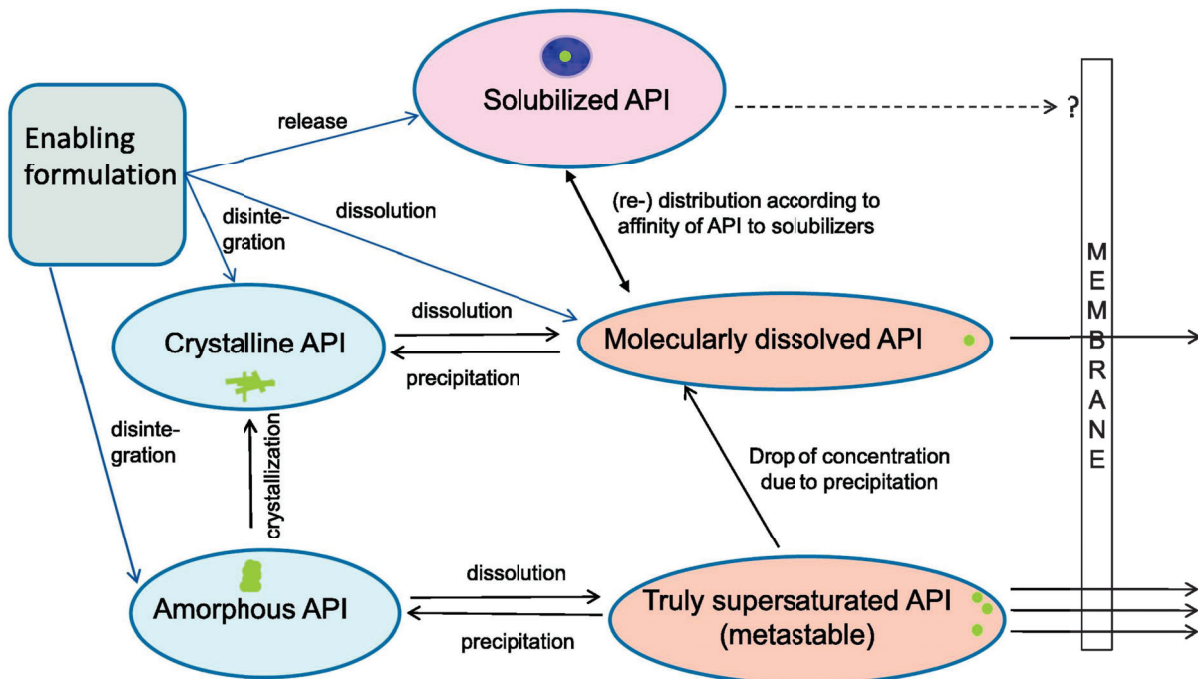


Figure 1.3: Schematic depiction of different states in which the API can occur in the GI tract and their role in terms of permeability across the GI membrane. From Buckley et al. [10]

1.2 Amorphous solid dispersions

As mentioned before, an improvement of the drug's dissolution behavior can be achieved by increasing the dissolution rate and/or the apparent solubility [17]. Amorphous solid dispersions (ASD) have emerged as an oral drug delivery strategy to ensure sufficient bioavailability of poorly soluble compounds of BCS class IIb. In 1971, Chiou and Riegelman [18] were the first to describe pharmaceutical applications of solid dispersions for solubility enhancement.

1.2.1 The amorphous form

The conversion from crystalline to amorphous increases the free energy, entropy and enthalpy, molecular mobility, free volume and chemical and thermodynamic activity of the API at a given temperature [19]. Amorphous materials lack long-range order symmetry operators which is e.g. detectable by a lack of X-Ray diffraction peaks or by the absence of a crystalline melting peak in differential scanning calorimetry (DSC). Instead, amorphous materials are characterized by a glass transition temperature T_g [20]. Below the T_g , the material exists in a glassy (solid-like) form and as a supercooled liquid above T_g . Heat content and molar volume change abruptly in the T_g region upon heating.

Due to their molecular disorder, it is not necessary to overcome the crystal lattice energy upon dissolution. In contrast to solubilization (e.g. by solubilizers, cyclodextrins or surfactants) which might be accompanied by a decrease in permeability [3, 21], kinetic supersaturation is related to enhanced free drug concentration which also is a beneficial driving force for enhanced passive transport across the GI membrane [22].

However, there are also hurdles associated with the amorphous form mainly caused by the inherent thermodynamic instability which might lead to relaxation, nucleation, precipitation and crystallization [23].

The glass forming ability (GFA) of drugs describes their propensity of existing in the amorphous form or - in other words - their crystallization tendency. This tendency is commonly described by the critical cooling rate (CCR) [24]. If cooling is performed faster than the CCR, the material is frozen in the amorphous form and recrystallization will not occur. While there are several possibilities to measure a material's GFA, this study refers to the GFA classification system proposed by Baird et al. [25] where GFA classes I, II and III are defined according to differential scanning calorimetry (DSC) experiments. Wyttenbach et al. [26] used this methodology to systematically assess the GFA of amorphous compounds in marketed drug products which, except for vemurafenib, belong to GFA class II or III with a high ease of amorphization.

In contrast to the thermodynamic solubility of a crystalline API, the "amorphous solubility" (=kinetic supersaturation) is hardly measurable due to fast precipitation. It can only be estimated by the ratio to which the chemical potential of the amorphous form exceeds that of the crystalline state [27].

1.2.2 Functional principle of ASD

Due to their inherent thermodynamic instability, pure amorphous drugs are usually not developed as commercial drug products but together with excipients used for stabilization. On the one hand, these stabilizing excipients, which are usually pharmacologically inert, can be non-polymeric carriers like e.g. amino acids, mesoporous silica, surfactants or solubilizers. On the other hand, polymeric excipients (non-ionic and ionic) are frequently used which were also in the focus of this work.

In this context, the combinations of API and excipients are called "solid dispersions" which arise in different solid state forms of API and carrier. Laitinen et al. [28] summarized these possibilities in Table 1.1.

Table 1.1: *Nomenclature and classification of solid dispersions. From Laitinen et al. [28]*

State of API	Number of phases	
	1	2
Crystalline	Solid solution	Eutectic mixture
Amorphous	Glass solution	Glass suspension

The term ASD covers the stabilization of the API by a polymeric carrier both as glass suspensions (two phase systems) as well as glass solutions (one phase systems). If the API exists in its amorphous form and is fully miscible with its carrier and molecularly dissolved, a one-phase system with one T_g is generated. Depending on the solubility of the API within the polymer, which is therefore also related to the drug load (DL), the API might alternatively be dispersed in the matrix at a particle level resulting in glass suspensions with two separate T_g . However, phase separation is often difficult to detect if the phase domains are small. Short range crystalline clusters might not be detectable by standard powder X-Ray diffraction (PXRD) but only analytical techniques with higher resolution like small-angle X-Ray scattering (SAXS) [29] are suited in order to clearly differentiate between glassy solutions or suspensions.

A solid dispersion can be considered as a system consisting of the drug as solute and the polymer as solvent. As such, the phase behavior can be described by a schematic phase diagram which is exemplarily depicted in Figure 1.4. The system is thermodynamically stable as long as the drug load is below the solubility limit (solid black line). This is often only the case at low drug loads or at high temperatures. In all the other cases, the drug must be kinetically stabilized or "frozen" below the T_g . Not only recrystallization but also amorphous-amorphous phase separation (APS) can occur with different API-rich or polymer-rich phases. Above T_g , viscosity and molecular mobility drastically increase, lowering the kinetic stabilization and potentially enabling both APS and recrystallization.

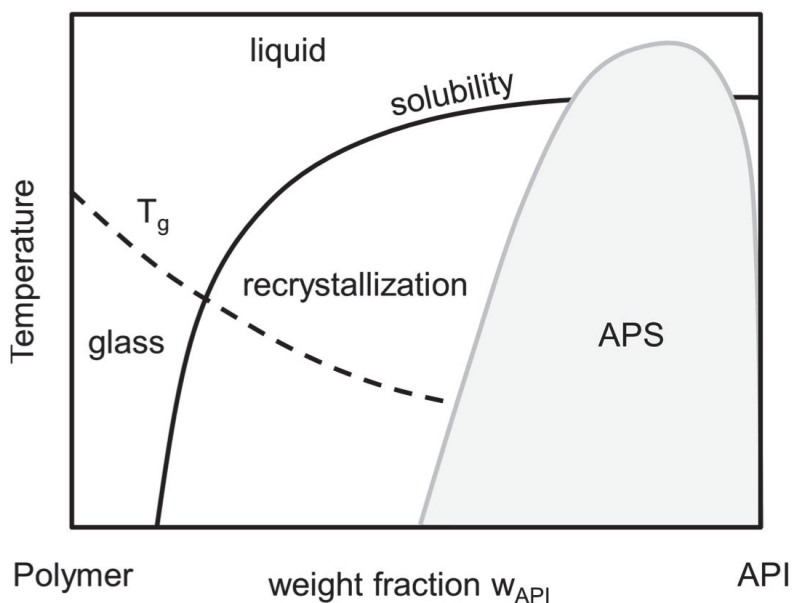


Figure 1.4: Schematic phase diagram for a two-component amorphous solid dispersion. From Luebbert et al. [30]

In both glass solutions as well as glass suspensions, the selected excipient stabilizes the API against crystal growth and recrystallization during storage as well as against precipitation during dissolution. Additionally, incorporation of the API molecules into hydrophilic carriers improves their wettability. If inhibition of precipitation and maintenance of supersaturation during dissolution is achieved for ASD, this then ends up in the so-called "spring and parachute effect" (Figure 1.5). Neat amorphous APIs can also exhibit pronounced supersaturation (spring) but normally quickly precipitate and return to the thermodynamic solubility of the crystalline state.

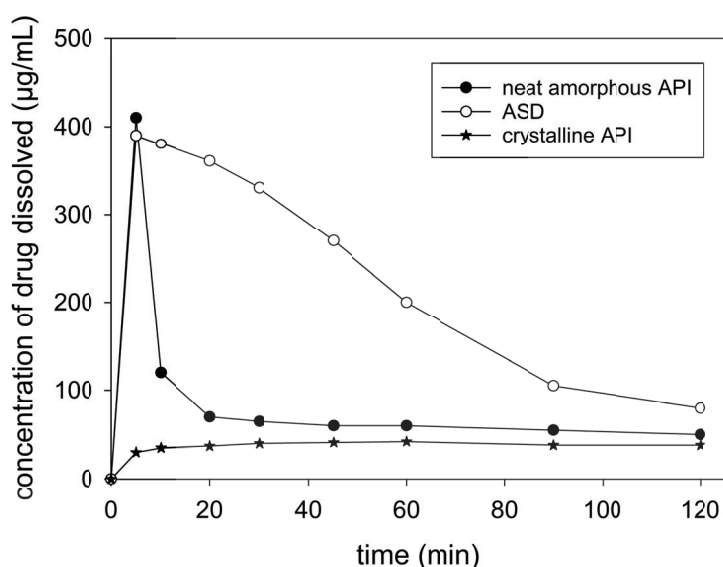


Figure 1.5: Schematic dissolution profiles of crystalline API, neat amorphous API and ASD with spring and parachute effect according to Baird et al. [25]

Hence, polymers significantly contribute to the functional principle of ASD. Table 1.2 summarizes the criteria that might influence performance and stability of these formulations. The enumeration shows the various factors that have to be considered during formulation development.

Table 1.2: *Factors that influence performance and stability of ASD. Modified and extended from Baghel et al. [31]*

Factors	Impact on performance and stability
Gibbs free energy	The lower the Gibbs free energy of a system the more stable it is. Amorphous forms possess higher free energies than the crystalline state.
Glass forming ability (GFA)	The GFA classification describes the propensity of a drug to recrystallize upon heating and cooling. It was possible to link the GFA assignment to supersaturation [32].
Glass transition temperature (T_g)	Stability increases with increasing T_g as mobility and viscosity change drastically [30]. Storage temperatures should be below T_g . T_g is also important for processability especially in hot-melt extrusion (HME).
Temperature	Temperature increases molecular mobility especially above T_g .
Humidity	Moisture acts as plasticizer which lowers the T_g of the formulation and can also lead to APS [30].
Degree of supersaturation	The higher the degree of supersaturation the higher the precipitation pressure to equilibrium solubility.
Precipitation	Precipitation inhibitors are used in ASD to maintain the supersaturated state during dissolution. It has to be prolonged for a certain timeframe to enable enhanced absorption in the GI tract.
Drug-polymer miscibility	Fully miscible components form one phase systems. Miscibility can be assessed experimentally (e.g. by DSC) where only one T_g is detected or by empirical parameters like the Flory-Huggins interaction parameter.
Drug-polymer solubility	If the DL is below the thermodynamic solubility of the API within the polymer, the system is not prone to recrystallization.
Drug-polymer interactions	Drug-polymer interactions may reduce recrystallization by increasing the T_g and reducing molecular mobilities.
Excipient functionalities	Functional groups that interact with the drug and molecular weight of excipients impact dissolution and stability of ASD [33, 34].
Molecular mobility	Molecular mobility of amorphous molecules in glass solutions should be reduced to hinder recrystallization (see also drug-polymer interactions). This is associated to macromolecular properties like viscosity. Quantification is e.g. possible by measurement of relaxation time.

Structural relaxation	Structural relaxation occurs in amorphous materials below their T_g and is a measure for molecular mobility. Molecular rearrangement that is also known as physical aging. Enthalpy and free volume decrease during relaxation [35].
Preparation method	Different preparation methods induce different thermal and mechanical histories.
Preparation conditions	Residence time in an extruder, downstream cooling rates [24] or evaporation rates [36] with spray-dried dispersions can affect the resulting stability of an ASD.
Mechanical stress	Mechanical stress can introduce seed crystals affecting recrystallization behavior.

1.2.3 Translational drawbacks - status quo

In 1999, Serajuddin et al. [37] analyzed promises and pitfalls of the formulation of ASD. The main problems were claimed as missing suitable (scale-up) manufacturing methods for ASD and subsequent dosage forms, reproducibility of physicochemical properties and physical stability issues. Although there is an ever increasing interest in formulating poorly soluble drugs and the numbers of publications on the topic of solid dispersions are continuously increasing (Figure 1.6), the number of marketed products does not rise to the same extent (Figure 1.7). Although there are multifactorial reasons to be considered in this context which are of course not only related to formulation aspects, this discrepancy is still evident and frequently discussed [29, 32, 38, 39].

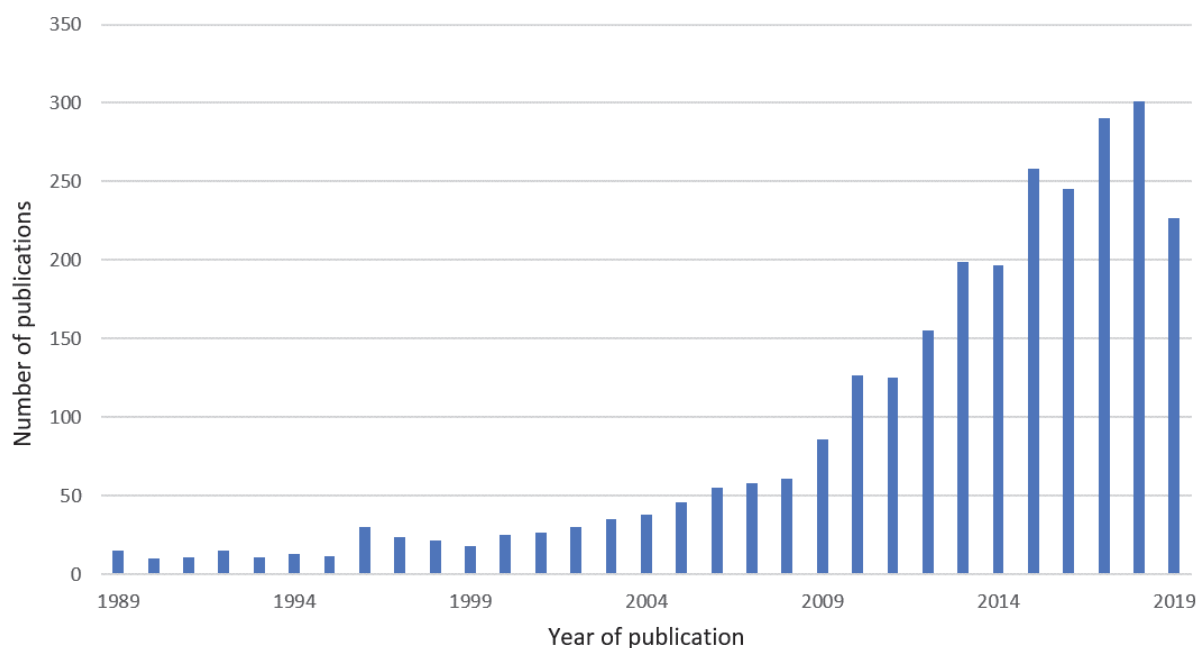


Figure 1.6: Publications in SciFinder database for the key words "amorphous solid dispersion", September 13th 2019

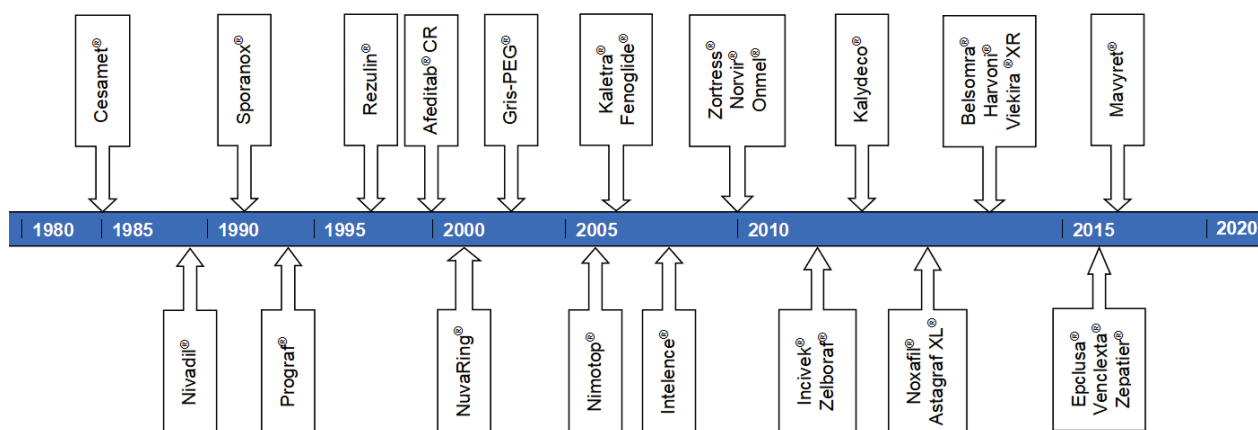


Figure 1.7: FDA approved drugs marketed as solid dispersions compiled with data from [11, 26, 40]

A lot of progress has been made especially in terms of manufacturing and scale-up but some of Serajuddin's concerns are still valid. This was also reflected by Shah et al. who discussed current reasons being mainly responsible for the discrepancy between research and access to the market. Hence, the following enumeration was adapted from Shah et al. [41] and additionally extended by the last point:

1. Limited knowledge about physicochemical properties of polymeric stabilizers
2. Insufficient knowledge about the interactions between API and polymer
3. Limited amounts of API available during early stages of development
4. Limited availability of representative processing techniques during preformulation development (miniaturized or small-scale formulation screening)
5. Insufficient predictability of physical stability
6. Lack of time for structured development
7. Lack of biorelevant dissolution methods providing better predictions for *in vivo* performance

Carrier selection - focus on screening methods

Table 1.2 lists many factors that have to be taken into account for selecting the best suited polymeric carrier. This selection is always dependent on the API in a case-by-case decision. As there are many pharmaceutically relevant polymers available, this results in a huge experimental setup of drug-polymer combinations with several drug loads to be tested. The number of experiments drastically increases if ternary systems (e.g. a combination of polymers or addition of plasticizers or surfactants) are needed. Additionally, the limited amount of API available during preclinical development intensifies the need for miniaturized screening methods with high throughput and fast readouts [42].

Therefore, 96-well plate based assays are attracting a lot of interest. Most popular are solvent-casting methods as described for example by Chiang et al. [43] or Wyttenbach et al. [44] named "Screening of Polymers for Amorphous Drug Stabilization (SPADS)". These provide a lot of information at a time but e.g. residual solvents have to be carefully monitored and evaporation must be sufficiently quick to avoid crystallization.

Second, there are solvent-shift screening methods described which induce supersaturation by either pH-shift or use of organic co-solvents with high concentration of the API dissolved that is being poured into aqueous media [45]. One of the most important drawbacks of the latter one is the impact of the co-solvent on the dissolution behavior. Both methods do not reflect dissolution kinetics from solid state but rather reflect an enforced induction of supersaturation.

Melt-fusion methods are also applied using hot plates, hot-stage microscopy or DSC. For the latter, e.g. melting point depression methods [46] or recrystallization trials are used [47]. One of the main restrictions here is intimate mixing of the components in solid state as melt rheological properties have to be considered [48]. Additionally, DSC methods can be used to measure the solubility of the API within the polymer matrix which allows for determination of maximum DL [49]. All of the techniques mentioned above provide a lot of information with minimal amounts of API. As decision-making in early formulation development often is very time challenging and straight forward, broad comparative studies between the different screening assays are missing. Further advanced analytics and scale-up trials are only being conducted with two or three of the most promising formulations lacking systematic evaluation of the predictability of these screenings. These limitations may impair reliability of the screening methods.

Drug-polymer interactions

Intermolecular drug-polymer interactions are considered one of the most important aspects for stabilization of the amorphous form which is of relevance both during dissolution and storage. Interactions may reduce the molecular mobility of API molecules which avoids nucleation or crystal growth and in consequence also recrystallization. Furthermore, they may prevent amorphous-amorphous phase separations (see Figure 1.4) with content inhomogeneities favoring the formation of one-phase systems [50]. Doing so, interactions may enable long-term physical stability during storage [19]. Additionally, interactions can also contribute to stabilization of the supersaturated state during dissolution hindering precipitation [51].

Many theoretical approaches exist which try to explain these stabilizing effects. However, they do not necessarily translate to *in vitro* or even *in vivo* performance [52]. Additionally, they are mainly focused on ionic interactions neglecting hydrogen bonding, dipole-dipole interactions, hydrophobic interactions or van der Waals forces although there are also several non-ionic drugs and carriers available (e.g. PVP derivatives, Soluplus™).

Quite some surrogate parameters are already known that should give an idea about drug-polymer interactions. These are for example the Flory-Huggins interactions parameter (FH) or deviations

from the calculated T_g value of a drug-polymer mixture via Gordon-Taylor equation (GT). However, these (semi-)empirical approaches often lack broad applicability and predictability. Where this is being investigated (e.g. Turpin et al. [53]) it turns out that systematic evidence is often missing.

From an experimental point of view, there are several possibilities to address interactions on a molecular level. Advanced characterization techniques like Fourier-transform infrared (FTIR) or Raman spectroscopy [54] and solid-state nuclear magnetic resonance (ss-NMR) [55] are used to elucidate interactions at a molecular level. However, they require at least small-scale manufacturing in gram scale and are normally quite time and cost intensive which excludes them for screening purposes.

Impact of manufacturing technique on excipients

There are several manufacturing techniques used for the preparation of solid dispersions including hot-melt extrusion (HME) and spray-drying (SD). The compilation of marketed ASD drug products depicted in Figure 1.8 indicates the significance of these two methods over other technologies like spray layering (e.g. on mesoporous silica), Kinetisol[®] Dispersing (high energy mixing [56]), electro spinning, supercritical fluids or coprecipitation.

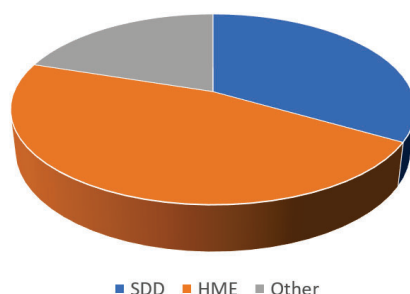


Figure 1.8: *FDA approved amorphous drugs according to the manufacturing technique compiled with data from [11, 26, 40]*

For selection of the appropriate manufacturing technique and process optimization, formulation scientists mostly rely on API properties (see also Figure 4.1). Thermostable compounds with a low melting point are usually applicable to HME whereas a high melting point combined with high solubility in volatile solvents favors SD. Only few studies systematically compare ASD prepared by HME and SD and analyze influencing factors [57, 58, 59]. However, the manufacturing technique may impact the final formulation in terms of crystalline content [60] or degree of relaxation and therefore presumably different levels of molecular mobility [61] and physical stability.

An increasing number of patents [62] reflects the importance of HME as one of the most widely used manufacturing techniques for ASD. Repka et al. [63] performed a S.W.O.T. (strengths, weaknesses, opportunities, threats) analysis for pharmaceutical application of this technology.

Considerable advantages over other ASD technologies were discussed: being solvent-free, applicability for continuous processing and suitability for further drug product formulation steps in terms of downstream processing. The biggest limitation is found in the restriction on thermally stable components, both API and polymers, as remarkable heat and shear stress are applied on the sample. Chemical and physicochemical degradation have to be monitored to ensure consistent quality of the formulation. As there is a twofold energy input from heating of the barrel as well as from viscous dissipation (shear stress), modelling of temperatures and exact mixing and dissolving processes within the barrel is quite complex [64].

In contrast, thermal stability for spray-drying processes is less critical as the contact times with heated air are very short. Instead, the choice of the solvent or mixture of solvents is crucial [65]. Both polymer and API should dissolve to a sufficient amount to ensure an efficient and economic process. Therefore, the solvent used should be volatile and residual solvents have to be carefully controlled observing the limits given in the ICH guidelines. Additionally, residual solvents may act as plasticizers which decrease the T_g and therefore potentially also stability of the formulation by increasing the molecular mobility.

The analytical setup to characterize ASD is also mostly focused on the API (see Chapter 3). Monitoring of chemical degradation, amorphization efficiency, physical stability during storage and determination of melting point and glass transition temperature are analytics assessed on a regular basis to just name a few. However, the polymer per se - often present in a higher mass fraction than the API - is not monitored to the same extent. The chemical stability of polymers was occasionally assessed e.g. for hydroxypropylmethylcellulose phthalate (HPMCP) [66] or hydroxypropylmethylcellulose acetate succinate (HPMCAS) [67]. Chen et al. [68] and Crowley et al. [69] published two of very few studies focusing on physicochemical characterization e.g. by means of gel permeation chromatography (GPC) for ASD relevant polymeric carriers. Broader application of this analytical technique would allow for process optimization with regard to the carrier without any API consumption.

Biorelevant *in vitro* dissolution

Friesen et al. [70] described the different drug, polymer and drug-polymer species that may form upon dissolution of a SDD with HPMCAS as carrier (Figure 1.9). The extent to which these species are formed could be correlated to the dosed drug level. The higher the dose the more colloids were formed instead of free drug. As the permeation through the GI membrane and hence oral absorption depend on the appearance of the drug (Figure 1.3), this should be taken into account to achieve a high bioavailability. Additionally, there are different possibilities how and when a drug is released from the solid dispersion [71] (e.g. either together with the polymer or separately). Hence, prediction of the dissolution behavior is very difficult. In contrast to other drug products, not only the dissolution rate or fraction of drug dissolved over a certain time is relevant but also the ability of the carrier to maintain supersaturation.

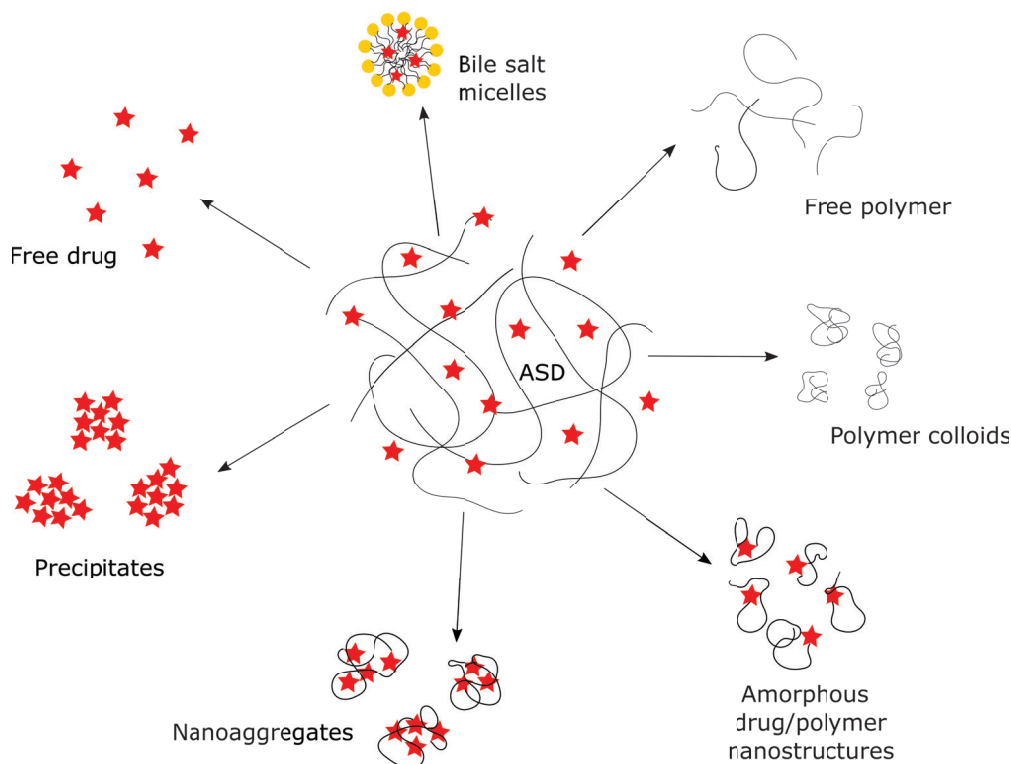


Figure 1.9: Potential species being formed upon dissolution of a SDD. Modified from Friesen et al. [70]

A careful selection of appropriate dissolution methods is absolutely necessary to discriminate between different formulations and select the best option in terms of polymeric carrier and drug load. The usage of simulated intestinal fluids (SIF) for fasted state (FaSSIF), fed state (FeSSIF) or gastric fluids (SGF) is highly recommended to account for bile salt, lecithin, fatty acids and pepsine present in the intestinal fluids *in vivo* [72, 73].

An additional effect has to be considered for biorelevant dissolution of weak bases (see also rDCS). Here, supersaturation can also be induced for crystalline drugs upon gastrointestinal transit [74]. The base is highly soluble in gastric media at low pH and reaches supersaturation when being released to the small intestine. Polymeric precipitation inhibitors likewise the carriers for ASD may stabilize the supersaturation and increase bioavailability. Such effects can be examined with a gastrointestinal transfer model as described by Kostewicz et al. [75]. Again, small-scale experimental setups are beneficial to account for limited API availability which was realized by Jede et al. [76] together with automated sampling. To date, such investigations were rarely conducted for ASD but give important insights into *in vitro-in vivo* correlation and the benefits of different formulation approaches.

1.3 Aim of work

This thesis deals with the formulation and characterization of amorphous solid dispersions which is one of the most promising strategies to overcome poor aqueous solubility. Although a lot of understanding was gained in the formulation of ASD within the last decade, there still is a need for further research as pointed out by Shah et al. (Chapter 1.2.3). These factors were taken into account to define the scope of this work. In this regard, ASD consisting of a weakly basic model compound should be developed with different pharmaceutically relevant polymeric carriers. Solubility enhancement, tested in discriminating *in vitro* non-sink dissolution assays, compared to crystalline API should be achieved. The different formulations should be manufactured by the two most common manufacturing techniques HME and SD to enable systematic comparison between the two manufacturing techniques. This broad objective setting was focused on the following three pillars:

1. **Predictability of miniaturized screening tools.** As the amount of API in preclinical development is very limited, miniaturized screening methods with high throughput and wide applicability are needed. Small-scale manufacturing can only be conducted with a limited number of carriers which are selected based on screening methods. Therefore, the reliability and predictability of such screenings is crucial for successful formulations. Hence, these criteria should be evaluated for a widely used solvent-based screening method. Furthermore, the transferability to different manufacturing techniques should be analyzed. Additionally, a screening method for detection of drug-polymer interactions should be developed.
2. **Physicochemical characterization of the polymeric carrier.** Most of the analytical techniques applied for characterization of amorphous solid dispersions only focus on the API as a surrogate for the success of the whole formulation. However, the polymeric carrier functionally contributes to the performance of the formulation to a great extent. Therefore, a characterization method should be developed to show the impact of the manufacturing technique on a polymer's molecular weight and PDI complementary to standard analytical tools. The impact of such changes on the performance of an ASD in dissolution should be examined.
3. **Biorelevant dissolution testing.** Only few publications deal with the comparison between supersaturation of amorphous formulations vs. physiologically induced supersaturation due to the gastrointestinal transfer for weakly basic compounds. It was the goal to evaluate this in a gastrointestinal transfer model considering the high variability of gastric pH in correlation to drug-polymer interactions.

A standardized set of analytical methods for assessment of critical quality parameters should be applied to enable systematic comparison of the different formulations.

2 Cumulative part

2.1 Overview of journals

Table 2.1: *Overview of journals where peer-reviewed articles were published*

Journal	Impact factor (2019)	5-year impact factor	Publisher
European Journal of Pharmaceutical Sciences (EJPS)	3.62	3.71	Elsevier
International Journal of Pharmaceutics (IJP)	4.85	4.44	Elsevier
Molecular Pharmaceutics (MolPharm)	4.32	n.a.	American Chemical Society

2.2 Peer-reviewed publications

The four publications described in this section were subject to a peer-review publication process as full research articles. They have been published in the journals listed above (Table 2.1).

Table 2.2 references the four articles with a declaration on the contribution of the first author to the experimental part as well as to the preparation of the manuscript.

These publications reflect the major part of the experiments that were conducted in the course of this doctoral thesis. As such, all methods used are described in detail in the articles and the results acquired were carefully discussed.

In **Publication I**, the predictability regarding dissolution performance of miniaturized screening methods for polymer selection in ASD was examined. A commonly used solvent evaporation procedure that was derived from the SPADS assay by Wyttenbach et al. [44] was compared with a newly developed melt-based method. The incorporation of the API within the polymeric carrier was assumed to be dependent on the amorphization technique used - either by rapid solvent evaporation or heat fusion. The dissolution results from the screenings were compared to ASD intermediates from either hot-melt extrusion or spray-drying which did not perform equally either. False negative results were found for polyvinylpyrrolidone (PVP) derivatives, namely the copolymer PVP-co-vinyl-acetate 60:40 (PVP-VA64) and PVP K30, in the solvent screening which was not the case in the melt-based approach. The solvent-based screening well predicted the performance of the solvent-based spray-drying process for the polymeric carriers hydroxypropyl methyl cellulose acetate succinate (HPMCAS) and cellulose acetate phthalate (CAP) whereas the performance of hot-melt extrudates was better reflected by the melt-based screening.

Publication II focuses on the physicochemical characterization of the polymeric carrier PVP-VA64. As such, the impact of hot-melt extrusion on molecular weight (M_w) and polydispersity index (PDI) was examined. A gel permeation chromatography (GPC) method with refractive index (RI) and multi-angle light scattering (MALS) detection was developed. This enabled absolute molar mass determination of the polymer with high reproducibility and sensitivity towards chain-scission and high molecular weight species. Different extrusion temperatures were used and minute changes of M_w and PDI could be detected while chemical integrity was proven by solution NMR. In a second step, KTZ was incorporated into the differently HME pre-stressed PVP-VA64 samples via spray-drying. The amorphous spray-dried dispersions (SDD) were tested in FaSSIF dissolution buffer for 120 min. As the SDD were manufactured with exactly the same process parameters, the changes detected in the dissolution profiles could be ascribed unambiguously to the changes in M_w and PDI of the polymeric carrier which were previously induced by HME.

As the assessment of drug-polymer interactions lacks high-throughput miniaturized methods, **Publication III** describes a new screening method based on changes in viscosity between polymer and polymer-KTZ solutions. The fluorescent molecular rotor 9-(2-Carboxy-2-cyanovinyl)julolidine (CCVJ) which emits different fluorescent yields depending on the viscosity of the surrounding solvent was used to rank drug-polymer interactions. A relative increase between polymer solutions and polymer-API solutions served as surrogate for interactions. ^{13}C ss-NMR spin-lattice relaxation time measurements ($T_{1\rho}$) were applied to investigate the interactions at a molecular level and confirmed the fluorescent viscosity screening (FluViSc) results for the two systems KTZ/HPMCAS and KTZ/PVP-VA64 that were chosen for proof of concept. The results were additionally correlated to the empiric Gordon-Taylor equation and shifts in Raman spectra where the FluViSc turned out to be both more accurate and discriminating.

One of the most important aspects in carrier selection for ASD is the generation and stabilization of supersaturation. Therefore, biorelevant dissolution methods are required that allow for small-scale testing and differentiation between different excipients. For ASD, this is usually realized by discriminative non-sink dissolution testing.

For weakly basic compounds, a second pathway of inducing supersaturation caused by the gastrointestinal transit is possible. Therefore, **Publication IV** compares the performance of ASD versus physical mixtures with the same carrier at different gastric pH. The precipitation inhibition was examined for different grades of HPMCAS and a ternary system with the basic polymer EudragitTME PO to further analyze the influence of acidity and drug-polymer interactions for stabilization of supersaturation.

Table 2.2: Declaration of contributions to the different publications. A: Planning, execution, analysis and evaluation of the corresponding experiments, B: Contribution to the manuscript

Publication	Title	Contribution
Publication I	C. Auch, M. Harms, K. Mäder <i>Melt-based screening method with improved predictability regarding polymer selection for amorphous solid dispersions.</i> European Journal of Pharmaceutical Sciences 124 (2018) 339-348	A: 90% B: 85%
Publication II	C. Auch, M. Harms, K. Mäder <i>How molecular weight and PDI of a polymer impact dissolution performance.</i> International Journal of Pharmaceutics 556 (2019) 372-382	A: 90% B: 85%
Publication III	C. Auch, M. Harms, Y. Golitsyn, D. Reichert, K. Mäder <i>Miniaturized measurement of drug-polymer interactions via viscosity increase for polymer selection in amorphous solid dispersions.</i> Molecular Pharmaceutics 16 (2019) 2214–2225	A: 75% B: 75%
Publication IV	C. Auch, C. Jede, M. Harms, C. Wagner, W. Weitschies, K. Mäder <i>Impact of amorphization and GI physiology on supersaturation and precipitation of poorly soluble weakly basic drugs using a small-scale in vitro transfer model.</i> International Journal of Pharmaceutics 574 (2020) 118917	A: 60% B: 75%

2.2.1 Melt-based screening method for polymer selection

Title: Melt-based screening method with improved predictability regarding polymer selection for amorphous solid dispersions

European Journal of Pharmaceutical Sciences

DOI: <https://doi.org/10.1016/j.ejps.2018.08.035>

Link: <https://www.sciencedirect.com/science/article/pii/S0928098718304007>

Supplementary Material:

<https://ars.els-cdn.com/content/image/1-s2.0-S0928098718304007-mmc1.pdf>

Abstract The predictability of preformulation screening tools for polymer selection in amorphous solid dispersions (ASD) regarding supersaturation and precipitation was systematically examined. The API-polymer combinations were scaled up by means of hot-melt extrusion and spray-drying to verify the predictions. As there were discrepancies between a solvent-based screening and performance of ASD, a new screening tool with improved predictability at minimal investments of time and material is presented. The method refinement resulted in a better correlation between the screening and ASD prototypes. So far, a purely solvent-based screening was used which consisted of film casting by rapid solvent evaporation. This approach was improved by applying a heating step after film casting. Four representative polymers were tested with two different model active pharmaceutical ingredients (API) under non-sink dissolution conditions. Polyvinylpyrrolidone (PVP) based polymers showed no benefit towards pure API in the solvent-based screening but good supersaturation as ASD formulations. The extrudates with cellulose derivatives hydroxypropylmethylcellulose acetate succinate (HPMCAS) and cellulose acetate

phthalate (CAP) showed lower supersaturation than predicted by the solvent-based screening but performed especially well as spray-dried dispersions (SDD). False negative results for PVP-co-vinyl acetate (PVP-VA64) could be avoided by using the new melt-based screening. Furthermore, comparing the results from the two different screening methods allowed to predict the performance of extrudates vs. SDD with cellulose derivatives as polymeric excipients.

Graphical Abstract

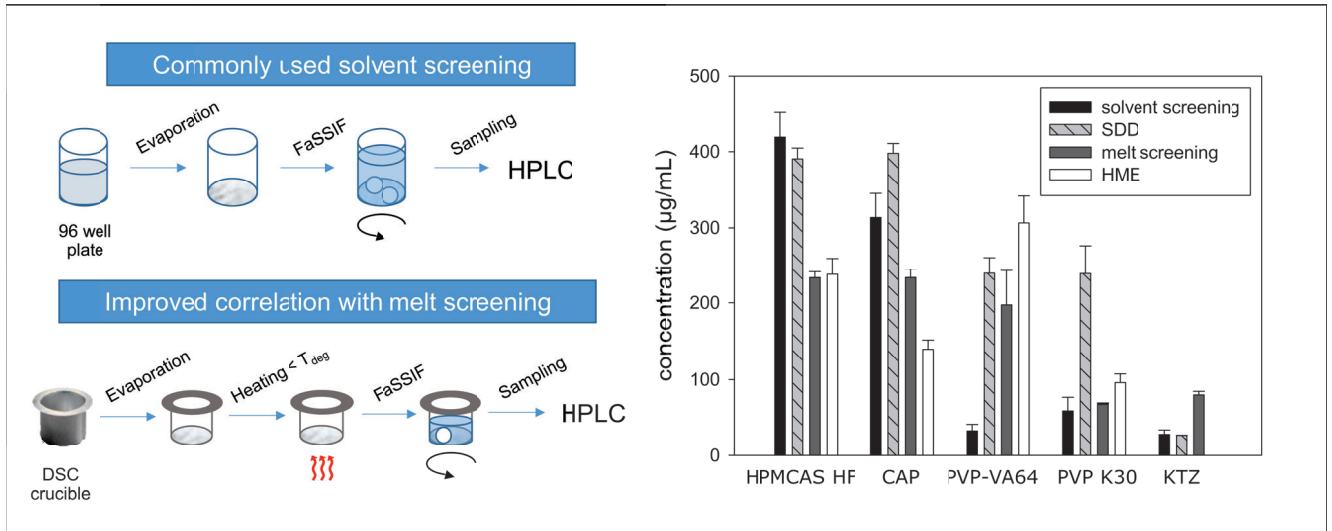


Figure 2.1: Graphical abstract to Auch et al. [77]

2.2.2 Impact of polymer degradation in HME

Title: How changes in molecular weight and PDI of a polymer in amorphous solid dispersions impact dissolution performance

International Journal of Pharmaceutics

DOI: <https://doi.org/10.1016/j.ijpharm.2018.12.012>

Link: <https://www.sciencedirect.com/science/article/pii/S0378517318309189?via%3Dihub>

Supplementary Material:

<https://ars.els-cdn.com/content/image/1-s2.0-S0378517318309189-mmc1.pdf>

Abstract Polymers functionally contribute to supersaturation and precipitation inhibition of the active pharmaceutical ingredient (API) in amorphous solid dispersions (ASD). Therefore, it is necessary to monitor physicochemical changes of the polymeric carrier caused by the manufacturing process. This is especially important when the material is exposed to heat and shear stress as in case of hot-melt extrusion (HME). This study evaluated the impact of HME process conditions on physical characteristics of poly(vinylpyrrolidone-co-vinyl-acetate) 60:40 (PVP-VA64) which is a widely used polymer for HME. Focus was set on molecular weight (M_w) and polydispersity index (PDI), by means of absolute molar mass detection via multi-angle light scattering. The generation of a high M_w fraction together with a decrease of the average M_w was detected. In a next step, the influence of these changes on the dissolution behavior of ASD was evaluated. Different stress conditions were applied onto PVP-VA64 in placebo extrusions. The obtained stressed polymer samples were subsequently used to prepare verum ASD with ketoconazole by spray drying (SD). SD dispersions (SDD) of thermally stressed PVPVA64 were compared to SDD prepared with bulk powder. Although there were only slight changes in M_w and PDI, they significantly impacted supersaturation and precipitation of the formulation.

Graphical Abstract

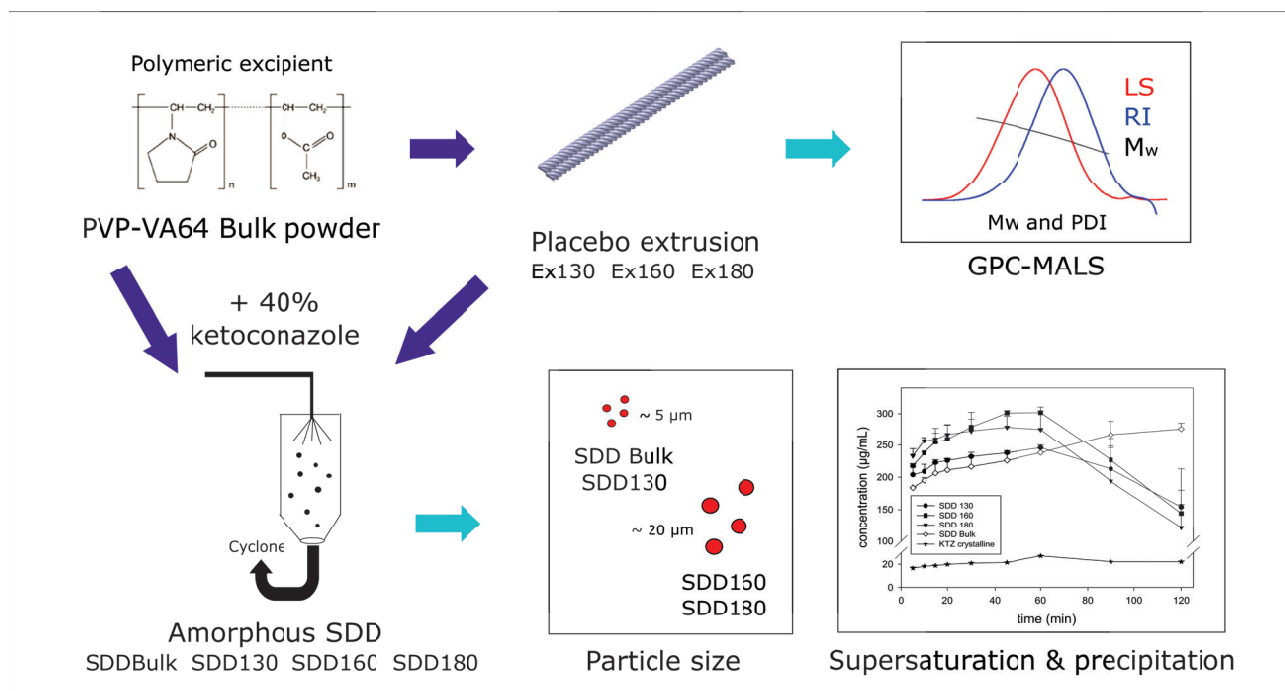


Figure 2.2: Graphical abstract to Auch et al. [34]

2.2.3 Analysis of API-polymer interactions in ASD

Title: Miniaturized measurement of drug-polymer interactions via viscosity increase for polymer selection in amorphous solid dispersions

Molecular Pharmaceutics

DOI: 10.1021/acs.molpharmaceut.9b00186

Link: <https://pubs.acs.org/doi/10.1021/acs.molpharmaceut.9b00186>

Supporting Information:

https://pubs.acs.org/doi/suppl/10.1021/acs.molpharmaceut.9b00186/suppl_file/mp9b00186_si_001.pdf

Abstract Drug–polymer interactions have a substantial impact on stability and performance of amorphous solid dispersions (ASD) but are difficult to analyze. Whereas there are many screening methods described for polymer selection based for example on glass forming ability, drug–polymer miscibility, supersaturation, or inhibition of recrystallization, the distinct detection of physico-chemical interactions mostly lacks miniaturized techniques. This work presents an interaction screening assessing the relative viscosity increase between highly concentrated polymer solutions with and without the model drug ketoconazole (KTZ). The fluorescent molecular rotor 9-(2-carboxy-2-cyanovinyl)julolidine was added to the solutions in a miniaturized setup in μL -scale. Due to its environment-sensitive emission behavior, the integrated fluorescence intensity can be used as a viscosity dye within this screening approach (FluViSc). Differences in relative viscosity increases through addition of KTZ were proposed to rank polymers regarding KTZ–polymer interactions. Absolute viscosities were measured with a cone–plate rheometer as a complementary method and supported the results acquired by the FluViSc. Solid-state nuclear magnetic resonance (ss-NMR) relaxation time measurements and Raman spectroscopy were utilized to investigate drug–polymer interactions at a molecular level. Whereas Raman spectroscopy was not suited to reveal KTZ–polymer interactions, ss-NMR relaxation time measurements differentiated between the selected polymeric carriers hydroxypropylmethylcellulose acetate succinate (HPM-CAS) and polyvinylpyrrolidone vinyl acetate 60:40 (PVP-VA64). Interactions were detected for HPMCAS/KTZ ASD while there was no hint for interactions between KTZ and PVP-VA64. These results were in correlation with the FluViSc. The findings were correlated with the dissolution performance of ASD and found to be predictive for supersaturation and inhibition of precipitation during dissolution.

Graphical Abstract

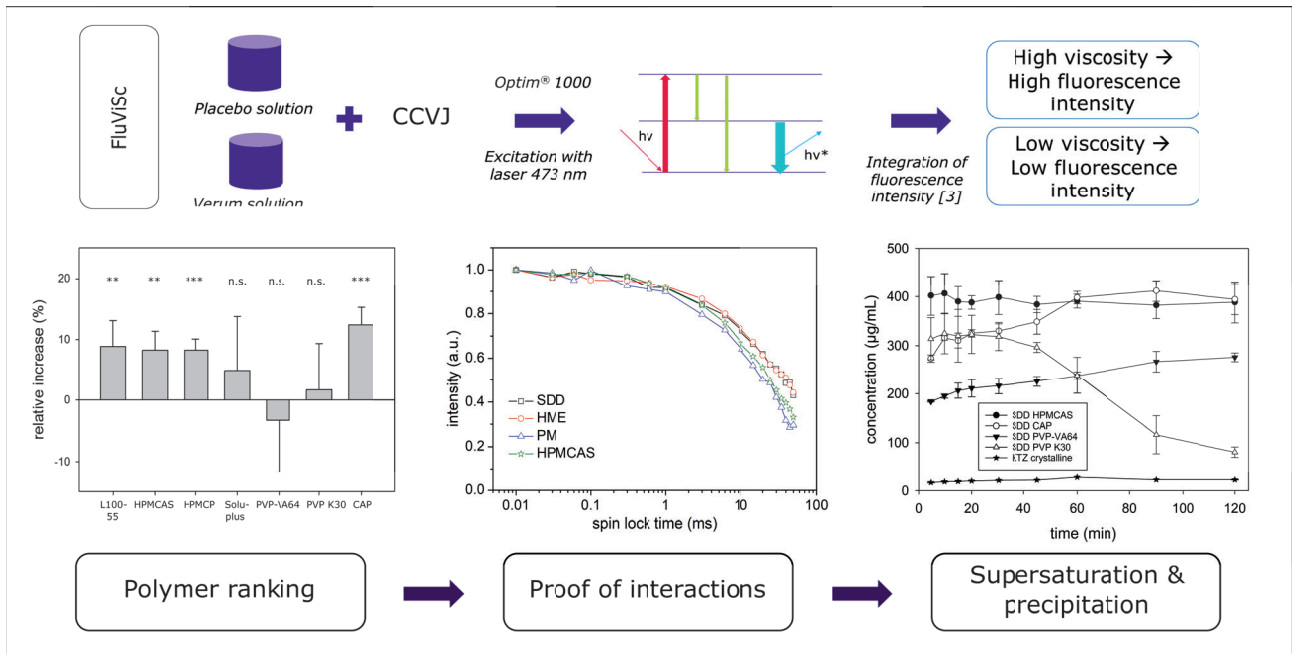


Figure 2.3: Graphical abstract to Auch et al. [78]

2.2.4 Application of gastrointestinal transfer model for ASD

Title: Impact of amorphization and GI physiology on supersaturation and precipitation of poorly soluble weakly basic drugs using a small-scale in vitro transfer model

International Journal of Pharmaceutics

DOI: <https://doi.org/10.1016/j.ijpharm.2019.118917>

Link: <https://www.sciencedirect.com/science/article/pii/S0378517319309627?via%3Dihub>

Supporting Information:

<https://ars.els-cdn.com/content/image/1-s2.0-S0378517319309627-mmc1.xml>

Abstract Formulation of amorphous solid dispersions (ASD) is one possibility to improve poor aqueous drug solubility by creating supersaturation. In case of weakly basic drugs like ketoconazole (KTZ), supersaturation can also be generated during the gastrointestinal (GI) transfer from the stomach to the intestine due to pH-dependent solubility. In both cases, the supersaturation during dissolution can be stabilized by polymeric precipitation inhibitors. A small-scale GI transfer model was used to compare the dissolution performance of ASD versus crystalline KTZ with the polymeric precipitation inhibitor HPMCAS. Similar in vitro AUCs were found for the transfer from SGF pH 2 into FaSSIF. Moreover, the impact of variability in gastric pH on drug dissolution was assessed. Here, the ASD performed significantly better at a simulated hypochlorhydric gastric pH of 4. Last, the importance of drug-polymer interactions for precipitation inhibition was evaluated. HPMCAS HF and LF grades with and without the basic polymer Eudragit E PO were used. However, E PO caused a faster precipitation probably due to competition for the interaction sites between KTZ and HPMCAS. Thus, the results are suited to assess the benefits of amorphous formulations vs. precipitation inhibitors under different gastrointestinal conditions to optimize the design of such drug delivery systems.

Graphical Abstract

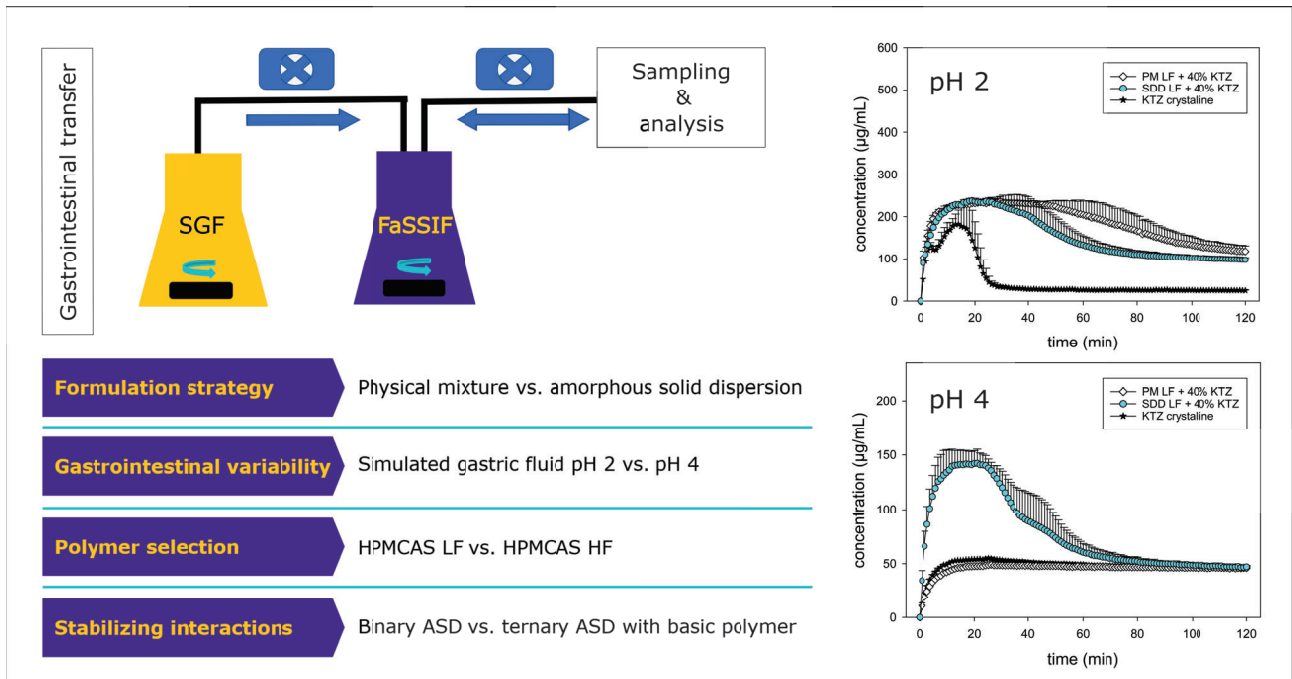


Figure 2.4: Graphical abstract to Auch et al. [79]

3 Results and discussion

The work presented in this thesis aimed at developing tools to improve the translation from pre-formulation research to formulation development in the field of ASD. Several gaps were identified throughout the formulation development of ASD (see Chapter 1.2.3) which were thus investigated within this thesis. The special circumstances to be considered in terms of gastrointestinal transfer of weakly basic compounds were accounted for by using the model API ketoconazole (KTZ) (chemical structure see Figure 3.1). KTZ was carefully selected to represent relevant API properties in terms of melting point (149°C), log P (4.3), solubility (23 µg/mL in FaSSIF) and GFA. KTZ belongs to GFA class III similar to most marketed ASD compounds [32] which means that there is a high propensity for amorphization (no recrystallization observed after quench-cooling in a DSC heating-cooling-heating cycle).

To systematically analyze certain aspects like supersaturation, precipitation, storage stability, miscibility or drug-polymer interactions, a broad set of formulations for comparison was needed. These formulations were developed with different polymeric carriers which are summarized in Table 3.1. These were non-ionic, anionic or cationic in nature with different T_g and T_{deg} as well as molecular weights; factors which are of relevance when selecting a polymeric carrier as outlined in Table 1.2. This enabled the comparison across various pharmaceutically relevant polymers and different manufacturing techniques. Four formulations where a complete dataset was acquired were additionally tested regarding physical stability under different storage conditions (2-8°C, 25°C/60% relative humidity (r.h.) and 40°C/75% r.h. according to ICH Q1A(R2) guideline) for up to one year.

Table 3.1: *Summary of formulations consisting of the listed excipient and KTZ that were developed and analyzed within PhD thesis*

Excipient	Solvent Screening	Melt Screening	FluViSc	HME	SDD	Stability
HPMCAS HF	x	x	x	x	x	x
HPMCAS LF	x	-	-	-	x	-
HPMCAS HME	x	-	-	x	x	x
CAP	x	x	x	x	x	x
HPMCP HP50	x	-	x	x	-	-
Soluplus	x	-	x	x	x	-
PVP K30	x	x	x	x	x	-
PVP-VA64	x	x	x	x	x	x
Eudragit E PO	x	-	-	x	-	-
Eudragit L100-55	x	-	x	x	-	-

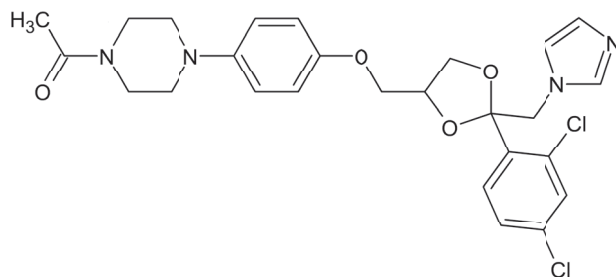


Figure 3.1: Chemical structure of model compound ketoconazole

The first aspect under closer investigation was the predictability of a preformulation screening tool for polymer selection. A modification of the SPADS assay by Wytenbach et al. in a 96 well quartz plate was used as starting point which can be considered as a standard miniaturized screening method based on solvent film casting. Stability testing was conducted by storage of the amorphous films under accelerated conditions (40 °C/75% r.h.). Two different drug loads of 20 and 40% were tested both giving amorphous films. For further experiments, it was decided to continue with the higher DL (40%) to challenge physical stability and pose a potential risk for recrystallization and instabilities during a manageable timeframe. The corresponding dissolution results are depicted in Figure 3.2.

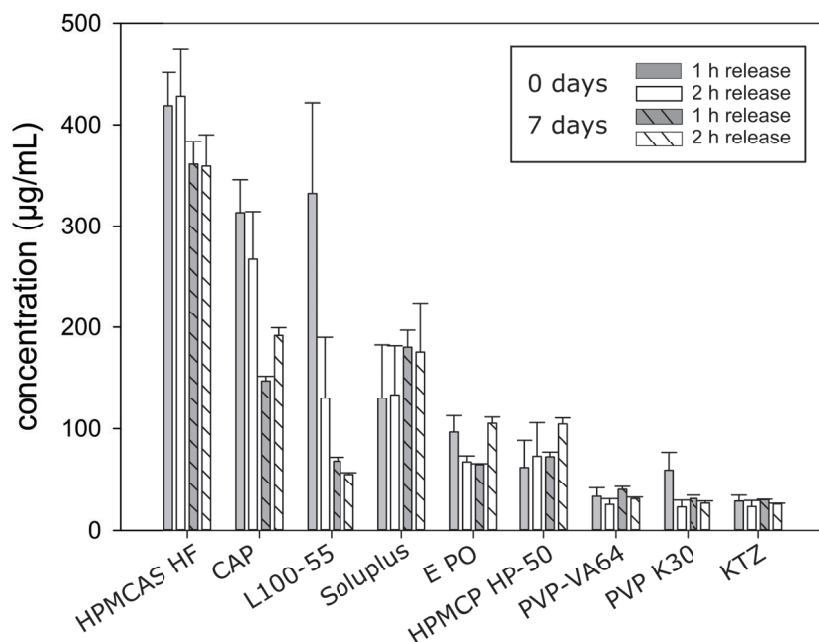


Figure 3.2: Solvent screening for KTZ with various polymers and 40% DL. Non-sink dissolution testing in FaSSIF-V1 pH 6.5. Arithmetic means of $n=3 + S.D.$

The casted film of neat KTZ was used as reference which showed slightly higher concentrations of drug dissolved than the thermodynamic solubility of crystalline KTZ. Different degrees of supersaturation were achieved for all formulations except for PVP-VA64 and PVP K30.

The best result was achieved with HPMCAS HF in terms of supersaturation, precipitation inhibition as well as storage stability. CAP and L100-55 showed a quite strong decrease in concentration of drug dissolved after seven days whereas Soluplus, E PO and HPMCP stabilized the supersaturation well but on a generally lower level.

The ranking derived from solvent screening results (Figure 3.2) should be correlated to ASD intermediates in terms of supersaturation and precipitation inhibition. Therefore, all polymers were first employed for manufacturing of ASD via HME as the predictability of the screening should be systematically investigated. The non-sink dissolution results for the milled extrudates correlated well with the solvent screening except for HPMCAS HF, CAP, PVP-VA64 and PVP K30 which is seen when comparing the concentrations of drug dissolved in Figure 3.3 A with Figure 3.2. Therefore, these four formulations were additionally formulated as SDD to examine the impact of the manufacturing technique. Figure 3.3 B shows the concentrations of drug dissolved that were achieved from dissolution of SDD particles.

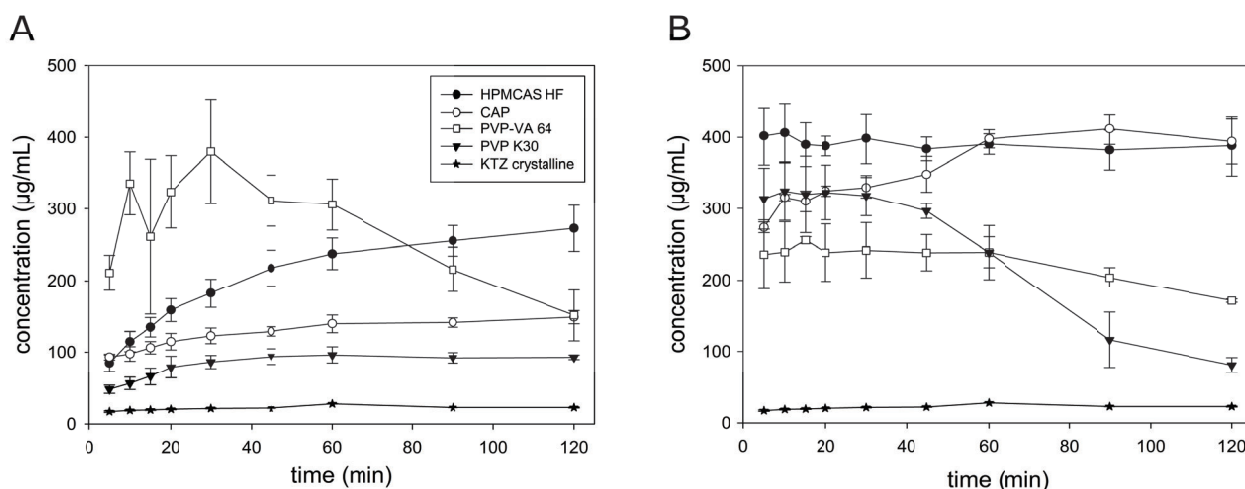


Figure 3.3: Concentration of KTZ dissolved in a non-sink dissolution of A) milled hot-melt extrudates and B) SDD powder (legend see A) with 40% DL in FaSSIF-V1 pH 6.5 compared to crystalline KTZ. Arithmetic means of $n=3 \pm S.D.$ From [77]

For in depth characterization of the formulations, the following setup of analytical methods was developed:

1. Reversed-phase high-performance liquid chromatography (RP-HPLC) - content analysis (for dissolution testing and content uniformity) and purity
2. Differential scanning calorimetry - measurement of T_m and T_g , miscibility assessment
3. Powder X-Ray diffraction (PXRD) - solid state analysis
4. Microscopy with standard light/polarized light (PLM) - particle size assessment, crystallinity

-
5. Gel permeation chromatography (GPC) with RI and MALS detection - determination of polymers' molecular weight and polydispersity index
 6. Viscosity measurements (FluViSc, cone-plate rheometer) - analysis of drug-polymer interactions via viscosity increase
 7. Raman spectroscopy - solid state analysis and detection of drug-polymer interactions
 8. Solution NMR - quantification of residual solvents, chemical integrity of polymer
 9. Solid-state NMR - detection of drug-polymer interactions via relaxation time measurements
 10. Thermogravimetric analysis (TGA) - T_{deg} , water content
 11. Loss on drying - monitoring of powders' humidity during processing and stability testing
 12. Static light scattering - particle size distribution
 13. Non-sink dissolution testing in different scales (96 well, Eppendorf Caps)
 14. Gastrointestinal transfer model - dissolution testing under simulated GI conditions

The analytical methods 1-4 were routinely applied to all ASD intermediates. Fulfillment of preset specifications for these analytical methods was considered as a prerequisite for comparability among the different formulations allowing further interpretation of the data. Fully amorphous formulations with 40% DL for all formulations listed in Table 3.1 were produced according to DSC, PLM and PXRD together with 95-105% content uniformity and >98% purity (n=4).

Exemplary results of the analytics (where applicable) for crystalline API, solvent casted films, physical mixtures (PM), SDD and HME are depicted in Figure 3.4 for KTZ formulations with the carrier HPMCAS. The absence of a crystalline melting peak in the HME and SDD samples as well as a single T_g indicate formation of one phase amorphous systems in the DSC thermograms (Figure 3.4 A). A melting point depression from 149°C (crystalline KTZ) to 141°C onset temperature in the PM was detected in the DSC runs which is considered as a hint for miscibility and interaction as explained in detail by Marsac et al. [80]. The amorphous halo for both HME and SDD formulations can be clearly differentiated from crystalline Bragg peaks (also present in PM) in the PXRD diffractograms acquired via long-term measurements (Figure 3.4 B). As HPMCAS is semi-crystalline in nature, special attention is needed for judging residual crystallinity via PLM which is only possible by comparison with placebo films, SDD particles or milled extrudates (Figure 3.4 C).

The two manufacturing techniques resulted in different performances of the ASD although the analytical results did not reveal any differences between extrudates and SDD in terms of amorphization, T_g , content or purity. As this discrepancy in performance would heavily influence the decision for the most suited manufacturing technique, a predictive screening tool should be established to assist in choosing the best formulation technique.

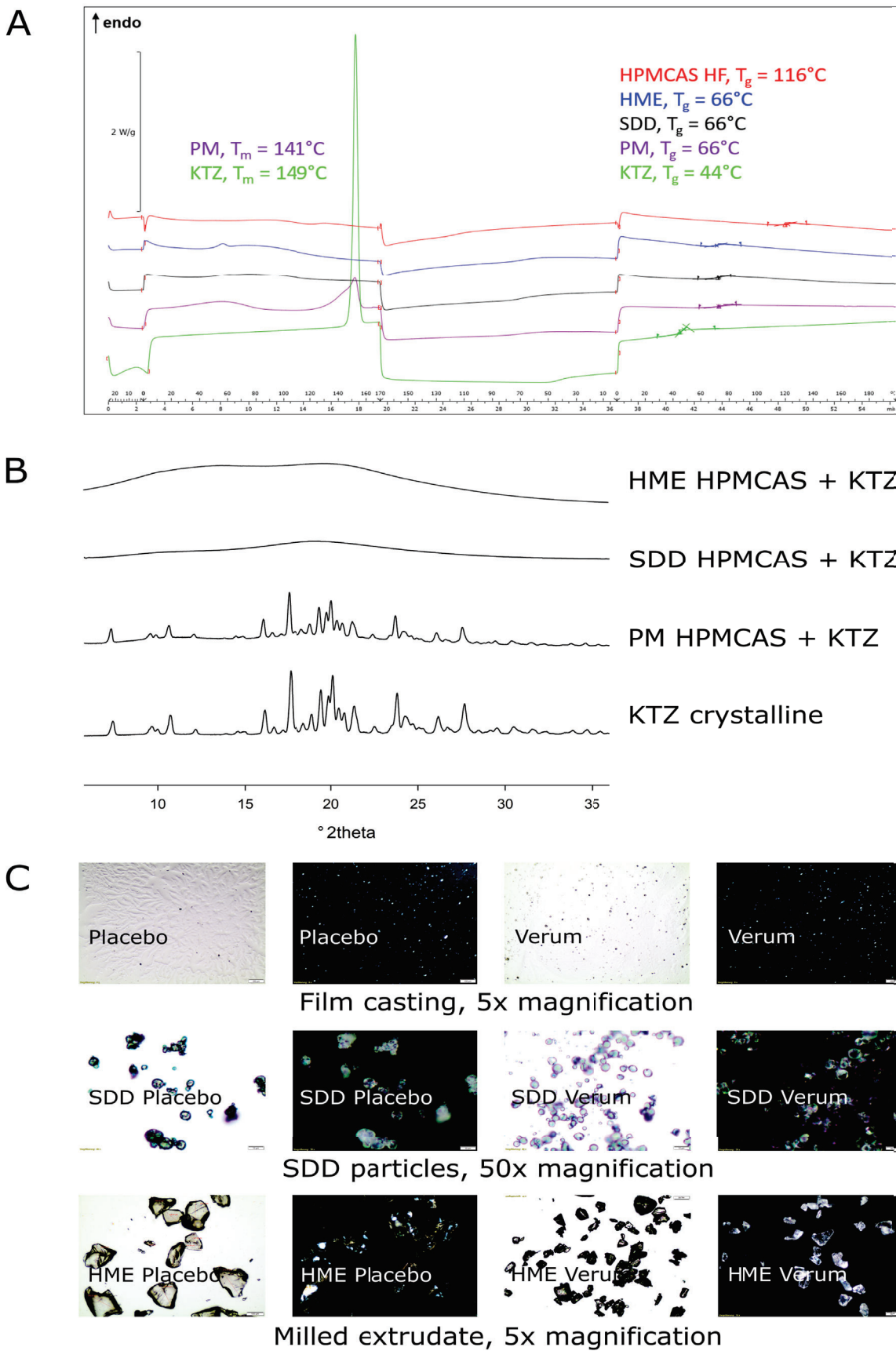


Figure 3.4: Exemplary results of A) DSC, B) PXRD and C) microscopy and PLM for HPMCAS with 40% DL KTZ

Therefore, a melt screening was developed [77] to better mimick the conditions in a HME process. The temperatures chosen for heating were selected to be below T_{deg} but above T_g of the drug-polymer films to enable certain mobility for molecular rearrangement.

The comparison between both screening approaches showed clear differences as depicted in Figure 3.5. On the one hand, both cellulose derivatives performed better in the solvent screening than in the melt screening. On the other hand, there was a pronounced supersaturation predicted for PVP-VA64 by the melt screening which was not seen at all in the solvent-based approach.

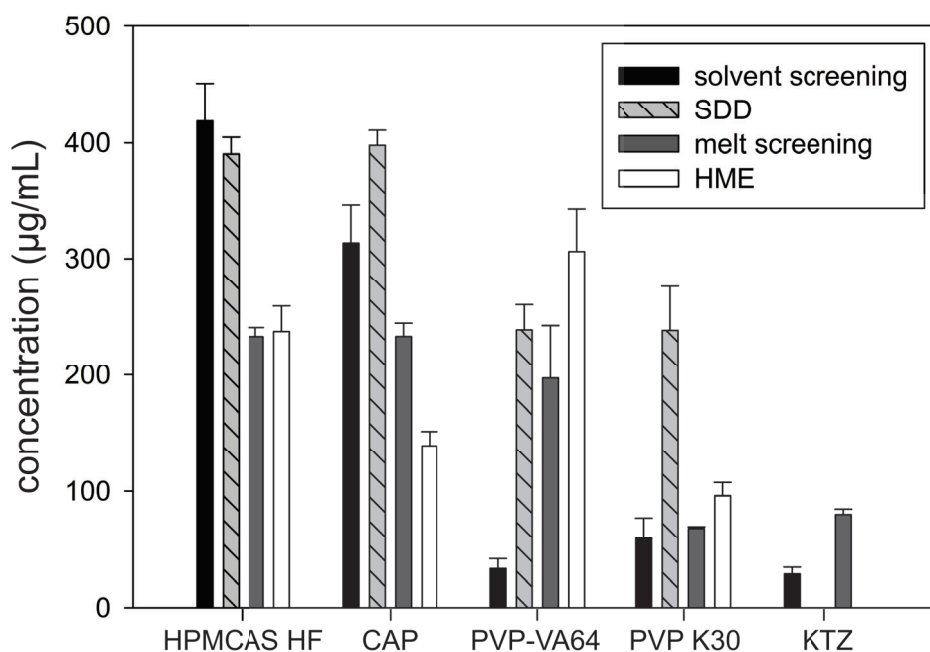


Figure 3.5: Overall comparison of concentration of drug dissolved with both screening tools (melt-based and solvent-based), SDD and HME with 40% drug load KTZ each after 60 min dissolution time. Arithmetic means of $n=3 \pm S.D.$ Pure KTZ was not fully amorphous as SDD without polymeric excipient and was not processed by means of HME. From [77]

It could be shown that the way the screening is conducted can be correlated to the manufacturing technique. Furthermore, it was demonstrated that the solvent screening underpredicted the performance of the two polyvinylpyrrolidone derivatives for KTZ solubility enhancement. This would lead to systematically false-negative results that unnecessarily limit the formulation options of ASD.

These findings were subsequently confirmed with an internal pipeline compound (MC1) in formulation with PVP-VA64 and HPMCAS (chemical structure and results are shown in [77]). Again, PVP-VA64 did not lead to supersaturation in the solvent screening but only in the melt screening which was proven by HME and SD. In contrast to KTZ, MC1 belongs to GFA class I with additional melt degradation effects which was considered a worst case example for the melt screening.

Nevertheless, the good correlation detected for KTZ could be directly transferred to MC1. For further interpretation, a closer investigation on the reasons for different performances depending on the manufacturing technique was necessary. One of the hypotheses was the creation of different drug-polymer interactions being built either upon solvent evaporation (solvent screening and SD) or upon heat fusion (melt screening and HME).

Drug-polymer interactions are generally known to contribute to the functional principle of ASD as discussed in Chapter 1.2.3. However, miniaturized and simple screening tools that give an idea on interactions during preformulation development were missing. Therefore, a μL -scale polymer screening based on viscosity measurements via fluorescent molecular rotors was developed named fluorescent viscosity screening (FluViSc). Placebo polymer stock solutions and solutions additionally containing the API with 40% DL were prepared. The fluorescent molecular rotor 9-(2-carboxy-2-cyanovinyl)julolidine (CCVJ) was added to the solutions and the fluorescence emission intensity was measured after excitation. An increase in fluorescence intensity of these rotors is a marker of increased viscosity [81]. To rank the extent of interactions between different polymers, a relative increase in fluorescence intensity between polymer and polymer-KTZ was calculated.

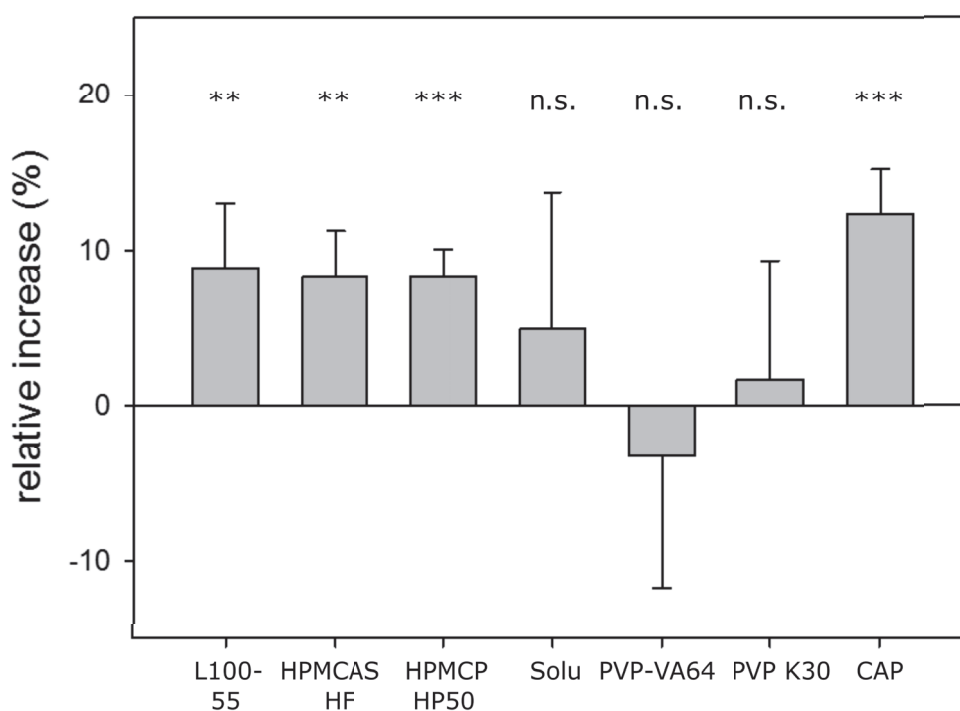


Figure 3.6: Relative viscosity increase between placebo and verum solutions with 50 mg/mL polymer each w/wo 40% DL. Arithmetic means of $n=3 \pm S.D.$ with asterisks indicating statistical significance in *t*-tests between polymer and polymer-KTZ (*: $p < 0.05$, **: $p < 0.01$, ***: $p < 0.001$). From [78]

The FluViSc (Figure 3.6) showed a strong increase for the acidic polymers (L100-55, HPMCAS, HPMCP, CAP) and non-significant results for the PVP derivatives and Soluplus. As KTZ is a weakly basic compound, ionic interactions between acidic polymers and KTZ are likely to occur. As these are much stronger compared to hydrophobic interactions or hydrogen bonds, they were expected to dominate the results which was indeed seen in the screening. For the stabilizing effect of Soluplus in ASD, its solubilization capacity caused by its amphiphilic nature is frequently discussed in literature. This might explain a subordinate manifestation of drug-polymer interactions in this case.

Of course, this completely new approach had to be subsequently verified by complimentary methods and also transferred to the dissolution performance and storage stability of selected ASD. Therefore, absolute viscosity measurements with a cone-plate rheometer as orthogonal method were conducted which confirmed the findings of the FluViSc. Deviations from the Gordon-Taylor equation were also fitting the data with a clear positive deviation towards higher T_g of the mixture than calculated for L100-55 and CAP which is depicted in Auch et al. [78].

To give a proof of concept regarding molecular interactions, ss-NMR measurements were conducted. HPMCAS and PVP-VA64 were chosen as positive and negative controls from the screening. The ^{13}C ss-NMR spectra for neat substances PVP-VA64, HPMCAS and KTZ are shown in Figure 3.7.

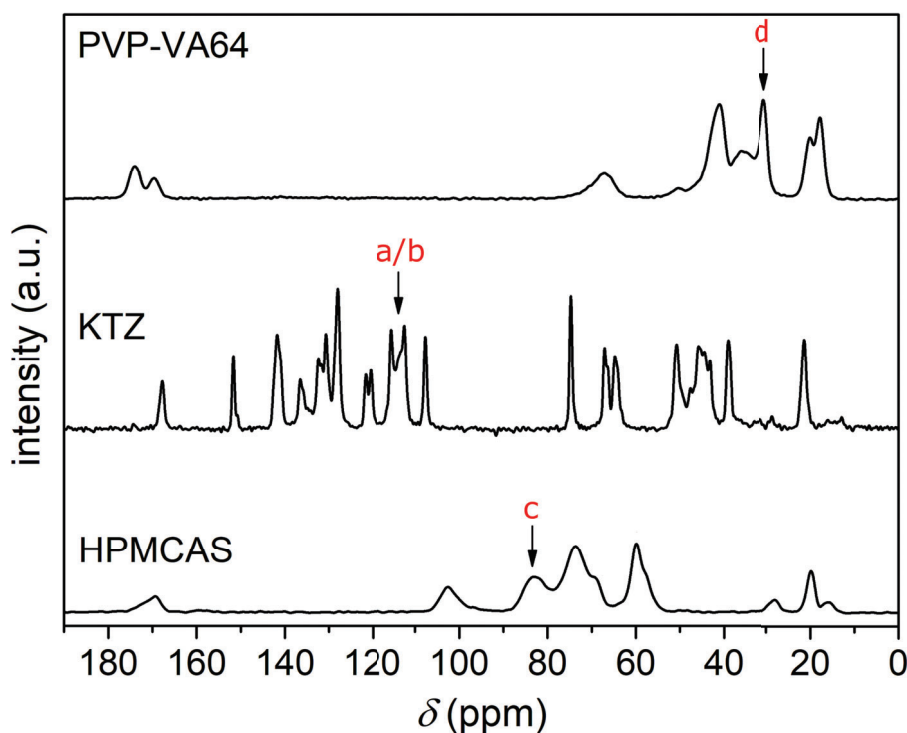


Figure 3.7: ^{13}C ss-NMR spectra for neat PVP-VA64, HPMCAS and KTZ as references for peak assignment in Figure 3.8. Modified from [78]

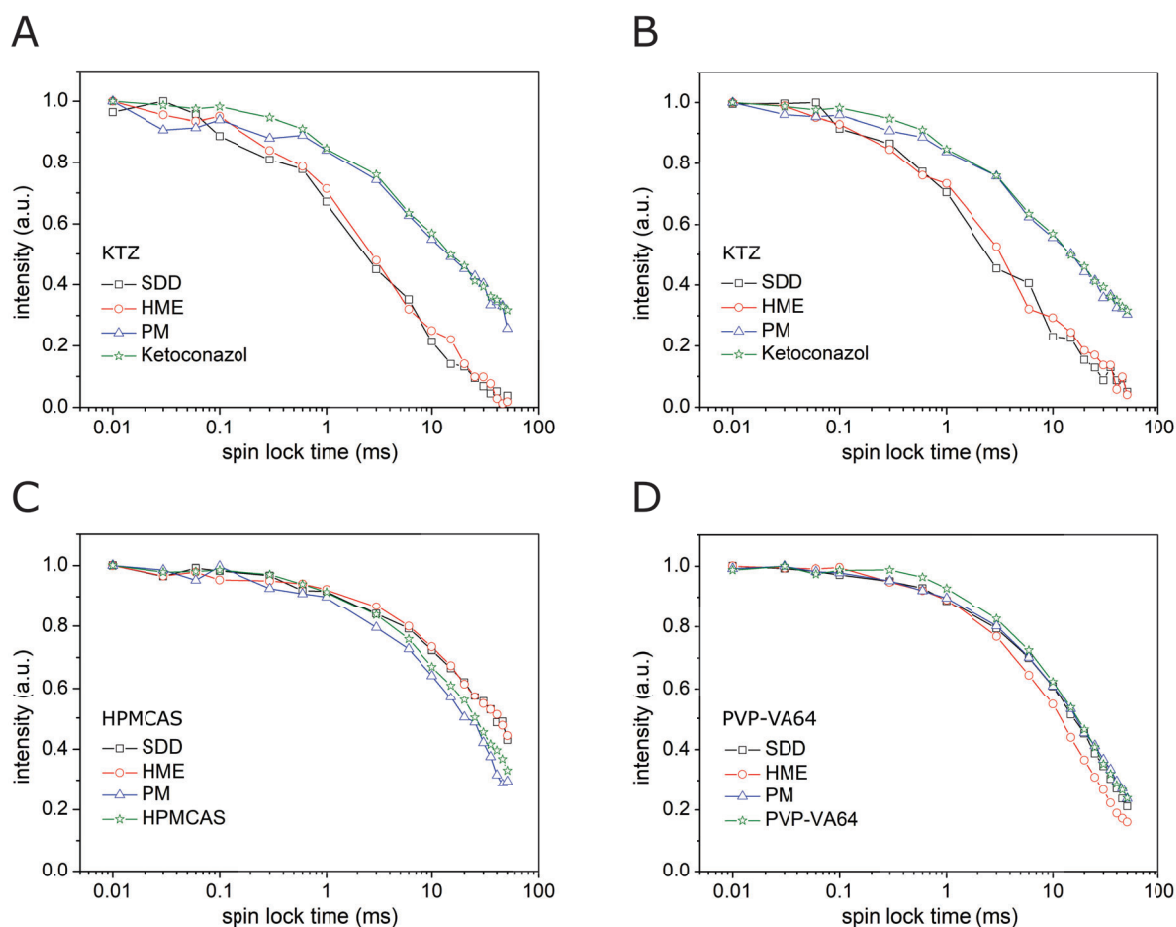


Figure 3.8: $T_{1\rho}$ decay curves from ^{13}C ss-NMR spin-lattice relaxation time measurements of references and formulations. A) Ketoconazole (peak a/b) alone and 40% DL in HPMCAS formulations B) Ketoconazole (peak a/b) alone and 40% DL in PVP-VA64 formulations C) HPMCAS matrix (peak c) D) PVP-VA64 matrix (peak d). From [78]

The spectra of crystalline KTZ were clearly different from its amorphous form within the ASD formulation (HME and SDD, data shown in [78]). However, there were no distinct peak shifts observed that could have been related to interactions. This was somehow expected as signals in ss-NMR are very broad compared to solution NMR. Nevertheless, they provide the possibility to examine interactions in the undissolved state.

Therefore, additional spin-lattice relaxation time ($T_{1\rho}$) measurements were performed. Figure 3.7 shows the peak assignment for neat KTZ, HPMCAS and PVP-VA64. The corresponding relaxation times of these distinct peaks are depicted in Figure 3.8. The decay curves showed a strong effect in relaxation times of KTZ due to amorphization of the API (Figure 3.8 A and B). This was observed to a similar extent in both systems with either HPMCAS (A) or PVP-VA64 (B). Here, the conversion from crystalline to amorphous was expected to dominate the relaxation behavior compared to drug-polymer interactions.

As the polymers did not undergo a change in solid state, it was investigated if their relaxation times change due to generation of drug-polymer interactions.

This was indeed found for the amorphous HPMCAS formulations (Figure 3.8 C) which correlated to high and stable supersaturation profiles and physical stability up to one year at 25 °C and 60% r.h. In total, three HPMCAS peaks were tested and gave reproducible results (see [78]).

In contrast, the PVP-VA64 relaxation times were not influenced but overlaid in their decays of the reference neat polymer curve, PM and SDD. The HME sample even showed faster relaxation. One possible explanation would have been a higher water content causing plasticization and therefore faster relaxation. However, this was not the case as confirmed in TGA trials and gave rise to the question what could be the discriminating factor between the HME and SDD samples which remained unexplained by the analytical techniques used at this stage of work.

Both screening studies (solvent/melt and FluViSc) revealed extraordinary results for PVP-VA64. The solvent screening gave false negative results for PVP-VA64 which could be mitigated by the development of the new melt screening method. In addition, there was a different relaxation behavior observed for distinct PVP-VA64 peaks after processing by HME which was not seen for SDD samples.

This confirmed the hypothesis regarding formation of different stabilizing mechanisms depending on the manufacturing technique. Hence, there was a clear rationale for closer evaluating the physicochemical properties of PVP-VA64 in correlation with the HME process and in comparison to SD.

PVP-VA64 has a high degradation temperature as declared by the manufacturers (230 °C) which enables a broad HME processing window between T_g and T_{deg} . Within this range, the polymer is claimed to be thermally stable. However, it has to be considered that exact temperatures of the melt within a HME process with mechanical energy contributions are difficult to access.

To detect minute differences caused by the manufacturing process, a GPC method was developed with a refractive index (RI) and multi-angle light scattering (MALS) detector coupling. It allowed for highly sensitive absolute molar mass measurement with approx. 97% mass recovery. To ensure comparability between different samples and measurements, the elution peak was always divided in three subsections according to Figure 3.9 A. The analysis of molecular weight and PDI was always conducted for peak 2 where appropriate size separation was achieved (Figure 3.9 B).

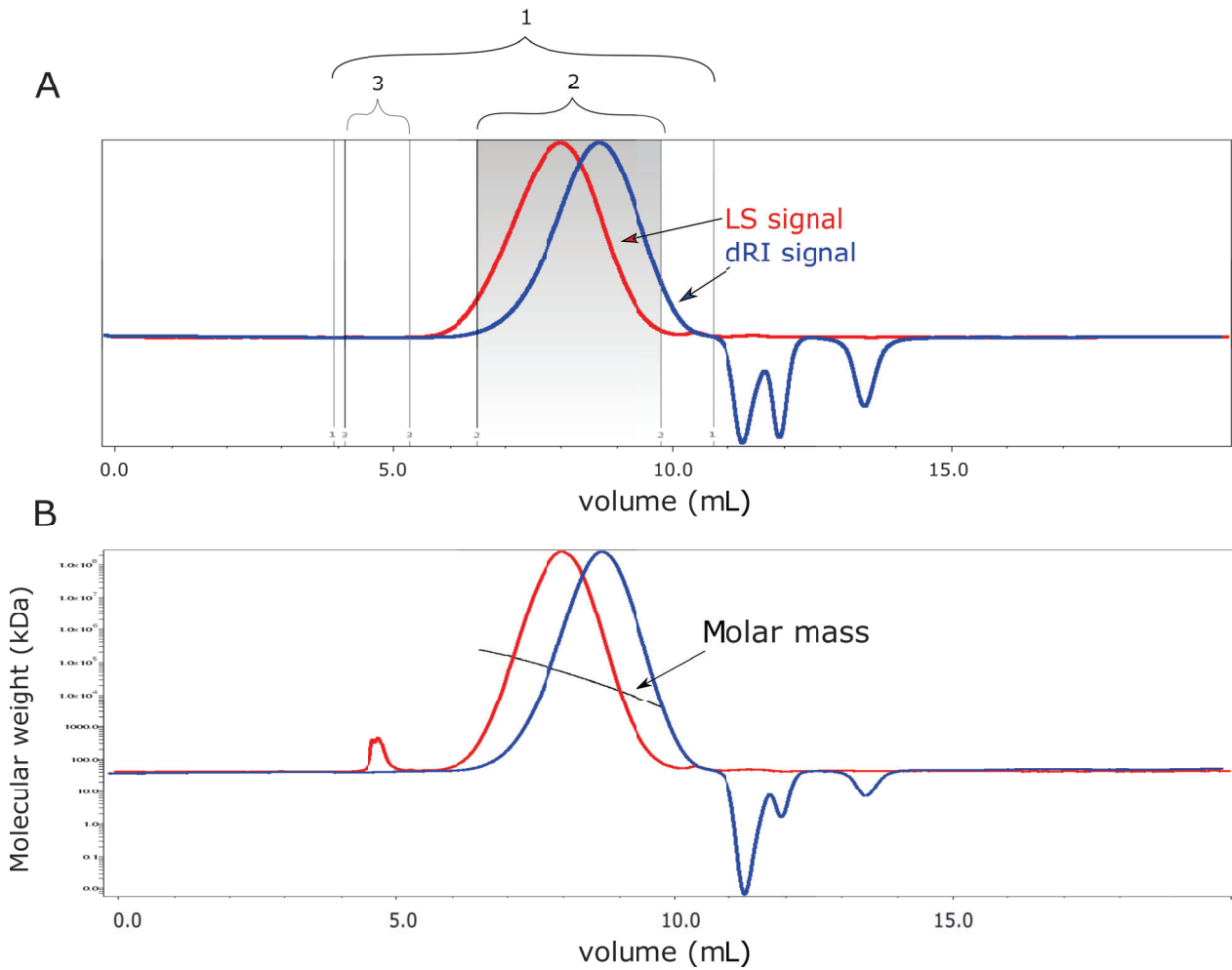


Figure 3.9: A) Chromatogram of PVP-VA64 bulk powder. Light scattering signal (LS) depicted in red, differential refractive index (dRI) depicted in blue. The polymer peak is divided into three sections. 1) Total peak for calculation of mass recovery, 2) polymer main peak with appropriate size separation for calculation of M_w and PDI and 3) high molecular weight peak B) Molar mass plot of peak 2 acquired for thermally stressed PVP-VA64 sample with high molecular weight fraction. Modified from [34]

Neat PVP-VA64 was exposed to different heat and shear stress in a small-scale extruder (co-rotating twin-screw extruder with three heating zones) with process temperatures far below the T_{deg} (130°C, 160°C and 180°C) resulting in the different extrudates Ex 130, Ex 160 and Ex 180. M_w and PDI were measured and compared to unprocessed bulk material (Figure 3.10). The highest decrease in molecular weight was observed for Ex 130 which was the sample with the lowest extrusion temperature applied. As lower temperatures are related to higher melt viscosity, this might result in higher shear stress.

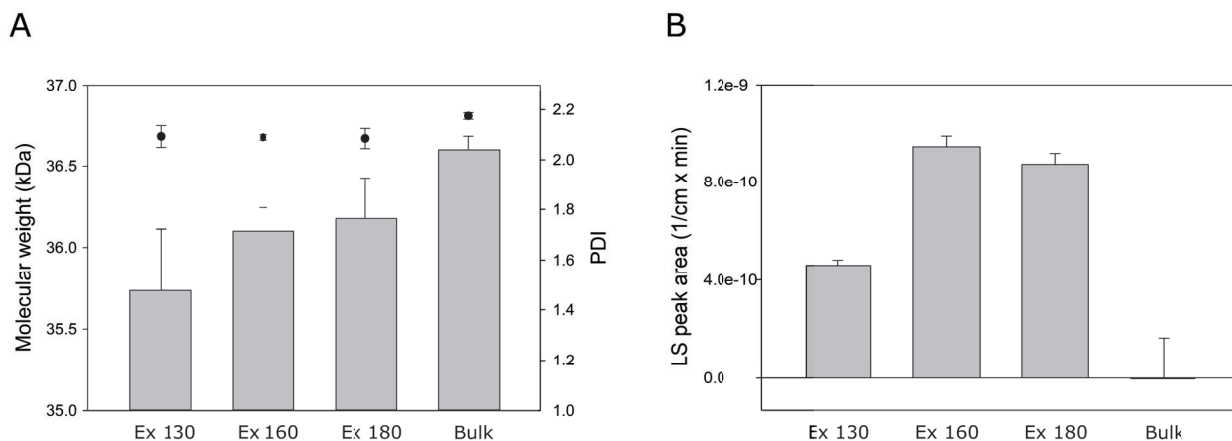


Figure 3.10: *Molecular weight and PDI of unprocessed PVP-VA64 versus stress-samples. A) Bars indicate molecular weight, PDI is depicted as dots of three different process conditions for PVP-VA64 extrudates versus unprocessed PVP-VA64 bulk powder. B) Integrated light scattering intensity of high molecular weight peak (peak 3, definition according to Figure 3.9). Arithmetic means of $n=4 + S.D.$ From [34]*

Hence, it could be shown that the shear stress was the dominant root cause compared to temperature induced changes in M_w and PDI.

To exclude chemical degradation effects, solution NMR spectra were acquired (Figure 3.11). They confirmed the chemical integrity of PVP-VA64. Furthermore, a shift for the peak at 2.1 ppm was detected which points towards conformational changes of the polymer. These are very likely to be induced when changes of M_w occur which influences coiling and dissolution behavior of the polymer.

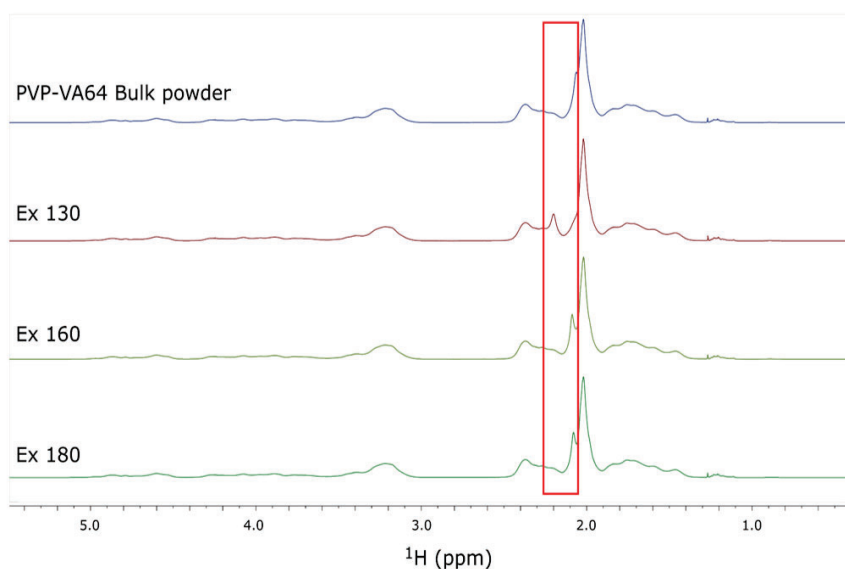


Figure 3.11: *¹H NMR solution spectra of PVP-VA64 bulk powder, Ex 130, Ex 160 and Ex 180. The samples were dissolved in deuterated chloroform containing tetramethylsilane for signal referencing. Modified from [34]*

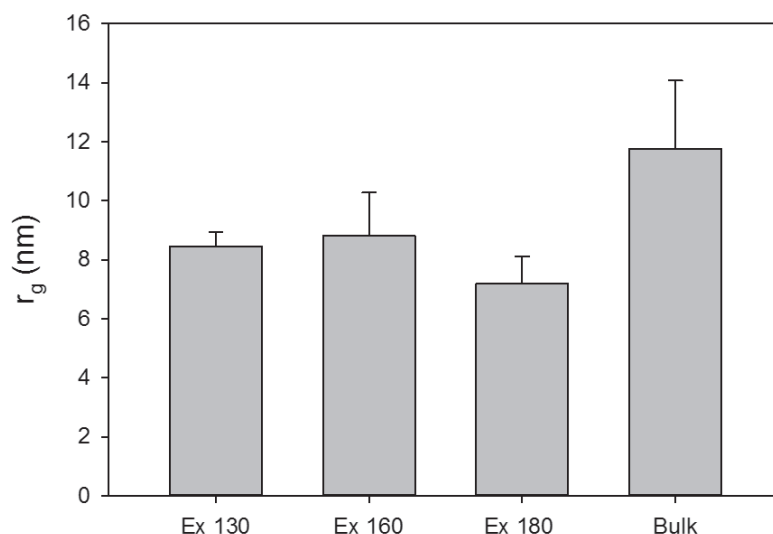


Figure 3.12: Radius of gyration (r_g) of the differently stressed PVP-VA64 extrudates (Ex 130, Ex 160 and Ex 180) versus unprocessed bulk powder. Arithmetic means of $n=4 + S.D.$ Statistical significance was shown with One-Way ANOVA ($p=0.006$). From [34]

The impact on the polymer coiling could additionally be confirmed by comparing the radii of gyration (r_g) acquired by GPC-MALS measurements as depicted in Figure 3.12. Although the limit of quantification of the MALS detector for (r_g) is around 10 nm, the trend between unprocessed bulk material and heat stressed extrudates towards smaller radii could be clearly seen.

The stressed polymeric extrudates were subsequently used for preparation of ASD with 40% KTZ via SD. In contrast to HME, SD did not alter the physicochemical properties of PVP-VA64 (neither M_w , PDI nor high molecular weight fraction) and was therefore considered suitable for subsequent incorporation of the API (data shown in [34]). This was conducted in exactly the same way for the stressed samples as well as for unprocessed bulk powder. The changes that were detected in supersaturation and precipitation of KTZ in a non-sink dissolution (Figure 3.13) could therefore unambiguously be correlated to polymer characteristics that were induced by the HME process.

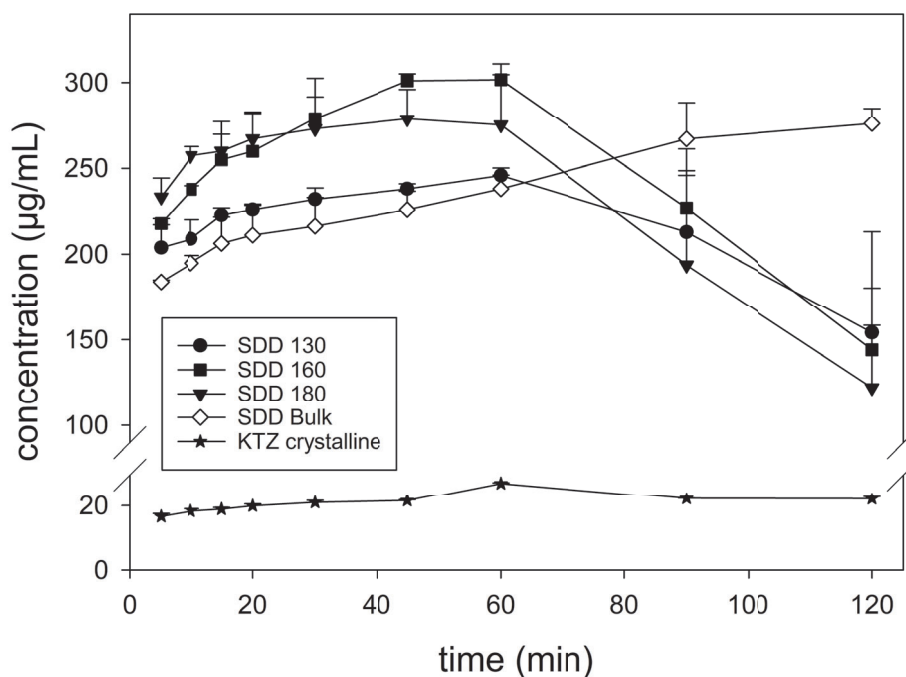


Figure 3.13: Concentration of KTZ dissolved in non-sink dissolution setup of SDD produced with PVP-VA64 and 40% drug load. SDD 130/160/180 were prepared with thermally stressed PVP-VA64 (Ex 130/160/180). SDD Bulk contains PVP-VA64 bulk powder. Comparison versus crystalline KTZ. Dissolution was conducted in FaSSiF-V1 at pH 6.5. Arithmetic means of $n=3 + S.D.$ Modified from [34]

The dissolution data of the ASD prepared with differently stressed or unstressed PVP-VA64 confirmed the relevance of these findings resulting in different performances of the ASD. The precipitation inhibition was much better for unstressed PVP-VA64 whereas the stressed polymer partly induced stronger supersaturation. This might in turn explain the different behavior of SDD and HME samples in the first part of this thesis (Figure 3.3). In both cases, supersaturation from SDD samples was lower compared to HME whereas a better stabilization was achieved.

Additionally, these results did underline the findings from the relaxation time measurements (Figure 3.8 D) where a different behavior for the HME of PVP-VA64 was observed compared to the SDD. As a different coiling of the polymer chains of course may impair the interaction sites available for the drug, this might well explain the different relaxation times.

The results of PVP-VA64 could not only be seen for other polymers (E PO and Soluplus) on a small-scale extruder but could furthermore be transferred to manufacturing scale [34]. Thus, the high relevance for ASD in general was shown as well as the importance of these insights for the translation from preclinical development towards manufacturing.

The last part of this work addressed the biorelevant dissolution testing of ASD as one of the most decisive *in vitro* assays to guide formulation selection. As it was pointed out before, the amorphous formulations of weakly basic KTZ should be evaluated in a two-compartmental transfer model and compared to potential supersaturation of crystalline KTZ which can be physiologically induced during the gastrointestinal transit.

As HPMCAS is known as one of the best precipitation inhibitors and showed specific interactions with KTZ (Figure 3.8), it was selected for closer evaluation. Therefore, not only the previously used grade HPMCAS HF but also HPMCAS LF (with slightly different pKa due to different contents of acetyl and succinyl groups) was deployed. As such, potentially different drug-polymer interactions were also in scope again.

Both SDD formulations with HPMCAS HF and LF (40% DL each) were evaluated in a non-sink dissolution testing in FaSSIF pH 6.5 as well as in the gastrointestinal transfer model by Jede et al. [82].

Figure 3.14 A depicts the non-sink dissolution behavior in FaSSIF where a strong precipitation was detected for the system with HPMCAS LF. In contrast, HPMCAS HF stabilized the supersaturation without recrystallization of the drug over two hours. The dissolution curves of the transfer model are shown in Figure 3.14 B.

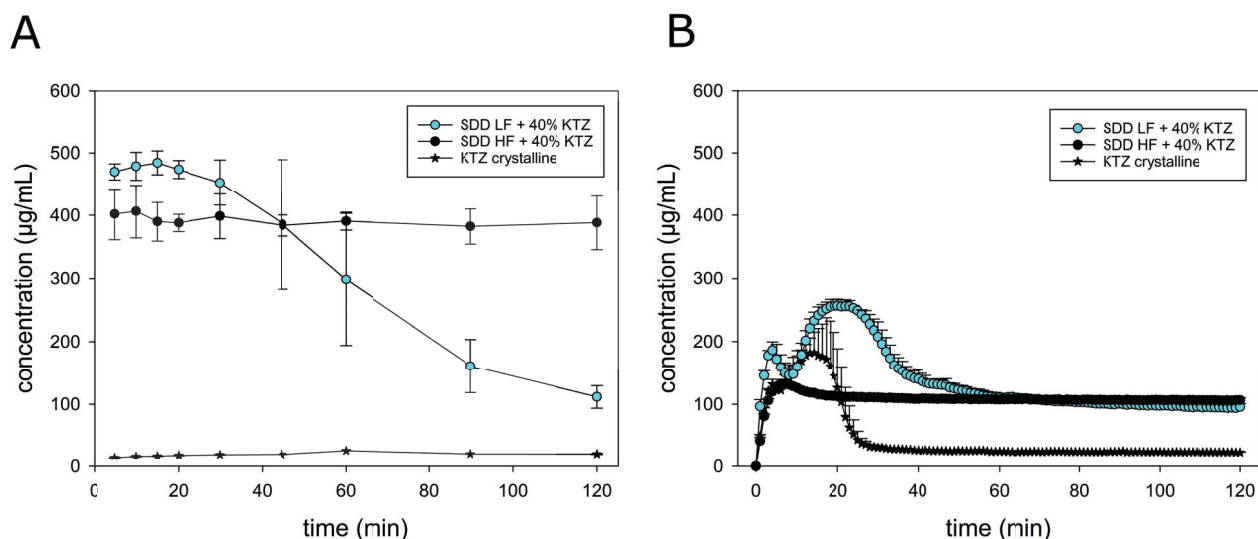


Figure 3.14: A) Non-sink dissolution testing of SDD HPMCAS LF versus SDD HPMCAS HF with 40% DL each in FaSSIF-V1. Arithmetic means of $n=3 \pm S.D.$ B) Transfer model of SDD with HPMCAS LF compared to SDD HPMCAS HF with 40% DL each. Transfer was conducted from SGF pH 2 into double-concentrated FaSSIF-V1 pH 6.5. Arithmetic means of $n=3 + S.D.$

As the predominant interaction forces are usually ionic in nature, which was confirmed by the FluViSc results (Figure 3.6), it was hypothesized that the more acidic HPMCAS LF grade might better stabilize supersaturation of the basic KTZ. However, the non-sink dissolution experiments showed that this was not the case at least for the difference between HPMCAS LF and HF. Instead, a hydrophobic interaction effect was assumed which was supported by data on drug-polymer colloids and aggregation behavior by Wang et al. [83]. These stabilizing mechanisms were found to be pH-dependent (correlating to the pH-dependent solubility of the polymer).

In a next step, the SDD were compared to physical mixtures containing the crystalline API and the precipitation inhibitor in the GI transfer model. Surprisingly, the amorphous formulations did not outperform the simple physical mixtures with HPMCAS as precipitation inhibitor (Figure 3.15) in contrast to non-sink dissolution trials where no supersaturation of crystalline KTZ in presence of precipitation inhibitors was observed [77].

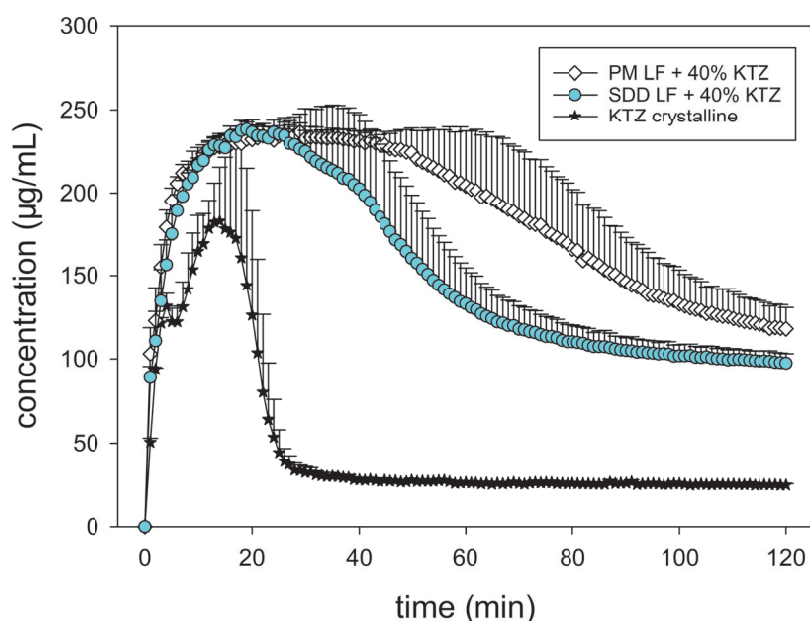


Figure 3.15: *Transfer model for SDD and PM of HPMCAS LF with 40% KTZ. Transfer was conducted from SGF pH 2 into double-concentrated FaSSIF-V1 pH 6.5. Arithmetic means of $n=3 + S.D.$*

Hence, the solubilities of SDD and crystalline KTZ in SGF were examined. Its solubility at pH 2 above 2 mg/mL led to fully dissolved API even in its crystalline form. Thus, a comparable effect in the transfer model could be expected retrospectively although the higher AUC of the PM remained unexplained.

The gastrointestinal transfer model was additionally applied to model variability of gastric pH which frequently occurs in human individuals. Dressman et al. [84] have shown a decreasing effect of co-administered cimetidine on plasma concentrations of crystalline ketoconazole. pH 4 was chosen as hypochlorhydric gastric pH which might be caused by intake of proton pump inhibitors, decreased secretion of gastric acid or food intake [82, 85]. Again, the performance of amorphous formulations was compared to PM. A clear benefit could be detected for the SDD with HPMCAS LF (Figure 3.16).

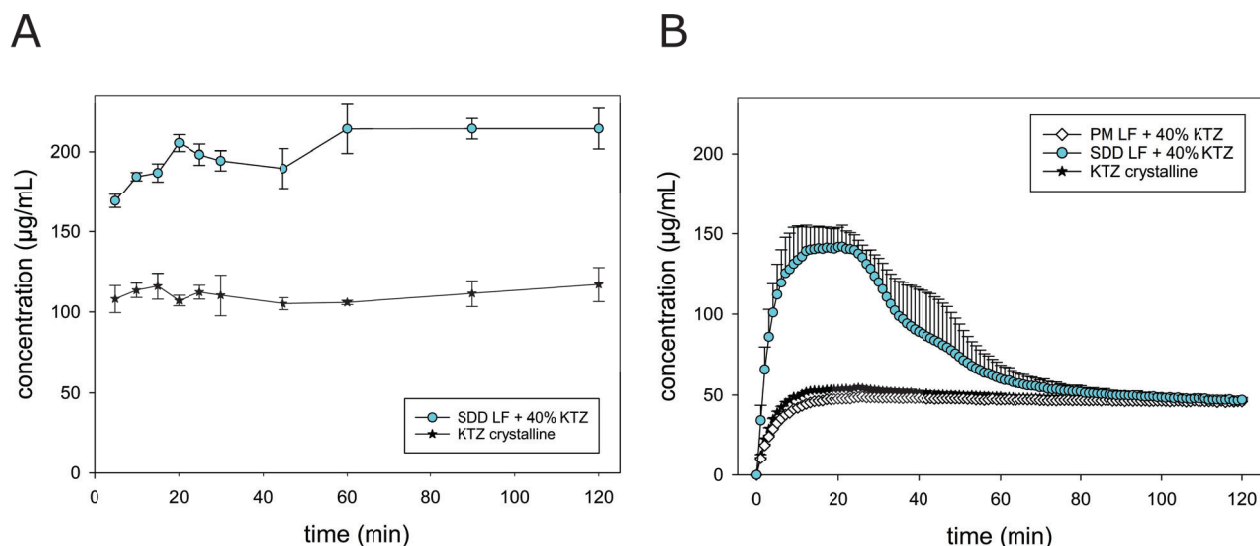


Figure 3.16: A) Non-sink dissolution testing of SDD HPMCAS LF versus crystalline KTZ in SGF pH 4. Arithmetic means of $n=3 \pm S.D.$ B) Transfer model of PM with HPMCAS LF compared to SDD HPMCAS LF with 40% DL each. Transfer was conducted from SGF pH 4 into double-concentrated FaSSIF-V1 pH 6.5. Arithmetic means of $n=3 \pm S.D.$

The amorphous solubility at pH 4 was much higher than the one of crystalline API which was also translated into higher supersaturation in the transfer model. This in turn ensures higher concentrations of drug dissolved in the small intestine under variable GI conditions or acid-reducing co-medications. This pharmacokinetic variability also has to be considered in terms of food effect which was found to be less marked in case of the ASD of ritonavir/lopinavir [86].

To further pursue the hypothesis of drug-polymer interactions being responsible for supersaturation and inhibition of precipitation, a ternary ASD with the basic polymer Eudragit E PO in a 3:1 weight ratio (m/m%) HPMCAS:E PO was developed. The formulation containing 40% KTZ was produced via SD resulting in a fully amorphous ASD with single T_g while also fulfilling all other specifications set up beforehand. The results of the corresponding transfer experiments are depicted in Figure 3.17.

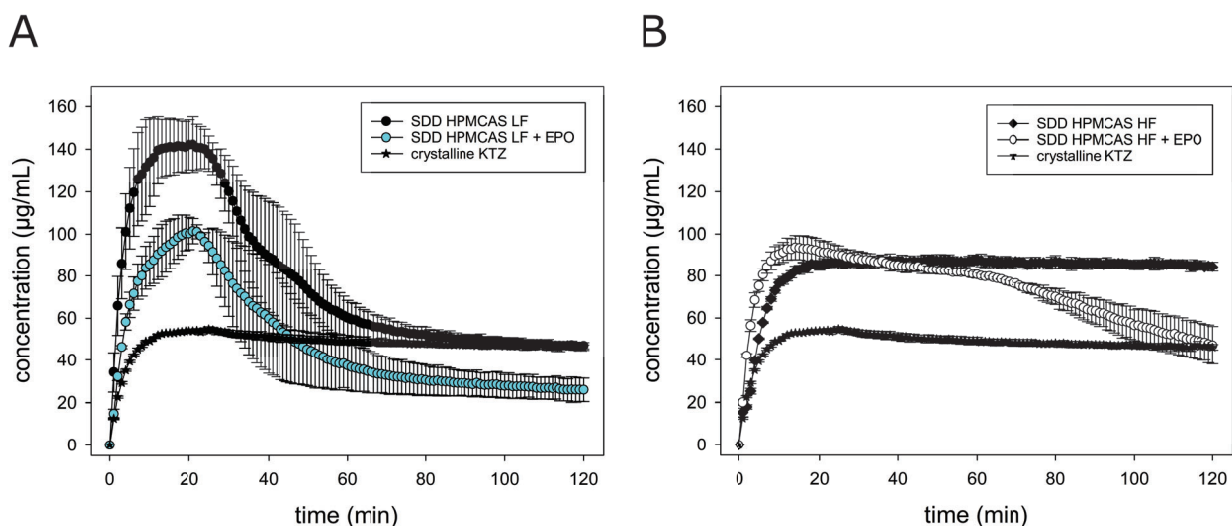


Figure 3.17: *Transfer model of ternary ASD formulations with A) HPMCAS LF + E PO versus B) HPMCAS HF + E PO with 40% DL each. Transfer was conducted from SGF pH 4 into double-concentrated FaSSIF-V1 pH 6.5. Arithmetic means of $n=3 + S.D.$*

Part A shows the combination of HPMCAS LF and E PO whereas HPMCAS HF is covered in part B. In both cases, the replacement of 25% HPMCAS by E PO decreased the AUC compared to HPMCAS alone. For HPMCAS LF, the absolute concentration of drug dissolved was lowered as well as the plateau that was reached after 120 min and hence also the AUC. As HPMCAS LF is the more acidic derivative, it is likely to form stronger interactions with E PO thus showing more impact in the overall performance. For HPMCAS HF, the overall supersaturation was almost constant with only a slight decrease in precipitation inhibition supporting the hypothesis of stabilizing hydrophobic interactions and drug-polymer aggregates rather than ionic forces.

The experiments with this multicomponent ASD again underlined the complexity of creating stable ASD and optimizing the formulation. In contrast to HPMCAS, E PO is soluble at gastric pH which was assumed to support in stabilization of initial supersaturation after the transfer. However, this was not seen, quite the contrary, the basic E PO probably blocked possible interaction sites of KTZ leading to reduced stabilization of supersaturation. Thus, ternary ASD - not only with polymer-polymer but also polymer-surfactant combinations - should be carefully evaluated as they may have both favorable or adverse effects on the primary formulation.

4 Summary and outlook

4.1 Summary

The development of pharmaceutical products requires thorough characterization of both API and drug product to guarantee the pharmaceutical principles of efficacy and safety and to provide the highest possible quality for the patient. Amorphous solid dispersions are a valuable option to improve the bioavailability of poorly soluble drugs. Aim of this thesis was to provide understanding and tools to improve the transition from preclinical research to successful formulation development. Therefore, the focus was set on physicochemical and *in vitro* characterization of ASD. Emphasis was put on getting information from miniaturized or small-scale methods during preclinical research with high predictability and reliability for later development stages.

This was covered by the preparation, characterization and *in vitro* evaluation of various formulations of the model compound ketoconazole. Additionally, the applicability for industrial pipeline compounds was shown in case of the melt screening. All formulations were analyzed as drug product intermediates rather than final oral dosage forms.

The goal was to address the unmet needs connected with predictability of screening methods and biorelevant dissolution testing for ASD with polymeric carriers. Especially with regard to the matrix excipient, profound physicochemical characterizations were conducted which was so far mostly neglected in the field of ASD.

The high complexity of amorphous formulations still poses many challenges to the formulation scientist. Therefore, a structured development approach is needed which is built of five main steps with different experimental effort which is depicted in Figure 4.1. This workflow was pursued and refined in the course of this work.

At first, focus was set on miniaturized screening methods that are of vital importance in preclinical research and development. As the optimal carrier is individually dependent on each API, these methods need to be optimized regarding high throughput, broad applicability, easy handling and robustness. Two new miniaturized screening methods for polymer selection of ASD were developed within this thesis as there were several gaps identified. The melt-based screening method provided the advantage of avoiding false negative results compared to the benchmark solvent screening at least for PVP based polymeric carriers. As differences in the preparation methods for ASD were detected, it was examined if these can be addressed by miniaturized screening methods. Indeed, a correlation between the screening technique and the manufacturing method was detected which helps a lot in reducing API consumption for testing different manufacturing processes as well as giving potential hints regarding degradation.

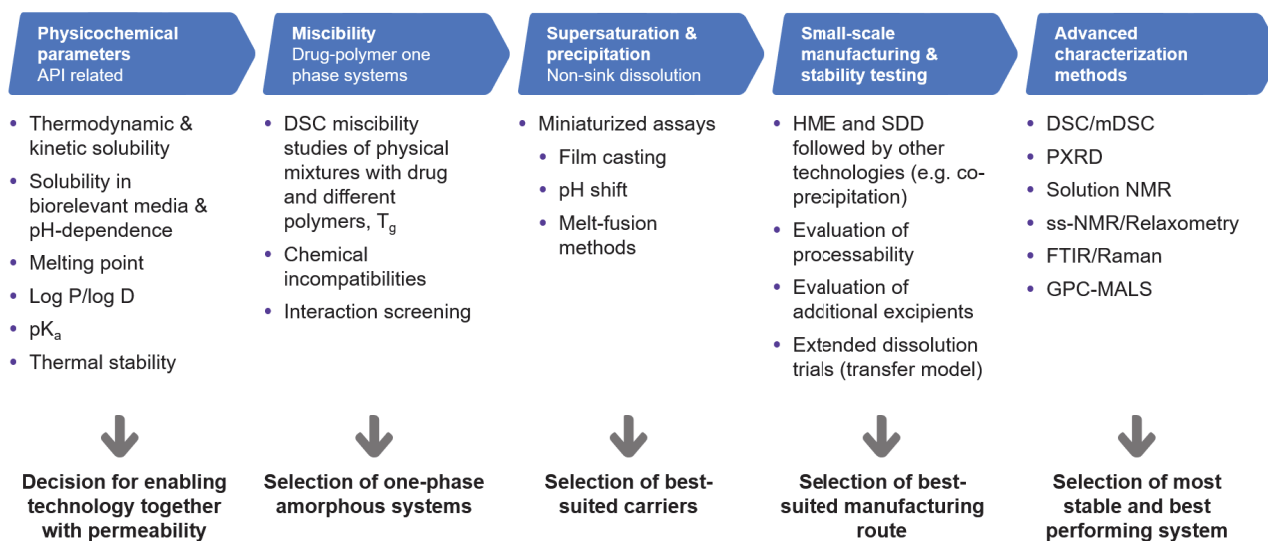


Figure 4.1: *Systematic formulation development of ASD*

The second tool, the FluViSc, can be considered as a meaningful extension of existing screening tools to detect drug-polymer interactions. A ranking among the different polymeric carriers could be set up based on viscosity increase of KTZ-polymer solutions. So far, there were only few methods known like FTIR or Raman spectroscopy to analyze interactions. HME and SD formulations of KTZ-HPMCAS and KTZ-PVP-VA64 were manufactured to give a proof of concept for the new approach. Differences in the relaxation times between the different carriers could be detected in the ss-NMR experiments. Additionally, there was a hint towards drug-polymer interactions depending on the preparation method at least for PVP-VA64. This underlined the importance of closer evaluating the properties of this polymeric carrier.

Therefore, the second aim of this thesis was addressed with the development of a physicochemical characterization method to describe changes in molecular weight and polydispersity index of the polymeric carrier that might occur due to heat and shear stress upon hot-melt extrusion. GPC methods with RI and MALS detector coupling were developed for the polymeric carriers used within this thesis. An impact of hot-melt extrusion on M_w and PDI was found for all of the three polymers tested (Eudragit E PO, Soluplus and PVP-VA64) although they were all claimed thermally stable up to far above the temperatures tested in the extrusion process.

To examine the implication of such changes on the performance of the ASD, focus was set on PVP-VA64. PVP-VA64 was outstanding in many experiments beforehand: false negative results in the miniaturized solvent based screening, differences between SDD and HME regarding non-sink dissolution and differences in the relaxation times depending on the manufacturing technique. Therefore, the GPC-MALS-RI method was applied on PVP-VA64 extrudates and the impact of slight changes in M_w and PDI that were detected upon the dissolution performance of ASD was closely examined.

This was completely new to the field and added various important benefits like (i) optimization of the HME process with regards of the polymeric carrier and not only on the API and amorphization (ii) monitoring of critical quality attributes of excipients and not only API and (iii) better understanding which factors influence dissolution performance.

The release from the amorphous formulations was routinely examined in this study by non-sink dissolution testing using the biorelevant FaSSiF medium. However, ketoconazole as a weakly basic compound necessitated further examination on suitable dissolution methods as supersaturation can not only be induced by amorphization but also by the pH shift during gastrointestinal transfer from the stomach to the small intestine. A physical mixture of KTZ and precipitation inhibitor HPMCAS was compared to the amorphous SDD of KTZ and HPMCAS. The AUC were comparable at gastric pH of 2, however there were pronounced differences for elevated gastric pH. One more time, the study also took into account drug-polymer interactions and different HPMCAS grades were compared in terms of the precipitation inhibition potential. With the addition of Eudragit E PO as a basic polymer, potential ionic interaction sites of HPMCAS with KTZ should be blocked which indeed led to the expected decrease of the AUC.

To conclude, important new insights were gained and several gaps discussed beforehand could be closed. The predictability of screening tools to select suitable carriers was examined and could be improved to avoid false negative results. These early restrictions in the selection of the best suited polymeric carrier would otherwise be a huge drawback for formulation development. This was shown for KTZ as well as for the Merck pipeline compound MC1. By applying two different ways of screening and two different manufacturing techniques, a correlation between them could be partly detected which might help in saving time and material in the assessment of the best process. The utilization of the FluViSc was shown to be a valuable additional option in the detection of drug-polymer interactions that are essential in the stabilization and generation of supersaturation while it was hardly possible to address them at such an early development stage beforehand. With the thorough physicochemical characterization of the polymeric carrier and separation of its properties from the amorphization itself, it was accounted for its functional contribution to the ASD system. Last but not least, an important comparison between physiologically induced supersaturation and amorphous supersaturation was sought which should never be neglected for weakly basic compounds.

The different aspects of this work provided mechanistic insights and are suited to optimize the formulation development of ASD in terms of selecting the best suited polymeric carrier that improves the apparent solubility, provides high physical stability against recrystallization upon storage and maintains this supersaturated state during a timeframe relevant for physiological absorption.

4.2 Future perspectives

The following section will discuss future perspectives in the context of this work based on the promising results that were acquired within this thesis. Three approaches are being described which could serve as a basis for further research.

The thermodynamic solubility of the API within the polymeric carrier is an important aspect for the physical stability of ASD. If the thermodynamic solubility is not exceeded and full miscibility is given, recrystallization or phase separation will not occur [87]. Hence, this is a possibility to find the maximum drug load without a risk for physical instabilities. There are many methods described in literature to approximate this solubility limit. In many cases, solubility parameters (Hansen or Hildebrand solubility parameter) or Flory-Huggins models [80] are used but they often fail in prediction of physical stability [88]. A completely different approach is pursued by DSC experiments where the solubility limit is determined via the melting point depression or recrystallization method [47]. Both approaches are somehow limited by the prerequisite of defined melting and recrystallization behavior and thermal stability.

One of the currently emerging methods is the modeling of thermodynamic phase diagrams for ASD via perturbed-chain statistical associated fluid theory (PC-SAFT) [89]. Effects of temperature and humidity are already taken into account [90, 91]. Reliable estimations on the solubility of the drug within the polymer would spare long-term stability studies and help addressing the gap regarding predictions of physical stability pointed out in Chapter 1.2.3.

In the context of this thesis, the drug load was kept constant to get normalized dissolution results with the same amounts of API and polymeric carrier and utmost comparability of the supersaturation and precipitation behavior. However, it would also be of interest to put the findings of this work e.g. on supersaturation and precipitation in context of the solubility limit of the API in each carrier. These interdependencies were not examined with this thermodynamic model so far to the best knowledge of the author and the combination of simulations and screening methods would add significant contributions to polymer design.

The molecular arrangement of API and polymer is of importance for the functional principle of ASD. API-rich or polymer-rich phases might be present which do not necessarily result in recrystallization but they increase the risk thereof e.g. when exceeding the solubility limit of the drug within the polymer as explained in the previous paragraph. Methods like SAXS can be used to detect short range orders of crystalline contents. The existence of such clusters might be dependent on the manufacturing process [32] and could be monitored by SAXS-DSC coupling for the melt screening described in this work to further elucidate on differences in the preparation technique.

The application of the GPC-MALS method showed the importance of better understanding the polymeric carrier. This highly sensitive analytical method allows advanced characterization in terms of polymer coiling in liquids and effects of different molecular weights on the dissolution performance. These insights could be used in the context of the studies by Frank et al. [33, 92] who modified polymers in their side chains functionalities to improve interactions with the drug and polymer solubility - in this case deconvoluted from the polymer chain length. Though it is known that also the polymer's molecular weight and the correlation to viscosity and T_g are crucial for successful stabilization of ASD [49].

Regulatory authorities require a declaration on "the ability of excipients to provide their intended functionality, and to perform throughout the intended drug product shelf life..." (ICH Q8 R2) in dossiers for new drug submissions. The importance of polymers for the functional principle of amorphous formulations was demonstrated in detail in the previous chapters. A comprehensive toolbox for the selection of the carrier is already available but what if we lack the right polymers? Excipient manufacturers are willing to develop a customized polymer for an API in ASD to conduct joint toxicological studies and get access to the market as regulatory authorities demand descriptions of manufacture, characterization and controls, as well as supporting safety data for novel excipients [93]. If there were more methods established to design and analyze these new excipients, the hurdle for the pharmaceutical industry to file their products with new excipients would be lowered with the perspective of increasing the amount of successfully marketed ASD.

The combination of GPC analysis, structural insights on phase separation and modelling of thermodynamic solubilities applied on new polymers would further help in designing the optimal excipient candidate - maybe even customized for each new chemical entity. Thus, the proposals for further research given beforehand would not only mean an additional scientific progress but again improve the translation from research contributions to formulation development and commercialization.

Bibliography

- [1] Gordon L Amidon, Hans Lennernäs, Vinod P Shah, and John R Crison. A theoretical basis for a biopharmaceutic drug classification: the correlation of in vitro drug product dissolution and in vivo bioavailability. *Pharmaceutical Research*, 12(3):413–420, 1995.
- [2] *Waiver of In Vivo Bioavailability and Bioequivalence Studies for Immediate-Release Solid Oral Dosage Forms Based on a Biopharmaceutics Classification System. Guidance for Industry*. U.S. Food and Drug Administration, Center for Drug Evaluation and Research, 2017.
- [3] Arik Dahan and Jonathan M Miller. The solubility–permeability interplay and its implications in formulation design and development for poorly soluble drugs. *The AAPS Journal*, 14(2):244–251, 2012.
- [4] Rebecca L Carrier, Lee A Miller, and Imran Ahmed. The utility of cyclodextrins for enhancing oral bioavailability. *Journal of Controlled Release*, 123(2):78–99, 2007.
- [5] James M Butler and Jennifer B Dressman. The developability classification system: application of biopharmaceutics concepts to formulation development. *Journal of Pharmaceutical Sciences*, 99(12):4940–4954, 2010.
- [6] M Sherry Ku. Use of the biopharmaceutical classification system in early drug development. *The AAPS Journal*, 10(1):208–212, 2008.
- [7] Julian Rosenberger, James Butler, and Jennifer Dressman. A refined developability classification system. *Journal of Pharmaceutical Sciences*, 107(8):2020–2032, 2018.
- [8] Robert O Williams III, Alan B Watts, and Dave A Miller. *Formulating poorly water soluble drugs*. Springer, 2012.
- [9] Leslie Z Benet, Chi-Yuan Wu, and Joseph M Custodio. Predicting drug absorption and the effects of food on oral bioavailability. *Bulletin Technique Gattefosse*, 99:9–16, 2006.
- [10] Stephen Timothy Buckley, Kerstin Julia Frank, Gert Fricker, and Martin Brandl. Biopharmaceutical classification of poorly soluble drugs with respect to “enabling formulations”. *European Journal of Pharmaceutical Sciences*, 50(1):8–16, 2013.
- [11] Jeffrey M Ting, William W Porter III, Jodi M Mecca, Frank S Bates, and Theresa M Reineke. Advances in polymer design for enhancing oral drug solubility and delivery. *Bioconjugate Chemistry*, 29(4):939–952, 2018.

- [12] Aurijit Sarkar and Glen E Kellogg. Hydrophobicity-shake flasks, protein folding and drug discovery. *Current Topics in Medicinal Chemistry*, 10(1):67–83, 2010.
- [13] Kinam Park. Controlled drug delivery systems: past forward and future back. *Journal of Controlled Release*, 190:3–8, 2014.
- [14] Jing Jin, Grant Edward Sklar, Vernon Min Sen Oh, and Shu Chuen Li. Factors affecting therapeutic compliance: A review from the patient's perspective. *Therapeutics and Clinical Risk Management*, 4(1):269, 2008.
- [15] Geoff GZ Zhang, Devalina Law, Eric A Schmitt, and Yihong Qiu. Phase transformation considerations during process development and manufacture of solid oral dosage forms. *Advanced Drug Delivery Reviews*, 56(3):371–390, 2004.
- [16] Srikonda Venkateswara Sastry, Janaki Ram Nyshadham, and Joseph A Fix. Recent technological advances in oral drug delivery—a review. *Pharmaceutical Science & Technology Today*, 3(4):138–145, 2000.
- [17] Christian Leuner and Jennifer Dressman. Improving drug solubility for oral delivery using solid dispersions. *European Journal of Pharmaceutics and Biopharmaceutics*, 50(1):47–60, 2000.
- [18] Win Loung Chiou and Sidney Riegelman. Pharmaceutical applications of solid dispersion systems. *Journal of Pharmaceutical Sciences*, 60(9):1281–1302, 1971.
- [19] Igor Ivanisevic. Physical stability studies of miscible amorphous solid dispersions. *Journal of Pharmaceutical Sciences*, 99(9):4005–4012, 2010.
- [20] Amjad Alhalaweh, Ahmad Alzghoul, Denny Mahlin, and Christel AS Bergström. Physical stability of drugs after storage above and below the glass transition temperature: Relationship to glass-forming ability. *International Journal of Pharmaceutics*, 495(1):312–317, 2015.
- [21] Beth A Miller-Chou and Jack L Koenig. A review of polymer dissolution. *Progress in Polymer Science*, 28(8):1223–1270, 2003.
- [22] Na Li and Lynne S Taylor. Tailoring supersaturation from amorphous solid dispersions. *Journal of Controlled Release*, 279:114–125, 2018.
- [23] Minoru Yoshioka, Bruno C Hancock, and George Zografi. Crystallization of indomethacin from the amorphous state below and above its glass transition temperature. *Journal of Pharmaceutical Sciences*, 83(12):1700–1705, 1994.
- [24] P Karmwar, Johan Peter Bøtker, KA Graeser, CJ Strachan, Jukka Rantanen, and T Rades. Investigations on the effect of different cooling rates on the stability of amorphous indomethacin. *European Journal of Pharmaceutical Sciences*, 44(3):341–350, 2011.

- [25] Jared A Baird, Bernard Van Eerdenbrugh, and Lynne S Taylor. A classification system to assess the crystallization tendency of organic molecules from undercooled melts. *Journal of Pharmaceutical Sciences*, 99(9):3787–3806, 2010.
- [26] Nicole Wyttenbach and Martin Kuentz. Glass-forming ability of compounds in marketed amorphous drug products. *European Journal of Pharmaceutics and Biopharmaceutics*, 112:204–208, 2017.
- [27] Siyuan Huang, Chen Mao, Robert O Williams III, and Chia-Yi Yang. Solubility advantage (and disadvantage) of pharmaceutical amorphous solid dispersions. *Journal of Pharmaceutical Sciences*, 105(12):3549–3561, 2016.
- [28] Riikka Laitinen, Petra A Priemel, Sachin Surwase, Kirsten Graeser, Clare J Strachan, Holger Grohgan, and Thomas Rades. Theoretical considerations in developing amorphous solid dispersions. In *Amorphous solid dispersions*, pages 35–90. Springer, 2014.
- [29] Mark Davis, Catherine Potter, Maryam Mohammadpour, Ahmad B Albadarin, and Gavin Walker. Design of spray dried ternary solid dispersions comprising itraconazole, soluplus and HPMCP: Effect of constituent compositions. *International Journal of Pharmaceutics*, 519(1-2):365–372, 2017.
- [30] Christian Luebbert, Fabian Huxoll, and Gabriele Sadowski. Amorphous-amorphous phase separation in API/polymer formulations. *Molecules*, 22(2):296, 2017.
- [31] Shrawan Baghel, Helen Cathcart, and Niall J O'Reilly. Polymeric amorphous solid dispersions: a review of amorphization, crystallization, stabilization, solid-state characterization, and aqueous solubilization of biopharmaceutical classification system class II drugs. *Journal of Pharmaceutical Sciences*, 105(9):2527–2544, 2016.
- [32] Lasse Ingerslev Blaabjerg, Eleanor Lindenberg, Korbinian Löbmann, Holger Grohgan, and Thomas Rades. Is there a correlation between the glass forming ability of a drug and its supersaturation propensity? *International Journal of Pharmaceutics*, 538(1-2):243–249, 2018.
- [33] Derek S Frank and Adam J Matzger. Probing the interplay between amorphous solid dispersion stability and polymer functionality. *Molecular Pharmaceutics*, 15(7):2714–2720, 2018.
- [34] Carolin Auch, Meike Harms, and Karsten Mäder. How changes in molecular weight and PDI of a polymer in amorphous solid dispersions impact dissolution performance. *International Journal of Pharmaceutics*, 556:372–382, 2019.
- [35] George Zografi and Ann Newman. Interrelationships between structure and the properties of amorphous solids of pharmaceutical interest. *Journal of Pharmaceutical Sciences*, 106(1):5–27, 2017.

- [36] Jian X Wu, Mingshi Yang, Frans van den Berg, Jari Pajander, Thomas Rades, and Jukka Rantanen. Influence of solvent evaporation rate and formulation factors on solid dispersion physical stability. *European Journal of Pharmaceutical Sciences*, 44(5):610–620, 2011.
- [37] Abu TM Serajuddin. Solid dispersion of poorly water-soluble drugs: Early promises, subsequent problems, and recent breakthroughs. *Journal of Pharmaceutical Sciences*, 88(10):1058–1066, 1999.
- [38] Abhishek Singh, Zelalem Ayenew Worku, and Guy Van den Mooter. Oral formulation strategies to improve solubility of poorly water-soluble drugs. *Expert Opinion on Drug Delivery*, 8(10):1361–1378, 2011.
- [39] Guy Van den Mooter. The use of amorphous solid dispersions: A formulation strategy to overcome poor solubility and dissolution rate. *Drug Discovery Today: Technologies*, 9(2):79–85, 2012.
- [40] Scott V Jermain, Chris Brough, and Robert O Williams III. Amorphous solid dispersions and nanocrystal technologies for poorly water-soluble drug delivery—an update. *International Journal of Pharmaceutics*, 535(1-2):379–392, 2018.
- [41] Navnit Shah, Harpreet Sandhu, Duk Soon Choi, Oskar Kalb, Susanne Page, and Nicole Wyttenbach. *Formulating poorly water soluble drugs*, chapter Structured development approach for amorphous systems. Springer, 2012.
- [42] Esther S Bochmann, Dirk Neumann, Andreas Gryczke, and Karl G Wagner. Micro-scale solubility assessments and prediction models for active pharmaceutical ingredients in polymeric matrices. *European Journal of Pharmaceutics and Biopharmaceutics*, 141:111–120, 2019.
- [43] Po-Chang Chiang, Yingqing Ran, Kang-Jye Chou, Yong Cui, Amy Sambrone, Connie Chan, and Ryan Hart. Evaluation of drug load and polymer by using a 96-well plate vacuum dry system for amorphous solid dispersion drug delivery. *AAPS PharmSciTech*, 13(2):713–722, 2012.
- [44] Nicole Wyttenbach, Christine Janas, Monira Siam, Matthias Eckhard Lauer, Laurence Jacob, Emmanuel Scheubel, and Susanne Page. Miniaturized screening of polymers for amorphous drug stabilization (SPADS): rapid assessment of solid dispersion systems. *European Journal of Pharmaceutics and Biopharmaceutics*, 84(3):583–598, 2013.
- [45] Jan Bevernage, Thomas Forier, Joachim Brouwers, Jan Tack, Peter Annaert, and Patrick Augustijns. Excipient-mediated supersaturation stabilization in human intestinal fluids. *Molecular Pharmaceutics*, 8(2):564–570, 2011.

- [46] Amrit Paudel, Jan Van Humbeeck, and Guy Van den Mooter. Theoretical and experimental investigation on the solid solubility and miscibility of naproxen in poly(vinylpyrrolidone). *Molecular Pharmaceutics*, 7(4):1133–1148, 2010.
- [47] Malte Bille Rask, Matthias Manne Knopp, Niels Erik Olesen, René Holm, and Thomas Rades. Comparison of two DSC-based methods to predict drug-polymer solubility. *International Journal of Pharmaceutics*, 540(1-2):98–105, 2018.
- [48] Esther S Bochmann, Elgin E Üstüner, Andreas Gryczke, and Karl G Wagner. Predicting melt rheology for hot-melt extrusion by means of a simple Tg-measurement. *European Journal of Pharmaceutics and Biopharmaceutics*, 119:47–55, 2017.
- [49] Matthias Manne Knopp, Niels Erik Olesen, Per Holm, Peter Langguth, René Holm, and Thomas Rades. Influence of polymer molecular weight on drug-polymer solubility: a comparison between experimentally determined solubility in PVP and prediction derived from solubility in monomer. *Journal of Pharmaceutical Sciences*, 104(9):2905–2912, 2015.
- [50] Karine Khougaz and Sophie-Dorothee Clas. Crystallization inhibition in solid dispersions of MK-0591 and poly(vinylpyrrolidone) polymers. *Journal of Pharmaceutical Sciences*, 89(10):1325–1334, 2000.
- [51] Navnit Shah, Harpreet Sandhu, Duk Soon Choi, Hitesh Chokshi, and A. Waseem Malick, editors. *Amorphous Solid Dispersions*. Springer New York, 2014.
- [52] Wiebke Saal, Nicole Wyttenbach, Jochem Alsenz, and Martin Kuentz. Interactions of dimethylaminoethyl methacrylate copolymer with non-acidic drugs demonstrated high solubilization in vitro and pronounced sustained release in vivo. *European Journal of Pharmaceutics and Biopharmaceutics*, 125:68–75, 2018.
- [53] Eleanor Turpin, Vincenzo Taresco, Wathiq Al-Hachami, Jonathan Booth, Kevin Treacher, Simone Tomasi, Cameron Alexander, Jonathan Burley, Charles A Loughton, and Martin C Garnett. In silico screening for solid dispersions: the trouble with solubility parameters and χ_{FH} . *Molecular Pharmaceutics*, 15(10):4654–4667, 2018.
- [54] Marja Savolainen, Andrea Heinz, Clare Strachan, Keith C Gordon, Jouko Yliruusi, Thomas Rades, and Niklas Sandler. Screening for differences in the amorphous state of indomethacin using multivariate visualization. *European Journal of Pharmaceutical Sciences*, 30(2):113–123, 2007.
- [55] Joseph W Lubach and Jonathan Hau. Solid-state NMR investigation of drug-exciipient interactions and phase behavior in indomethacin-Eudragit E amorphous solid dispersions. *Pharmaceutical Research*, 35(3):65, 2018.

- [56] James C DiNunzio, Chris Brough, Dave A Miller, Robert O Williams III, and James W McGinity. Applications of KinetiSol® dispersing for the production of plasticizer free amorphous solid dispersions. *European Journal of Pharmaceutical Sciences*, 40(3):179–187, 2010.
- [57] Anjali M Agrawal, Mayur S Dudhedia, Ashwinkumar D Patel, and Michelle S Raikes. Characterization and performance assessment of solid dispersions prepared by hot melt extrusion and spray drying process. *International Journal of Pharmaceutics*, 457(1):71–81, 2013.
- [58] Michal Beneš, Tomáš Pekárek, Josef Beranek, Jaroslav Havlíček, Lukáš Krejčík, Michal Šimek, Marcela Tkadlecová, and Pavel Doležal. Methods for the preparation of amorphous solid dispersions—a comparative study. *Journal of Drug Delivery Science and Technology*, 38:125–134, 2017.
- [59] Sunny P Bhardwaj, Kapildev K Arora, Elizabeth Kwong, Allen Templeton, Sophie-Dorothee Clas, and Raj Suryanarayanan. Mechanism of amorphous itraconazole stabilization in polymer solid dispersions: role of molecular mobility. *Molecular Pharmaceutics*, 11(11):4228–4237, 2014.
- [60] Abbe Haser, Tu Cao, Joe Lubach, Tony Listro, Larry Acquarulo, and Feng Zhang. Melt extrusion vs. spray drying: The effect of processing methods on crystalline content of naproxen-povidone formulations. *European Journal of Pharmaceutical Sciences*, 102:115–125, 2017.
- [61] Rahul Surana, Abira Pyne, and Raj Suryanarayanan. Effect of preparation method on physical properties of amorphous trehalose. *Pharmaceutical Research*, 21(7):1167–1176, 2004.
- [62] Michael M Crowley, Feng Zhang, Michael A Repka, Sridhar Thumma, Sampada B Upadhye, Sunil Kumar Battu, James W McGinity, and Charles Martin. Pharmaceutical applications of hot-melt extrusion: part I. *Drug Development and Industrial Pharmacy*, 33(9):909–926, 2007.
- [63] Michael A Repka, Suresh Bandari, Venkata Raman Kallakunta, Anh Q Vo, Haley McFall, Manjeet B Pimparade, and Ajinkya M Bhagurkar. Melt extrusion with poorly soluble drugs—an integrated review. *International Journal of Pharmaceutics*, 535(1-2):68–85, 2018.
- [64] Rachel Evans, Esther Bochmann, Samuel Kyeremateng, Andreas Gryczke, and Karl G Wagner. Holistic QbD approach for hot-melt extrusion process design space evaluation: Linking materials science, experimentation and process modeling. *European Journal of Pharmaceutics and Biopharmaceutics*, 141:149–160, 2019.
- [65] Naila A Mugheirbi, Laura I Mosquera-Giraldo, Carlos H Borca, Lyudmila V Slipchenko, and Lynne S Taylor. Phase behavior of drug-hydroxypropyl methylcellulose amorphous solid dispersions produced from various solvent systems: mechanistic understanding of the role of polymer using experimental and theoretical methods. *Molecular Pharmaceutics*, 15(8):3236–3251, 2018.

- [66] Hrushikesh Karandikar, Rohan Ambardekar, Adrian Kelly, Tim Gough, and Anant Paradkar. Systematic identification of thermal degradation products of HPMCP during hot melt extrusion process. *International Journal of Pharmaceutics*, 486(1-2):252–258, 2015.
- [67] Ashish L Sarode, Sakae Obara, Fumie Tanno, Harpreet Sandhu, Raman Iyer, and Navnit Shah. Stability assessment of hypromellose acetate succinate (HPMCAS) NF for application in hot melt extrusion (HME). *Carbohydrate Polymers*, 101:146–153, 2014.
- [68] Raymond Chen, Nicholas Ilassi, and Sonja S Sekulic. Absolute molecular weight determination of hypromellose acetate succinate by size exclusion chromatography: Use of a multi angle laser light scattering detector and a mixed solvent. *Journal of Pharmaceutical and Biomedical Analysis*, 56(4):743–748, 2011.
- [69] Michael M Crowley, Feng Zhang, John J Koleng, and James W McGinity. Stability of polyethylene oxide in matrix tablets prepared by hot-melt extrusion. *Biomaterials*, 23(21):4241–4248, 2002.
- [70] Dwayne T Friesen, Ravi Shanker, Marshall Crew, Daniel T Smithey, WJ Curatolo, and JAS Nightingale. Hydroxypropyl methylcellulose acetate succinate-based spray-dried dispersions: an overview. *Molecular Pharmaceutics*, 5(6):1003–1019, 2008.
- [71] Yanbin Huang and Wei-Guo Dai. Fundamental aspects of solid dispersion technology for poorly soluble drugs. *Acta Pharmaceutica Sinica B*, 4(1):18–25, 2014.
- [72] Jennifer B Dressman, Gordon L Amidon, Christos Reppas, and Vinod P Shah. Dissolution testing as a prognostic tool for oral drug absorption: immediate release dosage forms. *Pharmaceutical Research*, 15(1):11–22, 1998.
- [73] Alexander Fuchs, Mathew Leigh, Bastian Kloefer, and Jennifer B Dressman. Advances in the design of fasted state simulating intestinal fluids: FaSSIF-V3. *European Journal of Pharmaceutics and Biopharmaceutics*, 94:229–240, 2015.
- [74] Joachim Brouwers, Marcus E Brewster, and Patrick Augustijns. Supersaturating drug delivery systems: The answer to solubility-limited oral bioavailability? *Journal of Pharmaceutical Sciences*, 98(8):2549–2572, 2009.
- [75] Edmund S Kostewicz, Martin Wunderlich, Ulrich Brauns, Robert Becker, Thomas Bock, and Jennifer B Dressman. Predicting the precipitation of poorly soluble weak bases upon entry in the small intestine. *Journal of Pharmacy and Pharmacology*, 56(1):43–51, 2004.
- [76] Christian Jede, Christian Wagner, Holger Kubas, Christian Weber, and Werner Weitschies. In-line derivative spectroscopy as a promising application to a small-scale in vitro transfer model in biorelevant supersaturation and precipitation testing. *Journal of Pharmacy and Pharmacology*, 70(10):1315–1323, 2018.

- [77] Carolin Auch, Meike Harms, and Karsten Mäder. Melt-based screening method with improved predictability regarding polymer selection for amorphous solid dispersions. *European Journal of Pharmaceutical Sciences*, 124:339–348, 2018.
- [78] Carolin Auch, Meike Harms, Yury Golitsyn, Detlef Reichert, and Karsten Mäder. Miniaturized measurement of drug–polymer interactions via viscosity increase for polymer selection in amorphous solid dispersions. *Molecular Pharmaceutics*, 16(5):2214–2225, 2019.
- [79] Carolin Auch, Christian Jede, Meike Harms, Christian Wagner, and Karsten Mäder. Impact of amorphization and GI physiology on supersaturation and precipitation of poorly soluble weakly basic drugs using a small-scale in vitro transfer model. *International Journal of Pharmaceutics*, 574:118917, 2020.
- [80] Patrick J Marsac, Sheri L Shamblin, and Lynne S Taylor. Theoretical and practical approaches for prediction of drug–polymer miscibility and solubility. *Pharmaceutical Research*, 23(10):2417, 2006.
- [81] Christopher Rumble, Kacie Rich, Gang He, and Mark Maroncelli. CCVJ is not a simple rotor probe. *The Journal of Physical Chemistry A*, 116(44):10786–10792, 2012.
- [82] Christian Jede, Christian Wagner, Holger Kubas, Christian Weber, Markus Weigandt, Mirko Koziolok, and Werner Weitschies. Automated small-scale in vitro transfer model as screening tool for the prediction of in vivo-dissolution and precipitation of poorly solubles. *International Journal of Pharmaceutics*, 556:150–158, 2019.
- [83] Shan Wang, Chengyu Liu, Yuejie Chen, Alan Zhu, and Feng Qian. Aggregation of hydroxypropyl methylcellulose acetate succinate under its dissolving pH and the impact on drug supersaturation. *Molecular Pharmaceutics*, 15(10):4643–4653, 2018.
- [84] Jennifer B Dressman and Christos Reppas. In vitro–in vivo correlations for lipophilic, poorly water-soluble drugs. *European Journal of Pharmaceutical Sciences*, 11:73–80, 2000.
- [85] Chara Litou, Maria Vertzoni, Wei Xu, Filippos Kesisoglou, and Christos Reppas. The impact of reduced gastric acid secretion on dissolution of salts of weak bases in the fasted upper gastrointestinal lumen: data in biorelevant media and in human aspirates. *European Journal of Pharmaceutics and Biopharmaceutics*, 115:94–101, 2017.
- [86] Cheri Enders Klein, Yi-Lin Chiu, Walid Awni, Tong Zhu, Renee S Heuser, Thao Doan, Joerg Breitenbach, John B Morris, Scott C Brun, and George J Hanna. The tablet formulation of lopinavir/ritonavir provides similar bioavailability to the soft-gelatin capsule formulation with less pharmacokinetic variability and diminished food effect. *JAIDS Journal of Acquired Immune Deficiency Syndromes*, 44(4):401–410, 2007.

-
- [87] Kristin Lehmkemper, Samuel O Kyeremateng, Oliver Heinzerling, Matthias Degenhardt, and Gabriele Sadowski. Long-term physical stability of PVP-and PVPVA-amorphous solid dispersions. *Molecular Pharmaceutics*, 14(1):157–171, 2016.
- [88] Piero Piccinni, Yiwei Tian, Alyn McNaughton, Jane Fraser, Stephen Brown, David S Jones, Shu Li, and Gavin P Andrews. Solubility parameter-based screening methods for early-stage formulation development of itraconazole amorphous solid dispersions. *Journal of Pharmacy and Pharmacology*, 68(5):705–720, 2016.
- [89] Anke Prudic, Yuanhui Ji, and Gabriele Sadowski. Thermodynamic phase behavior of API/polymer solid dispersions. *Molecular Pharmaceutics*, 11(7):2294–2304, 2014.
- [90] Christian Luebbert and Gabriele Sadowski. Moisture-induced phase separation and recrystallization in amorphous solid dispersions. *International Journal of Pharmaceutics*, 532(1):635–646, 2017.
- [91] Kristin Lehmkemper, Samuel O Kyeremateng, Oliver Heinzerling, Matthias Degenhardt, and Gabriele Sadowski. Impact of polymer type and relative humidity on the long-term physical stability of amorphous solid dispersions. *Molecular Pharmaceutics*, 14(12):4374–4386, 2017.
- [92] Derek S Frank, Qingyuan Zhu, and Adam J Matzger. Inhibiting or accelerating crystallization of pharmaceuticals by manipulating polymer solubility. *Molecular Pharmaceutics*, 16(8):3720–3725, 2019.
- [93] Zedong Dong and Hasmukh Patel. Scientific and regulatory considerations for development and commercialization of poorly water-soluble drugs. In *Formulating Poorly Water Soluble Drugs*, pages 741–767. Springer, 2016.

Acknowledgement

Die vorliegende Dissertation entstand unter der Betreuung von Prof. Dr. Karsten Mäder der Martin-Luther Universität Halle-Wittenberg und Dr. Meike Harms der Firma Merck KGaA im Rahmen meiner Tätigkeit als Doktorandin bei der Merck KGaA in der Abteilung Pharmaceutical Technologies. An dieser Stelle möchte ich mich herzlich bei all jenen Personen bedanken, die mich in den vergangenen drei Jahren bei der Anfertigung dieser Arbeit mit Rat und Tat unterstützt haben.

An erster Stelle gilt mein Dank meinem Doktorvater Prof. Dr. Karsten Mäder für die Betreuung meiner Promotion und seine Unterstützung beim Verfassen der Publikationen und dieser Dissertation. Ich danke ihm für seine fachliche Expertise und persönlichen Ratschläge, die mir stets sehr weitergeholfen haben.

Des Weiteren möchte ich mich bei Dr. Meike Harms bedanken, die für mich stets eine offene Tür hatte, um sich in Diskussionen um Ergebnisse zu stürzen und dabei gerne auch mal Rohdaten zu analysieren. Sie hat meine Fähigkeiten zum wissenschaftlichen Denken und Arbeiten maßgeblich gefördert und dabei wertvolle Unterstützung für neue Ideen und Lösungsansätze gegeben.

Mein Dank gilt weiterhin Dr. Simon Geissler, der meine Arbeit stets unterstützt und Rücken- deckung für alle Entscheidungen gegeben hat.

Dr. Markus Weigandt danke ich für die Ermöglichung der Promotion in der Abteilung Pharmaceutical Technologies. Die Teilnahme an nationalen und internationalen Kongressen und die Einblicke in die vielen Aktivitäten bei Pharmaceutical Technologies haben mich fachlich und persönlich weitergebracht.

Besonders hervorzuheben ist die gemeinsame Zeit mit meinen Kollegen und Kolleginnen bei der Firma Merck. Sie alle haben meine Promotionszeit bereichert, sowohl während der Arbeitszeit als auch oft und gerne darüber hinaus. Die herrschende große Diskussionskultur und das kritische Hinterfragen jeglicher Hypothesen haben meine Denkweise geprägt. Besonders erwähnen möchte ich Robert Hennig, Markus Riehl, Magdalena Münster, Martina Jeschke und Steffen Wöll, die als Reviewer layout-technisches und sprachliches Feedback zu meinen Publikationen und dieser Dissertation gegeben haben. Christian Jede und Karsten Flügel möchte ich meinen ganz besonderen Dank für die Zusammenarbeit und die spannenden Diskussionen aussprechen. Zusätzlich dürfen Corinna Schoch, Dirk Schiroky, Katrin Grieser, Melanie Hofmann, Mira Oswald, Stefan Schiller und Vicky Schmitt und die fantastischen Momente mit der Unternehmensgruppe nicht unerwähnt bleiben.

Außerdem danke ich Martina Jeschke, Jessica Grieser, Katrin Grieser und Simone Hansmann für die gemeinsame Zeit in den besten Büros der Welt und allen Kollegen und Kolleginnen aus DDI und PharmTech für die tollen gemeinsamen Errungenschaften und Erlebnisse - nicht zuletzt bei Sommer- und Winterfrischen.

Die Beanspruchung durch Job und Doktorarbeit stellt Freundschaften manchmal auf eine harte Probe und lässt oft zu wenig Zeit für die Menschen, die einem am Herzen liegen. Dies betrifft vor allem Wegbegleiter/innen aus Kindergarten- und Schulzeiten, Nachbarn, Studienfreunde aus Freiburg, eine einmalige Pharmaziepraktikantenrunde und Freundschaften, die durch die gemeinsame Liebe zur Musik entstanden sind beim Musikverein Ludwigsburg-Oßweil e.V. Stadtkapelle Ludwigsburg, Kreisjugendorchester Ludwigsburg und Sinfonischen Blasorchester Ludwigsburg. Zahlreiche Bindungen jedoch sind über die Jahre nur stärker geworden und diese Menschen sind hoffentlich auf immer ein Teil meines Lebens. Ich würde beim Aufzählen sicherlich jemanden vergessen, daher danke ich Euch allen, dass ihr immer wieder auch ganz andere Aspekte des Lebens in den Fokus gerückt habt und beinahe unendliche Geduld für den zeitlichen Aufwand einer Dissertationsarbeit gezeigt habt.

Meinen Eltern und meiner gesamten Familie danke ich für ihre bedingungslose Unterstützung, die Ermöglichung von Studium und Promotion, ihr offenes Ohr und ihr unerschütterliches Vertrauen in mich. Ohne diesen Rückhalt wären Studium und Promotion nicht möglich gewesen. Darüber hinaus möchte ich meinem Bruder Marcus von Herzen danken für seine Hilfe in LaTeX-Fragen, der zum Layout dieser Arbeit einen großen Beitrag geleistet hat.

Zuletzt möchte ich mich bei Markus bedanken, der mit einer ehrlichen Meinung zu vielen Fragen und mit seinem Verständnis für die unterschiedlichen Phasen der Entstehung dieser Arbeit stets ein großer Rückhalt war. Er besitzt die einzigartige Gabe Probleme in die richtige Relation zu setzen und ich bin sehr glücklich ihn an meiner Seite zu wissen.

Eidesstattliche Erklärung

der

Naturwissenschaftliche Fakultät I

- Biowissenschaften -

Martin-Luther-Universität Halle-Wittenberg

Ich erkläre gemäß § 5 der Promotionsordnung der Naturwissenschaftlichen Fakultäten I, II und III der Martin-Luther-Universität Halle-Wittenberg an Eides statt, dass ich die Arbeit selbstständig und ohne fremde Hilfe verfasst, keine anderen als die von mir angegebenen Quellen und Hilfsmittel benutzt und die den benutzten Werken wörtlich oder inhaltlich entnommenen Stellen als solche kenntlich gemacht habe. Weiterhin erkläre ich, dass ich mich mit der vorliegenden Dissertationsarbeit erstmals um die Erlangung eines Doktorgrades bewerbe.

Datum

Unterschrift

Curriculum vitae

Persönliche Daten

Name	Carolin Christina Auch
Geburtsdatum	15. Juli 1991
Geburtsort	Ludwigsburg
Staatsangehörigkeit	Deutsch

Beruflicher Werdegang

Seit 11/2018	Post Doc Pharmaceutical Technologies, Merck KGaA
01/2016-10/2018	Doktorandin Pharmaceutical Technologies, Merck KGaA & Martin-Luther-Universität, Halle-Wittenberg
12/2015	Approbation als Apothekerin
05/2015-10/2015	Praktisches Jahr, 2. Halbjahr Bahnhof-Apotheke, Ludwigsburg
11/2014-04/2015	Praktisches Jahr, 1. Halbjahr Pharmaceutical Technologies, Merck KGaA
10/2010-10/2014	Pharmaziestudium Albert-Ludwigs-Universität, Freiburg

Datum

Unterschrift

List of publications

Peer-reviewed publications

Auch, Carolin; Harms, Meike; Mäder, Karsten: *Melt-based screening method with improved predictability regarding polymer selection for amorphous solid dispersions*. In: European Journal of Pharmaceutical Sciences 2018, 124, 339-348

Auch, Carolin; Harms, Meike; Mäder, Karsten: *How molecular weight and PDI of a polymer impact dissolution performance*. In: International Journal of Pharmaceutics 2019, 556, 372-382

Auch, Carolin; Harms, Meike; Golitsyn, Yury; Reichert, Detlef; Mäder, Karsten: *Miniaturized measurement of drug-polymer interactions via viscosity increase for polymer selection in amorphous solid dispersions*. In: Molecular Pharmaceutics 2019, 16, 2214-2225

Auch, Carolin; Jede, Christian; Harms, Meike; Wagner, Christian; Mäder, Karsten: *Impact of amorphization and GI physiology on supersaturation and precipitation of poorly soluble weakly basic drugs using a small-scale in vitro transfer model*. In: International Journal of Pharmaceutics 2020, 574, 118917

Oral presentations

Auch, Carolin: *Melt screening with improved predictability for ASD polymers*. Pharmaceutics and Biopharmaceutics World Meeting. In: Granada, Spain, March 22nd, 2018

Auch, Carolin: *Correlating screening tools to formulation feasibility*. Losan Drug Delivery Conference. In: Frankfurt, Germany, February 6th, 2018

Auch, Carolin: *Amorphous solid dispersions: screening tools in polymer selection*. German Local Chapter of Controlled Release Society. In: Saarbrücken, Germany, March 2nd, 2017

Conference abstracts

Auch, Carolin; Harms, Meike; Mäder, Karsten: *Molar mass matters - impact of excipient's molecular weight on dissolution performance of ASD*. AAPS PharmSci 360. In: San Antonio, Texas, USA, November 04th, 2019

Auch, Carolin; Harms, Meike; Mäder, Karsten: *Measurement of drug-polymer interactions as preclinical screening tool*. Annual Meeting Controlled Release Society. In: New York City, USA, July 22nd, 2018

Auch, Carolin; Harms, Meike; Mäder, Karsten: *Characterization of pharma polymers via GPC-UV-RI-MALS detection*. German Local Chapter of Controlled Release Society. In: Halle/Saale, Germany, March 1st, 2018

Auch, Carolin; Harms, Meike; Mäder, Karsten: *Amorphous solid dispersions: screening tools in polymer selection*. German Local Chapter of Controlled Release Society. In: Marburg, Germany, March 2nd, 2017



Melt-based screening method with improved predictability regarding polymer selection for amorphous solid dispersions

Carolin Auch^{a,b}, Meike Harms^b, Karsten Mäder^{a,*}

^a Institute of Pharmacy, Faculty I of Natural Sciences, Martin Luther University Halle-Wittenberg, 06120, Halle/Saale, Germany

^b Department of Pharmaceutical Technologies, Merck KGaA, 64293 Darmstadt, Germany



ARTICLE INFO

Keywords:

Amorphous solid dispersions
Manufacturing
Polymer selection
Screening
Preformulation

ABSTRACT

The predictability of preformulation screening tools for polymer selection in amorphous solid dispersions (ASD) regarding supersaturation and precipitation was systematically examined. The API-polymer combinations were scaled up by means of hot-melt extrusion and spray-drying to verify the predictions. As there were discrepancies between a solvent-based screening and performance of ASD, a new screening tool with improved predictability at minimal investments of time and material is presented. The method refinement resulted in a better correlation between the screening and ASD prototypes.

So far, a purely solvent-based screening was used which consisted of film casting by rapid solvent evaporation. This approach was improved by applying a heating step after film casting. Four representative polymers were tested with two different model active pharmaceutical ingredients (API) under non-sink dissolution conditions. Polyvinylpyrrolidone (PVP) based polymers showed no benefit towards pure API in the solvent-based screening but good supersaturation as ASD formulations. The extrudates with the cellulose derivatives hydroxypropylmethylcellulose acetate succinate (HPMCAS) and cellulose acetate phthalate (CAP) showed lower supersaturation than predicted by the solvent-based screening but performed especially well as spray-dried dispersions (SDD).

False negative results for PVP-co-vinyl acetate (PVP-VA64) could be avoided by using the new melt-based screening. Furthermore, comparing the results from the two different screening methods allowed predicting the performance of extrudates vs. SDD with cellulose derivatives as polymeric excipients.

1. Introduction

An increasing number of new active pharmaceutical ingredients (API) belong to biopharmaceutical classification system (BCS) class II (Amidon et al., 1995) with low bioavailability due to poor aqueous solubility. One way to overcome these solubility issues is by formulating amorphous solid dispersions (ASD). ASD contain the API in its amorphous form in a stabilizing matrix, which consists mostly of polymers. The polymer stabilizes the inherently thermodynamically unstable amorphous form of the API by reducing its molecular mobility and hindering recrystallization both upon storage and dissolution (Alonzo et al., 2011; Leuner and Dressman, 2000).

Several manufacturing techniques are used for the preparation of solid dispersions including hot-melt extrusion (HME) and spray-drying (SD). The compilation of marketed ASD drug products by Wyttenbach et al. (Wyttenbach and Kuentz, 2017) indicates the significance of these two methods with 29% prepared by SD, 38% manufactured via HME and another 33% by other techniques like spray layering or coprecipitation. The choice of the technique is mostly guided by API characteristics. Thermostable compounds with a low melting point are usually applicable to HME whereas a high melting point combined with high solubility in volatile solvents favors SD (Navnit Shah et al., 2014). Only few studies systematically compare amorphous solid dispersions prepared by HME and SD and analyze influencing factors (Agrawal

Abbreviations: ACN, acetonitrile; API, active pharmaceutical ingredient; ASD, amorphous solid dispersion; BCS, biopharmaceutical classification system; CAP, cellulose acetate phthalate; DCM, dichloromethane; DMF, *N,N*-dimethylformamide; DL, drug load; DSC, differential scanning calorimetry; FaSSIF, fasted-state simulating intestinal fluid; GFA, glass forming ability; HME, hot-melt extrusion; HPMCAS, hydroxypropylmethylcellulose acetate succinate; KTZ, ketoconazole; MeOH, methanol; PI, precipitation inhibitors/inhibition; PVP, Polyvinylpyrrolidone; PVP-VA64, PVP-co-vinyl acetate 60:40; PXRD, powder X-ray diffraction; RP-HPLC, Reversed-phase high-performance liquid chromatography; SD, spray-drying; SDD, spray-dried dispersion; T_{deg} , degradation temperature; T_g , glass transition temperature; T_m , melting temperature

* Corresponding author.

E-mail addresses: carolin.auch@external.merckgroup.com (C. Auch), meike.harms@merckgroup.com (M. Harms), karsten.maeder@pharmazie.uni-halle.de (K. Mäder).

<https://doi.org/10.1016/j.ejps.2018.08.035>

Received 4 July 2018; Received in revised form 23 August 2018; Accepted 25 August 2018

Available online 30 August 2018

0928-0987/ © 2018 Elsevier B.V. All rights reserved.

et al., 2013; Beneš et al., 2017; Bhardwaj et al., 2018; Haser et al., 2017a; Joe et al., 2010). Surana et al. (Surana et al., 2004) found that different preparation methods produce different degrees of relaxation and therefore presumably different levels of molecular mobility.

A large polymer excipient portfolio is available for the formulation of ASD (Navnit Shah et al., 2014). To date, it is not possible to predict e.g. only by knowledge of the drug's chemical structure which polymers or polymer mixtures are most suitable to achieve stable ASD and to preserve a high supersaturation after administration. Although there are promising *in-silico* approaches (Prudic et al., 2014; Van Eerdenbrugh and Taylor, 2011), experimental data is still needed to guide the drug product formulation strategy (Repka et al., 2018). Formulation screenings with HME or SD for several polymers are time consuming and demand considerable amounts of material even when using small-scale equipment. As new compounds are usually very limited in the amount available, miniaturized screening methods providing reliable results especially for complex questions like a polymer decision for ASD are desirable.

There are different screening tools available such as pretests with supersaturated drug solutions (Vandecruys et al., 2007) and differential scanning calorimetry (DSC) (Bhugra, 2016; Rask et al., 2018). More advanced and comprehensive preformulation approaches have been developed that handle dissolution behavior of ASD films together with imaging and interaction studies (Wyttenbach et al., 2013). Miniaturized approaches were mostly pursued in 96 well plate format e.g. by solvent evaporation (Chiang et al., 2012; Dai et al., 2007; Shanbhag et al., 2008) or solvent shift methods (Yamashita et al., 2011). Recently, there was also a comparative study of commonly used solvent-based screenings for polymer selection (Banda et al., 2018). A solvent casting and a solvent displacement method were evaluated for different APIs and selected formulations were scaled up via spray-drying. However, HME was not included as a preparation method although this technique has considerable advantages like being a solvent-free and therefore environmentally friendly process and providing applicability for continuous manufacturing and downstream-processing technologies (Repka et al., 2018).

Standardized high-throughput screening tools that cannot be fully optimized for every single polymer-API combination might especially neglect influences of scale-up manufacturing. In comparison to the solvent evaporation in a screening, spray-drying at elevated temperatures provides a faster evaporation and phase transition. Thus, complete amorphization is more likely which in turn reduces the risk for recrystallization caused by remaining seed crystals. In addition, residual solvents might influence the dissolution results by acting as a co-solvent or maintaining high molecular mobilities within the film and therefore reducing their stability during storage (Kawakami, 2009). Depending on the solvent used, polymer dissolution results either in entangled chains or coiled spheres (Miller-Chou and Koenig, 2003). This probably influences the way the API is embedded within the polymer matrix leading to different molecular mobilities. Finding the perfect solvent for each polymer is a tremendous work (Chen et al., 2011) and together with solubility issues for every single API it is an enormous task to create a fully comprehensive screening tool.

Table 1
Physicochemical properties of model API.

API	M _w (g/mol)	logP	T _m (°C)	T _g (°C)	pKa	Solubility in FaSSiF (µg/mL) ^c
Ketoconazole	531.4 ^b	4.3 ^b	148.9 ± 0.1 ^a	43.9 ± 0.2 ^a	6.51; 2.94 ^b	22.2 ± 0.70 ^c
MC1	481.9 ^d	2.5 ^d	209.8 ± 0.1 ^a	147.5 ± 0.4 ^a	1.8; 3.2 ^d	4.3 ± 0.03 ^c

^a In-house determination of T_m and T_g as onset values from raw materials using a standard DSC method (Section 2.6.1) with heating and cooling rates of ± 10 K/min, arithmetic mean of n ≥ 3 ± S.D.

^b Extracted from PubChem database (<https://pubchem.ncbi.nlm.nih.gov/>).

^c Solubility of crystalline drugs in FaSSiF-V1, pH 6.5 at 37 °C, arithmetic means ± S.D. (n = 3) after 2 h in mini-dissolution setup (method description see Section 2.7)

^d Internal data.

Nevertheless, solvent based processes have the advantages of easy handling, they enable efficient mixing of different components and can be conducted in miniaturized scale like 96 well plates. Furthermore, it allows for the assessment of glassy state together with non-sink dissolution in one film casting step which both provide valuable information at a time.

The desired characteristics for screening processes in general are (i) high predictability and reproducibility, (ii) low amount of required materials and (iii) fast output. In this study, predictability and reliability were investigated in more detail as these are crucial for making decisions in the drug product development process. Due to the complexity of ASD formulations, there are many factors desirable to be predicted out of screening tools: dissolution behavior, assessment of thermodynamic solubility of the drug within the polymer, glass transition temperature (T_g) of the mixture, long-term physical stability and storage conditions, drug-polymer interactions, amorphous phase separation or manufacturing parameters. The authors decided to focus on the prediction of supersaturation and precipitation as the most prominent parameters for bioavailability enhancement. Nevertheless, the other factors should not be neglected in the final decision for the best suited polymeric carrier and must be evaluated by different approaches.

In a first step, the authors performed a solvent-based screening derived from the miniaturized screening of polymers for amorphous drug stabilization (SPADS) by Wyttenbach et al. (Wyttenbach et al., 2013). Second, formulations were scaled-up via hot-melt extrusion and spray-drying to elucidate differences in the manufacturing technique. Last, the current study aimed to adapt the existing miniaturized screening method to predict the performance in dissolution in correlation with the manufacturing process.

The model drugs used in this study – ketoconazole (KTZ) and MC1 – are BCS class II compounds. Their physicochemical-properties are summarized in Table 1.

They were carefully selected to represent different properties in terms of melting point, log P, glass forming ability (GFA) (Baird et al., 2013; Blaabjerg et al., 2016; Blaabjerg et al., 2018) and glass forming stability (Uhlmann, 1972). KTZ belongs to GFA class III similar to most marketed ASD compounds (Wyttenbach and Kuentz, 2017). GFA class III comprises compounds which exhibit no recrystallization of the pure API in a DSC heating-cooling-heating cycle. MC1 was selected as an example for thermolabile APIs where a GFA class attribution by melt quenching is not possible due to its decomposition above the melting temperature. The kinetic amorphization pathway by ball milling (Blaabjerg et al., 2017) did not result in fully amorphous samples indicating a GFA class I assignment (data not shown).

The excipient portfolio is focused on ionic and non-ionic polymers of different chemical classes that are often used in solid dispersions (Navnit Shah et al., 2014; Wyttenbach and Kuentz, 2017). In this study, HPMCAS HF, CAP, PVP-VA64 and PVP K30 were chosen as representative polymers. These four polymers were also part of the polymer setup in the SPADS approach by Wyttenbach et al. (HPMCAS MF derivative instead of HF) where scaled-up formulations were only prepared by SD.

To our knowledge, the present work is the first investigation on

correlating the way the polymer screening is conducted to the manufacturing technique for formulating ASD.

2. Materials and methods

2.1. Materials

Ketoconazole (KTZ, purity $\geq 98\%$) was purchased from Biotrend Chemicals AG (Switzerland). Analytical standard of KTZ (Ph.Eur. reference standard) for HPLC calibration was purchased from Sigma Aldrich (USA). An internal pipeline API (MC1) was additionally used as model drug. The chemical structures of KTZ and MC1 are depicted in Fig. 1.

Polyvinylpyrrolidone-co-vinyl acetate 60:40 (PVP-VA64) and polyvinylpyrrolidone K30 (PVP K30) were obtained from BASF (Germany). Hydroxypropylmethylcellulose acetate succinate (HPMCAS) grade HF was kindly provided by Shin Etsu (Japan). Cellulose acetate phthalate (CAP) was delivered by Eastman (USA). Acetonitrile (ACN), dichloromethane (DCM), 25% ammonia solution and formic acid were purchased from Merck KGaA (Germany) and *N,N*-dimethylformamide was supplied by VWR Chemicals (Belgium). All solvents were of HPLC grade (purity $\geq 99.7\%$).

Powder for preparation of fasted-state simulating intestinal fluid V1 (FaSSIF-V1) was obtained from Biorelevant.com (UK). The following substances were used for dissolution media preparation: sodium hydroxide (VWR Chemicals, Belgium), sodium chloride, di-sodium hydrogen phosphate, hydrochloric acid 1 M and sodium hydroxide solution 1 M (Merck KGaA, Germany). All aqueous solutions were prepared with purified water (Millipore-Milli-Q® integral water purification system, Merck KGaA, Germany).

2.2. Solvent-based screening

The miniaturized solvent-based screening for polymer selection was derived from [Wyttenbach et al. \(2013\)](#). Drug-polymer films were cast in 96 well quartz plates (Hellma Analytics, Germany). For this purpose, DMF stock solutions were prepared in concentrations of 10 mg/mL for both API and polymers. The stock solutions were mixed in ratios

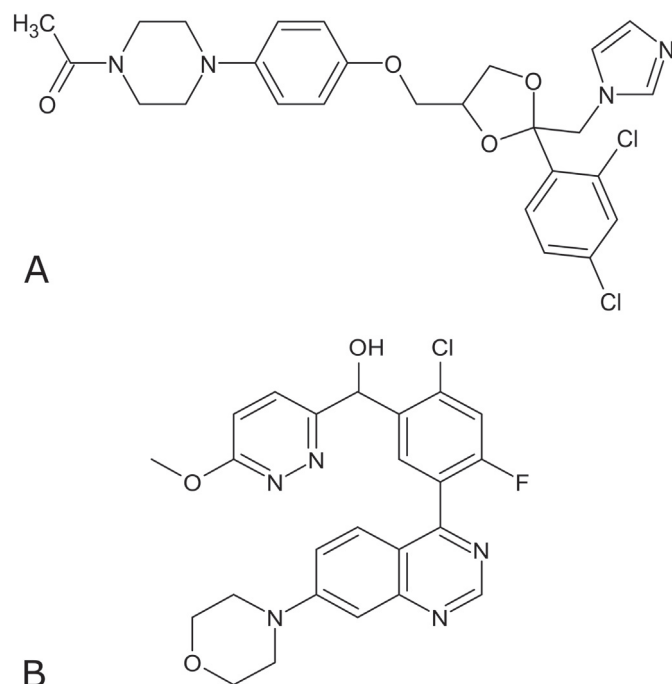


Fig. 1. Chemical structures of A) ketoconazole and B) MC1.

providing the desired drug loads (DL) directly in the wells with 20% and 40% (w/w) DL for KTZ and 30% (w/w) DL for MC1. Each well ended up with 1000 μg solid content for polymer-API mixtures and 200 μg , 300 μg or 400 μg for API control groups, depending on the drug load ($n = 6$). After mixing, the solvent was rapidly evaporated with a freeze dryer apparatus (Alpha 2–4, Christ, Germany) at 0.1 mbar for 30 min at 25 °C. The volume of control groups was filled up with DMF and full evaporation was monitored with a control well with neat solvent ($V = 100 \mu\text{L}$ according to volume of stock solutions).

Dissolution experiments were conducted with 200 μL pre-warmed FaSSIF-V1 pH 6.5 at 37 °C in a thermo microplate shaker (THERMOstar®, BMG Labtech, Germany). Two glass balls ($\varnothing 2.5\text{--}3.5 \text{ mm}$, VWR Chemicals Prolabo, Belgium) were added to each well for agitation. Wells were sealed with an adhesive foil to avoid evaporation and shaken at 700 rpm. 100 μL of sample were taken after 60 min and residual volume after 120 min and transferred to a 0.45 μm PTFE filter plate (AcroPrep™ Advance, USA). The filter plate was centrifuged at 2500g (Heraeus Multifuge X3R, Thermo Scientific, Germany) and the filtrate was collected in a 96 well polypropylene plate. 50 μL of filtrate were immediately diluted with 150 μL of ACN/MilliQ 50:50 (v/v). Drug concentration was quantified by RP-HPLC (Section 2.5, $n = 6$).

Dissolution testing was re-conducted after seven days storage under accelerated conditions (40 °C, 75% relative humidity).

2.3. Preparation of amorphous solid dispersions

2.3.1. Preparation of physical mixtures

Polymer and API were exactly weighed with 40% (w/w) DL for KTZ and 30% (w/w) DL for MC1 and pre-mixed with mortar and pestle. The pre-mixture was afterwards filled in a Turbula® (T2F, Willy A. Bachofen AG, Switzerland) container and mixed at 32 rpm for 15 min. Drug load was subject to HPLC analysis (Section 2.5, $n = 4$).

2.3.2. Hot-melt extrusion

Extrudates were produced in a small-scale twin-screw extruder (ZE5 ThreeTec, Switzerland) with 5 mm screw diameter and three heating zones. The split barrel was equipped with double-concave co-rotating screws with conveying elements and a 1.0 mm die. The maximum screw speed was 300 rpm. The powder blend was added by manual feeding. The feeding zone was constantly cooled to 12.5 °C with a cryostat (WK4600, Lauda, Germany). Different extrusion temperatures and screw speeds were tested to obtain glassy, smooth extrudate strands. Process parameters for each formulation are summarized in Table 2. Drug load and impurities were monitored with $n = 4$ by HPLC analysis (Section 2.5), the solid state was assessed by DSC (Section 2.6.1) and powder X-ray diffraction (PXRD, Section 2.6.3).

2.3.3. Milling

Formulations with cellulose derivatives were cut with 25,000 rpm for $2 \times 1 \text{ min}$ (IKA® Tube mill control, USA) whereas PVP polymers were milled with a vibrational ball mill with 30 Hz for $2 \times 2 \text{ min}$

Table 2

Extrusion parameters ThreeTec ZE5 for formulations with 40% drug load KTZ.

Formulation	Screw speed (rpm)	Zone 1 (°C)	Zone 2 (°C)	Zone 3 (°C)
KTZ				
HPMCAS HF + 40% KTZ	300	120	170	170
CAP + 40% KTZ	300	130	160	160
PVP-VA64 + 40% KTZ	300	120	160	160
PVP K30 + 40% KTZ	200	120	160	160
MC1				
HPMCAS HF + 30% MC1	300	135	175	175
PVP-VA64 + 30% MC1	300	90	160	160

Table 3
Spray-drying parameters 4M8-TriX.

Formulation	Inlet temperature (°C)	Feed rate (mL/min)	Outlet temperature readout (°C)
KTZ			
100% KTZ	80; 100	1.0	42.6; 48.6
HPMCAS HF + 40% KTZ	80	2.0	41.1
CAP + 40% KTZ	100	2.0	45.4
PVP-VA64 + 40% KTZ	80	2.0	42.3
PVP K30 + 40% KTZ	120	2.0	52.3
MC1			
HPMCAS HF + 30% MC1	80	2.0	45.1
PVP-VA64 + 30% MC1	100	1.0	53.1

(Pulverisette® 23, Fritsch, Germany). A 15 mL volume zirconium oxide vessel and two ZrO₂ milling balls (Ø 10 mm) were used.

2.3.4. Spray-drying

Solutions with 2% (w/w) solid content of placebo and API-polymer mixture in DCM:MeOH 9:1 (v/v) were spray-dried with a 4 M8-TriX Spray-Dryer (ProCepT, Belgium). Drug load (30% MC1 and 40% KTZ, w/w with respect to polymer), nozzle diameter (1.0 mm), atomizing nitrogen (10 L/min) and air speed (70%) were kept constant. Inlet temperature and feed rate varied through the different formulations to obtain fully amorphous SDD. To generate amorphous KTZ as a reference, a 1% (w/w) solid solution was prepared. Parameters are depicted in Table 3. Spray-dried powder was dried overnight in a desiccator with silica gel (Merck KGaA, Germany) at 100 mbar. Drug load and impurities were monitored with $n = 4$ by HPLC analysis (Section 2.5), the solid-state properties were assessed by DSC, PLM and PXRD (Section 2.6).

2.4. Melt-based screening

Drug-polymer films were casted according to the solvent-based screening (Section 2.2) in 160 µL aluminum crucibles with pin. The mixing of stock solutions and solvent evaporation was maintained as a process step to ensure homogeneous mixing and keep the advantage of high throughput assays. A scale-down to 550 µg solid content was necessary with respect to reduced maximum filling volume of 110 µL FaSSiF in comparison to 200 µL FaSSiF in the solvent-based screening (Section 2.2).

A DSC 1 (Mettler Toledo GmbH, Germany) was used for heating and quench cooling of the films. The API's melting temperature (T_m) could not be reached if T_m was higher than the polymer's degradation temperature (T_{deg}). In this case, heating was performed up to 20 K below T_{deg} of the polymer. An equilibration step of 10 min at the respective temperature was integrated, followed by a rapid cooling to room temperature with -50 K/min. T_g , T_{deg} and respective annealing temperatures within the melt-based screening are summarized in Table 4.

The annealing temperatures were partly below T_m of KTZ and below T_m of MC1 for all formulations but always exceeded the glass transition temperatures of the drug-polymer combinations (Tables 5 and 6). The dissolution of the tempered films was conducted according to Section 2.2. 110 µL FaSSiF-V1 instead of 200 µL were used and one glass ball was inserted into each DSC crucible. 55 µL of sample were taken after 60 and 120 min and filtered. 20 µL of filtrate were diluted with 60 µL of ACN/MilliQ 50:50 (v/v) and analyzed by RP-HPLC (Section 2.5, $n = 3$).

2.5. HPLC analysis

API and degradation products were analyzed with an Agilent Technologies (USA) 1260 HPLC System. Purity was reported as area percent. All analyses maintained linearity in the range tested

Table 4

Glass transition, degradation and annealing temperatures of polymers used in melt-based screening.

Polymer	T_g (°C)	T_{deg} (°C)	Annealing temperatures (°C)
HPMCAS HF	117.8 ± 0.4 ^a	175 ^b	155
CAP	144.4 ± 0.8 ^a	165 ^b	145
PVP-VA64	105.4 ± 1.5 ^a	230 ^c	210 (KTZ) 190 (MC1)
PVP K30	156.2 ± 1.0 ^a	175 ^c	155

^a In-house determination as onset values from raw materials using a standard DSC method (Section 2.6.1) with heating and cooling rates of ± 10 K/min, arithmetic means ± S.D. ($n = 3$)

^b In-house determination from raw materials using a TGA method with heating rate of + 5 K/min from 25 °C to 350 °C.

^c As indicated by manufacturer BASF (Kolter et al., 2012) determined via TGA.

($r^2 = 0.9999$). Content specifications were set to 95–105%, purity had to be > 98%.

2.5.1. Ketoconazole

10 µL of sample were injected and quantified by a diode array detector working at 225 nm. The eluents used were binary mixtures of 95:5 and 5:95 (v/v) ammonium-formiate buffer pH 4 and ACN. The linear gradient ran from 100% phase A to 100% B within 10 min. A Waters XSelect® CSH Phenyl-Hexyl reverse phase column (4.6 × 100 mm with 3.5 µm packing, Waters Corporation, USA) was used, constantly heated up to 60 °C.

2.5.2. MC1

10 µL of sample were injected and quantified by a diode array detector working at 298 nm. The eluents used were binary mixtures of 95:5 and 5:95 (v/v) MilliQ water with 0.1% trifluoroic acid and ACN. The linear gradient ran from 90% phase A to 100% B within 13 min. A YMC-Triart reverse phase column (4.6 × 50 mm with 3 µm packing) was used, constantly heated up to 35 °C.

2.6. Solid-state characterization

2.6.1. Differential scanning calorimetry (DSC)

DSC studies were performed on a DSC 1 (Mettler Toledo, Switzerland). 7–10 mg of the samples were exactly weighed into 100 µL DSC aluminum crucibles without pin and crimped. Lids were pierced by the DSC piercing unit directly before measurement. Two heating cycles were applied, heating and cooling was conducted with ± 10 K/min. For KTZ, the first heating ramp reached from 25 °C up to 170 °C (above T_m), afterwards the melt was cooled down to 0 °C and heated again up to 200 °C.

Nitrogen was used as purging gas. The amorphous form – characterized by the absence of the API's melting peak – for all formulations was checked in the first heating cycle. Glass transition temperatures (T_g) were determined for both unprocessed raw material and ASD in the second cycle as onset temperature as the T_g in the first cycle is overlaid by a water evaporation peak. Any numerical values reported are arithmetic means with standard deviation of three independently prepared samples.

2.6.2. Microscopy

An Olympus BX60 microscope (Germany) was used for optical assessment. Extrudate strands, milled extrudates and SD powder were analyzed. Particle sizes were determined from light microscopy and polarized light microscopy was applied to check for crystalline traces. Pictures were taken with a SC-30 camera (Olympus) and processed with Stream Essentials software.

Table 5
Thermal properties of amorphous formulations with 40% drug load KTZ. Arithmetic means \pm S.D. ($n = 3$)

Formulation	T _g blank ^a (°C)	T _g SDD (°C)	T _g HME (°C)	Melting point depression of KTZ in PM (°C)
100% KTZ	43.9 \pm 0.2	Not fully amorphous	n/a	n/a
HPMCAS HF + KTZ	117.8 \pm 0.4	67.3 \pm 1.1	66.2 \pm 1.0	142.8 \pm 1.2
CAP + KTZ	144.4 \pm 0.8	101.5 \pm 2.6	85.6 \pm 2.9	136.1 \pm 1.1
PVP-VA64 + KTZ	105.4 \pm 1.5	65.0 \pm 2.6	68.3 \pm 1.0	143.9 \pm 0.6
PVP K30 + KTZ	156.2 \pm 1.0	81.3 \pm 1.3	83.7 \pm 1.0	144.2 \pm 1.8

^a The term “blank” describes either 100% KTZ without polymeric excipients (in case of KTZ blank) or 100% polymer bulk powder without KTZ.

Table 6
Thermal properties of amorphous formulations with 30% drug load MC1. Arithmetic means \pm S.D. ($n = 3$)

Formulation	Glass transition temperature blank (°C)	Glass transition temperature SDD (°C)	Glass transition temperature HME (°C)
100% MC1	n/a (degradation above T _m)	Not fully amorphous	n/a
HPMCAS HF + MC1	117.8 \pm 0.4	89.2 \pm 2.8	86.7 \pm 1.4
PVP-VA64 + MC1	105.4 \pm 1.5	106.2 \pm 0.7	105.3 \pm 2.2

2.6.3. Powder X-ray diffraction (PXRD)

Powder X-ray diffraction analyses were conducted on a Stoe StadiP 611 instrument (Stoe, Germany) equipped with Mythen1K Si-strip detector (PSD). Measurements were performed in transmission geometry with Cu-K α 1 radiation source generated at 40 kV and 40 mA. Approximately 20 mg of the sample were prepared on a combinatorial 96 well plate sample holder comprising a Kapton[®] foil on the bottom of the wells. Samples were scanned with an angular resolution of 0.03° 2 θ over a 2 θ range from -36° 2 θ to $+36^\circ$ 2 θ with measurement times of 30 s/PSD-step and a PSD step width of 0.09° 2 θ . After the measurements, the diffractograms were folded to the range from 0° 2 θ to 36° 2 θ .

2.7. Non-sink dissolution

Amounts of formulation containing 600 μ g of API were exactly weighed and filled into 2 mL round bottom Eppendorf caps. 1.2 mL of pre-warmed FaSSIF-V1 were added. The caps were shaken for 1 min at 1500 rpm (Vortex-Genie[®] 2, Scientific Industries, USA) and afterwards heated to 37 °C again in an incubator (Thermomixer[®] comfort, Eppendorf, Germany). Two minutes before each sampling, the suspensions were centrifuged (Mikro 200R centrifuge, Hettich, Germany) for 1 min at 15000g. 50 μ L of supernatant were then removed (without replacement) after 5, 10, 15, 20, 30, 45, 60, 90 and 120 min. All dissolution experiments were conducted in triplicate. Quantification of dissolved API in the dissolution samples was determined by HPLC (Section 2.5).

Saturation solubility of each KTZ-polymer system was also measured to evaluate the extent of supersaturation. The corresponding polymers were dissolved in FaSSIF in the same concentration as for the non-sink dissolution. Crystalline KTZ was added to the polymer solutions to result in a concentration of 1 mg/mL which is above the saturation solubility of KTZ. After centrifugation, the amount of KTZ dissolved in the supernatant was analyzed by RP-HPLC ($n = 3$). Samples were taken after 1 h, 2 h and 24 h.

2.8. Statistical analysis

Analyses of variance (Holm-Sidak method, Dunnett's test) and *t*-tests were conducted using Sigma-Plot 12.5 (Systat Software Inc., USA). A *p*-value < 0.05 was considered as statistically significant.

3. Results

3.1. Ketoconazole

3.1.1. Solvent-based screening

The solvent-based screening was conducted with two different drug loads (20 and 40% (w/w)). 40% DL was chosen for further experiments to challenge the physical stability of the systems. The results of the solvent-based screening are shown in Fig. 2 (data for 20% DL see Supplementary 1). KTZ without a polymeric excipient but treated the same as the API-polymer systems was used as reference.

HPMCAS HF performed best in the dissolution experiment immediately after film casting as well as after seven days storage under accelerated conditions. CAP also provided a high supersaturation which decreased after storage. The PVP derivative PVP-VA64 could not provide any benefit in comparison to pure API, whereas PVP K30 showed at least little supersaturation in the 60 min sampling.

3.1.2. Hot-melt extrusion

HME prototypes with 40% DL were manufactured with the

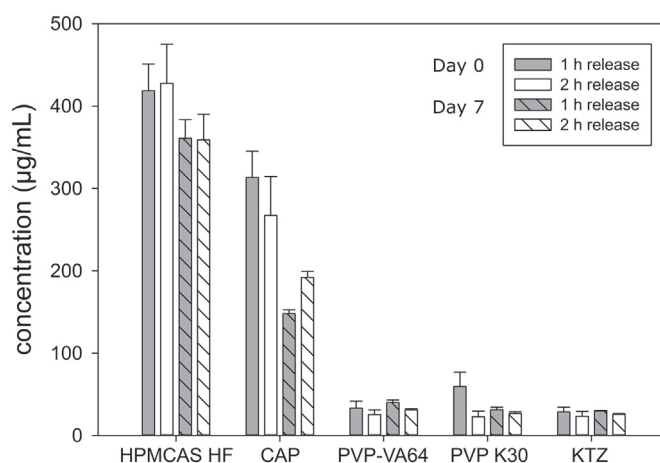


Fig. 2. Concentration of KTZ dissolved in the solvent-based screening with 40% drug load. Dissolution experiments were conducted directly after film casting and after seven days storage at 40 °C and 75% relative humidity. Dissolution medium was FaSSIF-V1 pH 6.5. Arithmetic means \pm S.D. ($n = 6$).

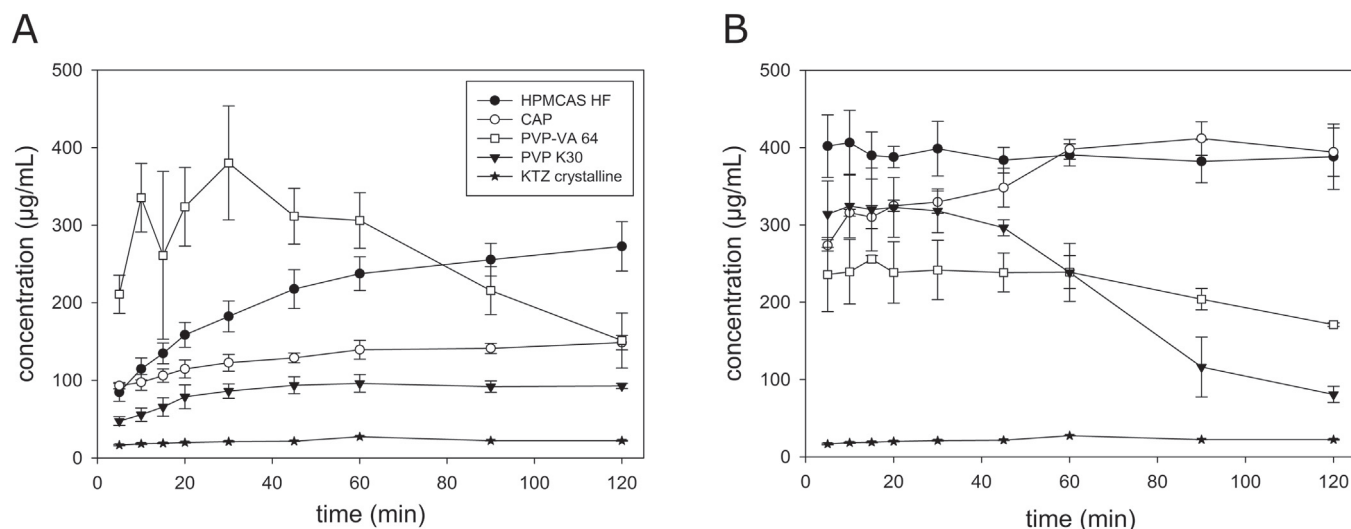


Fig. 3. A) Dissolution kinetics of milled hot-melt extrudates with 40% drug load KTZ in FaSSIF-V1 pH 6.5. Arithmetic means \pm S.D. ($n = 3$). B) Dissolution kinetics of SDD powder with 40% drug load KTZ in FaSSIF-V1 pH 6.5. Arithmetic means \pm S.D. ($n = 3$). Legend see 3A.

polymers tested in the solvent-based screening. All formulations resulted in clear and glassy strands indicating successful amorphization. This was confirmed by solid-state characterization (Section 3.1.6). The corresponding results of the non-sink dissolution experiments are shown in Fig. 3A.

Formulations with HPMCAS and CAP showed similar kinetics with slow dissolution of the API but no precipitation. As both cellulose derivatives seem to prevent recrystallization of KTZ effectively, the variability of the dissolution curves is strongly reduced compared to PVP-VA64. PVP-VA64 provided high supersaturation together with high variability and precipitation after 60 min. In general, PVP-VA64 formulations showed quite high variabilities indicated by large error bars. As nucleation can be caused by many different triggers and can also occur spontaneously (Mullin, 2012), variability in a non-sink dissolution setup – especially in small-scale – is not unlikely. At the same time, this also indicates that PVP-VA64 has a certain potential to generate supersaturation but is not capable to stabilize high concentrations of drug dissolved. PVP K30 showed a clear benefit towards crystalline API but the concentrations of KTZ dissolved were the lowest compared to the other extrudates.

Physical mixtures of API and polymer without further processing did not show an enhanced solubility for KTZ in FaSSIF (Supplementary 2). Thus, the amorphous form is needed to generate supersaturation.

3.1.3. Spray-drying

Spray-drying experiments were performed additionally to HME to investigate whether certain polymers are more suitable for solvent-based manufacturing processes.

Spray-dried formulations with HPMCAS HF and CAP provided very high and stable supersaturations (Fig. 3B). In both cases, SDDs performed better than the corresponding extrudates (Fig. 3).

The PVP derivatives showed a clear benefit compared to crystalline KTZ also as spray-dried amorphous solid dispersions in contrast to the solvent-based screening. The obtained supersaturation with PVP-VA64 from an SDD was slightly lower than from the extrudate. PVP K30 provided high concentrations of drug dissolved at the beginning but precipitated quickly after 45 min. Concentrations after 120 min were comparable to the extrudate.

3.1.4. Melt-based screening KTZ

As there was a clear gap in correlation of the results from solvent-based screening to scaled up prototype formulations, an investigation for improvement of the screening tool was started. To closer mimic

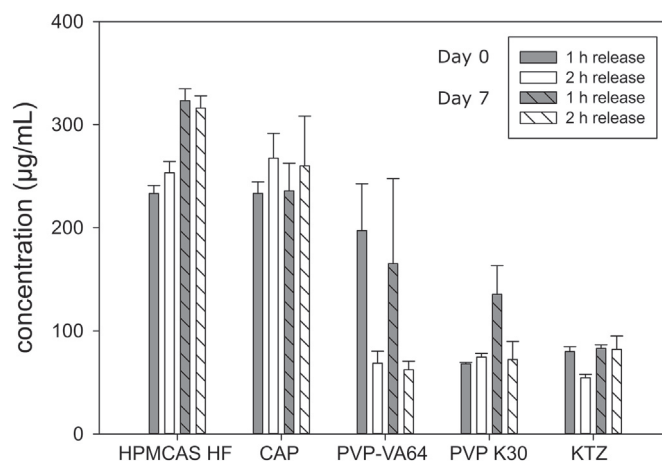


Fig. 4. Concentration of drug dissolved in the melt-based screening for 40% drug load KTZ after 60 and 120 min. Dissolution experiments were conducted directly after film preparation and after seven days storage at 40 °C and 75% relative humidity. Dissolution medium was FaSSIF-V1 pH 6.5. Arithmetic means \pm S.D. ($n = 3$).

processes and results in hot-melt extrusion, an additional heating step after film casting was introduced. API degradation due to the heating step was always monitored by stability-indicating RP-HPLC analysis. No generation of API impurities was detected.

Fig. 4 shows the dissolution results of the melt-based screening. HPMCAS and CAP gave high concentrations of drug dissolved which in this screening approach was also seen for PVP-VA64. Again, PVP-VA64 results were associated with high standard deviations but significant supersaturation was observed after 60 min compared to pure KTZ (t -test, $p = 0.01$). PVP K30 performed comparable to API without polymeric carrier.

3.1.5. Comparison

Fig. 5 shows the concentration of drug dissolved reached after 60 min for the two different screening tools and both manufacturing methods. The solvent-based screening gave an excellent fit to spray-drying results for HPMCAS HF whereas the additional heating step led to dissolution results in accordance with the hot-melt extrudates. This comparison did not only provide a ranking of suitable polymers but even predicted the absolute concentrations of drug dissolved at the respective sampling points (Supplementary 3). Results for CAP SDD and

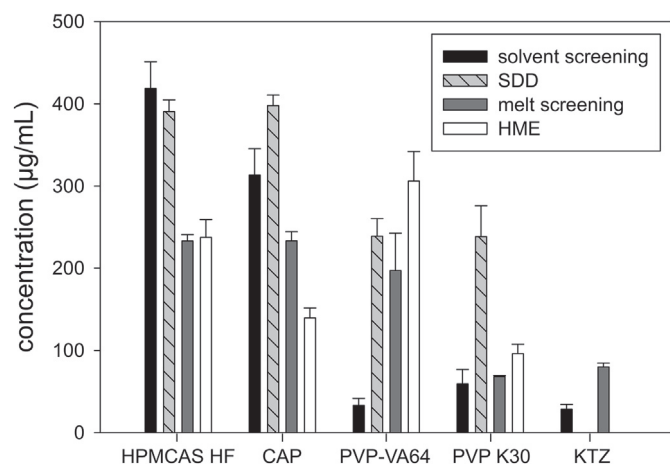


Fig. 5. Overall comparison of concentration of drug dissolved with both screening tools (melt-based and solvent-based), SDD and HME with 40% drug load KTZ each after 60 min dissolution time. Arithmetic means + S.D. ($n = 3$). Pure KTZ was not fully amorphous as SDD without polymeric excipient and was not processed by means of HME.

HME formulations could also be correlated with the corresponding solvent-based and melt-based screening tools. The absolute concentrations of KTZ dissolved that were achieved after 60 and 120 min (in accordance with sampling points of the screenings), as well as the maximum concentration that was achieved in the non-sink dissolution testing of extrudates and SD powder are summarized in Supplementary 3.

Only the new melt-based screening predicted supersaturation for the PVP-VA64 formulations which was significantly higher (t-test, $p = 0.004$) compared to the solvent-based screening. PVP K30 provided high supersaturations as a spray-dried dispersion with very quick precipitation kinetics (Fig. 3B). This was not reflected by any of the screening methods. However, the melt-based screening predicted the concentration of drug dissolved after 120 min for both HME and SDD.

3.1.6. Analytical results for amorphous formulations - KTZ

All formulations manufactured either by spray-drying or hot-melt extrusion were fully amorphous according to PXRD (Supplementary 4)

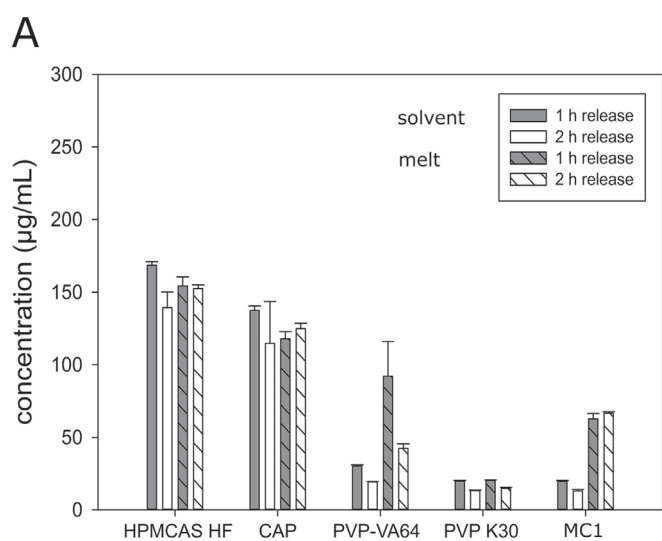


Fig. 6. A) Concentration of drug dissolved for MC1 from melt-based screening (full bars) and solvent screen (hatched bars). Dissolution in FaSSiF-V1 pH 6.5. Arithmetic means + S.D. ($n = 3$). B) Dissolution kinetics of milled extrudate and spray-dried powder with PVP-VA64 and HPMCAS HF in comparison to crystalline MC1. All formulations have a drug load of 30% (w/w) MC1. Dissolution in FaSSiF-V1 pH 6.5. Arithmetic means \pm S.D. ($n = 3$).

and DSC measurements (Supplementary 5). The amorphous form was evaluated in the first heating cycle as absence of a crystalline melting peak. Glass transition temperatures (Table 5) were determined in the second heating cycle. There were no melting peaks and only one single T_g was detected which indicated formation of a one-phase amorphous system. The T_g with different preparation methods were comparable except for CAP, where a discrepancy between the T_g of SDD and HME was detected. The chemical degradation of the CAP polymer (especially by hydrolysis of the phthalic acid group) may have been more pronounced in the HME process than during spray-drying leading to different T_g .

Content specifications were set to 95–105%, purity had to be $> 98\%$ which was met for all samples.

Particle sizes of milled extrudates and SD powder were measured with standard light under the microscope. The spray-dried particles were in the size range of 1–10 μm . Milled extrudates showed a broader particle size distribution and had sizes of 20–80 μm .

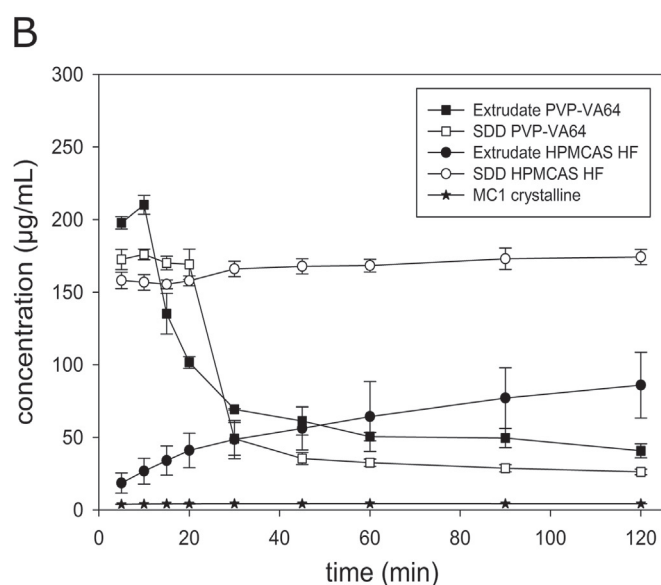
3.2. MC1

MC1 was chosen for this study as it comprises different physico-chemical properties regarding $\log P$, pKa values and intrinsic solubility compared to KTZ (Table 1). It has a high melting point of 210 $^{\circ}\text{C}$ and undergoes thermal degradation at temperatures above T_m . This has to be considered when using a heat related screening tool.

Dissolution results from the solvent-based screening and the melt-based screening were evaluated to obtain a proof of concept for the four polymers tested. The authors did not aim to find the best-suited polymer for MC1, but wanted to derive regularities for the correlation between screening and scale-up for certain polymers. Since HPMCAS did show the biggest difference in performance depending on the manufacturing technique and PVP-VA64 was underpredicted by the solvent-based screening it was decided to focus on these two excipients.

3.2.1. Screening results for polymers with 30% drug load MC1

HPMCAS HF, CAP and PVP K30 performed similarly in both screening approaches for MC1 (Fig. 6A). Film casting with HPMCAS resulted in the highest concentration of drug dissolved which was stable during dissolution and after seven days stability testing. A similar performance was seen for the CAP polymer whereas PVP K30 did not



provide a benefit in comparison to pure MC1. Again, PVP-VA64 showed much better results in the melt-based than in the solvent-based screening. The concentrations of drug dissolved with PVP-VA64 were significantly different (*t*-test, *n* = 3) between solvent- and melt-based screening for both sampling points. The dissolution results for pure MC1 were about 3-fold higher in the melt-based screening than in the solvent-based screening. For stability testing, dissolution was performed again after seven days under accelerated conditions (Supplementary 6). The concentrations of drug dissolved were similar compared to start data.

3.2.2. Scaled-up formulations with 30% drug load MC1

The extrusion process was conducted below T_m of MC1 to avoid chemical degradation. HPLC analysis with a purity indicating method did not show any API degradants. During the HME process, clear and glassy strands were formed indicating successful amorphization. Dissolution curves of HME and SD formulations with MC1 are shown in Fig. 6B.

PVP-VA64 provided very high supersaturation (> 200 $\mu\text{g}/\text{mL}$) with quick precipitation. Milled extrudate and SDD showed similar concentrations of drug dissolved and precipitation kinetics for MC1.

As already seen for KTZ there were differences in the dissolution performance when using different manufacturing techniques with HPMCAS HF. The SDD again performed better than the extrudate with high and stable concentrations of drug dissolved. All formulations provided significant solubility enhancement compared to crystalline MC1.

3.2.3. Comparison

The high supersaturations reached with PVP-VA64 in the non-sink dissolution (during the first 20 min) were not fully reflected in both screenings (Fig. 6). With respect to the quick precipitation, this is not surprising as sampling in the screenings was only conducted after 60 and 120 min. Nevertheless, the melt-based screening correctly indicated a supersaturation potential for use of PVP-VA64 as excipient in contrast to the solvent-based screening. Hence, it was possible to avoid false negative results for PVP-VA64 as already seen for KTZ (Fig. 5). The precipitation of HME and SDD corresponded to the measured decrease in concentration of drug dissolved from 60 min to 120 min in the melt-based screening. Additionally, the concentration of MC1 dissolved after 120 min in the melt-based screening was in accordance with the PVP-VA64 extrudate.

The performance of the HPMCAS SDD was correctly predicted by the solvent-based screening as expected from the good correlation results for KTZ. The melt-based screening indicated the same performance for SDD as well as for HME with HPMCAS. This was not completely reached with the HME scale-up formulation.

3.2.4. Analytical results of amorphous formulations - MC1

Formulations with 30% drug load MC1 were fully amorphous according to PXRD and DSC measurements (data not shown). Glass transition temperatures of the amorphous formulations are summarized in Table 6.

4. Discussion

An important question in the development of ASD is how to ensure that the screening tools used for polymer selection are representative for the performance of the later formulation. The discrepancy found between the solvent-based screening and the two most common manufacturing techniques for ASD (HME and SD) showed a clear need for improvement of the solvent-based screening used so far.

To discuss the differences between melt-based screening and solvent-based screening, the effect of particle sizes and surface area obtainable for wetting can be excluded to the greatest extent possible. Both screening approaches work with casted films and the contact area

between film and FaSSiF dissolution buffer nearly stays the same. In addition, the difference between solvent-based screening and melt-based screening cannot be explained by simple melting of API seed crystals which was demonstrated by inclusion of MC1. Here, the annealing temperature in the melt-based screening remained below T_m of MC1 (20 K below degradation temperature of the polymers see Table 4; API DSC thermograms see Supplementary 7). Nevertheless, there were significant differences detected between both screenings and the subsequent correlation to ASD performance.

The discrepancy between solvent-based screening and ASD was especially striking for PVP-VA64 with both compounds tested in this study. The polymer is easily extrudable with a T_g of 105 °C (Table 4) and has a high solubility in many volatile solvents. Therefore, it is a valuable formulation option for both HME as well as SD. Correspondingly, it enabled high supersaturation for both KTZ and MC1 as an extrudate as well as a SDD (Figs. 3 and 6B). However, the results of the solvent-based screening would not have indicated any benefit for using PVP-VA64 (Figs. 2 and 6A), resulting in false negative screening results unnecessarily limiting the formulation options. In contrast, the melt-based screening presented herein (Fig. 4) could demonstrate the capability of PVP-VA64 providing pronounced supersaturation. The factors that might have contributed to this improvement will be discussed in the following.

If less potent precipitation inhibitors (PIs) like the PVP derivatives are used (Konno et al., 2008), tiny seed crystals left after solvent evaporation may lead to a collapse of the amorphous system caused by crystal growth and subsequent precipitation. Additionally, PVP-VA64 solutions have low viscosities in comparison to HPMCAS and CAP at the same concentrations. As the crystal growth rate is inversely related to the solution's viscosity (Haser et al., 2017a), PVP-based systems are more prone to undergo complete API precipitation after nucleation. Therefore, PVP derivatives may especially benefit from reducing seed crystals. The additional heating step applied in the melt-based screening could thus lead to a better amorphization. Hence, by applying the method described in this study, the risk of false negative results – especially for weak PIs – is reduced.

Not only nucleation and crystal growth but also amorphous-amorphous phase separation (Luebbert et al., 2017) with API-rich clusters can cause instabilities of amorphous systems. Amorphous API clusters still present after solvent-evaporation might be dissolved and homogenized in the polymeric matrix during the additional heating step even below T_m of the API (Haser et al., 2017b; Marsac et al., 2006). Additionally, it is possible that a better dissolution of the API within the polymer is achieved by heating in case the thermodynamic solubility of the API in the polymer matrix has not been reached yet. The temperature increase enables a certain molecular mobility and subsequently might result in molecular re-orientation and formation of drug-polymer interactions as well as rearrangement of structures within the film. As the annealing step was conducted at temperatures above the T_g of the corresponding drug-polymer mixture (Tables 4, 5, 6), such effects are quite likely.

Unlike PVP-VA64, PVP K30 did not stand out in any of the screenings for the different APIs. Indeed, it showed a high supersaturation as SDD with 40% KTZ at the beginning (Fig. 3B). The higher initial supersaturation of the spray-dried powder compared to HME may be caused by smaller particle sizes, bigger surface area and different morphology. Subsequently, the dissolved drug precipitated quickly which was not inhibited by the polymer. This could demonstrate a weak point of these screening tools in general. The impact of particle size, porosity or morphology of spray-dried particles or milled extrudates is not reflected. Furthermore, the sampling frequency is too low to capture a complete dissolution profile. Nevertheless, it is still reasonable to focus on sampling after 60 and 120 min as the supersaturation needs to be maintained at a certain level throughout the absorption window to effectively increase the bioavailability (Price et al., 2018).

Wyttenbach et al. have also used different preparation techniques in the SPADS assays for dissolution, interaction and imaging. In the imaging assay established by Lauer et al. (Lauer et al., 2011), samples prepared via quench-cooling melt mixtures were assessed by atomic force microscopy. The assay did not predict phase separation for 20% drug load with PVP-VA64. In contrast, the spray-dried powder used for stability testing did so after six months storage at 40 °C/75% relative humidity. Hence, there were differences seen in stability of ASD depending on the manufacturing technique which has of course an impact on dissolution behavior. However, the formulations were not scaled-up by means of HME to further examine this effect.

In contrast to PVP derivatives, there was an excellent correlation between solvent-based screening and SDD performance seen for the cellulose derivatives with both KTZ and MC1 (Figs. 5 and 6). HPMCAS is known as one of the best PIs (Alonzo et al., 2011), reliably stabilizing the API in its supersaturated state during dissolution which was also seen in this study (Figs. 3B and 6B). This allows for the assumption that seed crystals which might be present in the solid dispersion films pose a lower risk for crystal growth and precipitation still leading to a good correlation between solvent-based screening and SDD (Figs. 5 and 6). However, it did not provide a satisfying correlation to HME formulations (Figs. 3A and 6B) which was only achieved with the melt-based screening. Such a different behavior between HME and SDD might be related to different structures within the amorphous phase (Shalaev and Zograf, 2002) depending on the manufacturing process. The generation of an ASD leads to destruction of the API's long-range order. Nevertheless, short-range orders may still vary depending on the manufacturing technique which was already found by Surana et al. (Surana et al., 2004).

It is well known that both HPMCAS and CAP undergo certain degradation effects like loss of acidic groups (phthalate, acetate, succinate) even below their degradation temperature (Sarode et al., 2014). The melt-based screening provides the possibility to reveal such degradation effects or incompatibilities between polymer and API or API degradation during heating. This can be measured by dissolving the molten films and analyzing drug content and purity via RP-HPLC and is a valuable information for the next step of ASD manufacturing. No such effects were observed for the APIs tested in this study.

5. Conclusion

As the amount of API during drug product development is often very limited, broad feasibility studies for development of ASD with many different polymers are not possible. This study demonstrated how small-scale screening results may differ from performance of scaled up HME and SDD formulations. Since screening methods are intended for polymeric carrier selection for further development, they should mimic the relevant processes as much as possible.

The simple solvent-based screening method gave false negative results for PVP-VA64, leading to exclusion as a potential polymeric carrier. By applying the herein described melt-based screening method, such discrepancies can be minimized. Furthermore, by conducting both the solvent-based screening and the refined melt-based screening, it is possible to anticipate the in-vitro performance of HME vs. SDD with minimal investments of API. The different ways to perform a miniaturized screening might already reflect the processes and interactions that are formed during SD or HME. As these are the most established manufacturing techniques for ASD this can be of great value for the decision which manufacturing process to choose. A more accurate ranking of polymers in terms of their potential to provide and stabilize supersaturation of an API in non-sink dissolution is the consequence, guiding the formulation scientist towards the best suited excipient and manufacturing technique.

Acknowledgement

The authors gratefully acknowledge Michael Lange for his analytical support in conducting the PXRD measurements and Robert Hennig, Magdalena Münster, Markus Riehl and Peter Tate for the scientific discussion.

Declaration of interest

The authors declare that they have no conflict of interest. This research did not receive any specific grant from funding agencies in the public, commercial or not-for-profit sectors.

Appendix A. Supplementary data

Supplementary data to this article can be found online at <https://doi.org/10.1016/j.ejps.2018.08.035>.

References

- Agrawal, A.M., Dudhedia, M.S., Patel, A.D., Raikes, M.S., 2013. Characterization and performance assessment of solid dispersions prepared by hot melt extrusion and spray drying process. *Int. J. Pharm.* 457, 71–81.
- Alonzo, D.E., G.Y., Zhou, D., Mo, H., Zhang, G.G., Taylor, L.S., 2011. Dissolution and precipitation behavior of amorphous solid dispersions. *J. Pharm. Sci.* 100, 3316–3331.
- Amidon, G.L., L.H., Shah, V.P., Crison, J.R., 1995. A theoretical basis for a biopharmaceutical drug classification: the correlation of in vitro drug product dissolution and in vivo bioavailability. *Pharm. Res.* 12, 413–420.
- Baird, J.A., Thomas, L.C., Aubuchon, S.R., Taylor, L.S., 2013. Evaluating the non-isothermal crystallization behavior of organic molecules from the undercooled melt state using rapid heat/cool calorimetry. *CrystEngComm* 15, 111–119.
- Banda, A., Manchanda, A., Zhang, W., Alba, G.M., Nagapudi, K., 2018. Comparative assessment of miniaturized screening approaches for selection of polymers for amorphous drug stabilization. *J. Pharm. Sci.* 107, 897–908.
- Beneš, M., Pekárek, T., Beránek, J., Havlíček, J., Krejčík, L., Šimek, M., Tkadlecová, M., Doležal, P., 2017. Methods for the preparation of amorphous solid dispersions – a comparative study. *J. Drug Delivery Sci. Technol.* 38, 125–134.
- Bhardwaj, V., Trasi, N.S., Zemlyanov, D.Y., Taylor, L.S., 2018. Surface area normalized dissolution to study differences in itraconazole-copovidone solid dispersions prepared by spray-drying and hot melt extrusion. *Int. J. Pharm.* 540, 106–119.
- Bhugra, C., Telang, C., Schwabe, R., Zhong, L., 2016. Reduced crystallization temperature methodology for polymer selection in amorphous solid dispersions - stability perspective. *Mol. Pharm.* 13, 3326–3333.
- Blaabjerg, L.I., Lindenberg, E., Löbmann, K., Grohgan, H., Rades, T., 2016. Glass forming ability of amorphous drugs investigated by continuous cooling and isothermal transformation. *Mol. Pharm.* 13, 3318–3325.
- Blaabjerg, L.I., Lindenberg, E., Rades, T., Grohgan, H., Löbmann, K., 2017. Influence of preparation pathway on the glass forming ability. *Int. J. Pharm.* 521, 232–238.
- Blaabjerg, L.I., Lindenberg, E., Löbmann, K., Grohgan, H., Rades, T., 2018. Is there a correlation between the glass forming ability of a drug and its supersaturation propensity? *Int. J. Pharm.* 538, 243–249.
- Chen, R., Ilassi, N., Sekulic, S.S., 2011. Absolute molecular weight determination of hypromellose acetate succinate by size exclusion chromatography: use of a multi angle laser light scattering detector and a mixed solvent. *J. Pharm. Biomed. Anal.* 56, 743–748.
- Chiang, P.-C., Ran, Y., Chou, K.-J., Cui, Y., Sambrone, A., Chan, C., Hart, R., 2012. Evaluation of drug load and polymer by using a 96-well plate vacuum dry system for amorphous solid dispersion drug delivery. *AAPS PharmSciTech* 13, 713–722.
- Dai, W.-G., Dong, L.C., Li, S., Pollock-Dove, C., Chen, J., Mansky, P., Eichenbaum, G., 2007. Parallel screening approach to identify solubility-enhancing formulations for improved bioavailability of a poorly water-soluble compound using milligram quantities of material. *Int. J. Pharm.* 336, 1–11.
- Haser, A., Cao, T., Lubach, J., Listro, T., Acquarulo, L., Zhang, F., 2017a. Melt extrusion vs. spray drying: the effect of processing methods on crystalline content of naproxen-povidone formulations. *Eur. J. Pharm. Sci.* 102, 115–125.
- Haser, A., Huang, S., Listro, T., White, D., Zhang, F., 2017b. An approach for chemical stability during melt extrusion of a drug substance with a high melting point. *Int. J. Pharm.* 524, 55–64.
- Joe, J.H., Lee, W.M., Park, Y.-J., Joe, K.H., Oh, D.H., Seo, Y.G., Woo, J.S., Yong, C.S., Choi, H.-G., 2010. Effect of the solid-dispersion method on the solubility and crystalline property of tacrolimus. *Int. J. Pharm.* 395, 161–166.
- Kawakami, K., 2009. Current status of amorphous formulation and other special dosage forms as formulations for early clinical phases. *J. Pharm. Sci.* 98, 2875–2885.
- Kolter, K., K.M., Grycze, A., 2012. Hot-melt Extrusion with BASF Pharma Polymers.
- Konno, H., Handa, T., Alonzo, D.E., Taylor, L.S., 2008. Effect of polymer type on the dissolution profile of amorphous solid dispersions containing felodipine. *Eur. J.*

- Pharm. Biopharm. 70, 493–499.
- Lauer, M.E., Grassmann, O., Siam, M., Tardio, J., Jacob, L., Page, S., Kindt, J.H., Engel, A., Alsenz, J., 2011. Atomic force microscopy-based screening of drug-excipient miscibility and stability of solid dispersions. *Pharm. Res.* 28, 572–584.
- Leuner, C., Dressman, J., 2000. Improving drug solubility for oral delivery using solid dispersions. *Eur. J. Pharm. Biopharm.* 50, 47–60.
- Luebbert, C., Huxoll, F., Sadowski, G., 2017. Amorphous-amorphous phase separation in API/polymer formulations. *Molecules* 22, 296.
- Marsac, P.J., Shamblin, S.L., Taylor, L.S., 2006. Theoretical and practical approaches for prediction of drug–polymer miscibility and solubility. *Pharm. Res.* 23, 2417.
- Miller-Chou, B.A., Koenig, J.L., 2003. A review of polymer dissolution. *Prog. Polym. Sci.* 28, 1223–1270.
- Mullin, J.W., 2012. Crystallization and Precipitation. *Ullmann's Encyclopedia of Industrial Chemistry*.
- Navnit Shah, H.S., Choi, Duk Soon, Chokshi, Hitesh, Malick, A.Waseem, 2014. *Amorphous Solid Dispersions*. Springer.
- Price, D.J., Ditzinger, F., Koehl, N.J., Jankovic, S., Tsakiridou, G., Nair, A., Holm, R., Kuentz, M., Dressman, J.B., Saal, C., 2018. Approaches to increase mechanistic understanding and aid in the selection of precipitation inhibitors for supersaturating formulations – a PEARRL review. *J. Pharm. Pharmacol.*
- Prudic, A., Ji, Y., Sadowski, G., 2014. Thermodynamic phase behavior of API/polymer solid dispersions. *Mol. Pharm.* 11, 2294–2304.
- Rask, M.B., Knopp, M.M., Olesen, N.E., Holm, R., Rades, T., 2018. Comparison of two DSC-based methods to predict drug-polymer solubility. *Int. J. Pharm.* 540, 98–105.
- Repka, M.A., Bandari, S., Kallakunta, V.R., Vo, A.Q., McFall, H., Pimparade, M.B., Bhagurkar, A.M., 2018. Melt extrusion with poorly soluble drugs – an integrated review. *Int. J. Pharm.* 535, 68–85.
- Sarode, A.L., Obara, S., Tanno, F.K., Sandhu, H., Iyer, R., Shah, N., 2014. Stability assessment of hypromellose acetate succinate (HPMCAS) NF for application in hot melt extrusion (HME). *Carbohydr. Polym.* 101, 146–153.
- Shalaev, E., Zografi, G., 2002. The concept of ‘structure’ in amorphous solids from the perspective of the pharmaceutical sciences. In: Levine, H. (Ed.), *Amorphous Food and Pharmaceutical Systems*. The Royal Society of Chemistry, pp. 11–30.
- Shanbhag, A., Rabel, S., Nauka, E., Casadevall, G., Shivanand, P., Eichenbaum, G., Mansky, P., 2008. Method for screening of solid dispersion formulations of low-solubility compounds—miniaturization and automation of solvent casting and dissolution testing. *Int. J. Pharm.* 351, 209–218.
- Surana, R., Pyne, A., Suryanarayanan, R., 2004. Effect of preparation method on physical properties of amorphous trehalose. *Pharm. Res.* 21, 1167–1176.
- Uhlmann, D.R., 1972. A kinetic treatment of glass formation. *J. Non-Cryst. Solids* 7, 337–348.
- Van Eerdenbrugh, B., Taylor, L.S., 2011. An ab initio polymer selection methodology to prevent crystallization in amorphous solid dispersions by application of crystal engineering principles. *CrystEngComm* 13, 6171–6178.
- Vandercruys, R., Peeters, J., Verreck, G., Brewster, M.E., 2007. Use of a screening method to determine excipients which optimize the extent and stability of supersaturated drug solutions and application of this system to solid formulation design. *Int. J. Pharm.* 342, 168–175.
- Wytenbach, N., Kuentz, M., 2017. Glass-forming ability of compounds in marketed amorphous drug products. *Eur. J. Pharm. Biopharm.* 112, 204–208.
- Wytenbach, N., Janas, C., Siam, M., Lauer, M.E., Jacob, L., Scheubel, E., Page, S., 2013. Miniaturized screening of polymers for amorphous drug stabilization (SPADS): rapid assessment of solid dispersion systems. *Eur. J. Pharm. Biopharm.* 84, 583–598.
- Yamashita, T., Ozaki, S., Kushida, I., 2011. Solvent shift method for anti-precipitant screening of poorly soluble drugs using biorelevant medium and dimethyl sulfoxide. *Int. J. Pharm.* 419, 170–174.



How changes in molecular weight and PDI of a polymer in amorphous solid dispersions impact dissolution performance



Carolin Auch^{a,b}, Meike Harms^b, Karsten Mäder^{a,*}

^a Institute of Pharmacy, Faculty I of Natural Sciences, Martin Luther University Halle-Wittenberg, Wolfgang-Langenbeck-Str. 4, 06120 Halle/Saale, Germany

^b Department of Pharmaceutical Technologies, Merck KGaA, Frankfurter Straße 250, 64293 Darmstadt, Germany

ARTICLE INFO

Keywords:

Amorphous solid dispersion
Molecular weight
Polymer degradation
Multi-angle light scattering
Hot-melt extrusion
PVP-VA64

ABSTRACT

Polymers functionally contribute to supersaturation and precipitation inhibition of the active pharmaceutical ingredient (API) in amorphous solid dispersions (ASD). Therefore, it is necessary to monitor physicochemical changes of the polymeric carrier caused by the manufacturing process. This is especially important when the material is exposed to heat and shear stress as in case of hot-melt extrusion (HME). This study evaluated the impact of HME process conditions on physical characteristics of poly(vinylpyrrolidone-co-vinyl-acetate) 60:40 (PVP-VA64) which is a widely used polymer for HME. Focus was set on molecular weight (M_w) and polydispersity index (PDI), by means of absolute molar mass detection via multi-angle light scattering. The generation of a high M_w fraction together with a decrease of the average M_w was detected. In a next step, the influence of these changes on the dissolution behavior of ASD was evaluated. Different stress conditions were applied onto PVP-VA64 in placebo extrusions. The obtained stressed polymer samples were subsequently used to prepare verum ASD with ketoconazole by spray drying (SD). SD dispersions (SDD) of thermally stressed PVP-VA64 were compared to SDD prepared with bulk powder. Although there were only slight changes in M_w and PDI, they significantly impacted supersaturation and precipitation of the formulation.

1. Introduction

One of the key areas that evolved for application of polymeric excipients is the use as matrices in solid dispersions (Chiou and Riegelman, 1971). The inherently thermodynamically unstable amorphous form of the active pharmaceutical ingredient (API) is stabilized by incorporation into a polymeric matrix. Hence, polymers functionally contribute to overcome the poor aqueous solubility of the API and improve its bioavailability (Leuner and Dressman, 2000). The beneficial effects of polymers in the formulation of amorphous solid dispersions (ASD) have been widely examined (Baghel et al., 2016). Suitable polymers must be selected carefully e.g. in terms of drug-polymer miscibility and solubility of the API within the polymer (Marsac et al., 2008; Pezzoli et al., 2018), glass transition temperature (T_g),

degradation temperature (T_{deg}), hygroscopicity and drug-polymer interaction sites (Lubach and Hau, 2018; Mori et al., 2018) amongst others. Furthermore, the choice of the manufacturing process necessitates different excipient properties. The ratio between T_g and T_{deg} affects the processing window in hot-melt extrusion (HME) and a high solubility in volatile solvents is needed for time and cost-efficient spray-drying (Shah et al., 2014).

HME is one of the most widely used manufacturing techniques for ASD which is also seen in an increasing number of patents (Crowley et al., 2007). It has considerable advantages over other ASD technologies like being a solvent-free and continuous process (Haser and Zhang, 2018) and is widely applicable for drug product formulation as summarized by Repka et al. (Repka et al., 2018). However, both API and polymer could undergo changes in their properties (and as a result, in

Abbreviations: ACN, acetonitrile; API, active pharmaceutical ingredient; ASD, amorphous solid dispersion; DCM, dichloromethane; DMF, N,N-dimethylformamide; dn/dc, refractive index increment; DL, drug load; DSC, differential scanning calorimetry; FaSSIF, fasted-state simulated intestinal fluid; GPC, gel permeation chromatography; HME, hot-melt extrusion; KTZ, ketoconazole; LiBr, lithium bromide; MALS, multi-angle light scattering; MeOH, methanol; M_w , weight-averaged molecular weight; NMR, nuclear magnetic resonance; PDI, polydispersity index; Ph.Eur., European Pharmacopoeia; PM, physical mixture; PS, polystyrene; PVP, polyvinylpyrrolidone; PVP-VA64, poly(vinylpyrrolidone-co-vinyl-acetate) 60:40; PXRD, powder X-ray diffraction; RI, refractive index; RP-HPLC, reversed-phase high-performance liquid chromatography; SD, spray-drying; SDD, spray-dried dispersion; T_{deg} , degradation temperature; T_g , glass transition temperature; T_m , melting temperature; TGA, thermogravimetric analysis; TMS, tetramethylsilane

* Corresponding author.

E-mail addresses: carolin.auch@merckgroup.com (C. Auch), karsten.maeder@pharmazie.uni-halle.de (K. Mäder).

<https://doi.org/10.1016/j.ijpharm.2018.12.012>

Received 30 October 2018; Received in revised form 5 December 2018; Accepted 7 December 2018

Available online 13 December 2018

0378-5173/ © 2018 Elsevier B.V. All rights reserved.

the properties of the solid dispersion) as heat and shear stress are applied on the sample. Therefore, it is necessary to monitor physicochemical properties of both drug and polymer in a HME process to ensure thermal stability of the system.

There are numerous analytical methods to assess ASD (Baghel et al., 2016; Crowley et al., 2007; Repka et al., 2018; Shah et al., 2014; Zografi and Newman, 2017). ASD put high requirements on comprehensive characterization due to the analytical complexity (Paudel et al., 2014). As ASD are multicomponent systems, it is often difficult to correlate certain effects (e.g. dissolution variability) unambiguously to the causative component. This might be of practical relevance e.g. in scale-up trials when one must elucidate which changes affected the performance of the formulation.

The different analytical techniques include thermoanalysis like differential scanning calorimetry (DSC) or thermogravimetric analysis (TGA) and spectroscopic techniques like powder X-ray diffraction (PXRD) and microscopy to analyze the amorphization efficiency and surface properties. Raman or infrared spectroscopy as well as solid-state nuclear magnetic resonance (NMR) can be utilized to detect interactions between drug and polymeric carrier at a molecular level. Dynamic vapor sorption is often applied to estimate hygroscopicity and stability during different storage conditions whereas chemical degradation can be detected by reversed-phase high-performance liquid chromatography (RP-HPLC). With regard to HME, rheological evaluations (Liu et al., 2012; Sarode et al., 2013) are valuable tools to evaluate melt viscosities and softening temperatures. DSC and TGA are commonly used to elucidate the thermal behavior of polymers prior to HME but they neglect the energy input by shear stress and are therefore not directly accountable for the effects in an extruder. Additionally, apparent melt temperatures and conditions within the barrel zones are still hardly accessible. There are different modeling approaches (Bochmann et al., 2018; Eitzlmayr et al., 2014; Reitz et al., 2013; Schittny et al., 2018; Zecevic et al., 2018) to estimate effects in the extruder, but experimental data is mostly missing.

Specific polymeric properties have been overlooked for a long time but are now attracting deservedly more interest in the field of ASD. Frank et al. (Frank and Matzger, 2018) examined the influence of polymeric side chain functionalities and respective drug-polymer interactions on recrystallization behavior. The influence of molecular weight (M_w) on ASD properties in a macromolecular scale (Prudic et al., 2014) especially for polyvinylpyrrolidone (PVP) derivatives (Knopp et al., 2015; Pacuř et al., 2018) has been subject to different studies.

During the HME process, it may come to both chain-scission and cross-linking with regard to the polymeric backbone (Lang et al., 2014). In addition, chemical degradation and hydrolysis of side-chain functionalities are possible (Jiannan et al., 2018; Sarode et al., 2014). The chemical stability of polymers was occasionally assessed (Karandikar et al., 2015; Sarode et al., 2014) by TGA or RP-HPLC. One of the seldom gel permeation chromatography (GPC) studies associated with HME (Crowley et al., 2002) examined the thermal stability of polyethylene oxide. There, the weight averaged M_w was found to be dependent on processing temperature and screw speed. The use of plasticizers, like e.g. Vitamin E TPGS, can of course prevent or reduce polymer degradation in the HME process (Repka and McGinity, 2000) but again increases the complexity of the formulation.

Table 1
Physicochemical properties of KTZ.

Compound	M_w (g/mol)	logP	T_m (°C)	T_g (°C)	pKa	Solubility in FaSSiF ($\mu\text{g/mL}$)
Ketoconazole	531.4 ^b	4.3 ^b	149 ± 0.1 ^a	44 ± 0.2 ^a	6.51; 2.94 ^b	22.2 ± 0.70 ^c

^a In-house determination of T_m and T_g as onset values from raw materials using a standard DSC method (2.6) with heating and cooling rates of ± 10 K/min, arithmetic means of $n \geq 3 \pm$ S.D.

^b Extracted from PubChem database (<https://pubchem.ncbi.nlm.nih.gov/>).

^c Solubility of crystalline drug in FaSSiF-V1, pH 6.5 at 37 °C, arithmetic mean of $n = 3 \pm$ S.D. after 2 h under non-sink dissolution conditions (2.8).

Although there exist several analytical techniques for ASD, the analysis of M_w and polydispersity index (PDI) of the polymeric carrier is often neglected despite their crucial importance in polymer analysis. GPC is the most commonly used technique for determination of M_w , but it still is not considered as a standard analytical technique in the field of ASD. Especially when it comes to minute changes induced by the manufacturing process, highly sensitive analytical techniques are required. To date, size standards or relative calibration are mostly used to determine M_w (Izunobi and Higginbotham, 2011; Suárez et al., 2013). This can only be considered as an approximation since the underlying separation principle is based on the molecule's hydrodynamic radius where solvation effects and coiling of the investigated sample influence the elution volume. Moreover, calibration standards are often not readily available. A more precise and accurate method to determine M_w was found with the development of multi-angle-light scattering (MALS) in combination with refractive index (RI) detection by (Wyatt, 1993). Here, absolute molar masses are determined which does not require monodisperse calibration standards. Furthermore, LS allows for determination of the molecular dimensions of a molecule in solution by absolute measurement of the radius of gyration (r_g). The RI detector has the additional benefit of measuring concentrations also for UV inactive molecules, which is the case for many polymers.

The polymer poly(vinylpyrrolidone-co-vinyl acetate) 60:40 (PVP-VA64) was chosen in this study to show how changes in M_w and PDI might impact the dissolution performance of ASD as it has an outstanding position as a polymeric carrier for ASD. With Kaletra®, it was used as excipient in one of the first marketed ASD products. PVP-VA64 is also widely used in several other marketed ASD (Wytttenbach and Kuentz, 2017). It is easily extrudable with a T_g of about 104 °C and it is considered as chemically stable during the HME process up to its T_{deg} . The PVP-VA64 monograph in the European Pharmacopoeia (Ph.Eur., 2018a) contains a section on functionality-related characteristics where viscosity, particle size distribution and density are mentioned as parameters that are “known to be relevant for certain uses of the excipient” (Ph.Eur., 2018b). That said, since viscosity is directly dependent on the M_w and mass distribution, M_w is also an important quality control parameter for polymers.

As the complexity of ASD and the multiple connections between API and its carrier make it hard to elucidate single influence factors, it was the aim of this study to investigate the polymer characteristics separately from API amorphization. M_w and PDI of PVP-VA64 should be examined as such quality parameters and the impact on the dissolution performance of the resulting drug product intermediate should be investigated. The experiments were mostly conducted in small-scale experiments to minimize API consumption.

To our knowledge, this is the first time that GPC-MALS-RI analysis was applied to monitor minute changes of PVP-VA64 caused by the extrusion process and to transfer these findings to the dissolution performance of ASD intermediates.

2. Materials and methods

2.1. Materials

Ketoconazole (KTZ) was purchased from Biotrend Chemicals AG

(Switzerland). Table 1 contains its physicochemical properties. Poly (vinylpyrrolidone-co-vinyl acetate) 60:40 (PVP-VA64) was supplied by BASF (Germany) with a K-value (1% in water) of 25–31 (Kolter and Gryczke, 2012). Simulated intestinal fluid (SIF) powder for the preparation of fasted-state SIF V1 (FaSSIF-V1) pH 6.5 was obtained from Biorelevant.com (UK). Silicone oil (10 cSt, $n_{20,D} = 1.403$, lit.) was acquired from Aldrich Chemistry. Sodium hydroxide (VWR Chemicals, Belgium), sodium chloride, di-sodium hydrogen phosphate, hydrochloric acid 1 M and sodium hydroxide solution 1 M (Merck KGaA, Germany) for preparation of the dissolution buffer were used in analytical grade. Anhydrous lithium bromide (LiBr, Alfa Aesar, USA) was used as additive for GPC analysis. N,N-Dimethylformamide (DMF, Alfa Aesar, USA) was of HPLC grade (purity $\geq 99.7\%$), filtered through 0.2 μm to avoid particles for GPC analysis. Acetonitrile (ACN), dichloromethane (DCM) and methanol (MeOH) were purchased from Merck KGaA, Germany. Purified water was obtained from a Millipore-Milli-Q® integral water purification system (Millipore Merck KGaA, Germany).

2.2. Experimental design

Fig. 1 schematically illustrates the experimental setup of this study. PVP-VA64 bulk powder was extruded on a small-scale extruder (Section 2.4.1) with three different temperature profiles (resulting in Ex 130, Ex 160, Ex 180) and subject to M_w and PDI analysis (Section 2.3). Afterwards, verum formulations with 40% (w/w) drug load (DL)

ketoconazole (KTZ) and either the obtained pre-stressed PVP-VA64 samples (resulting in SDD 130, SDD 160, SDD 180) or unprocessed PVP-VA64 bulk powder (SDD Bulk) were prepared by spray-drying according to Section 2.4.3. This approach was chosen as a model to evaluate degradation effects of the polymer separately from API amorphization. An impact on incorporation of the API due to different temperatures in the extrusion process (e.g. above and below the melting point (T_m) of KTZ) should be avoided. Therefore, spray-drying (SD) was used instead of HME for subsequent incorporation of the API to have identical and comparably low heat and shear stress during the preparation of the verum ASD.

Three references were selected to show the applicability of the experimental design. The first one was a physical mixture (PM) of PVP-VA64 bulk powder with 40% DL KTZ which was extruded in small-scale (ExPM 160, Section 2.4.1) in a one-step process. Second, a placebo spray-drying experiment was conducted to check for changes due to the spray-drying process (SDD Placebo). Last, relevance of the findings for manufacturing scale should be demonstrated. Therefore, PVP-VA64 that was pre-stressed on a Leistritz 18 mm extruder (Ex Scale-Up, Section 2.4.2) was used for preparation of the verum spray-dried dispersion (SDD Scale-Up).

2.3. GPC-MALS-RI analysis

A triple detector system consisting of UV, refractive index (RI, Optilab® T-rEX™, Wyatt Technology Corporation, USA) and multi-angle

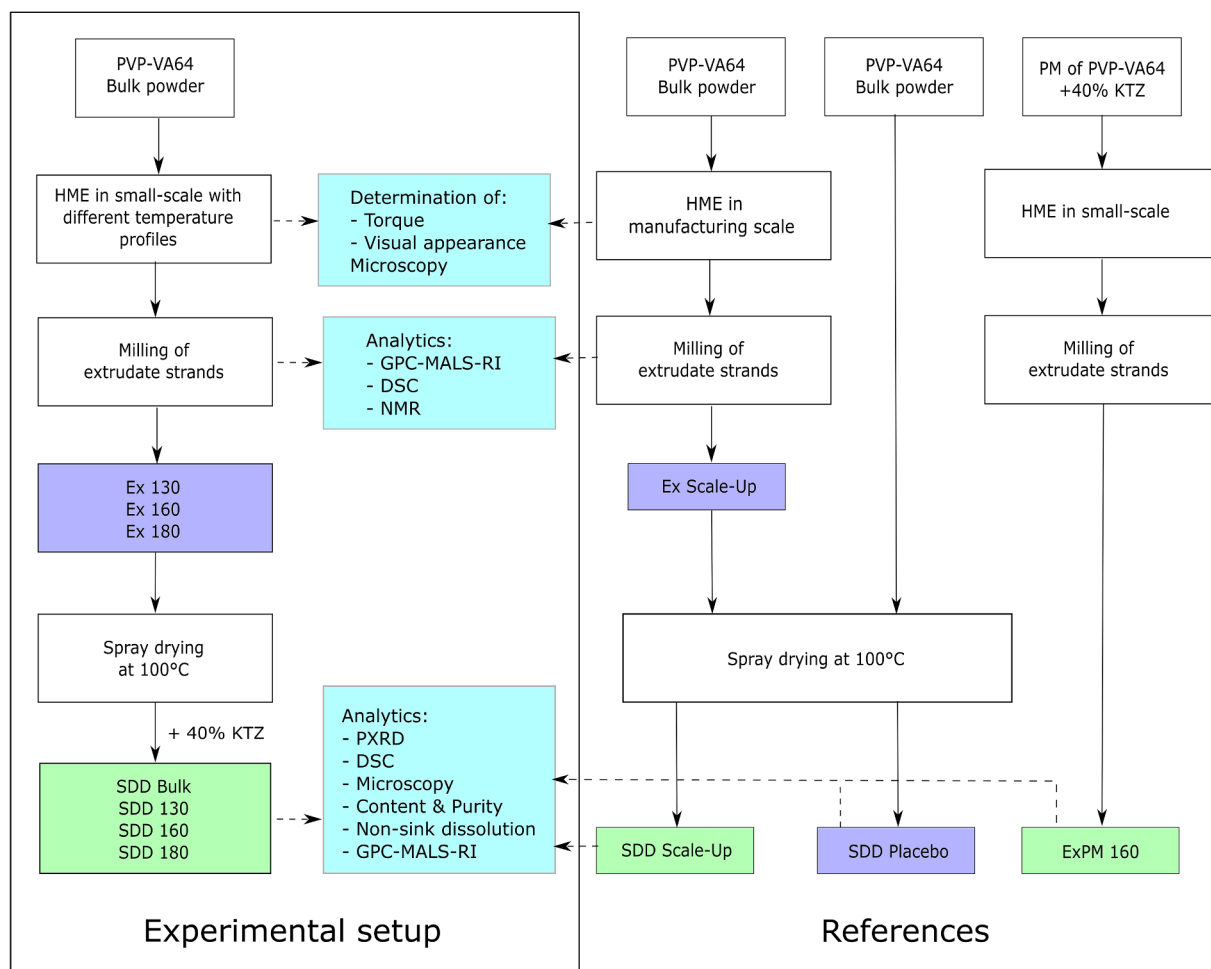


Fig. 1. Schematic illustration of experiments conducted in this study. Analytical steps are depicted in turquoise, placebo samples are depicted in violet and verum formulations are highlighted in green. References did not undergo the full analytical setup, depending on purpose. (For interpretation of the references to colour in this figure legend, the reader is referred to the web version of this article.)

light scattering (MALS, DAWN® Heleos™ II, Wyatt) with 18 angles was used for the analysis of M_w and PDI of the polymer. The correlation between LS intensity and M_w is given by Equation (1)

$$\frac{K \times c}{R_0} = \frac{1}{M_w \times P(\theta)} + 2 \times A_2 \times c \quad (1)$$

with R_0 as the Rayleigh ratio, A_2 as the second virial coefficient, c is defined as solute concentration in g/mL, $P(\theta)$ is a form factor relating the angular variation in scattering intensity to the mean square radius of the particle and M_w is the molecular weight.

K is a physical constant for polarized light defined according to Equation (2).

$$K = \frac{4\pi \times \left(\frac{dn}{dc}\right)^2 \times n_0^2}{N_a \times \lambda_0^4} \quad (2)$$

dn/dc is the refractive index increment of the sample, n_0 is the specific refractive index of the sample in mL/g, N_a is the Avogadro's number and λ_0 is defined as the vacuum wavelength of the incident laser. Theory and background of these equations are described in detail by (Wyatt, 1993).

A 1260 Agilent HPLC system was used for size-dependent separation of the polymer equipped with a TSK-GEL® Alpha-4000 GPC column (Tosoh Bioscience GmbH, Germany) with an exclusion limit of 10^6 Da (polystyrene (PS) in tetrahydrofuran). N,N-Dimethylformamide (DMF) with the addition of 10 mM LiBr to avoid polyelectrolyte interaction effects was used as solvent and eluent. All samples were dissolved in this solvent and stirred for 12 h at 150 rpm. 50 μ L of sample at a concentration of 4 mg/mL were injected and eluted with an isocratic pump rate of 0.5 mL/min over 40 min. An inline PTFE filter was installed to ensure particle-free analysis.

The refractive index increment (dn/dc) was acquired via stand-alone measurement with the RI detector. A calibration curve with concentrations of 0.5, 1.0, 2.0, 3.0 and 4.0 mg/mL was used. dn/dc values were determined in triplicate with an average of $0.0730 \text{ mL/g} \pm 0.0006$ (exemplary determination with $R^2 = 1.000$ see Supplementary Material Fig. S1) for PVP-VA64. The RI detector was set to 25 °C, the MALS detector operated at room temperature. Both detectors (RI and MALS) used a wavelength of 658 nm. The MALS detector was calibrated with toluene (90° diode, LS 11). Normalization coefficients, alignment and band broadening were determined with a 30 kDa PS standard (P8402-03001B, batch#80317, Wyatt Technology, USA). The molecular weight was defined with 28.5 ± 0.03 kDa and a PDI of 1.01 ± 0.01 according to certificate of analysis. All measurements were conducted with $n = 4$. The eluted peak was divided into three sections: 1) total peak for calculation of mass recovery, 2) main peak with good separation for determination of M_w and PDI, 3) high molecular weight fraction. This definition was held constant through all runs and is exemplarily shown for PVP-VA64 bulk powder in Fig. 2. Fig. 3 shows the molar mass plot for peak 2 of PVP-VA64 bulk powder with an ideal continuous molar mass distribution as targeted for polydisperse samples without column interactions.

The term molecular weight (M_w) always describes the weight-averaged molecular weight and will be consistently used as M_w from now on according to this definition.

2.4. Manufacturing of amorphous solid dispersion

2.4.1. Hot-melt extrusion – small-scale

Hot-melt extrusion was conducted on a small-scale twin-screw extruder (ZE5, ThreeTec, Switzerland) with 5 mm screw diameter and three heating zones. The extruder was equipped with double-concave co-rotating screws consisting of conveying elements and a 1.0 mm die. The feeding zone was constantly cooled to 12.5 °C with a cryostat (WK4600, Lauda, Germany), powder was fed manually. Extrusion temperatures were adjusted according to Table 2, a screw speed of 300 rpm was maintained.

The physical mixture for ExPM 160 was intimately mixed with mortar and pestle and subsequently homogenized by mixing in a Turbula® (Willy A. Bachofen, Germany) mixer for 15 min. The physical mixture was subject to HPLC analysis ($n = 4$, Section 2.9) to ensure content uniformity. The resulting strands were milled with a vibrational ball mill (Pulverisette 23, Fritsch, Germany) at 30 Hz for 2×2 min.

2.4.2. Hot-melt extrusion – manufacturing scale

Placebo extrusion in manufacturing scale was conducted on a Leistritz ZSE18 twin-screw extruder (L/D ratio 40:1) with two kneading zones and a process temperature of 160 °C with 600 rpm. Two venting ports were part of the barrel configuration in zones 3 and 7 and a 10 mm die was used. Feeding was conducted with a gravimetric feeder (KT20, Coperion) with a throughput of 6 kg/h. Cooling was realized with a water circulation system set to 15 °C. The extrudate (Ex Scale-Up) was subsequently milled with a L1A Fitzmill (Fitzpatrick, USA).

2.4.3. Spray-drying

API-polymer mixtures (40% DL (w/w) with respect to polymer) were dissolved in DCM:MeOH 9:1 (v/v) to result in a concentration of 2% (w/w) solid content. PVP-VA64 bulk powder as well as thermally stressed extrudates (Ex 130, Ex 160, Ex 180, Section 2.4.1 and Ex Scale-Up, Section 2.4.2) were used. Spray-dried dispersions (SDD) were prepared on a 4 M8-TriX Formatrix Spray Dryer (ProCepT, Belgium). The spray-dryer was set up with a 1.0 mm nozzle, 10 L/min atomizing nitrogen and 70% air speed. Air temperature and feed rate were adjusted to obtain fully amorphous (SDD). The outlet temperature varied slightly (Table 3), the cyclone pressure drop was constant at approximately 56 mbar. Spray-dried powders were dried in a desiccator over silica gel at 100 mbar overnight to ensure removal of residual solvents (residual DCM and MeOH were quantified by solution NMR). Content analytics were conducted with $n = 4$ according to Section 2.9. The samples were additionally analyzed via DSC (Section 2.6) and PXRD (Section 2.7).

2.5. Nuclear-magnetic resonance (NMR)

PVP-VA64 placebo samples (bulk powder, Ex 130, Ex 160, Ex 180) were dried in a vacuum oven at 60 °C for 24 h to reduce water content of the hygroscopic PVP-VA64. Residual water was measured by loss on drying with an infrared balance. The samples were dissolved in deuterated chloroform (CDCl_3) containing tetramethylsilane (TMS) for signal referencing. The sample solution (final concentration 10 mg/mL) was transferred into a 5 mm NMR sample tube. ^1H and heteronuclear single quantum coherence (HSQC) measurements were performed on a 700 MHz Bruker Avance III machine equipped with a TCI cryocooled probe. For the ^1H spectra the relaxation delay was set to 10 s to allow quantitative analysis. Measurements were conducted at 298 K.

To analyze if ester hydrolysis occurred during extrusion, the integrals of ester CH_3 groups and $\alpha\text{-CH}_2$ group vs. amide CH_2 group of the pyrrolidone ring were compared. It was assessed whether this ratio changed between PVP-VA64 bulk powder and the different extrudates.

2.6. Differential scanning calorimetry (DSC)

DSC measurements were conducted on a DSC 1 (Mettler Toledo, Switzerland). The samples were exactly weighed into 100 μ L DSC aluminum crucibles without pin. The first heating ramp reached from 25 °C up to 170 °C (above T_m of KTZ), afterwards the melt was cooled down to 0 °C and heated again up to 200 °C. Heating and cooling were conducted with ± 10 K/min.

Glass transition temperatures (T_g) were determined as onset values for placebo bulk powder as well as for extrudates with PVP-VA64 in the second heating cycle. The SDD were described by both heating cycles: absence of a melting peak of KTZ was checked in the first cycle for successful amorphization whereas the T_g of the mixture was analyzed in the second cycle.

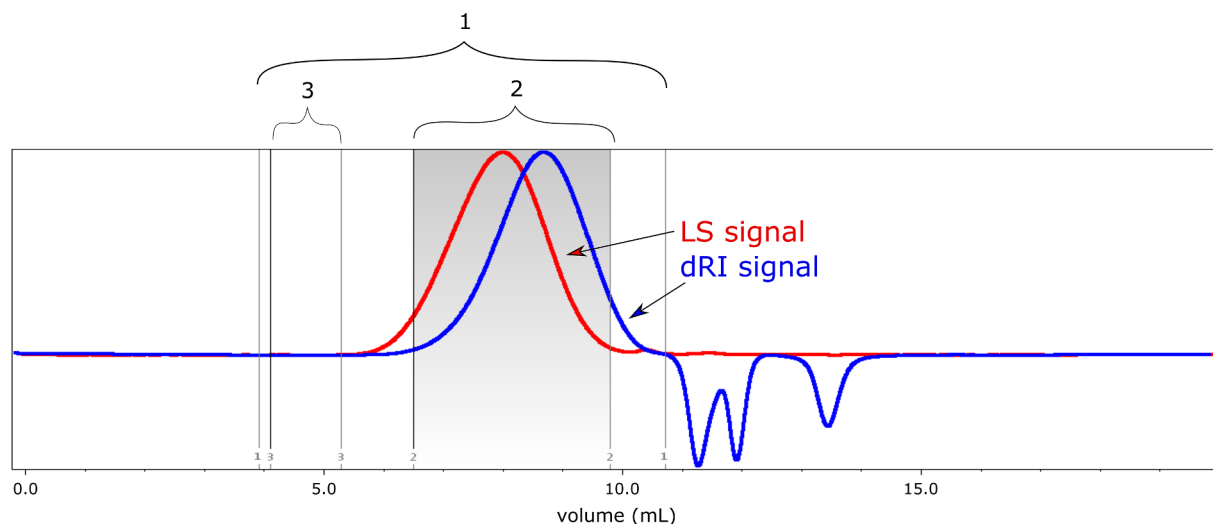


Fig. 2. Chromatogram of PVP-VA64 bulk powder. Light scattering signal (LS) depicted in red, differential refractive index (dRI) depicted in blue. The polymer peak is separated into three sections. 1) Total peak for calculation of mass recovery, 2) polymer main peak with appropriate size separation for calculation of M_w and PDI and 3) high molecular weight peak (only present in thermally stressed samples). (For interpretation of the references to colour in this figure legend, the reader is referred to the web version of this article.)

Table 2

Extrusion parameters on ThreeTec for stress-tests with placebo PVP-VA64 resulting in extrudates Ex 130, Ex 160, Ex 180 and extruded physical mixture of PVP-VA64 + 40% KTZ (ExPM 160).

Sample	Temp. Zone 1 (°C)	Temp. Zone 2 (°C)	Temp. Zone 3 (°C)	Torque (Nm)
PVP-VA64 (Ex 130)	100	130	130	1.39 ± 0.20
PVP-VA64 (Ex 160)	120	160	160	1.22 ± 0.16
PVP-VA64 (Ex 180)	140	180	180	0.83 ± 0.06
PVP-VA64 + 40% KTZ (ExPM 160)	120	160	160	0.78 ± 0.06

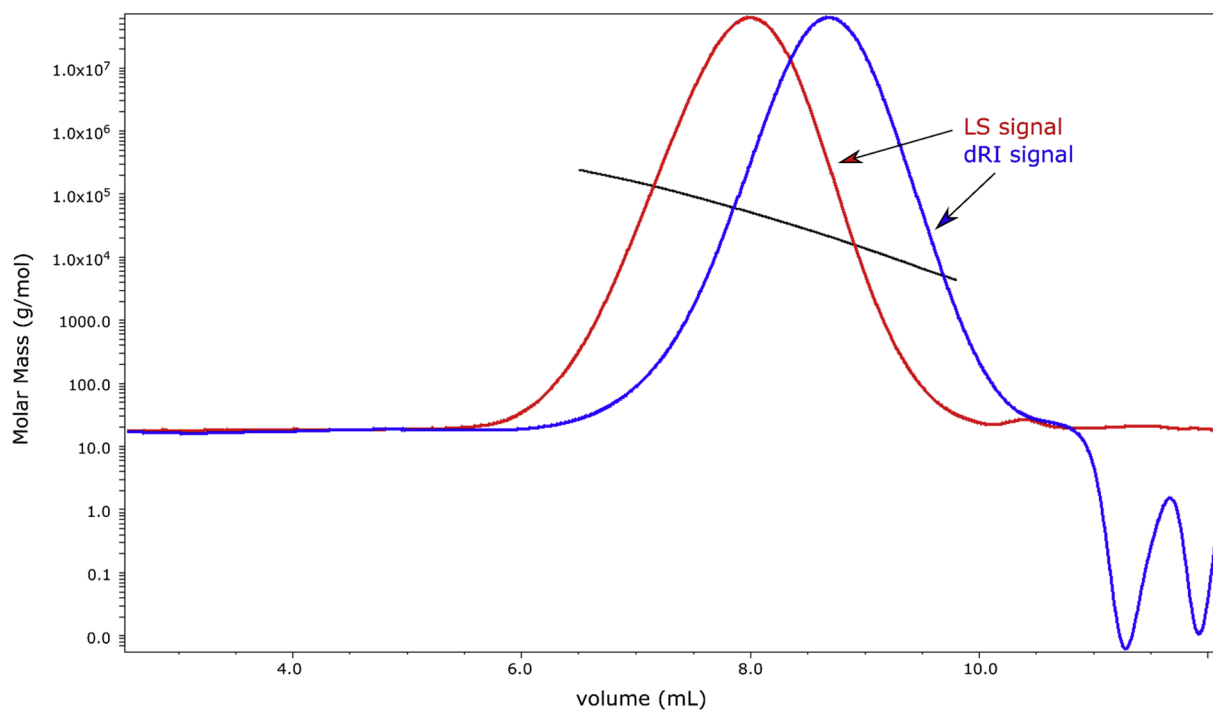


Fig. 3. Molar mass plot for PVP-VA64 bulk powder. Molecular weight distribution (straight black line) as expected for polydisperse samples like polymers. Range shown for peak 2. LS signal depicted in red, dRI signal in blue. (For interpretation of the references to colour in this figure legend, the reader is referred to the web version of this article.)

Table 3
Spray-drying parameters for PVP-VA64 placebo and formulations with 40% drug load KTZ.

Formulations	Inlet temperature (°C)	Feed rate (mL/min)	Outlet temperature readout (°C)
SDD Bulk PVP-VA64 (bulk powder) + 40% KTZ	100	2.0	42.5
SDD 130 PVP-VA64 (Ex 130) + 40% KTZ	100	2.0	42.7
SDD 160 PVP-VA64 (Ex 160) + 40% KTZ	100	2.0	43.2
SDD 180 PVP-VA64 (Ex 180) + 40% KTZ	100	2.0	44.2
SDD Placebo PVP-VA64 (bulk powder)	100	2.0	41.5
SDD Scale-Up PVP-VA64 (Ex Scale-Up) + 40% KTZ	100	2.0	42.7

Any numerical values reported are arithmetic means with standard deviation of three independently prepared samples.

2.7. Powder X-ray diffraction (PXRD)

A Stoe StadiP 611 instrument (Stoe, Germany) equipped with a Mythen1K Si-strip detector (PSD) was used for PXRD analysis. The measurements were performed in transmission mode with Cu-K_{α1} radiation source. The samples were prepared on a 96 well plate sample holder with a Kapton® foil on the bottom of the wells. An angular resolution of 0.03° 2θ over a 2θ range from −36° 2θ to +36° 2θ with measurement times of 30 sec/PSD-step and a PSD step width of 0.09° 2θ was applied. The diffractograms were folded to the range from 0° 2θ to 36° 2θ.

2.8. Non-sink dissolution

1.5 mg SDD containing 40% (w/w) KTZ were exactly weighed into 2 mL round bottom Eppendorf caps. The dissolution was started by addition of 1.2 mL FaSSiF-V1 at 37 °C. After vortexing for 1 min at 1500 rpm (Vortex-Genie® 2, Scientific Industries, USA), the caps were incubated at 37 °C in a block heater (Thermomixer® comfort, Eppendorf, Germany). Samples were taken after 5, 10, 15, 20, 30, 45, 60, 90 and 120 min. Suspensions were centrifuged (Mikro 200R centrifuge, Hettich, Germany) prior to sampling and 50 μL supernatant (without replacement) were transferred each time. Samples were immediately diluted 1:3 with ACN/water (50:50, v/v). The concentration of drug dissolved was determined via RP-HPLC (Section 2.9). Each SDD was analyzed in triplicate.

2.9. HPLC analysis

The concentration of KTZ dissolved was determined with an Agilent Technologies (USA) 1260 HPLC system equipped with a diode array detector working at 225 nm. 10 μL of sample were injected and

analyzed with a Waters XSelect® CSH Phenyl-Hexyl reverse phase column (4.6 × 100 mm with 3.5 μm packing, Waters Corporation, USA). The column temperature was constantly held at 60 °C. Mobile phases A and B consisted of binary mixtures of 95:5 and 5:95 (v/v) 10 mM ammonium-formiate buffer pH 4 and ACN. The linear gradient ran from 100% phase A to 100% B within 10 min. Purity was reported as area percent. Content specifications for SDD samples were set to 95–105%, purity was monitored and confirmed to be > 98% (a/a).

2.10. Statistical analysis

Analyses of variance (ANOVA, Holm-Sidak method, Dunnett's test) and t-tests were conducted using Sigma-Plot 12.5 (Systat Software Inc., USA). A p-value < 0.05 was considered as statistically significant.

3. Results and discussion

3.1. Small-scale extrusion of PVP-VA64 placebo

The extrusion experiments were conducted with placebo bulk powder above T_g of PVP-VA64 (104 °C ± 0.7, n = 3, DSC method Section 2.6). The barrel processing temperature was set below T_{deg} of 230 °C according to (Kolter and Gryczke, 2012) with a maximum of 180 °C (Ex 180). As there is an additional energy input from viscous dissipation caused by shear stress (Zecevic et al., 2018), temperatures within the melt might have been significantly higher. PVP-VA64 was continuously extruded without interruption of the process as residence times are known to influence product properties (Reitz et al., 2013). Increasing temperatures decrease the melt viscosity which was also reflected by a decreasing torque (Table 2). As expected, the strand thickness also decreased with increasing temperature and showed less die swelling. All process conditions resulted in macroscopically and microscopically (Supplementary Material Fig. S2) clear, glassy strands with smooth surface and no visible degradation or discoloration.

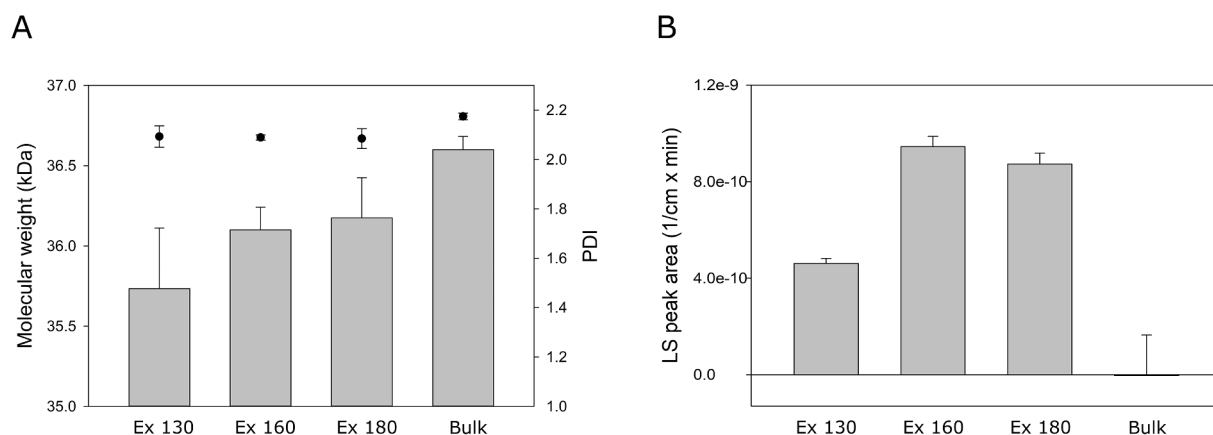


Fig. 4. A) Bars indicate molecular weight, PDI is depicted as dots of three different process conditions for PVP-VA64 extrudates and compared to unprocessed PVP-VA64 bulk powder. B) Integrated light scattering intensity of high molecular weight peak (peak 3, definition according to Fig. 2). Arithmetic means of n = 4 + S.D.

3.2. GPC-MALS-RI analysis of hot-melt extrudates

3.2.1. Reproducibility and mass recovery

The suitability of the developed GPC-MALS-RI method (Section 2.3) was tested regarding reproducibility and mass recovery of PVP-VA64 samples. Therefore, four independently prepared samples of the same bulk powder batch were analyzed with the described method. All samples were injected twice to additionally enable monitoring of the analytical variability and influence of data processing. The total of $n = 8$ showed mass recoveries (calculated for peak 1) of $100\% \pm 5\%$ and a relative standard deviation for M_w of 1.0%. This high accuracy of GPC-MALS-RI methods was also found by (Andersson et al., 2003).

3.2.2. Influence of HME in small-scale

The differently stressed placebo PVP-VA64 extrudates Ex 130, Ex 160 and Ex 180 were analyzed by GPC-MALS-RI analysis. The results for M_w and PDI are shown in Fig. 4A. The different extrusion profiles showed different impacts on M_w and PDI. Although alterations were only made with regard to process temperature whereas all the other input parameters were held constant to the greatest possible extent, there are still many inter-correlating factors in the extrusion process that might have caused these effects on M_w and PDI. As low temperatures result in higher melt viscosity (as also indicated by increasing torque), the shear stress increases which might also increase the product temperature. Keeping the process variables constant, higher melt viscosities also result in longer residence times (Lang et al., 2014). These considerations may explain why Ex 130 showed the strongest M_w decrease whereas Ex 160 and Ex 180 were only affected to a minor extent. Statistical significance of M_w was shown with a one-way ANOVA ($p = 0.002$) and Dunnett's method.

MALS analysis allows not only for absolute determination of M_w but also for detection of molecular dimensions of a molecule in solution by absolute measurement of the radius of gyration (r_g). The so-called scaling law (Suárez et al., 2013), describes the connection between M_w and r_g . Supplementary Material Fig. S3 shows how the decrease in M_w for Ex 130, Ex 160 and Ex 180 correlated with a decrease of r_g which reflects conformational changes of the polymer in solution.

Not only M_w and r_g but also the PDI slightly decreased. An explanation for that was found by integrating the LS peak area of a high molecular weight fraction (peak 3, definition according to Fig. 2) that was detected in the extrudates (Fig. 4B). PVP-VA64 bulk powder did not contain a significant amount of this high M_w fraction whereas it was quite pronounced in Ex 160 and Ex 180 that were extruded with higher temperatures. The peak area of Ex 130 was about half of that for Ex 160 and Ex 180.

The high molecular weight fraction was probably separated from

the polymer main peak leading to a more homogeneous size distribution reflected as a decrease in PDI (and M_w) for the polymer main peak of Ex samples (Fig. 4A). Additionally, this peak (eluted at lower retention volume meaning bigger hydrodynamic volume) could also be related to changes in the substitution pattern of PVP-VA64 resulting in a different solubility and hydrodynamic radius and therefore different pore penetration and retention volumes (Dawkins, 1976). To exclude chemical decomposition mainly by hydrolysis of the ester side chain functionality (chemical structure see graphical abstract), the samples were analyzed by NMR measurements (Fig. 6).

The M_w of peak 3 was not determinable as the RI signal-to-noise ratio was too low for calculation of M_w . As the LS signal's intensity is dependent on both – concentration and M_w according to Eq. (1) – a pronounced LS signal can be detected although the amount of that fraction is below the limit of detection of the RI detector. Consequently, the higher peak area of the LS signal for Ex 160 and 180 compared to Ex 130 could mean two things: 1) a higher amount of the high M_w fraction or 2) higher M_w . For reliable elucidation, higher amounts of the high M_w fraction need to be injected to enable RI detection and method development with a GPC column with appropriate molecular weight separation range is needed. Furthermore, correct determination of M_w would require collection of the high M_w fraction and separate determination of dn/dc as it is possible that cross-linking changed the refractive index. Calculating M_w with dn/dc of PVP-VA64 bulk powder would only be a rough approximation. Therefore, determination of the M_w of peak 3 poses an additional complex analytical challenge and will be subject to further studies.

3.2.3. Transfer to scale-up equipment

Extrusion was also conducted on a manufacturing scale equipment to verify the results from the small-scale process. The results cannot be directly transferred to larger scales even when using the same temperatures as the equipment design and energetic consumptions are completely different. In contrast to small-scale extrusion, the changes of M_w were not statistically significant ($p = 0.423$, Fig. 5A). However, a significant difference regarding high molecular weight fraction between unprocessed PVP-VA64 bulk powder and extrudate (Fig. 5B) was detected (t -test, $n = 4$, $p < 0.001$). This indicates that the findings of the small-scale equipment are also relevant for later scale-up trials at least in terms of high M_w fraction. The chromatogram of Ex Scale-Up with high M_w fraction is depicted in the Supplementary Material Fig. S4.

The authors want to point out that there was only one screw configuration and temperature profile tested in this setup to confirm the relevance of the GPC-MALS-RI analysis in general. The effects on M_w and PDI may be influenced by different process parameters (e.g. residence time distribution, feed rate, screw speed, screw configuration,

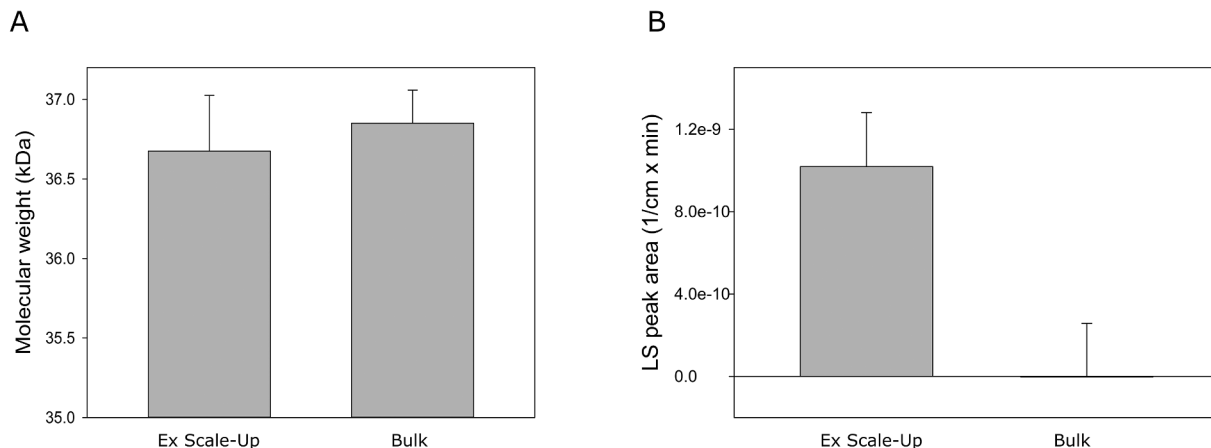


Fig. 5. A) Molecular weight of PVP-VA64 extrudate in manufacturing scale (process temperature 160 °C, 600 rpm) and unprocessed PVP-VA64 bulk powder. Difference is not statistically significant. B) Integrated light scattering intensity of high molecular weight peak (peak 3 see Fig. 2). Arithmetic means of $n = 4 + S.D.$

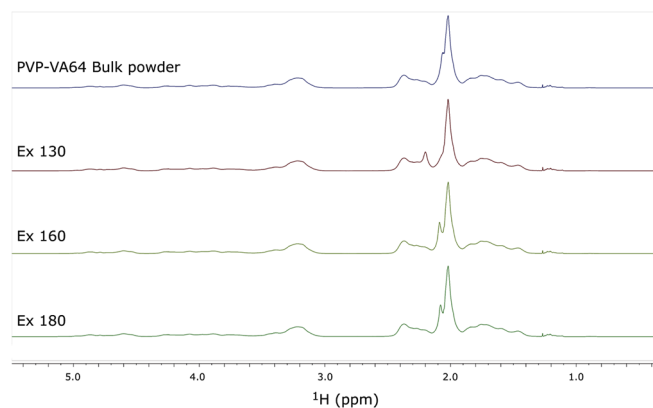


Fig. 6. ^1H NMR solution spectra of PVP-VA64 bulk powder, Ex 130, Ex 160 and Ex 180.

barrel temperature) which should be addressed in a design of experiment in further studies. To successfully develop ASD, it is necessary to define a processing window like demonstrated e.g. for HPMCAS (Jiannan et al., 2018) where T_g , yellowness index and free functional groups were used to monitor polymer degradation. As the melt temperature is influenced by different energetic consumptions, it is hardly predictable when degradation starts. The GPC-MALS-RI methodology proposed in this study is highly sensitive and capable to detect changes in the polymeric backbone and not only hydrolysis of side-chain functionalities. Thus, it provides a substantial contribution to quality control during formulation development.

3.3. NMR

NMR measurements were conducted to exclude chemical degradation effects like ester hydrolysis that could also lead to different dissolution performances. Relative integrals of ester- CH_3 groups and α - CH_2 group vs. amide- CH_2 group of the pyrrolidone ring did not change between PVP-VA64 bulk material (Supplementary Material Figs. S5 and S6) and the extrudates. Within the limit of detection of the proposed method, this indicates that the ester group did not undergo hydrolysis during the extrusion and there were no changes in the composition of the copolymer either. Additionally, there was no free acetic acid detected.

All peaks were assigned to their corresponding functional groups (Supplementary Material Fig. S5). There was no loss of signals observed. The NMR spectra are congruent except for slight peak shifts. This is shown in Fig. 6 with a stack plot of the ^1H NMR spectra of PVP-VA64 bulk powder and the three different ThreeTec extrudates (Ex 130, Ex 160, Ex 180).

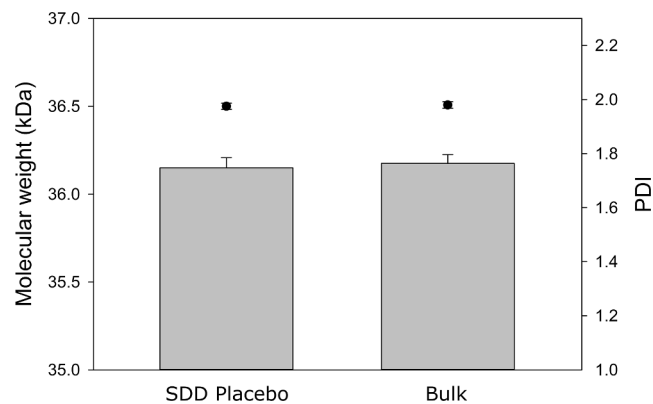


Fig. 7. Molecular weight (bars) and PDI (dots) of PVP-VA64 Bulk powder and PVP-VA64 placebo SDD. Arithmetic means of $n = 4 + \text{S.D.}$

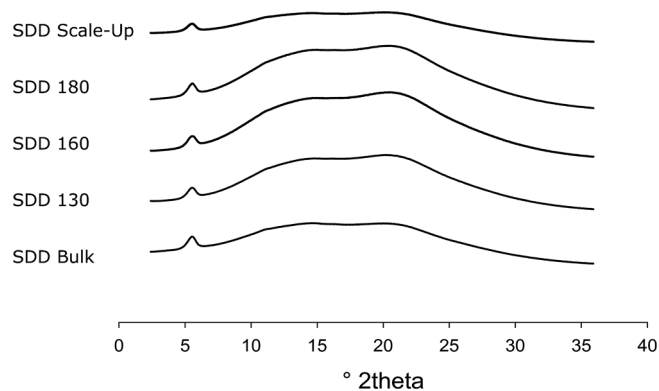


Fig. 8. PXRD Diffractograms for SDD with PVP-VA64 and 40% drug load KTZ. The reflex at $5^\circ 2\theta$ derives from the Kapton[®] foil.

The shifts point towards conformational changes of the polymer in solution (Saalwächter and Reichert, 2010). The NMR results were in very good correlation to GPC-MALS-RI measurements (Fig. 4A) as Ex 130 also showed the strongest decrease in M_w which is likely to be responsible for conformational changes. This was also reflected by the change in r_g compared to bulk material (Supplementary Material Fig. S3). The shifts were mostly pronounced in Ex 130 which can be clearly seen for the peak at 2.1 ppm. The high M_w fraction which was more pronounced in Ex 160 and Ex 180 (Fig. 4B) seemed to have less influence.

3.4. Spray-drying

3.4.1. Influence of SD on M_w and PDI

A two-step manufacturing process (HME of the placebo followed by SD of the verum formulation) was chosen to investigate how the changes in M_w and PDI of the polymer affect the formulation's performance in dissolution. First, it was necessary to demonstrate that SD does not adulterate the physicochemical properties of the polymer. Therefore, unprocessed bulk powder was compared to SDD Placebo in terms of M_w and PDI. The weight averaged M_w and PDI of the main polymer peak (peak 2 according to Fig. 2) are depicted in Fig. 7. Both samples showed nearly identical masses as well as PDI. Additionally, formation of a high molecular weight fraction was not observed. This allowed SD to be used as a non-adulterating manufacturing technique for ASD with differently stressed PVP-VA64. The polymer batch for these experiments (bulk and Placebo SDD) was different from the one in 3.2.2. A small batch-to-batch variability (compared to Fig. 4) was detected in M_w of the bulk material.

3.4.2. Manufacturing of SDD with 40% drug load KTZ

As spray-drying did not affect the polymer characteristics (Fig. 7), it was chosen as a second process step instead of a second HME run for

Table 4

Glass transition temperatures of placebo PVP-VA64 bulk powder and placebo extrudates as well as glass transition temperatures of verum SDD formulations with PVP-VA64 bulk powder or Ex 130/160/180 with 40% drug load KTZ. Arithmetic means of $n = 3 \pm \text{S.D.}$

	Placebo	PVP-VA64 Bulk (°C)	Ex 130 (°C)	Ex 160 (°C)	Ex 180 (°C)
T_g		103.6 \pm 0.7	104.0 \pm 1.2	104.2 \pm 1.2	103.6 \pm 0.2
	Verum	SDD Bulk (°C)	SDD 130 (°C)	SDD 160 (°C)	SDD 180 (°C)
T_g		69.3 \pm 0.6	69.6 \pm 0.8	70.3 \pm 1.8	69.3 \pm 1.8

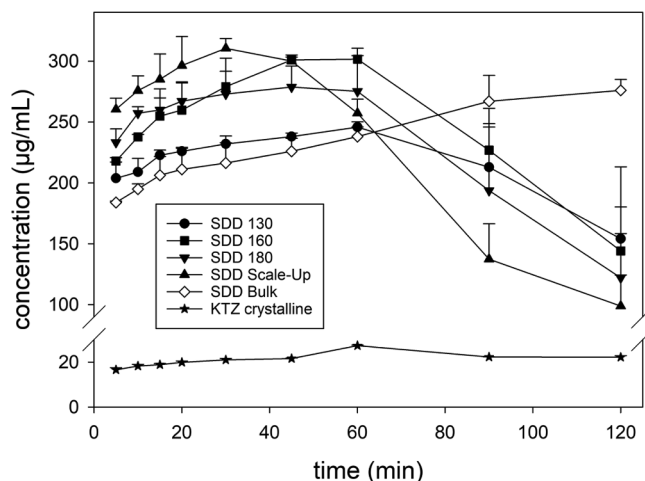


Fig. 9. Concentration of KTZ dissolved in non-sink dissolution setup of SDD with PVP-VA64 and 40% drug load. SDD 130/160/180 and SDD Scale-Up were prepared with thermally stressed PVP-VA64 (Ex 130/160/180 and Ex Scale-Up). SDD Bulk contains PVP-VA64 bulk powder. Comparison versus crystalline KTZ. Dissolution was conducted in FaSSiF-V1 at pH 6.5. Arithmetic means of $n = 3 + S.D.$

amorphously embedding the API into the polymeric matrix. An exponentiation of degradation effects by two heat and shear stress processes should be avoided. Thus, the amorphization could be conducted independently from the thermal and shear stress applied on the polymer during HME. This enabled non-adulterated analyses of the polymer's impact on dissolution parameters. Otherwise it would have been necessary to additionally discuss the influence of the process temperature (e.g. above or below T_g of KTZ) on amorphization. By using this approach, differences in the dissolution behavior of the ASD can be directly correlated to polymer characteristics. Particle sizes of the spray-dried particles were in the range of 3–17 μm (median, d_{10} and d_{90} values are given in [Supplementary Material Table S7](#)).

3.4.3. Solid-state – PXRD & DSC

The SDD were analyzed by PXRD to check for residual crystallinity. No crystalline reflections were detected ([Fig. 8](#)).

DSC analysis was conducted for HME placebo as well as for SDD verum. The thermograms indicated fully amorphous SDD by absence of the crystalline API's melting peak. Glass transition temperatures did not show differences between either different placebo extrudates or verum SDD ([Table 4](#)).

3.5. Non-sink dissolution

The SDD were tested in a non-sink dissolution setup to evaluate if the measured changes in M_w and PDI of PVP-VA64 influence supersaturation and precipitation behavior of the verum ASD. As KTZ was amorphously integrated into the polymeric matrix in the same way for each of the five formulations (SDD Bulk, SDD 130, SDD 160, SDD 180, SDD Scale-Up), the dissolution results should only be related to polymer characteristics.

All SDD samples with pre-stressed PVP-VA64 showed significantly stronger precipitation than the SDD sample with bulk powder ([Fig. 9](#)). Furthermore, SDD Scale-Up, SDD 160 and 180 enabled higher supersaturation than SDD 130 and SDD Bulk. Of course, the higher supersaturation results in a higher precipitation pressure and might therefore also explain the stronger precipitation observed for SDD Scale-Up, SDD 160 and 180. However, this doesn't hold true for the SDD 130 where the concentration of drug dissolved is almost equal to SDD Bulk whereas it precipitates much stronger anyway. GPC-MALS-RI analysis of Ex Scale-Up ([Fig. 5](#)) did only show a significant difference between

extrudate and bulk for the high M_w fraction in contrast to Ex 130, 160 and 180 where M_w and PDI were additionally affected. As the SDD Scale-Up did show the same precipitation behavior though as SDD 130, 160 and 180, this leads to the assumption that the high M_w fraction might contribute more strongly to this dissolution effect than the impact on M_w and PDI. This is additionally supported by the fact, that SDD Scale-Up, SDD 160 and SDD 180 contained very similar amounts of this high M_w fraction ([Fig. 4B](#) and [5B](#)) and showed the same supersaturations. In contrast, SDD 130 contained only half of the high M_w fraction detected in the other extrudates and showed concentrations of drug dissolved alike SDD Bulk up to 60 min.

The changes in M_w and PDI and degradation effects were not accessible to ASD standard analytical methods like PXRD, DSC or microscopy. Only GPC-MALS-RI analysis was capable to elucidate differences between PVP-VA64 bulk powder and the extrudates and therefore could explain the differences in dissolution performance.

The precipitation inhibitory effect of polymers in supersaturated systems is normally kinetic in nature and not related to an increase of thermodynamic solubility. Nucleation and crystal growth should be prevented to maintain high concentrations of drug dissolved which may be influenced by specific drug-polymer interactions ([Mullin, 2012](#)). Additionally, surface adsorption effects of the polymer to API nucleation crystals are discussed to inhibit crystal growth ([Lindfors et al., 2008](#)). Patel et al. ([Patel and Anderson, 2015](#)) correlated these adsorption effects to the molecular weight of PVP which is additionally dependent on chain length, chain conformation and rigidity ([Kramarenko et al., 1996](#)). The change in r_g ([Supplementary Material Fig. S3](#)) together with the NMR results ([Fig. 6](#)) showed that changes in M_w and PDI also affected the polymer conformation which could in turn lead to different interactions of the polymer chains with the drug ([Singh and Van den Mooter, 2015](#)). Pacult et al. ([2018](#)) investigated the effect of polymer chain length on precipitation inhibition by molecular dynamics analysis and positron annihilation lifetime spectroscopy for different M_w of PVP (PVP K10, PVP K30 and PVP K90). K90 was characterized by the greatest tendency to recrystallize. They found the largest free volume within the longest polymer chains and postulated that different chain lengths lead to different configurations and with that to different stabilizing effects. The polymer with the best stabilization efficiency though was not the one with the smallest M_w (K10) but the intermediate M_w (K30). The authors pointed out how important it is to find the optimal chain length and to monitor physical properties of the polymer. The results of Pacult et al. fully support the effects that were detected in this study. The changes in M_w and the high M_w fraction generated in Ex 130, Ex 160, Ex 180 and Ex Scale-Up might have

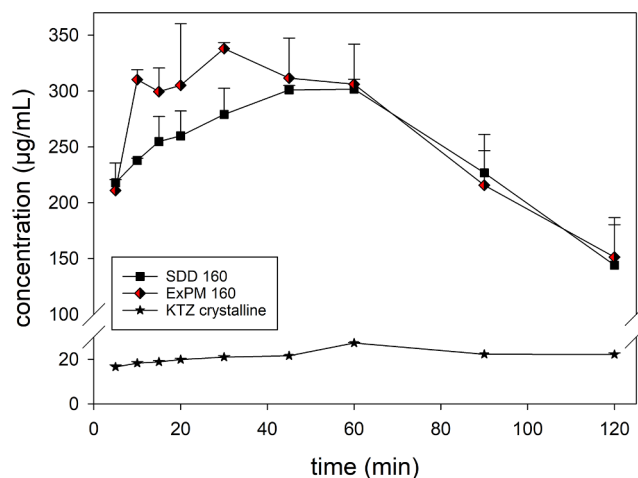


Fig. 10. Comparison of concentrations of KTZ dissolved of SDD 160 and ExPM 160 (directly extruded physical mixture of PVP-VA64 and 40% KTZ) vs. crystalline KTZ. Arithmetic means of $n = 3 + S.D.$

caused different conformations of the polymer in solution (which was supported by NMR results) leading to worse stabilization against recrystallization. As the chemical structure and conformation of the high M_w fraction is not known, all factors might contribute to a different polymer conformation resulting in different drug-polymer interactions and precipitation inhibitory behavior.

As the molecular weight directly influences intrinsic viscosities, differences in the dissolution might additionally be related to viscosity effects. The increase in viscosity might have also prolonged the core to surface transport of the solvent during the SD process for SDD 130, SDD 160, SDD 180 and SDD Scale-Up as they contain a high M_w fraction. In effect, this would have resulted in lower evaporation rates especially at the edge of particles (Wu et al., 2011) increasing the probability of recrystallization and explaining the stronger precipitation compared to SDD Bulk. This effect is certainly especially pronounced in the SD process which served as an ideal model system to demonstrate the impact of such changes. Therefore, comparability to extrusion of physical mixture (PM) of polymer and API should be demonstrated.

Amorphous strands (ExPM 160) were obtained at 160 °C process temperature (equivalent to Ex 160). As the incorporated KTZ acts as a plasticizer (T_g 44 °C, Table 1), the shear stress applied on the PM is not the same as for the placebo extrusion (torque of screws reduced in comparison to placebo, see Table 2). This might have led to slight differences in supersaturation between SDD 160 and HME 160 between 5 and 45 min dissolution testing (Fig. 10). However, the precipitation behavior of the SDD 160 is congruent with the ExPM 160 where the polymer was exposed to the same temperatures. Particle sizes of the milled extrudate and spray-dried particles were comparable in the range of 3–10 μ m.

These results show the complexity of optimizing extrusion process parameters and to find out how they affect the ASD formulation as tuning of only one parameter (in this case process temperature) might still have multiple unpredictable effects.

The experiments under 3.4. and 3.5. have been repeated independently in separate spray-drying and dissolution experiments and were always leading to the same findings.

4. Conclusion

This study demonstrated the importance of the polymers' physico-chemical properties for ASD formulation. On the one hand, it could be demonstrated how HME impacts the polymer PVP-VA64 (in contrast to SD) and how minute changes in M_w and PDI might influence supersaturation and precipitation of the API. On the other hand, it was shown that degradation effects occurred although they were not necessarily expected at the temperatures employed. These changes were not detected by standard analytical techniques but only by GPC-MALS-RI. Although all extrusions were performed at barrel temperatures that were set at minimum 50 °C below the theoretical T_{deg} of PVP-VA64, there was a considerable impact on the polymer's M_w and PDI. In consequence, not only the maximum concentration of drug dissolved was influenced but also the precipitation behavior of the API. It is quite likely that such changes might also impact the physical stability of ASD by influencing e.g. molecular mobility and drug-polymer interactions. GPC-MALS-RI analysis is a highly accurate and sensitive analytical method and allowed to monitor these minute changes. The results clearly indicate a need for advanced analytical tools for polymer characterization in the development of ASD in addition to API-related issues. PVP-VA64 was selected as an excipient with a high T_{deg} and broad processing window. If polymers with lower T_{deg} and thermal stability like e.g. cellulose derivatives are used, the problem gets even worse and careful tuning of the process is required. This methodology can be used as an additional quality control parameter to optimize HME process conditions to systematically develop HME formulations and subsequently ensure maximum performance of the ASD.

Acknowledgements

The authors gratefully acknowledge Karsten Flügel for providing the extrudate for the scale-up experiments. Andreas Marx is highly acknowledged for his analytical support regarding the NMR measurements. Furthermore, the authors want to thank Robert Hennig, Magdalena Münster and Markus Riehl for the scientific discussion on this manuscript.

Declaration of interest

The authors declare that they have no conflict of interest. This research did not receive any specific grant from funding agencies in the public, commercial, or not-for-profit sectors.

Appendix A. Supplementary data

Supplementary data to this article can be found online at <https://doi.org/10.1016/j.ijpharm.2018.12.012>.

References

- Andersson, M., Wittgren, B., Wahlund, K.-G., 2003. Accuracy in multiangle light scattering measurements for molar mass and radius estimations. Model calculations and experiments. *Anal. Chem.* 75, 4279–4291.
- Baghel, S., Cathcart, H., O'Reilly, N.J., 2016. Polymeric amorphous solid dispersions: a review of amorphization, crystallization, stabilization, solid-state characterization, and aqueous solubilization of biopharmaceutical classification system class II drugs. *J. Pharm. Sci.*
- Bochmann, E.S., Steffens, K.E., Gryczke, A., Wagner, K.G., 2018. Numerical simulation of hot-melt extrusion processes for amorphous solid dispersions using model-based melt viscosity. *Eur. J. Pharm. Biopharm.* 124, 34–42.
- Chiou, W.L., Riegelman, S., 1971. Pharmaceutical applications of solid dispersion systems. *J. Pharm. Sci.* 60, 1281–1302.
- Crowley, M.M., Zhang, F., Koleng, J.J., McGinity, J.W., 2002. Stability of polyethylene oxide in matrix tablets prepared by hot-melt extrusion. *Biomaterials* 23, 4241–4248.
- Crowley, M.M., Zhang, F., Repka, M.A., Thumma, S., Upadhye, S.B., Kumar Battu, S., McGinity, J.W., Martin, C., 2007. Pharmaceutical applications of hot-melt extrusion: Part I. *Drug Dev. Ind. Pharm.* 33, 909–926.
- Dawkins, J.V., 1976. Thermodynamic interpretation of polystyrene retention on cross-linked polystyrene gels in GPC with poor and theta solvents. *J. Polym. Sci.: Polym. Phys. Ed.* 14, 569–571.
- Eitzlmayr, A., Koscher, G., Reynolds, G., Huang, Z., Booth, J., Shering, P., Khinast, J., 2014. Mechanistic modeling of modular co-rotating twin-screw extruders. *Int. J. Pharm.* 474, 157–176.
- Frank, D.S., Matzger, A.J., 2018. Probing the interplay between amorphous solid dispersion stability and polymer functionality. *Mol. Pharmaceutics*.
- Haser, A., Zhang, F., 2018. New strategies for improving the development and performance of amorphous solid dispersions. *AAPS PharmSciTech* 19, 978–990.
- Izunobi, J.U., Higginbotham, C.L., 2011. Polymer molecular weight analysis by 1H NMR spectroscopy. *J. Chem. Educ.* 88, 1098–1104.
- Jiannan, L., Sakae, O., Nicolas, I., John, S., Costas, G., Shingo, K., 2018. Understanding the processing window of hypromellose acetate succinate for hot-melt extrusion, Part I: polymer characterization and hot-melt extrusion. *Adv. Polym. Tech.* 37, 154–166.
- Karandikar, H., Ambardekar, R., Kelly, A., Gough, T., Paradkar, A., 2015. Systematic identification of thermal degradation products of HPMCP during hot melt extrusion process. *Int. J. Pharm.* 486, 252–258.
- Knopp, M.M., Olesen, N.E., Holm, P., Langguth, P., Holm, R., Rades, T., 2015. Influence of polymer molecular weight on drug-polymer solubility: a comparison between experimentally determined solubility in PVP and prediction derived from solubility in monomer. *J. Pharm. Sci.* 104, 2905–2912.
- Kolter K., K.M., Gryczke A., 2012. Hot-Melt Extrusion with BASF Pharma Polymers. Kramarenko, E.Y., Winkler, R.G., Khalatur, P.G., Khokhlov, A.R., Reineker, P., 1996. Molecular dynamics simulation study of adsorption of polymer chains with variable degree of rigidity. I. Static properties. *J. Chem. Phys.* 104, 4806–4813.
- Lang, B., McGinity, J.W., Williams, R.O., 2014. Hot-melt extrusion – basic principles and pharmaceutical applications. *Drug Dev. Ind. Pharm.* 40, 1133–1155.
- Leuner, C., Dressman, J., 2000. Improving drug solubility for oral delivery using solid dispersions. *Eur. J. Pharm. Biopharm.* 50, 47–60.
- Lindfors, L., Forssén, S., Westergren, J., Olsson, U., 2008. Nucleation and crystal growth in supersaturated solutions of a model drug. *J. Colloid Interface Sci.* 325, 404–413.
- Liu, H., Zhang, X., Suwardie, H., Wang, P., Gogos, C.G., 2012. Miscibility studies of indomethacin and Eudragit® E PO by thermal, rheological, and spectroscopic analysis. *J. Pharm. Sci.* 101, 2204–2212.
- Lubach, J.W., Hau, J., 2018. Solid-state NMR investigation of drug-excipient interactions and phase behavior in indomethacin-eudragit E amorphous solid dispersions. *Pharm. Res.* 35, 65.
- Marsac, P.J., Li, T., Taylor, L.S., 2008. Estimation of drug-polymer miscibility and solubility in amorphous solid dispersions using experimentally determined interaction

- parameters. *Pharm. Res.* 26, 139–151.
- Mori, Y., Takahashi, M., Ohno, Y., Okura, R., Ishida, M., Higashi, T., Motoyama, K., Arima, H., 2018. Identification of molecular-interaction sites between lowly hydrolyzed polyvinyl alcohols and indomethacin by NMR spectroscopy. *Int. J. Pharm.* 549, 456–465.
- Mullin, J.W., 2012. Crystallization and Precipitation, *Ullmann's Encyclopedia of Industrial Chemistry*.
- Pacult, J., Rams-Baron, M., Chrzęszcz, B., Jachowicz, R., Paluch, M., 2018. Effect of polymer chain length on the physical stability of amorphous drug-polymer blends at ambient pressure. *Mol. Pharm.* 15, 2807–2815.
- Patel, D.D., Anderson, B.D., 2015. Adsorption of polyvinylpyrrolidone and its impact on maintenance of aqueous supersaturation of indomethacin via crystal growth inhibition. *J. Pharm. Sci.* 104, 2923–2933.
- Paudel, A., Meeus, J., Van den Mooter, G., 2014. Structural Characterization of Amorphous Solid Dispersions.
- Pezzoli, R., Lyons, J.G., Gately, N., Higginbotham, C.L., 2018. Investigation of miscibility estimation methods between indomethacin and poly(vinylpyrrolidone-co-vinyl acetate). *Int. J. Pharm.* 549, 50–57.
- Ph.Eur., 2018a. Copovidone, in: *Healthcare, E.D.f.t.Q.o.M. (Ed.)*. Council of Europe, pp. 4882–4884.
- Ph.Eur., 2018b. Functionality-related characteristics of excipients. In: *Healthcare, E.D.f.t.Q.o.M. (Ed.)*, European Pharmacopoeia Council of Europe, pp. 4411–4412.
- Prudic, A., Ji, Y., Sadowski, G., 2014. Thermodynamic phase behavior of API/polymer solid dispersions. *Mol. Pharm.* 11, 2294–2304.
- Reitz, E., Podhaisky, H., Ely, D., Thommes, M., 2013. Residence time modeling of hot melt extrusion processes. *Eur. J. Pharm. Biopharm.* 85, 1200–1205.
- Repka, M.A., Bandari, S., Kallakunta, V.R., Vo, A.Q., McFall, H., Pimparade, M.B., Bhagurkar, A.M., 2018. Melt extrusion with poorly soluble drugs – an integrated review. *Int. J. Pharm.* 535, 68–85.
- Repka, M.A., McGinity, J.W., 2000. Influence of Vitamin E TPGS on the properties of hydrophilic films produced by hot-melt extrusion. *Int. J. Pharm.* 202, 63–70.
- Saalwächter, K., Reichert, D., 2010. *Polymer Applications of NMR*.
- Sarode, A.L., Obara, S., Tanno, F.K., Sandhu, H., Iyer, R., Shah, N., 2014. Stability assessment of hypromellose acetate succinate (HPMCAS) NF for application in hot melt extrusion (HME). *Carbohydr. Polym.* 101, 146–153.
- Sarode, A.L., Sandhu, H., Shah, N., Malick, W., Zia, H., 2013. Hot melt extrusion (HME) for amorphous solid dispersions: predictive tools for processing and impact of drug-polymer interactions on supersaturation. *Eur. J. Pharm. Sci.* 48, 371–384.
- Schittny, A., Ogawa, H., Huwyler, J., Puchkov, M., 2018. A combined mathematical model linking the formation of amorphous solid dispersions with hot-melt-extrusion process parameters. *Eur. J. Pharm. Biopharm.* 132, 127–145.
- Shah, N.H.S., Choi, Duk Soon, Hitesh Chokshi, A., Malick, Waseem, 2014. *Amorphous Solid Dispersions*. Springer.
- Singh, A., Van den Mooter, G., 2015. Spray drying formulation of amorphous solid dispersions. *Adv. Drug Deliv. Rev.*
- Suárez, I., Losio, S., Coto, B., 2013. Polymer chain conformation of copolymers with different monomer size: 13C NMR spectroscopy and MALS study. *Eur. Polym. J.* 49, 3402–3409.
- Wu, J.X., Yang, M., Berg, F.V.D., Pajander, J., Rades, T., Rantanen, J., 2011. Influence of solvent evaporation rate and formulation factors on solid dispersion physical stability. *Eur. J. Pharm. Sci.* 44, 610–620.
- Wyatt, P., 1993. *Light Scattering and the Absolute Characterization of Macromolecules*.
- Wytenbach, N., Kuentz, M., 2017. Glass-forming ability of compounds in marketed amorphous drug products. *Eur. J. Pharm. Biopharm.* 112, 204–208.
- Zecevic, D.E., Evans, R.C., Paulsen, K., Wagner, K.G., 2018. From benchtop to pilot scale-experimental study and computational assessment of a hot-melt extrusion scale-up of a solid dispersion of dipyridamole and copovidone. *Int. J. Pharm.* 537, 132–139.
- Zograf, G., Newman, A., 2017. Interrelationships between structure and the properties of amorphous solids of pharmaceutical interest. *J. Pharm. Sci.* 106, 5–27.

Miniaturized Measurement of Drug–Polymer Interactions via Viscosity Increase for Polymer Selection in Amorphous Solid Dispersions

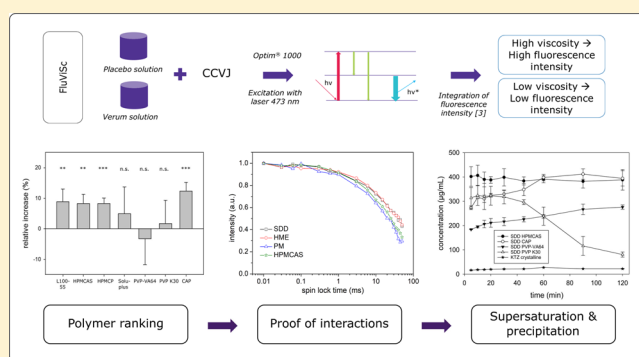
Carolin Auch,^{†,‡} Meike Harms,[‡] Yury Golitsyn,[§] Detlef Reichert,[§] and Karsten Mäder^{*,†,‡}[†]Institute of Pharmacy, Faculty of Natural Sciences I, Martin Luther University Halle-Wittenberg, Wolfgang-Langenbeck-Str. 4, 06120 Halle/Saale, Germany[‡]Department Pharmaceutical Technologies, Merck KGaA, Frankfurter Str. 250, 64293 Darmstadt, Germany[§]Department of Physics, Faculty of Natural Sciences II, Martin Luther University Halle-Wittenberg, Betty-Heimann-Str. 7, 06120 Halle/Saale, Germany

Supporting Information

ABSTRACT: Drug–polymer interactions have a substantial impact on stability and performance of amorphous solid dispersions (ASD) but are difficult to analyze. Whereas there are many screening methods described for polymer selection based for example on glass forming ability, drug–polymer miscibility, supersaturation, or inhibition of recrystallization, the distinct detection of physico-chemical interactions mostly lacks miniaturized techniques. This work presents an interaction screening assessing the relative viscosity increase between highly concentrated polymer solutions with and without the model drug ketoconazole (KTZ). The fluorescent molecular rotor 9-(2-carboxy-2-cyanovinyl)julolidine was added to the solutions in a miniaturized setup in μL -scale.

Due to its environment-sensitive emission behavior, the integrated fluorescence intensity can be used as a viscosity dye within this screening approach (FluViSc). Differences in relative viscosity increases through addition of KTZ were proposed to rank polymers regarding KTZ–polymer interactions. Absolute viscosities were measured with a cone–plate rheometer as a complimentary method and supported the results acquired by the FluViSc. Solid-state nuclear magnetic resonance (ss-NMR) relaxation time measurements and Raman spectroscopy were utilized to investigate drug–polymer interactions at a molecular level. Whereas Raman spectroscopy was not suited to reveal KTZ–polymer interactions, ss-NMR relaxation time measurements differentiated between the selected polymeric carriers hydroxypropylmethylcellulose acetate succinate (HPMCAS) and polyvinylpyrrolidone vinyl acetate 60:40 (PVP-VA64). Interactions were detected for HPMCAS/KTZ ASD while there was no hint for interactions between KTZ and PVP-VA64. These results were in correlation with the dissolution performance of ASD and found to be predictive for supersaturation and inhibition of precipitation during dissolution.

KEYWORDS: amorphous solid dispersions, viscosity, solid-state nuclear magnetic resonance, fluorescent molecular rotor, interaction, screening, ketoconazole, polymer selection



INTRODUCTION

Low aqueous solubility and correspondingly low bioavailability is one of the main deficiencies of new active pharmaceutical ingredients (API) in the industrial pipeline.¹ The formulation of amorphous solid dispersions (ASD) is one possibility to improve both the apparent solubility and the dissolution rate. However, the amorphous form is thermodynamically unstable and recrystallization must be delayed both upon storage and dissolution.^{2,3} This can be achieved for example by incorporating the API in a polymeric matrix, which reduces its molecular mobility. This effect can be enhanced by specific drug–polymer interactions.^{4,5} Therefore, such interactions are beneficial as they may enable long-term physical stability

during storage and hinder precipitation from the supersaturated state during dissolution⁶ as well as they may favor the formation of one-phase systems.⁷

Different types of interactions can occur in ASD like ionic interactions, hydrogen-bonding, dipole–dipole interactions, or hydrophobic interactions with diverse effects on the formulation.⁸ The interactions may involve specific functional groups of API and polymer or reflect nonspecific dispersion

Received: February 12, 2019

Revised: March 26, 2019

Accepted: March 28, 2019

Published: March 28, 2019

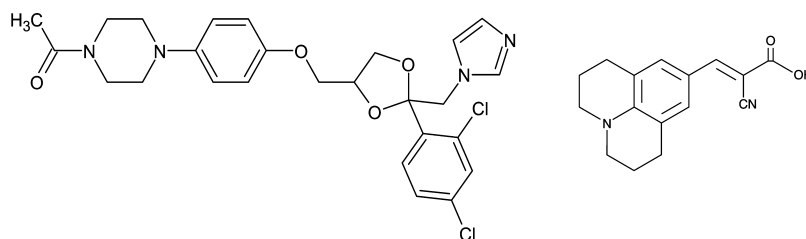


Figure 1. Chemical structures of KTZ (left) and the fluorescent molecular rotor CCVJ (right).

forces. Furthermore, it is challenging to link interactions detected in the solid state to drug–polymer interactions in dissolution environment as solvent molecules can disrupt interactions.⁹

Researchers currently aim to gain a deeper mechanistic understanding of interactions at the molecular level.^{10,11} Many of these studies primarily focus on ionic interactions which are not accountable for non-ionic systems.^{12,13} A widely used approach to estimate drug–polymer interactions is the *in silico* calculation of the Flory–Huggins (FH) interaction parameter.^{14,15} However, this parameter does neither account for specific interactions like hydrogen bonds nor viscosity and concentration dependence.¹⁶ Turpin et al.¹⁶ showed that systematic evidence of predictability of the FH parameter was missing and concluded that this approach was not suitable to screen or select excipients.

From an experimental perspective, spectroscopic techniques like infrared spectroscopy and Raman spectroscopy¹⁷ can be used to detect interactions at a molecular level. By applying solid-state nuclear magnetic resonance (ss-NMR),^{4,18} it is even possible to quantify interactions, but both analytical methods are time and cost intensive. Chiang et al.¹⁹ used ss-NMR to measure the long-range homogeneity of ASD formulations prepared by different manufacturing techniques and found the results to be predictive for the physical stability.^{20,21}

As the methods named above require at least small-scale manufacturing of ASD in gram scale, the present study aimed to develop a miniaturized screening tool in microgram scale to account for the limited API availability during early development. Such miniaturized methods should provide fast readouts with high information gain to quickly decide on formulation strategies and narrow-down the excipient portfolio to the most promising candidates. For ASD, there exist numerous screening tools which focus for example on glass forming ability,²² solubility enhancement in dissolution,²³ or *in silico* prediction of thermodynamic solubility of API within the polymer.²⁴ However, the detection of interactions between API and polymer is only rarely assessed by experimental miniaturized approaches²⁵ why the method described herein is of particular importance.

The screening presented in this study proposes to use the viscosity increase between polymer and drug–polymer solutions as a predictive factor for drug–polymer interactions. The idea was derived from protein–protein self-association by noncovalent bonds.^{26,27} Neergaard et al.²⁸ found a solution's viscosity proportional to attractive protein–protein interactions. Since the strength of interactions is dependent on the distance between molecules, high concentrations of drug and polymer in solution are necessary.

The feasibility of measuring drug–polymer interactions in organic solvents was previously shown by using ¹H NMR and NOESY, where intermolecular interactions between different

drugs and polymers like for example poly-(vinylpyrrolidone) (PVP), hydroxypropylmethylcellulose acetate succinate (HPMCAS), Eudragit E PO, polyacrylic acid, or polyvinyl alcohol were described.^{10,29,30}

To measure viscosities in a miniaturized scale, a derivative nonmechanical method with a fluorescent molecular rotor as viscosity dye³¹ is presented in this work. The general structure of these rotors consists of electron donor and acceptor functional subunits with a spacer in between around which an intramolecular twisting motion can occur in the fluorescent excited state.³² For the molecular rotor 9-(2-carboxy-2-cyanovinyl)julolidine (CCVJ), a julolidine malonitrile, which was used in this study, the return from the twisted state to the ground state happens nonradiatively while light is emitted when returning from planar state. As high viscosities reduce the twisting kinetic, increasing viscosities lead to higher fluorescent yields. The precision of this fluorescence-based method was found to be comparable to mechanical viscometry.³³ Additionally, there is no shear perturbation applied on the samples, which might be a bias for systems with non-Newtonian flow behavior. There are several applications described in the literature like surveillance of polymerization processes, plasma viscosity measurements connoted with certain diseases,³³ or fluidity of membranes.³² Zhu et al.³⁴ showed the application of molecular rotors to determine the viscosities of polymer-based fluids and polymeric melts with dependence on their molecular weight. The quantum yields are dependent on the free volume of the surrounding solvent, allowing the measurement of the microviscosity around the molecular rotor. For further explanation of the functional principles and underlying physical principles, the reader is referred to Rumble et al.³⁵ and Haidekker and Theodorakis.³²

The equipment used in this study (Optim 1000) provided the ability to measure the integrated fluorescence intensity of 48 samples in sealed cuvettes with only 9 μ L sample volume each within a few minutes. This allowed for very fast high-throughput screenings with minimal amounts of API.

The screening results were confirmed by absolute viscosity measurements and subsequently correlated with estimations from the Gordon–Taylor (GT) equation. Raman spectroscopy and ss-NMR were selected as complimentary methods to give a proof of interactions at a molecular level. Furthermore, the findings were interpreted in relation to the dissolution performance of the corresponding ASD. The influence of the preparation pathway on interactions at the molecular level was also examined and discussed, as the authors detected differences here in a previous study.²³ Therefore, amorphous formulations were prepared by both spray-drying dispersion (SDD) and hot-melt extrusion (HME), which are the most common techniques in the field of ASD.³⁶

Ketoconazole (KTZ), a BCS class II compound,³⁷ was used as a model drug as it comprises representative properties of

compounds on the market as ASD.²² Similar to many compounds in the pharmaceutical pipeline, KTZ is weakly basic, which is of special interest for ionic interactions.

This study describes a new screening tool that can be used to rank interactions between the drug and different polymers with only μg of API consumption. The results from this screening were compared with complimentary methods, and the effects of possible interactions on the dissolution performance were discussed.

EXPERIMENTAL SECTION

Materials. Crystalline KTZ was purchased from Biotrend Chemicals AG (Switzerland). The fluorescent molecular rotor 9-(2-carboxy-2-cyanovinyl)julolidine (CCVJ) was obtained from Sigma-Aldrich (USA). The chemical structures are given in Figure 1.

Evonik Industries (Germany) supplied the methacrylic acid copolymer Eudragit L100-55 (L100-55). HPMCAS grade HF was kindly donated by Shin Etsu (Japan). Poly-(vinylpyrrolidone-co-vinyl acetate) 60:40 (PVP-VA64), poly-(vinylpyrrolidone) K30 (PVP K30), and the polyvinylcaprolactam-polyvinyl acetate-polyethylene glycol graft copolymer (Soluplus) were provided by BASF (Germany). Hydroxypropylmethylcellulose phthalate (HPMCP) HP-50 was delivered by Dow Chemicals (USA); cellulose acetate phthalate (CAP) was obtained from Eastman (USA). The chemical structures are given in the Supporting Information, Figure S1.

Fasted-state simulating intestinal fluid V1 (FaSSIF-V1) pH 6.5 was prepared with SIF powder from Biorelevant.com (UK). Sodium hydroxide (VWR Chemicals, Belgium), sodium chloride, di-sodium hydrogen phosphate, hydrochloric acid 1 M, and sodium hydroxide solution 1 M (Merck KGaA, Germany) were used for preparation of the dissolution media in analytical grade or gradient grade. All solvents used were of high-performance liquid chromatography (HPLC) grade (purity $\geq 99.7\%$). *N,N*-Dimethylformamide (DMF) was purchased from Alfa Aesar (USA). A Millipore-Milli-Q integral water purification system (Millipore Merck KGaA, Germany) delivered purified water.

Miniaturized FluViSc. Highly concentrated polymer solutions (50 mg/mL) of L100-55, HPMCAS, HPMCP, Soluplus, PVP-VA64, PVP K30, and CAP with and without 20 mg/mL KTZ were prepared in DMF. The addition of 20 mg/mL KTZ refers to 40% (w/w) drug load (DL) with respect to polymer weight. CCVJ was prepared as a stock solution in DMF (3 mM) and added to the solutions to result in a concentration of 5 μM . An Optim 1000 (Unchained Labs Inc., USA) equipment was used for high-throughput measurements of fluorescence intensity. Each sample (9 μL) was pipetted into a microcuvette array. Neat DMF and solutions with different amounts of KTZ served as controls. The measurements were conducted at 10.0 °C with 473 nm laser wavelength. Exposure time was set to 5 s with a slit width of 300 μm . The fluorescence intensity was integrated between 475 and 560 nm. Results are given as relative increase (%) between polymer and KTZ-polymer solutions as a quotient of their fluorescence intensities. Arithmetic means with standard deviations according to Gaussian error propagation of three independently prepared samples are depicted.

Rheology. A rotational viscometer (Haake RheoStress 1, Thermo Scientific, USA) was used for rheological evaluation of polymer and KTZ-polymer solutions (identical to the FluViSc). The cone-plate setup was built up with 60 mm

diameter cone. Cone angle was 0.502°. The sample (500 μL) was pipetted on the plate surface, which was cooled to 10 °C. Frequency sweeps within the linear viscoelastic region were conducted with frequencies from 500 to 1000 s^{-1} . All rheometer measurements were conducted in triplicate.

Manufacturing of ASDs. *Preparation of Physical Mixtures.* KTZ-polymer mixtures with 40% (w/w) DL of crystalline API were prepared with a mortar and pestle. The mixtures were additionally homogenized afterward with a Turbula (T2F, Willy A. Bachofen AG, Switzerland) mixer at 32 rpm for 15 min.

Hot-Melt Extrusion. HME was conducted on a small-scale twin-screw extruder (ZES, ThreeTec, Switzerland) with 5 mm screw diameter and three heating zones. The double-concave co-rotating screws were equipped with conveying elements and a 1.0 mm die. The feeding zone was constantly cooled to 12.5 °C with a cryostat (WK4600, Lauda, Germany). The powder was fed manually. Extrusion temperatures were adjusted to result in clear and glassy extrudate strands, and a screw speed of 300 rpm was maintained. The extrusion parameters are given in Auch et al.²³ Afterward, the strands were milled either with a vibrational ball mill at 30 Hz for 2 \times 2 min (Pulverisette 23, Fritsch, Germany) or with a tube mill (IKA Tube mill control, USA) at 25 000 rpm for 2 \times 1 min.

Spray-Drying. SDD were prepared on a 4M8-TriX Formatrix Spray Dryer (ProCepT, Belgium). Neat polymer and KTZ-polymer mixtures [40% DL (w/w) with respect to polymer] were dissolved in dichloromethane/MeOH 9:1 (v/v) to result in a total solid concentration of 2% (w/w). The spray-dryer was set up with a 1.0 mm nozzle, 10 L/min atomizing nitrogen, and 70% air speed. Air temperature and feed rate were adjusted for the different formulations to obtain fully amorphous SDD. Outlet temperature varied with inlet temperature, the cyclone pressure drop was constant at approximately 56 mbar. The spray-drying parameters are given in Auch et al.²³ Spray-dried powder was dried over silica gel (Merck KGaA, Germany) at 100 mbar overnight.

Differential Scanning Calorimetry. A differential scanning calorimetry (DSC) 1 (Mettler Toledo, Switzerland) was used for acquisition of melting points and glass transition temperatures. The samples (7–10 mg) were exactly weighed into 100 μL aluminum pans without pin and crimped. A pinhole was pierced via an automated piercing unit into the lids to allow for water evaporation during measurement. A ramp of 10 K/min was used for heating and cooling in two heating cycles. The maximum temperature in the first heating cycle was 170 °C (above T_m of KTZ with 149 °C) and 200 °C in the second cycle. Glass transition temperatures (T_g) were determined in the second cycle and reported as onset temperatures. Temperatures are given as arithmetic means with standard deviation of three independently prepared samples.

Gordon-Taylor Equation. The GT eq 1³⁸ was used for the calculation of T_g of the drug-polymer mixtures with a simplified calculation of the constant K according to Hancock and Zograf³⁹ eq 2.

$$T_g(\text{mix}) = \frac{\omega_1 \cdot T_{g1} + K \cdot \omega_2 \cdot T_{g2}}{\omega_1 + K \cdot \omega_2} \quad (1)$$

$$K = \frac{T_{g1} \cdot \rho_1}{T_{g2} \cdot \rho_2} \quad (2)$$

T_{g1} and T_{g2} are the glass transition temperatures for KTZ and polymer. ω_1 and ω_2 are the weight fractions of KTZ and polymer in the mixture. ρ_1 and ρ_2 are the densities of pure KTZ and polymer. Density measurements were conducted using a Micromeritics AccuPyc 1330 helium pycnometer (Micromeritics Instrument Corporation, USA). Approximately 2 g of powder were filled into the measurement cell ($V = 10$ mL). Ten consecutive measurement cycles were performed and the average density of the last three runs was calculated (relative standard deviation < 0.9%). The equilibration rate was 0.005 psig/min. All measurements were conducted at room temperature.

Powder X-ray Diffraction. The solid-state of extrudate strands and SDD was assessed by powder X-ray diffraction (PXRD). Measurements were conducted on a Stoe StadiP 611 instrument (Stoe, Germany) with Cu $K\alpha 1$ radiation generated at 40 kV and 40 mA. A Mythen 1K Si-strip (PSD) served as detector. The samples were measured in transmission after preparation on a combinatorial 96-well plate sample holder (approximately 20 mg of each formulation) comprising a Kapton foil on the bottom of the wells. The angular resolution was $0.03^\circ 2\theta$ over a 2θ range from $-36^\circ 2\theta$ to $+36^\circ 2\theta$.

Solid-State Nuclear Magnetic Resonance. ss-NMR experiments were performed on a Bruker AVANCE II spectrometer (Bruker Optik GmbH, Germany) at ^1H and ^{13}C frequencies of 400.16 and 100.6 MHz, with a standard Bruker 4 mm magic-angle spinning (MAS) probe at MAS rates of 10 kHz. The sample temperature (30°C) was controlled by a standard Bruker VT-controller and calibrated with methanol. The proton 90° pulse length was $3.0\ \mu\text{s}$, corresponding to a radio frequency field strength of 83 kHz during cross-polarization. For the measurement of the spin–lattice relaxation times in the rotating frame ($T_{1\rho}$) of ^{13}C nuclei, the spin-locking time was varied from $10\ \mu\text{s}$ to 50 ms. The effective frequency of the spin-lock pulse was 70 kHz. A typical recycle delay of 15 until 30 s was used for the experiments. Integrated peaks for $T_{1\rho}(^{13}\text{C})$ measurements were clearly assigned to either KTZ or matrix component.

The Kohlrausch–Williams–Watts (KWW) fit, a stretched exponential function, was used to describe the relaxation in this disordered system.⁴⁰ The mathematical fit was performed according to eq 3 considering a monoexponential nature of a motional process in amorphous systems.

$$I = I_0 \cdot e^{-(t/T_{1\rho})^\beta} \quad (3)$$

The variables are defined as the spin–lattice relaxation times in the rotating frame ($T_{1\rho}$), time (t), stretching exponent (β), and intensity (I).

HPLC Analysis. A 1260 HPLC system (Agilent Technologies, USA) with a UV detector operating at 225 nm was used for quantification of KTZ. Content and degradants of physical mixtures (PMs), hot-melt extrudates, and spray-dried powders were analyzed as reported earlier.²³

Non-sink Dissolution. Non-sink dissolution testing was conducted as described in Auch et al.²³ in FaSSIF-V1 dissolution buffer pH 6.5 at 37°C . All formulations were tested in triplicate.

Statistical Analysis. Analyses of variance (ANOVA, with Holm–Sidak method) and t -tests were conducted using SigmaPlot 12.5 (Systat Software, Inc., USA). A p -value < 0.05 was considered as the threshold value for statistical

significance. Asterisks represent significance levels: * < 0.05, ** < 0.01, *** < 0.001.

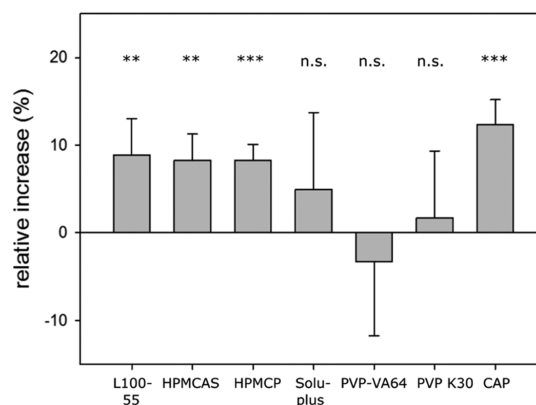


Figure 2. Relative viscosity increase or decrease between polymer solutions ($c = 50$ mg/mL polymer) and KTZ–polymer solutions ($c = 50$ mg/mL polymer plus 20 mg/mL KTZ). Arithmetic means of $n = 3 + \text{SD}$ from error propagation. Asterisks indicate statistical significance of increase in fluorescence intensity between polymer and KTZ–polymer solutions.

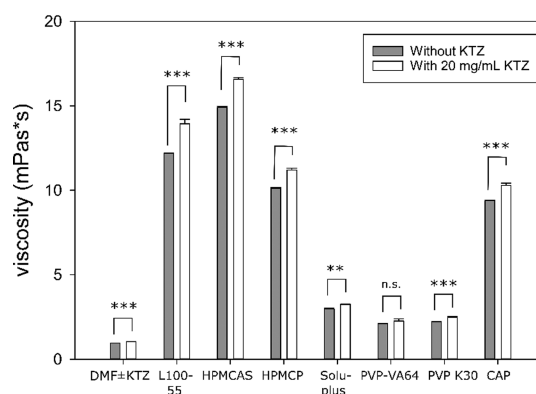


Figure 3. Absolute viscosities of polymer solutions (50 mg/mL polymer, filled bars) and KTZ–polymer solutions (50 mg/mL polymer plus 20 mg/mL KTZ, white bars) measured with the cone–plate setup via a rheometer. Neat DMF with addition of 20 mg/mL KTZ served as reference. Arithmetic means of $n = 3 + \text{SD}$. Asterisks indicate statistical significance of differences in viscosities between polymer and KTZ–polymer solutions.

RESULTS

Miniaturized FluViSc. Highly concentrated blank polymer solutions (50 mg/mL polymer) were compared to the same polymer solutions containing additional 20 mg/mL KTZ (equivalent to 40% (w/w) DL). The viscosity dye CCVJ was added to each solution in a concentration of $5\ \mu\text{M}$. The fluorescence intensities of both solutions were integrated, and the relative increase (or decrease) from neat polymer solutions to KTZ–polymer solutions was calculated. The percentage is depicted in Figure 2. Test solutions with different concentrations of neat KTZ in DMF compared to neat DMF did not show an effect on integrated fluorescence intensity with CCVJ (Figure S2, Supporting Information), meaning that there was no viscosity increasing effect due to KTZ without polymer.

The relative increase in viscosity did depend on the polymeric carrier. The addition of KTZ to CAP showed the

Table 1. Theoretical and Experimental Glass Transition Temperatures of Neat Polymers and Formulations with 40% DL KTZ^a

formulation	experimental T_g (°C) of polymers	theoretical T_g (°C) of KTZ–polymer	experimental T_g (°C) of KTZ–polymer	deviation
L100-55/KTZ	114.6 ± 1.6	71.6	91.0 ± 0.7	positive
HPMCAS/KTZ	117.8 ± 0.4	71.5	67.3 ± 1.1	none
HPMCP/KTZ	140.16 ± 2.8	76.0	78.2 ± 2.2	none
Soluplus/KTZ	65.03 ± 2.0	55.4	not detectable	n/a
PVP-VA64/KTZ	105.4 ± 1.5	68.4	65.0 ± 2.6	none
PVP K30/KTZ	156.2 ± 0.7	104.2	81.3 ± 1.3	negative
CAP/KTZ	144.4 ± 0.8	93.6	105.5 ± 2.6	positive

^aTheoretical data were calculated according to GT, and experimental values were measured by means of DSC (arithmetic means of $n = 3 \pm SD$).

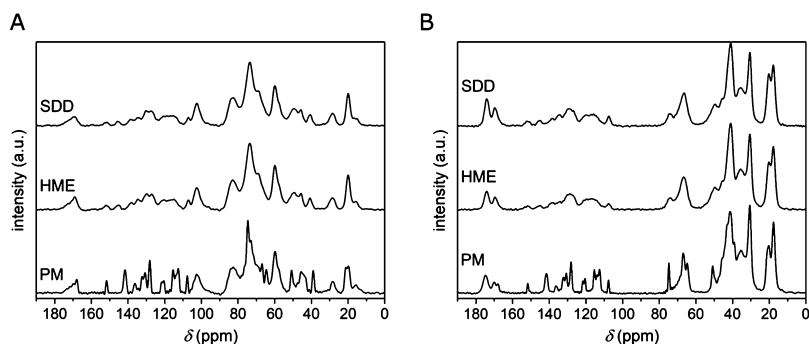


Figure 4. ¹³C ss-NMR spectra for KTZ formulations. (A) SDD, HME, and PM 40% DL in HPMCAS formulations. (B) SDD, HME, and PM 40% DL in PVP-VA64 formulations.

highest increase followed by Eudragit L100-55, HPMCAS, and HPMCP. The systems with Soluplus, PVP-VA64, and PVP K30 showed only a minor increase or even a decrease (PVP-VA64) in viscosity. Asterisks indicate the significance level of the mean difference in fluorescence intensities between polymer and KTZ–polymer solutions.

Rheometer Viscosity Data. A cone–plate rheometer was used for absolute determination of viscosities to confirm the derivative method with the viscosity dye CCVJ. The absolute viscosities of the KTZ–polymer solutions were in all cases higher than the neat polymer solutions (Figure 3). Highest relative increases between polymer and KTZ–polymer solutions were observed again for PMs of L100-55, HPMCAS, HPMCP, and CAP with KTZ (Figure S3, Supporting Information). No statistically significant differences between drug loaded and drug free systems were observed for PVP-VA64.

Gordon–Taylor Equation. Densities of KTZ and the polymeric excipients were measured with a He-pycnometer in duplicate (Table S4, Supporting Information). The densities and arithmetic means of experimental data were included in the calculation of theoretical T_g according to the GT equation. Table 1 shows the glass transition temperatures of the neat polymers as well as of the KTZ–polymer PMs (40% DL). There was always only one T_g detected in the second heating cycle. The glass transition temperature of amorphous KTZ (prepared via quench–cooling) was 43.9 ± 0.2 °C. Theoretical values were calculated according to GT, and experimental results were acquired via DSC in triplicate.

Positive deviations from theoretical T_g were observed for formulations with L100-55/KTZ and CAP/KTZ that also showed the highest increase in viscosity in both FluViSc (Figure 2) and rheometer measurements (Figure 3). PVP-K30/KTZ formulations showed negative deviations from calculated value. The T_g of Soluplus/KTZ formulations was

not detectable via DSC. For the other formulations, the experimental T_g values were in agreement with the predicted values of the GT equation (tolerability of ± 4 °C due to standard deviation of experimental data).

Solid-State Nuclear Magnetic Resonance. HPMCAS and PVP-VA64 were selected for ss-NMR measurements as positive and negative controls of the FluViSc. For both polymers, experimental and theoretical values predicted by the GT formula were in agreement (see Table 1). The ¹³C spectra of formulations with HPMCAS and PVP-VA64 and 40% DL KTZ each clearly showed differences between crystalline PM, amorphous SDD, or milled extrudates (Figure 4).

The spectral region between 100 and 160 ppm could be assigned to KTZ without overlaying signals from the polymers (Figure 5). Its amorphization was clearly visible by comparing PM versus HME or SDD as the KTZ signals was much broader and had a lower spectral resolution caused by a higher molecular disorder of amorphous versus crystalline API. Unfortunately, it was not possible to prepare powdery

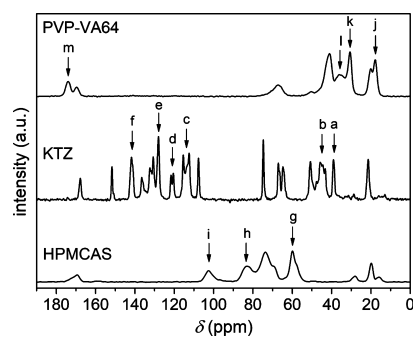


Figure 5. ¹³C ss-NMR spectra for neat substances PVP-VA64, HPMCAS, and KTZ as references for peak assignment.

amorphous KTZ via SDD or HME as reference, although several preparation techniques were tested. During the spray-drying process of KTZ, the outlet temperatures were above its T_g causing recrystallization. Quench-cooled films were not accessible to ss-NMR as they immediately recrystallized upon scratching. Thus, only hints on peak shifts and differences in peak shapes (Figure S7A + B, Supporting Information) could be drawn from the comparison of spectra with different matrix components (HPMCAS HF vs PVP-VA64). The same was true for differentiation between HME versus SDD with the same polymeric excipient over the whole spectra (Figure S7C + D).

In the next step, $T_{1\rho}$, which is the spin–lattice relaxation time in the rotating frame, was used to analyze molecular motions in more detail. In contrast to the NMR relaxation time T_1 which is sensitive to very fast motions on the ns time scale only, $T_{1\rho}$ is better suited to characterize molecular re-orientational motions at or around T_g . For correlation times down to the inverse of the cross-polarization field strength (which is 83 kHz in the present case), the change of the value of $T_{1\rho}$ for a given molecular geometry is in good agreement to the change of the value of the correlation time, that is a shorter $T_{1\rho}$ means a shorter correlation time and thus an increase in molecular mobility.⁴¹ The values of $T_{1\rho}$ were measured by acquiring a series of experiments with different spin-lock pulse-length, and the signal's intensity was plotted against the applied spin lock time, resulting in decay curves (Figure 6). The graphical relaxation time decays were also expressed in numerical values fitted to the KWW equation. Four representative peaks were exemplarily chosen (graphical analysis of all peaks is given in the Figures S8–S11, Supporting Information): one KTZ peak in both formulations with HPMCAS and PVP-VA64, one HPMCAS matrix peak, and one PVP-VA64 matrix peak. The peak assignment for relaxation time measurements is depicted in Figure 5. Tables 2 and 3 show the numerical fit of the relaxation time decay curves to the exponential KWW equation for two peaks (complete data are given in Table S12, Supporting Information).

PM, SDD, HME, and the references of the three compounds used (crystalline KTZ, neat HPMCAS, and neat PVP-VA64) were analyzed. The KTZ peaks showed almost the same behavior in HPMCAS as well as PVP-VA64 environment

Table 2. ^{13}C Relaxation Times ($T_{1\rho}$) of Peaks assigned to KTZ Integrated in Formulations with HPMCAS and PVP-VA64^a

peak	single component (ms)	in formulation with HPMCAS		
		PM (ms)	SDD (ms)	HME (ms)
KTZ (a)	31.8 ± 1.1	34.9 ± 1.8	4.8 ± 0.3	5.5 ± 0.4
KTZ (c)	285.1 ± 33.9	338.8 ± 63.1	28.4 ± 1.3	28.4 ± 1.8
peak	single component (ms)	in formulation with PVP-VA64		
		PM (ms)	SDD (ms)	HME (ms)
KTZ (a)	31.8 ± 1.1	31.5 ± 1.1	5.3 ± 0.5	6.1 ± 0.6
KTZ (c)	285.1 ± 33.9	322.6 ± 44.1	28.4 ± 1.6	36.2 ± 1.2

^aErrors indicate deviation from applied fit.

Table 3. Relaxation Times ($T_{1\rho}$) of Peaks assigned to Matrix Component Integrated^a

Peak	single component (ms)	in formulation with KTZ		
		PM (ms)	SDD (ms)	HME (ms)
HPMCAS (h)	44.1 ± 0.6	36.2 ± 1.3	74.2 ± 2.8	73.3 ± 2.3
HPMCAS (i)	48.1 ± 1.3	39.3 ± 2.3	92.4 ± 7.8	71.5 ± 3.5
peak	single component (ms)	in formulation with KTZ		
		PM (ms)	SDD (ms)	HME (ms)
PVP-VA64 (j)	29.2 ± 0.7	30.3 ± 0.4	28.4 ± 0.3	21.0 ± 0.3
PVP-VA64 (k)	29.0 ± 0.5	29.6 ± 0.3	27.2 ± 0.2	19.7 ± 0.2

^aErrors indicate deviation from applied fit.

(Figure 6A,B). Crystalline KTZ (crystalline reference and KTZ in the PM) showed much ^{13}C $T_{1\rho}$ longer relaxation times than amorphous KTZ in SDD and HME formulations. The absolute relaxation times were very similar for both KTZ incorporated in HPMCAS and as well as in PVP-VA64 (see Table 2) and could not be used to rank drug–polymer interactions.

However, the results for the polymeric peaks clearly showed differences between HPMCAS and PVP-VA64 (Figure 6C,D, Table 3). $T_{1\rho}$ relaxation times of HPMCAS were prolonged in amorphous formulations with KTZ, whereas the PM had the same decay curve as the HPMCAS reference. In contrast, PVP-VA64 formulations did not show this effect.

The HME curve of PVP-VA64 even showed faster relaxation than the other samples. Higher water content of the extrudate was assumed as the most likely reason for higher molecular mobility. However, loss on drying via thermogravimetric analysis (TGA) showed a 3% weight loss for all PVP-VA64 samples (Table S13, Supporting Information), which could therefore not explain the effect. Another possible explanation would be the creation of a different amorphous form, which could however not be elucidated so far.

β , as a factor for distribution of relaxation times, was between 0.38 and 0.79 for all integrated peaks (see Table S12, Supporting Information). As the factor β is a measure for the Gaussian distribution of the relaxation times, the values should be in the same order of magnitude to enable comparability of the fitted data, which was fulfilled for these experiments.

The solid-state was analyzed via PXRD before and after ss-NMR measurements. Diffractograms are given in Figure S14, Supporting Information and confirmed the maintenance of the amorphous state of KTZ.

Performance of ASD. The formulations prepared by SD were additionally examined regarding dissolution behavior under non-sink conditions. Polarized light microscopy (data not shown), PXRD (Figures S15–S17, Supporting Information), and DSC analysis (data not shown) did not reveal any crystalline fractions in all formulations with 40% DL KTZ. Content analysis was conducted for all samples tested and showed uniformity in the range from 98 to 102%. Purity was higher than 98% with respect to KTZ reference.

SDD formulations with HPMCAS and CAP showed high and stable supersaturations over 120 min (Figure 7A,B) with a maximum concentration of 400 $\mu\text{g}/\text{mL}$ KTZ dissolved.

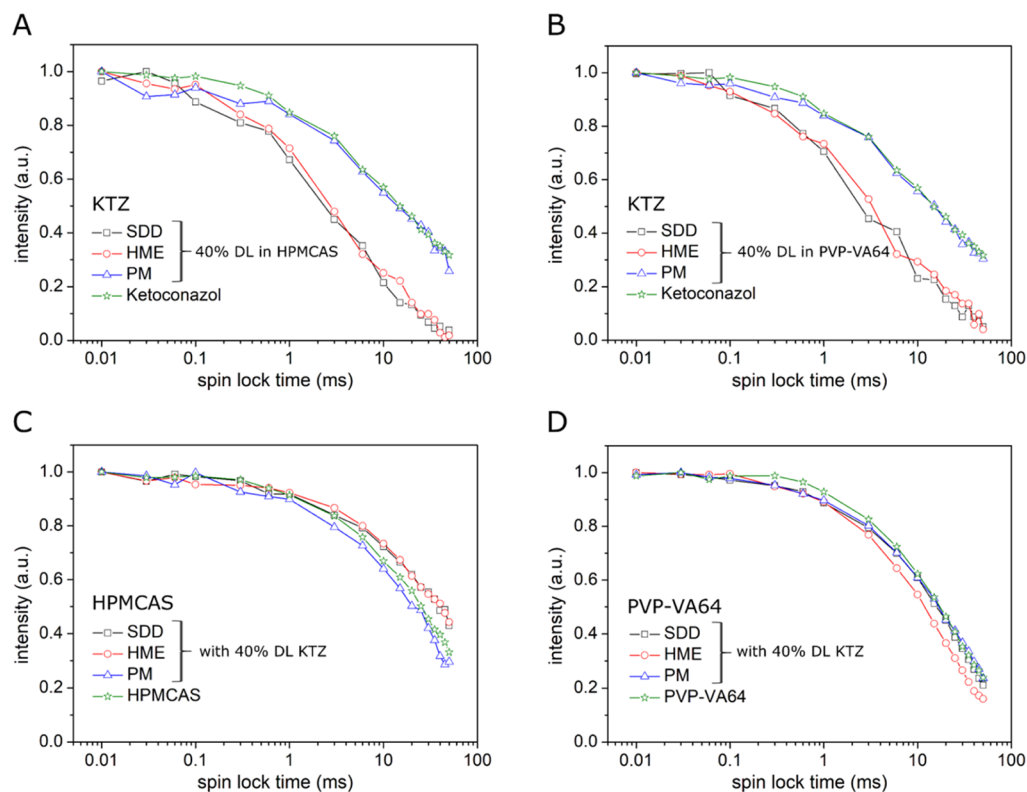


Figure 6. $T_{1\rho}$ decay curves of references and formulations, peak definition according to Figure 5. (A) KTZ (peak c) alone and 40% DL in HPMCAS formulations. (B) KTZ (peak c) alone and 40% DL in PVP-VA64 formulations. (C) HPMCAS matrix (peak h). (D) PVP-VA64 matrix (peak k).

Formulations with PVP-VA64 generated lower absolute concentrations of drug dissolved in general (Figure 7C). PVP K30 enabled similar supersaturation like PVP-VA64 but could not prevent drug precipitation (Figure 7D).

DISCUSSION

Analytics should provide the advantages of low API consumption, easy handling, high throughput, and wide applicability in terms of suitability for many API, especially when the amount of API is very limited. These prerequisites were met by using the viscosity fluorescence screening tool (FluViSc). The fluorescent molecular rotor CCVJ and the measurement of its fluorescence intensity were successfully used to rank drug–polymer interactions, according to the viscosity increase between polymer and KTZ–polymer solutions in an organic solvent. The interactions were measured in highly concentrated solutions in μL -scale requiring only a few mg of API for the whole screening. No time-intensive ASD manufacturing steps were needed, and fluorescence intensities are easily measurable as a surrogate for viscosity with the prerequisite of proper temperature control. As on the one hand, viscosity is highly dependent on temperature, which in turn also influences the fluorescent yields. On the other hand, interactions are influenced by temperature changes as the molecular motions increase at higher temperatures and interactions might become weaker.⁴²

The limited solubility of the API (which holds true for BCS class II and IV compounds in general) did not allow us to use water or buffer systems as solvent, although an aqueous environment would have better mimicked biorelevant conditions. DMF was chosen mainly as it dissolved KTZ and

all polymers used. As DMF is an aprotic solvent, protonation of CCVJ by DMF resulting in bias of the fluorescence intensity measurements was excluded.³² Furthermore, DMF is poorly volatile, which enabled absolute viscosity measurements in the cone–plate setup. However, solvent specific parameters like permittivity, polarity, or formation of hydrogen bonds may influence drug–polymer interactions.

A measured viscosity increase was hypothesized to be caused by KTZ–polymer interactions. The opposite case, namely a reduction of viscosity probably due to disturbance of intrapolymer chain interactions and coiling, was also observed namely for the system of PVP-VA64 and KTZ (Figure 2). Consequently, the FluViSc resulted in a ranking of polymers with the hypothesis of indicating decreasing strengths of interaction in the following order: CAP > L100-55 \approx HPMCAS HF \approx HPMCP HP-50 > Soluplus \approx PVP K30 > PVP-VA64. The extent of standard deviations was also considered for the ranking and stability of the drug–polymer interactions, which were much higher for the latter three polymers. A high standard deviation (also leading to nonsignificant viscosity increases) was interpreted as a hint for unstable and weak drug–polymer interactions in contrast to very specific and strong interactions like different electric charges. As KTZ is a weakly basic drug with two basic functional groups, interactions with acidic polymers were expected. Furthermore, KTZ contains hydrogen bonding acceptor groups⁴³ allowing interactions with hydrogen donors like CAP, L100-55, HPMCAS, or HPMCP.⁴⁴ In contrast, PVP K30 and PVP-VA64 are neutral polymers with hydrogen bonding acceptor sites only. Hydrophobic interactions must be additionally taken into account, which is often claimed an

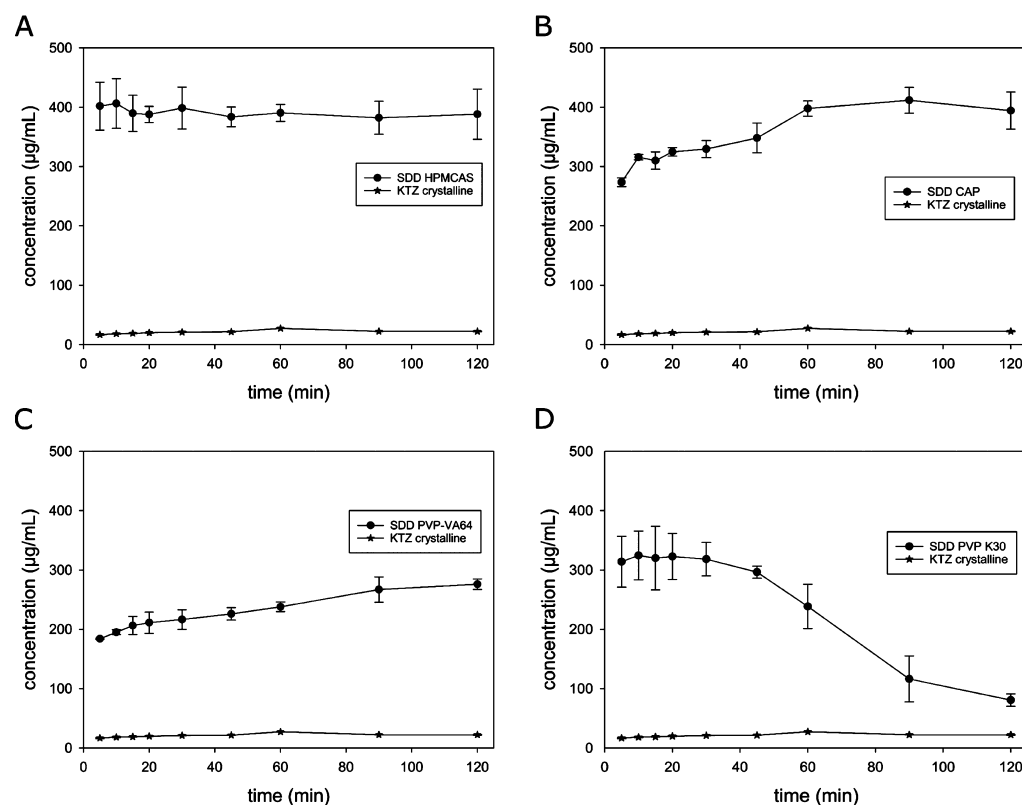


Figure 7. Concentration of KTZ dissolved in non-sink dissolution experiments with FaSSIF dissolution buffer pH 6.5. Arithmetic means of $n = 3 \pm$ SD. (A) SDD HPMCAS with 40% DL KTZ. (B) SDD CAP with 40% DL KTZ. (C) SDD PVP-VA64 with 40% DL KTZ. (D) SDD PVP K30 with 40% DL KTZ.

essential stabilization mechanism for HPMCAS which contains both hydrophilic and hydrophobic functional groups.⁴⁵

A change in polymer conformation resulting in a change of viscosity is an additional possibility of showing interactions with another component (comparable to the effect of theta vs nontheta solvents). Small molecules might occupy interaction sites (e.g., weakly charged functional groups of the polymer) that formerly exerted repulsive forces between the polymer chains leading to different coiling and conformations in solution.

In this study, the authors do not want to claim specific elucidation of interaction sites as this is still hard to grasp. A review by Warren et al.⁴⁶ provides a thorough summary on drug–polymer interactions. Hypotheses on the most likely interactions can be frequently found in the literature sometimes also with contradicting claims and are always drug-dependent. In contrast, the FluViSc provides an experimental tool for quantification, irrespective of whether the mode of interaction is known or not. Additionally, it reflects a paper-based probability of forming interactions, which was shown in this study for KTZ–polymer combinations.

Absolute viscosities of polymer and KTZ–polymer solutions were additionally measured in a cone–plate setup with 55 \times material consumption and much longer measurement times compared to the FluViSc, which is a major drawback of mechanical viscometry methods in general.⁴⁷ HPMCAS, HPMCP, Eudragit L100-55, and CAP were again among the excipients showing the highest viscosity increase with 40% DL KTZ (Figure 3). The ranking that was derived thereof (L100-55 > CAP \approx HPMCAS \approx HPMCP > Soluplus > PVP-VA64)

was confirming the FluViSc results (Figure S3). The only exception was found for PVP K30, where a high increase was detected in the cone–plate setup. However, the absolute viscosities of the PVP K30 (as well as PVP-VA64) solutions were around the limit of quantification for this measurement principle.

To confirm the ranking of polymers based on viscosity increase, the existence of drug–polymer interactions was analyzed by complimentary methods.

This was first examined by using the GT equation, a well-known and easy experimental way to estimate interactions. The T_g of a mixture can be calculated as a function of its composition by applying this empirical equation.^{48,49} A positive deviation from the predicted value is recognized as a hint for drug–polymer interactions. This was extensively examined for example for indomethacin–PVP systems by Yoshioka et al.,⁵⁰ who concluded that also other mechanisms except for antiplasticization must be involved to explain this stabilizing effect. These might for example either be ionic interactions⁵¹ or hydrogen bonding.⁵²

Again, formulations with L100-55/KTZ and CAP/KTZ showed the strongest positive deviation from GT-calculated values (Table 1) as indicated by both the FluViSc and rheometer results. Measured T_g values of both HPMCAS/KTZ and PVP-VA64/KTZ did not deviate from calculated GT data, whereas the FluViSc predicted interactions for HPMCAS/KTZ in contrast to PVP-VA64/KTZ.

Besides this thermoanalytical technique, spectroscopic solid-state analyses were conducted. HPMCAS and CAP were selected as positive controls of the FluViSc and absolute

viscosity data, and PVP-VA64 and PVP K30 served as negative control group.

The corresponding formulations were prepared by either SDD or HME and assessed by Raman spectroscopy (Supporting Information, Figure S6). The Raman spectra were supposed to provide the following: (i) a discrimination between crystalline and amorphous material, (ii) a ranking between the different polymeric excipients, and (iii) differentiation between the preparation technique used (SDD and HME) as the authors previously found differences in the behavior of the formulations prepared by different manufacturing techniques.²³ While the amorphous state of KTZ could be proven (Figure S5), drug–polymer interactions could not be detected by Raman spectroscopy. Additionally, a differentiation regarding the manufacturing technique was not possible. In summary, the Raman data suggested the interactions created in solid dispersions to be very similar irrespectively of the manufacturing technique or the polymer used.

For the ¹³C ss-NMR analysis and $T_{1\rho}$ relaxation time measurement, it was decided to focus on two polymeric carriers that were clearly differentiated by the FluViSc but were not discriminated by GT. Furthermore, these polymers have high relevance for ASD as both HPMCAS (e.g., Kalydeco, Noxafil, Incivec, Zelboraf) as well as PVP-VA64 (e.g., Onmel, Kaletra, Norvir) are commonly used in marketed solid dispersions. HPMCAS had shown an increase in the FluViSc, whereas PVP-VA64 interestingly showed a viscosity decrease. The expectations on ss-NMR experiments were the same as on Raman spectroscopy (i–iii). Differences in the chemical shifts for API-specific signals between HPMCAS and PVP-VA64 formulations could not be detected (Figure 4). Additionally, it was not possible to discriminate between SDD versus HME from the ¹³C spectra. This was somehow expected due to the broad peaks of the amorphous form in ss-NMR.

Hence, the measurement of molecular mobility was considered the most promising technique to detect drug–polymer interactions. Relaxation time measurements were previously often used to evaluate physical stability⁵³ of ASD and drug–polymer miscibility.^{54,55} Molecular mobilities vary with changes in solid state like the transition from crystalline to amorphous. Therefore, the strong increase in molecular mobility (meaning faster relaxation times) found for amorphous versus crystalline KTZ was expected due to the lack of molecular order in the amorphous form. As the change in the solid state was the dominant factor for $T_{1\rho}$ relaxation times of KTZ and an amorphous reference was not obtainable, these values could not be used to differentiate drug–polymer interactions in formulations with HPMCAS versus PVP-VA64 (Figure 6A,B). However, the polymer itself is also influenced by drug–polymer interactions and—in contrast to the API—does not undergo a change in the solid state. Therefore, relaxation times of the polymer peaks were analyzed as well. HPMCAS in formulation with amorphous KTZ (HME and SDD) showed longer relaxation times, meaning reduced molecular mobility in comparison to the PM and pure polymer (Figure 6C). Interactions with KTZ might have generated a more rigid and less flexible system, which would at the same time also mean better stabilization of the API in its amorphous form and a more efficient inhibition of recrystallization. The reduced molecular mobility might also be the explanation for the increase in viscosity.

ASD with PVP-VA64, that were included as a negative control based on viscosity measurements, did not show this decrease in molecular mobility (Figure 6D). To the contrary, there was even an increase in molecular mobility found for the PVP-VA64 HME (correlating with a viscosity decrease measured in the FluViSc). Interactions between KTZ and PVP-VA64 are therefore quite unlikely, and a stabilizing effect due to drug–polymer interactions would be missing.

As water strongly decreases the glass transition temperature⁵⁶ and increases molecular mobility, water contents must be monitored. This potential bias could be excluded as the water contents were approximately the same for neat polymer, PM, HME, and SDD for each HPMCAS and PVP-VA64 (Table S13, Supporting Information).

In summary, the findings of the relaxation time measurements supported the results of the FluViSc as an appropriate screening tool to rank drug–polymer interactions and enabled a better understanding of the stabilization mechanisms in correlation to viscosity effects. As HPMCAS and PVP-VA64 were not discriminated by the GT approach but interactions were proven to be different by ss-NMR, the benefits and better predictability of the FluViSc could be shown. The estimations by GT were found to be insufficient and nondiscriminating among the polymeric carriers.

Furthermore, it was the aim of this study to better understand the implications of interactions on dissolution performance and physical stability. They can have an enhancing effect on the drug's supersaturation by preventing drug precipitation during dissolution caused by an increased activation energy for nucleation.^{57,58} Interactions may also prolong the physical stability of the amorphous form during storage. Several studies for example on co-amorphous systems^{59–61} support the hypothesis of a stabilizing effect due to interactions. Hence, the analytical results should be linked to dissolution performance of the ASD (Figure 7).

The FluViSc results were evaluated for the formulations with CAP, HPMCAS, PVP-VA64, and PVP K30 in a non-sink dissolution setup. First, HPMCAS and CAP enabled higher maximum concentrations of drug dissolved (400 $\mu\text{g}/\text{mL}$) compared to the PVP derivatives (300 $\mu\text{g}/\text{mL}$). A solubilizing effect of each of the polymers increasing the solubility of crystalline KTZ was not observed in previous trials.²³ Although the precipitation pressure to reach equilibrium solubility again increases with higher degrees of supersaturation, HPMCAS and CAP completely prevented drug precipitation during dissolution. In contrast, PVP K30 was not able to stabilize the supersaturation and the drug dissolved precipitated quickly. The FluViSc proposed stronger interactions for HPMCAS and CAP compared to PVP-VA64 and PVP K30, which was found to result in better stabilization of supersaturation despite of the higher precipitation pressure.

On the other hand, interactions might also prolong the physical stability of the amorphous API by efficiently hindering recrystallization in the solid state. Here, the thermodynamic solubility of the API within the polymer is of crucial importance. This was not in the scope of this study but might add further important insights in follow-up trials.

CONCLUSIONS

The results of the FluViSc were supported by ss-NMR measurements and correlated well with the behavior of different formulations during non-sink dissolution. Therefore, it can be used to rank drug–polymer systems regarding the

extent of interactions formed. The FluViSc was superior compared to GT and Raman spectroscopy that were not discriminating between different polymeric carriers to the same extent. The screening might not be suited to elucidate the specific sites of interaction in a drug–polymer system but it is able to provide a ranking amongst different polymers and their potential to stabilize the amorphous state. Its application is of course limited if there is an interaction between the fluorescent molecular rotor and either API or polymer, leading to fluorescence quenching effects. In addition, the inherently low photostability of these rotors has to be considered. However, the experiments can be conducted with much lower experimental expenditure compared to ss-NMR, and the method is applicable for high-throughput screening studies. Hence, the FluViSc is proposed as an additional miniaturized screening technique for selection of polymeric carriers in ASD.

■ ASSOCIATED CONTENT

■ Supporting Information

The Supporting Information is available free of charge on the ACS Publications website at DOI: [10.1021/acs.molpharmaceut.9b00186](https://doi.org/10.1021/acs.molpharmaceut.9b00186).

Chemical structures of the polymers; fluorescence intensity (FluViSc) with different amounts of neat KTZ; additional depiction of relative viscosity increase from cone–plate rheometer measurements; tabulated data on pycnometric densities of the raw materials; water content of ss-NMR samples based on TGA measurements and detailed $T_{1\rho}$ (13C) relaxation times of all the peaks integrated; relaxation time curves from $T_{1\rho}$ measurements for all the peaks integrated; Raman spectra of crystalline versus amorphous KTZ and overlay of SDD Raman spectra in aromatic and carbonyl region; and diffractograms for the formulations tested in this study (PDF)

■ AUTHOR INFORMATION

Corresponding Author

*E-mail: karsten.maeder@pharmazie.uni-halle.de. Phone: +49-345-55-25167. Fax: +49-345-55-27029 (K.M.).

ORCID

Detlef Reichert: [0000-0002-6876-1901](https://orcid.org/0000-0002-6876-1901)

Karsten Mäder: [0000-0003-1613-6976](https://orcid.org/0000-0003-1613-6976)

Notes

The authors declare no competing financial interest.

■ ACKNOWLEDGMENTS

The authors want to thank Axel Becker for the scientific discussion on multivariate data analysis of Raman spectral data. Jörg Plaschke and Heike Lehr are gratefully acknowledged for their analytical support in developing the FluViSc method. Furthermore, I would also like to extend my thanks to Magdalena Münster, Robert Hennig, and Markus Riehl for the scientific discussions.

■ REFERENCES

- (1) Di, L.; Fish, P. V.; Mano, T. Bridging solubility between drug discovery and development. *Drug Discovery Today* **2012**, *17*, 486–495.
- (2) Leuner, C.; Dressman, J. Improving drug solubility for oral delivery using solid dispersions. *Eur. J. Pharm. Biopharm.* **2000**, *50*, 47–60.

- (3) Alonzo, D. E.; Gao, G.; Zhou, D.; Mo, H.; Zhang, G. G. Z.; Taylor, L. S. Dissolution and precipitation behavior of amorphous solid dispersions. *J. Pharm. Sci.* **2011**, *100*, 3316–3331.

- (4) Paudel, A.; Geppi, M.; Mooter, G. V. d. Structural and Dynamic Properties of Amorphous Solid Dispersions: The Role of Solid-State Nuclear Magnetic Resonance Spectroscopy and Relaxometry. *J. Pharm. Sci.* **2014**, *103*, 2635–2662.

- (5) Weuts, I.; Kempen, D.; Verreck, G.; Peeters, J.; Brewster, M.; Blaton, N.; Van den Mooter, G. Salt formation in solid dispersions consisting of polyacrylic acid as a carrier and three basic model compounds resulting in very high glass transition temperatures and constant dissolution properties upon storage. *Eur. J. Pharm. Sci.* **2005**, *25*, 387–393.

- (6) Shah, N.; Sandhu, H. S.; Choi, D. S.; Chokshi, H.; Malick, A. W. *Amorphous Solid Dispersions*; Springer, 2014.

- (7) (a) Khougaz, K.; Clas, S.-D. Crystallization Inhibition in Solid Dispersions of MK-0591 and Poly(vinylpyrrolidone) Polymers. *J. Pharm. Sci.* **2000**, *89*, 1325–1334. (b) Marsac, P. J.; Shamblyn, S. L.; Taylor, L. S. Theoretical and Practical Approaches for Prediction of Drug-Polymer Miscibility and Solubility. *Pharm. Res.* **2006**, *23*, 2417.

- (8) Taylor, L. S.; Zografi, G. Spectroscopic Characterization of Interactions Between PVP and Indomethacin in Amorphous Molecular Dispersions. *Pharm. Res.* **1997**, *14*, 1691–1698.

- (9) (a) Rumondor, A. C. F.; Konno, H.; Marsac, P. J.; Taylor, L. S. Analysis of the moisture sorption behavior of amorphous drug-polymer blends. *J. Appl. Polym. Sci.* **2010**, *117*, 1055–1063. (b) Konno, H.; Taylor, L. S. Influence of different polymers on the crystallization tendency of molecularly dispersed amorphous felodipine. *J. Pharm. Sci.* **2006**, *95*, 2692–2705.

- (10) Higashi, K.; Yamamoto, K.; Pandey, M. K.; Mroue, K. H.; Moribe, K.; Yamamoto, K.; Ramamoorthy, A. Insights into Atomic-Level Interaction between Mefenamic Acid and Eudragit EPO in a Supersaturated Solution by High-Resolution Magic-Angle Spinning NMR Spectroscopy. *Mol. Pharm.* **2014**, *11*, 351–357.

- (11) Saal, W.; Ross, A.; Wyttenbach, N.; Alsenz, J.; Kuentz, M. A Systematic Study of Molecular Interactions of Anionic Drugs with a Dimethylaminoethyl Methacrylate Copolymer Regarding Solubility Enhancement. *Mol. Pharm.* **2017**, *14*, 1243–1250.

- (12) Kojima, T.; Higashi, K.; Suzuki, T.; Tomono, K.; Moribe, K.; Yamamoto, K. Stabilization of a Supersaturated Solution of Mefenamic Acid from a Solid Dispersion with EUDRAGIT EPO. *Pharm. Res.* **2012**, *29*, 2777–2791.

- (13) Song, Y.; Zemlyanov, D.; Chen, X.; Su, Z.; Nie, H.; Lubach, J. W.; Smith, D.; Byrn, S.; Pinal, R. Acid-base interactions in amorphous solid dispersions of lumefantrine prepared by spray-drying and hot-melt extrusion using X-ray photoelectron spectroscopy. *Int. J. Pharm.* **2016**, *514*, 456–464.

- (14) Konno, H.; Handa, T.; Alonzo, D. E.; Taylor, L. S. Effect of polymer type on the dissolution profile of amorphous solid dispersions containing felodipine. *Eur. J. Pharm. Biopharm.* **2008**, *70*, 493–499.

- (15) Marsac, P. J.; Li, T.; Taylor, L. S. Estimation of Drug-Polymer Miscibility and Solubility in Amorphous Solid Dispersions Using Experimentally Determined Interaction Parameters. *Pharm. Res.* **2008**, *26*, 139–151.

- (16) Turpin, E. R.; Taresco, V.; Al-Hachami, W. A.; Booth, J.; Treacher, K.; Tomasi, S.; Alexander, C.; Burley, J.; Laughton, C. A.; Garnett, M. C. In Silico Screening for Solid Dispersions: The Trouble with Solubility Parameters and χ FH. *Mol. Pharm.* **2018**, *15*, 4654–4667.

- (17) Savolainen, M.; Heinz, A.; Strachan, C.; Gordon, K. C.; Yliruusi, J.; Rades, T.; Sandler, N. Screening for differences in the amorphous state of indomethacin using multivariate visualization. *Eur. J. Pharm. Sci.* **2007**, *30*, 113–123.

- (18) Lubach, J. W.; Hau, J. Solid-State NMR Investigation of Drug-Excipient Interactions and Phase Behavior in Indomethacin-Eudragit E Amorphous Solid Dispersions. *Pharm. Res.* **2018**, *35*, 65.

- (19) Chiang, P.-C.; Cui, Y.; Ran, Y.; Lubach, J.; Chou, K.-J.; Bao, L.; Jia, W.; La, H.; Hau, J.; Sambrone, A.; Qin, A.; Deng, Y.; Wong, H. In

Vitro and In Vivo Evaluation of Amorphous Solid Dispersions Generated by Different Bench-Scale Processes, Using Griseofulvin as a Model Compound. *AAPS J.* **2013**, *15*, 608–617.

(20) Song, Y.; Yang, X.; Chen, X.; Nie, H.; Byrn, S.; Lubach, J. W. Investigation of Drug-Excipient Interactions in Lapatinib Amorphous Solid Dispersions Using Solid-State NMR Spectroscopy. *Mol. Pharm.* **2015**, *12*, 857–866.

(21) Policianova, O.; Brus, J.; Hruba, M.; Urbanova, M.; Zhigunov, A.; Kredatusova, J.; Kobera, L. Structural Diversity of Solid Dispersions of Acetylsalicylic Acid As Seen by Solid-State NMR. *Mol. Pharm.* **2014**, *11*, 516–530.

(22) Wyttenbach, N.; Kuentz, M. Glass-forming ability of compounds in marketed amorphous drug products. *Eur. J. Pharm. Biopharm.* **2017**, *112*, 204–208.

(23) Auch, C.; Harms, M.; Mäder, K. Melt-based screening method with improved predictability regarding polymer selection for amorphous solid dispersions. *Eur. J. Pharm. Sci.* **2018**, *124*, 339–348.

(24) Prudic, A.; Ji, Y.; Sadowski, G. Thermodynamic Phase Behavior of API/Polymer Solid Dispersions. *Mol. Pharm.* **2014**, *11*, 2294–2304.

(25) Wyttenbach, N.; Janas, C.; Siam, M.; Lauer, M. E.; Jacob, L.; Scheubel, E.; Page, S. Miniaturized screening of polymers for amorphous drug stabilization (SPADS): Rapid assessment of solid dispersion systems. *Eur. J. Pharm. Biopharm.* **2013**, *84*, 583–598.

(26) Saluja, A.; Kalonia, D. S. Nature and consequences of protein-protein interactions in high protein concentration solutions. *Int. J. Pharm.* **2008**, *358*, 1–15.

(27) Hofmann, M.; Winzer, M.; Weber, C.; Gieseler, H. Prediction of Protein Aggregation in High Concentration Protein Solutions Utilizing Protein-Protein Interactions Determined by Low Volume Static Light Scattering. *J. Pharm. Sci.* **2016**, *105*, 1819–1828.

(28) Neergaard, M. S.; Kalonia, D. S.; Parshad, H.; Nielsen, A. D.; Møller, E. H.; van de Weert, M. Viscosity of high concentration protein formulations of monoclonal antibodies of the IgG1 and IgG4 subclass - Prediction of viscosity through protein-protein interaction measurements. *Eur. J. Pharm. Sci.* **2013**, *49*, 400–410.

(29) Ueda, K.; Yamazoe, C.; Yasuda, Y.; Higashi, K.; Kawakami, K.; Moribe, K. Mechanism of Enhanced Nifedipine Dissolution by Polymer-Blended Solid Dispersion through Molecular-Level Characterization. *Mol. Pharm.* **2018**, *15*, 4099–4109.

(30) Baghel, S.; Cathcart, H.; O'Reilly, N. J. Understanding the generation and maintenance of supersaturation during the dissolution of amorphous solid dispersions using modulated DSC and ¹H NMR. *Int. J. Pharm.* **2018**, *536*, 414–425.

(31) *Relative Viscosity Measurement Using the Unit*. Unchained Labs. Application Note, 2015.

(32) Haidekker, M. A.; Theodorakis, E. A. Environment-sensitive behavior of fluorescent molecular rotors. *J. Biol. Eng.* **2010**, *4*, 11.

(33) Akers, W. J.; Haidekker, M. A. Precision Assessment of Biofluid Viscosity Measurements Using Molecular Rotors. *J. Biomech. Eng.* **2005**, *127*, 450–454.

(34) Zhu, D.; Haidekker, M. A.; Lee, J.-S.; Won, Y.-Y.; Lee, J. C.-M. Application of Molecular Rotors to the Determination of the Molecular Weight Dependence of Viscosity in Polymer Melts. *Macromolecules* **2007**, *40*, 7730–7732.

(35) Rumble, C.; Rich, K.; He, G.; Maroncelli, M. CCVJ Is Not a Simple Rotor Probe. *J. Phys. Chem. A* **2012**, *116*, 10786–10792.

(36) Agrawal, A. M.; Dudhedia, M. S.; Patel, A. D.; Raikes, M. S. Characterization and performance assessment of solid dispersions prepared by hot melt extrusion and spray drying process. *Int. J. Pharm.* **2013**, *457*, 71–81.

(37) Amidon, G. L.; Lennernäs, H.; Shah, V. P.; Crison, J. R. A theoretical basis for a biopharmaceutical drug classification: the correlation of in vitro drug product dissolution and in vivo bioavailability. *Pharm. Res.* **1995**, *12*, 413–420.

(38) Gordon, M.; Taylor, J. S. Ideal copolymers and the second order transitions of synthetic rubbers. I. Non-crystalline copolymers. *J. Appl. Chem.* **1952**, *2*, 493–500.

(39) Hancock, B. C.; Zografi, G. The Relationship Between the Glass Transition Temperature and the Water Content of Amorphous Pharmaceutical Solids. *Pharm. Res.* **1994**, *11*, 471–477.

(40) Williams, G.; Watts, D. C. Non-symmetrical dielectric relaxation behaviour arising from a simple empirical decay function. *Trans. Faraday Soc.* **1970**, *66*, 80–85.

(41) Fedotov, V. D.; Schneider, H. Structure and dynamics of bulk polymers by NMR method. In *NMR Basic Principles and Progress/NMR Grundlagen und Fortschritte*; Diehl, P.; Fluck, E.; Kosfeld, R., Eds.; Springer Science and Business Media, 2012; Vol. 21.

(42) Alonzo, D. E.; Zhang, G. G. Z.; Zhou, D.; Gao, Y.; Taylor, L. S. Understanding the behavior of amorphous pharmaceutical systems during dissolution. *Pharm. Res.* **2009**, *27*, 608–618.

(43) Ullrich, A.; Schiffer, H. A. The influence of polymer excipients on the dissolution and recrystallization behavior of ketoconazole: Application, variation and practical aspects of a pH shift method. *Eur. J. Pharm. Biopharm.* **2018**, *133*, 20–30.

(44) Van Eerdenbrugh, B.; Taylor, L. S. An ab initio polymer selection methodology to prevent crystallization in amorphous solid dispersions by application of crystal engineering principles. *CrystEngComm* **2011**, *13*, 6171–6178.

(45) Wang, S.; Liu, C.; Chen, Y.; Zhu, A.; Qian, F. Aggregation of Hydroxypropyl Methylcellulose Acetate Succinate under its Dissolving pH and the Impact on Drug Supersaturation. *Mol. Pharm.* **2018**, *15*, 4643–4653.

(46) Warren, D. B.; Benameur, H.; Porter, C. J. H.; Pouton, C. W. Using polymeric precipitation inhibitors to improve the absorption of poorly water-soluble drugs: A mechanistic basis for utility. *J. Drug Targeting* **2010**, *18*, 704–731.

(47) Sutharsan, J.; Lichlyter, D.; Wright, N. E.; Dakanali, M.; Haidekker, M. A.; Theodorakis, E. A. Molecular rotors: synthesis and evaluation as viscosity sensors. *Tetrahedron* **2010**, *66*, 2582–2588.

(48) Rask, M. B.; Knopp, M. M.; Olesen, N. E.; Holm, R.; Rades, T. Influence of PVP/VA copolymer composition on drug-polymer solubility. *Eur. J. Pharm. Sci.* **2016**, *85*, 10–17.

(49) Couchman, P. R.; Karasz, F. E. A Classical Thermodynamic Discussion of the Effect of Composition on Glass-Transition Temperatures. *Macromolecules* **1978**, *11*, 117–119.

(50) Yoshioka, M.; Hancock, B. C.; Zografi, G. Inhibition of indomethacin crystallization in poly(vinylpyrrolidone) coprecipitates. *J. Pharm. Sci.* **1995**, *84*, 983–986.

(51) Warren, D. B.; Bergström, C. A. S.; Benameur, H.; Porter, C. J. H.; Pouton, C. W. Evaluation of the Structural Determinants of Polymeric Precipitation Inhibitors Using Solvent Shift Methods and Principle Component Analysis. *Mol. Pharm.* **2013**, *10*, 2823–2848.

(52) Miller, D. A.; DiNunzio, J. C.; Yang, W.; McGinity, J. W.; Williams, R. O. Enhanced In Vivo Absorption of Itraconazole via Stabilization of Supersaturation Following Acidic-to-Neutral pH Transition. *Drug Dev. Ind. Pharm.* **2008**, *34*, 890–902.

(53) Schantz, S.; Hoppu, P.; Juppo, A. M. A Solid-State NMR Study of Phase Structure, Molecular Interactions, and Mobility in Blends of Citric Acid and Paracetamol. *J. Pharm. Sci.* **2009**, *98*, 1862–1870.

(54) Aso, Y.; Yoshioka, S.; Kojima, S. Explanation of the Crystallization Rate of Amorphous Nifedipine and Phenobarbital from Their Molecular Mobility as Measured by ¹³C Nuclear Magnetic Resonance Relaxation Time and the Relaxation Time Obtained from the Heating Rate Dependence of the Glass Transition Temperature. *J. Pharm. Sci.* **2001**, *90*, 798–806.

(55) Aso, Y.; Yoshioka, S.; Kojima, S. Molecular mobility-based estimation of the crystallization rates of amorphous nifedipine and phenobarbital in poly(vinylpyrrolidone) solid dispersions. *J. Pharm. Sci.* **2004**, *93*, 384–391.

(56) Oksanen, C. A.; Zografi, G. The Relationship Between the Glass Transition Temperature and Water Vapor Absorption by Poly(vinylpyrrolidone). *Pharm. Res.* **1990**, *7*, 654–657.

(57) Raghavan, S. L.; Trividic, A.; Davis, A. F.; Hadgraft, J. Crystallization of hydrocortisone acetate: influence of polymers. *Int. J. Pharm.* **2001**, *212*, 213–221.

(58) Chauhan, H.; Kuldipkumar, A.; Barder, T.; Medek, A.; Gu, C.-H.; Atef, E. Correlation of Inhibitory Effects of Polymers on Indomethacin Precipitation in Solution and Amorphous Solid Crystallization Based on Molecular Interaction. *Pharm. Res.* **2014**, *31*, 500–515.

(59) Löbmann, K.; Laitinen, R.; Strachan, C.; Rades, T.; Grohgan, H. Amino acids as co-amorphous stabilizers for poorly water-soluble drugs - Part 2: Molecular interactions. *Eur. J. Pharm. Biopharm.* **2013**, *85*, 882–888.

(60) Chavan, R. B.; Thipparaboina, R.; Kumar, D.; Shastri, N. R. Co amorphous systems: A product development perspective. *Int. J. Pharm.* **2016**, *515*, 403–415.

(61) Allesø, M.; Chieng, N.; Rehder, S.; Rantanen, J.; Rades, T.; Aaltonen, J. Enhanced dissolution rate and synchronized release of drugs in binary systems through formulation: Amorphous naproxen–cimetidine mixtures prepared by mechanical activation. *J. Controlled Release* **2009**, *136*, 45–53.



Impact of amorphization and GI physiology on supersaturation and precipitation of poorly soluble weakly basic drugs using a small-scale in vitro transfer model



Carolin Auch^{a,b}, Christian Jede^c, Meike Harms^b, Christian Wagner^b, Karsten Mäder^{a,*}

^a Institute of Pharmacy, Faculty I of Natural Sciences, Martin Luther University Halle-Wittenberg, Wolfgang-Langenbeck-Str. 4, 06120 Halle/Saale, Germany

^b Department of Pharmaceutical Technologies, Merck Healthcare KGaA, Frankfurter Straße 250, 64293 Darmstadt, Germany

^c Department of Analytical Development, Merck Healthcare KGaA, Frankfurter Straße 250, 64293 Darmstadt, Germany

ARTICLE INFO

Keywords:

Amorphous solid dispersion
Transfer model
Precipitation inhibitor
Gastrointestinal
Biorelevant
GI variability

ABSTRACT

Formulation of amorphous solid dispersions (ASD) is one possibility to improve poor aqueous drug solubility by creating supersaturation. In case of weakly basic drugs like ketoconazole (KTZ), supersaturation can also be generated during the gastrointestinal (GI) transfer from the stomach to the intestine due to pH-dependent solubility. In both cases, the supersaturation during dissolution can be stabilized by polymeric precipitation inhibitors. A small-scale GI transfer model was used to compare the dissolution performance of ASD versus crystalline KTZ with the polymeric precipitation inhibitor HPMCAS. Similar *in vitro* AUCs were found for the transfer from SGF pH 2 into FaSSiF. Moreover, the impact of variability in gastric pH on drug dissolution was assessed. Here, the ASD performed significantly better at a simulated hypochlorhydric gastric pH of 4. Last, the importance of drug-polymer interactions for precipitation inhibition was evaluated. HPMCAS HF and LF grades with and without the basic polymer Eudragit E PO were used. However, E PO caused a faster precipitation probably due to competition for the interaction sites between KTZ and HPMCAS. Thus, the results are suited to assess the benefits of amorphous formulations vs. precipitation inhibitors under different gastrointestinal conditions to optimize the design of such drug delivery systems.

1. Introduction

The Biopharmaceutical Classification System (BCS) by Amidon et al. (1995) serves as a tool to classify active pharmaceutical ingredients (API) in terms of solubility and permeability. Many new API in the industrial pipeline are classified as BCS class II or IV drugs expressing poor aqueous solubility (Ting et al., 2018).

The main causes for poor aqueous solubility are high lipophilicity and high intermolecular forces within the crystal lattice (Ishikawa and Hashimoto, 2011; Yalkowsky and Valvani, 1980). For the latter, especially the formulation as amorphous solid dispersions (ASD) represents a possibility to increase the apparent solubility and the dissolution rate (Leuner and Dressman, 2000). This results in supersaturation upon dissolution which can be stabilized by using polymeric carriers that

hinder nucleation and/or crystal growth, and, thus, recrystallization and precipitation of the API to the thermodynamically stable crystalline state.

However, at least for ionic drugs, the aqueous solubility may also depend on the pH value which changes under physiologically relevant conditions during the gastrointestinal (GI) transfer. The high relevance of pH-dependent API solubility was demonstrated in studies by Manallack (2009); Manallack et al. (2013) who reviewed the pK_a dependent distribution of 907 orally administered drugs. The authors found almost half of them being single or bi-basic meaning that they contain physiologically relevant ionizable groups (with about 25% acid compounds and another 25% being ampholytes).

Weakly basic drugs express higher solubility under the acidic conditions of the stomach which decreases at elevated pH under intestinal

Abbreviations: ACN, acetonitrile; API, active pharmaceutical ingredient; ASD, amorphous solid dispersion; AUC, area under the curve; BCS, Biopharmaceutical Classification System; DCM, dichloromethane; DMF, N,N-dimethylformamide; DSC, differential scanning calorimetry; FaSSiF, fasted state simulated intestinal fluid; GI, gastrointestinal; HPMCAS, hydroxypropylmethylcellulose acetate succinate; KTZ, ketoconazole; MeOH, methanol; N_{agg} , aggregation number; PM, physical mixture; PXRD, powder X-ray diffraction; RP-HPLC, reversed-phase high-performance liquid chromatography; SD, spray-drying; SDD, spray-dried dispersion; SGF, simulated gastric fluid; T_g , glass transition temperature; T_m , melting temperature

* Corresponding author.

E-mail address: karsten.maeder@pharmazie.uni-halle.de (K. Mäder).

<https://doi.org/10.1016/j.ijpharm.2019.118917>

Received 28 September 2019; Received in revised form 27 November 2019; Accepted 28 November 2019

Available online 04 December 2019

0378-5173/© 2019 Elsevier B.V. All rights reserved.

conditions (Dressman and Reppas, 2000). Hence, the GI transfer of dissolved drug from the stomach into the small intestine also generates supersaturated drug solutions (Kostewicz et al., 2004; Psachoulas et al., 2011). As these are, likewise ASD, prone to recrystallization (Vertzoni et al., 2005; Wagner et al., 2012), stabilizing polymeric precipitation inhibitors are needed. For drugs that are mainly absorbed in the small intestine, the supersaturation in the intestinal lumen must be stabilized during the transit time (Brouwers et al., 2009). In this context, Jankovic et al. (2019) recently assessed the GI absorption of ASD *in vitro* in a biphasic dissolution test together with a simulated GI transfer. Only if stabilization in the small intestine is given – and if the drug is well permeable – the higher concentration of molecularly dissolved drug in the intestinal lumen can lead to a higher fraction absorbed and higher bioavailability (Buckley et al., 2013).

However, the physiologically induced supersaturation depends on gastric conditions which are highly variable within different patients (Abuhelwa et al., 2017; Schneider et al., 2016) as well as under fasting standardized conditions (Grimm et al., 2018). This might in turn result in high pharmacokinetic variability (Shah et al., 2014). Furthermore, the intake of acid-reducing agents such as proton-pump inhibitors reduces acid secretion in the stomach and causes higher pH values which can subsequently affect drug solubility (Budha et al., 2012) and pharmacokinetics in general (Segregur et al., 2019).

Dissolution experiments in a single intestinal medium (e.g. fasted-state simulated intestinal fluid FaSSIF) might work sufficiently well for neutral and acidic drugs. However, the increased solubility under gastric pH of poorly soluble weak bases needs to be considered for formulation testing and development. Therefore, an *in vitro* transfer model (Jede et al., 2018) was used in the present study to simulate the transfer of dissolved drug from a simulated stomach to a simulated small intestine.

The first part of this study aimed at investigating the induction of supersaturation in two different ways under specified GI conditions: by formulation of an amorphous solid dispersion or by physiologically induced supersaturation. Therefore, the model drug ketoconazole (KTZ) was selected as a weakly basic BCS class II compound with a strong pH-dependent solubility *in vitro* and a high dependence of oral bioavailability on gastric pH *in vivo* (Dressman and Reppas, 2000; Van Der Meer et al., 1980). ASD with KTZ and two different hydroxypropylmethylcellulose acetate succinate grades (HPMCAS, HF and LF) were manufactured as ASD via spray-drying (SD) and compared to the performance of physical mixtures (PM) of crystalline KTZ in presence of HPMCAS HF/LF in a direct dissolution approach in FaSSIF as well as in the GI transfer model developed by Jede et al. Most recently, Ullrich and Schiffter (2018) were among the first to examine the behavior of ASD in a pH shift method which was so far mostly neglected. However, the authors did not describe the effect of amorphous formulations vs. crystalline drug polymer mixtures, which represents an important question in terms of appropriate formulation strategies.

The two different HPMCAS grades that were used in this study differ in their contents of acetyl and succinoyl endgroups (Table 4) which leads to different pK_a values as well as different polarities. This was also of interest for further elucidation of the mechanism of precipitation inhibition and evaluation of acid/base interactions between the drug and the polymeric carrier. Therefore, polymer combinations of the HPMCAS grades with Eudragit® E PO were tested as ASD as well as PM. E PO represents a basic polymer, that is used for different formulation purposes, e.g. manufacturing of amorphous formulations, taste masking or moisture protection (Saal et al., 2018). Up to date, the effect of the presence of a basic polymer next to an acidic polymer, its correlation to drug-polymer interactions and the overall impact on drug dissolution, has not been carried out.

Additionally, the influence of elevated gastric pH on the transfer of the amorphous systems as well as on the crystalline PM was examined in the present study.

In early development phases, formulations of poorly soluble drugs

are being developed with the aim to increase the solubility and subsequent *in vivo* absorption. Therefore, discriminative *in vitro* assays are needed of which the results are fed e.g. into *in silico* tools for bioavailability predictions (Patel et al., 2019) and used to address the question which formulation effort, i.e. elaborative amorphous formulations vs. time-effective PM, should be pursued. The small-scale approach used in this study is well suited for preclinical formulation development as it allows rapid assessment of different formulations based on biorelevant dissolution methods.

2. Materials and methods

2.1. Materials

KTZ was obtained from Biotrend Chemicals AG (Switzerland). Hydroxypropyl methylcellulose acetate succinate (HPMCAS) in HF and LF grade were donated by Shin Etsu (Japan). Eudragit® E PO (E PO) was obtained from Evonik (Germany). Sodium hydroxide (VWR Chemicals, Belgium), sodium chloride, di-sodium hydrogen phosphate, hydrochloric acid 1M and sodium hydroxide solution 1M (Merck KGaA, Germany) for preparation of the different dissolution buffers were used in analytical grade. N,N-Dimethylformamide (DMF, Alfa Aesar, USA) was of HPLC grade (purity $\geq 99.7\%$). Acetonitrile (ACN), dichloromethane (DCM) and methanol (MeOH) were purchased from Merck KGaA, Germany. Purified water was taken from a Millipore-Milli-Q® integral water purification system (Millipore Merck KGaA, Germany).

2.2. Dissolution media

Simulated Gastric Fluid (SGF) pH 2, SGF_{hypo} pH 4 and fasted-state simulated intestinal fluid pH 6.5 (FaSSIF-V1) were used as compendial media for dissolution testing. SGF was prepared according to USP and adjusted to pH 2 (instead of pH 1.2) to avoid substantial pH decrease during the *in vitro* transfer of SGF into FaSSIF (Ruff et al., 2017). This was also considered for preparation of FaSSIF, where a double-concentrated phosphate buffer was used (Jede et al., 2019). SGF_{hypo} pH 4 were prepared according to Jede et al. (2019).

2.3. Miscibility testing of binary polymer combinations

A DSC 1 from Mettler Toledo (Switzerland) was used for evaluation of miscibility between the two polymers HPMCAS HF/LF and E PO. The polymers were tested in ratios of 3:1, 1:1 and 1:3 (w/w). Stock solutions of the different polymers were prepared in DMF in concentrations of 20 mg/mL.

The stock solutions were premixed in PTFE screw cap vials and poured out onto PTFE non-adhesive foils. The resulting films were peeled off after solvent evaporation in the freezer dryer and subsequently weighed into 100 μ L DSC crucibles with piercing lid. A heating and cooling rate of ± 10 K/min was applied. The DSC heating ramp was defined from 25 °C to above the glass transition temperature of the polymer with the higher T_g . All glass transition temperatures (T_g) are reported as onset values of three independently prepared samples with standard deviation.

2.4. Spray-drying

A 4M8-TriX Formatrix Spray Dryer (ProCepT, Belgium) was used for preparation of spray-dried dispersions (SDD). API and polymer or polymer combinations were dissolved in DCM:MeOH 9:1 (v/v), which resulted in a concentration of 2% (w/w) solid content. The drug load (DL) was kept constant with 40% (w/w) with respect to the polymer for HPMCAS LF, HPMCAS HF and the combinations with Eudragit E PO. The spray-dryer was equipped with a 1.0 mm nozzle, 10 L/min atomizing nitrogen and 70% air speed. Air temperature and feed rate were

Table 1
Spray-drying parameters for binary and ternary SDD formulations with 40% (w/w) drug load KTZ.

Formulations	Drying air temperature (°C)	Feed rate (mL/min)	Outlet temperature readout (°C)	Yield (%)
SDD HPMCAS LF + 40% KTZ	80	2.0	52.8	66.7
SDD HPMCAS HF + 40% KTZ	80	2.0	54.3	81.4
SDD HPMCAS LF + E PO + 40% KTZ	80	2.0	55.0	65.8
SDD HPMCAS HF + E PO + 40% KTZ	80	2.0	51.1	68.9

Table 2
Parameters for in vitro transfer model.

Parameter	Automated small-scale transfer model
Gastric compartment	25 mL SGF (pH 2.0/4.0)
Intestinal compartment	25 mL FaSSiF (pH 6.5)
Amount of KTZ	20 mg
Amount of polymer	30 mg
Paddle/stirrer speed	150 rpm
Transfer rate first order	$t_{1/2} = 5$ min
Temperature	37 ± 0.5 °C

adjusted to result in fully amorphous SDD. Process details of the formulations are given in Table 1. The samples were subsequently dried in a desiccator over silica gel at 100 mbar to ensure removal of residual solvents. SDD formulations were tested in terms of crystallinity (DSC 2.5.1, PLM, PXRD 2.5.2), content and impurities (RP-HPLC, Section 2.5.3), particle size (microscopy) and dissolution performance under non-sink conditions (Section 2.5.4).

2.5. SDD analytics

2.5.1. DSC

Sample preparation was conducted according to Section 2.3.1. Two heating cycles were applied: the first reached from 25 °C up to 170 °C (above T_m of KTZ), afterwards the melt was cooled down to 0 °C and heated again up to 200 °C.

Glass transition temperatures (T_g) were determined in the second heating cycle. The SDD were described by both heating cycles: absence of a melting peak of KTZ was checked in the first cycle for successful amorphization. T_g of the resulting mixtures were analyzed in the second cycle by the analysis of onset values ($n = 3$).

2.5.2. PXRD

A Stoe StadiP 611 instrument (Stoe, Germany) with Cu- $K_{\alpha 1}$ radiation source and a Mythen1K Si-strip detector (PSD) was used to investigate crystallinity of the SDD. The samples were measured at room temperature and were prepared on a 96 well plate sample holder with a Kapton® foil on the bottom of the wells. An angular resolution of $0.03^\circ 2\theta$ over a 2θ range from $-36^\circ 2\theta$ to $+36^\circ 2\theta$ was applied and the spectra were folded to $0-36^\circ 2\theta$. Measurement times of 30 sec/PSD-step and a PSD step width of $0.09^\circ 2\theta$ were used.

2.5.3. RP-HPLC analysis

Monitoring of content and impurities was conducted with an Agilent Technologies (USA) 1260 HPLC system at 225 nm. A detailed description of the corresponding method is given in (Auch et al., 2019).

2.5.4. Non-sink dissolution

The small-scale dissolution testing of SDD was conducted in 2 mL rounded bottom Eppendorf Caps. Pre-warmed FaSSiF-V1 was added to 1.2 mg of formulation. Samples were taken after 5, 10, 15, 20, 30, 45, 60, 90 and 120 min. Suspensions were centrifuged for 2 min at 15,000 rpm (Mikro 200R centrifuge, Hettich, Germany) prior to sampling and 50 μ L supernatant (without replacement) was transferred each time and diluted 1:3 with ACN/water (50:50, v/v). The

concentration of drug dissolved was determined via RP-HPLC with $n = 3$ (Section 2.6.3). A detailed description is given in (Auch et al., 2018).

2.6. In vitro transfer model

The model applied reflects a 1:10 scale-down (25 mL instead of 250 mL gastric volume after water administration for drug intake). Therefore, 20 mg KTZ (corresponding to a 1:10 scale-down of 200 mg human dose) and the respective amounts of different polymers (40% DL, w/w) were dissolved (in case of KTZ) and suspended (in case of HPMCAS) in 25 mL SGF (donor compartment). API and polymer were suspended individually as PM or together as existing SDD. After 30 min pre-conditioning, the acid drug-polymer suspension was transferred into FaSSiF (acceptor compartment) using a first order transfer rate ($t_{1/2} = 5$ min). The solutions/suspensions were constantly stirred at 150 rpm using magnetic stirrers. The complete set-up of the small-scale transfer model was placed in a GFL 3033 incubator (GFL, Germany) heated to 37 °C. All transfer experiments described in this study were performed in triplicate. The area under the curve (AUC) of the time frame explored (0–120 min) was calculated based on the concentration–time profiles obtained from the *in vitro* transfer experiments. Table 2 summarizes the experimental parameters. For more details on method development and set-up evaluations, the reader is referred to previous publications (Jede et al., 2019, 2018).

3. Results and discussion

3.1. Spray-dried formulations

The SD experiments resulted in powdery solid formulations and high yields for all combinations. The API content ($> 98\%$ recovery) and purity ($> 98\%$ with respect to API main peak) of all formulations were tested by RP-HPLC. Eudragit® E PO has a low T_g and is therefore normally difficult to handle in a SD process in case the outlet temperature exceeds the T_g which causes high molecular mobility and sticky material. Additionally, the risk of recrystallization due to enhanced molecular mobility above T_g is strongly increased (Yoshioka et al., 1994; Zhao et al., 2012). However, in combination with HPMCAS HF and LF this could be mitigated. It was not possible to prepare fully amorphous KTZ as a reference via spray-drying which was also described by Ullrich and Schiffter, 2018.

3.2. SDD analytics

3.2.1. DSC

The T_g of the single components as well as of binary and ternary systems were determined in the second DSC heating cycle (Section 2.5.1.). The values are summarized in Table 3. The T_g of the binary polymer combinations were determined of film casted polymer foils which represented full miscibility (and subsequent detection of single T_g) in contrast to powdery PM (Section 2.3.). The thermograms of SDD verum did not contain a KTZ melting peak but always showed a single T_g . The plasticizing effect of KTZ in all formulations is clearly visible, expressed by a decreased T_g .

The T_g of the two HPMCAS grades were very similar. However, in

Table 3
Glass transition temperatures of neat components, binary and ternary systems. Arithmetic means of $n = 3 \pm S.D.$

Formulations		T_g ($^{\circ}C$)	T_g ($^{\circ}C$) according to GT
HPMCAS LF	Polymer	115.1 ± 0.5	n.n.
HPMCAS HF	Polymer	117.8 ± 0.4	n.n.
E PO	Polymer	39.1 ± 0.8	n.n.
Ketoconazole	API	43.9 ± 0.2	n.n.
SDD HPMCAS LF + 40% KTZ	SDD Verum	72.9 ± 0.4	70.9
SDD HPMCAS HF + 40% KTZ	SDD Verum	67.3 ± 1.1	71.5
SDD HPMCAS LF + E PO + 40% KTZ	SDD Verum	63.8 ± 1.1	63.4
SDD HPMCAS HF + E PO + 40% KTZ	SDD Verum	58.5 ± 1.9	63.8

Table 4
Acetyl and succinoyl contents of HPMCAS HF and LF grades (AQOAT[®]), data provided by manufacturer ShinEtsu.

HPMCAS grade	Acetyl content (%)	Succinoyl content (%)	Solubility at pH
HF	10.0–14.0	4.0–8.0	≥ 6.8
LF	5.0–9.0	14.0–18.0	≥ 5.5

both cases, the T_g of their combinations either in a binary system with 40% KTZ or in a ternary system with KTZ and E PO was found to be slightly higher for HPMCAS LF.

The T_g of mixtures can be calculated according to the Gordon-Taylor equation (Hancock and Zografi, 1994). Positive deviations from the calculated values (given in Table 3) are commonly considered to be a hint for drug-polymer interactions. In turn, positive deviations of measured T_g values for formulations with HPMCAS LF compared to HPMCAS HF might indicate potentially stronger interactions.

3.2.2. Analytics – PXR D

The PM and spray-dried formulations were tested using PXR D to confirm successful amorphization. In contrast to the PM with KTZ, the SDD did not show reflections from crystalline API with 40% DL in any of the formulations which indicated amorphous samples (Fig. 1) in alignment to DSC results.

3.3. Transfer model HPMCAS LF – SDD vs. physical mixture (SGF pH 2)

At first, the transfer model was used to compare the performance of the amorphous SDD with the PM containing crystalline KTZ and the

respective polymer. The transfer experiment was started with a dissolution step in SGF pH 2. Due to its physicochemical properties, the enteric HPMCAS is not soluble at pH values less than 5.5 (Table 4).

PM of KTZ, that were tested with different polymers in a non-sink dissolution testing in FaSSIF at pH 6.5, did not provide any supersaturation compared to neat KTZ (Auch et al., 2018). Only the amorphous SDD generated supersaturation in a single compartment non-sink dissolution experiment (Fig. 2A). In contrast, the transfer model showed that amorphization of KTZ was not the only possibility to increase the AUC. In contrast, under consideration of the GI pH shift, also the PM showed prolonged supersaturation compared to neat KTZ and did even slightly outperform the SDD (Fig. 2B). The reasons for this difference in performance could not be elucidated so far as both formulations showed immediate release of the full amount of KTZ in a single compartment dissolution testing in SGF pH 2 (data not shown). In effect, a benefit for the amorphous formulation was not found when applying a simulated gastric pH of 2 in the transfer model experiment in contrast to the non-sink dissolution testing where the apparent solubility was increased.

This underlines the necessity of performing a systematic series of experiments as conducted in the present study in single buffers as well as in the transfer model to elucidate benefits and differences between the formulations under physiologically relevant conditions.

3.4. Transfer model HPMCAS LF – Hypochlorhydric conditions (SGF pH 4)

To account for the high variability of gastric pH in human individuals (Abuhelwa et al., 2017; Grimm et al., 2018; Schneider et al., 2016), the dissolution tests were additionally conducted under hypochlorhydric conditions, i.e. SGF pH 4 instead of pH 2. Several studies report on decreased bioavailability of weakly basic drugs under altered gastric conditions (Budha et al., 2012; Monschke and Wagner, 2019). Due to inter- and intra-individual variability in patients, it is generally favorable to focus on pH-independent formulation strategies like it was realized e.g. with OMS-based formulation for itraconazole compared to the powder in capsule product Sporanox[®] or a melt extrudate of lopinavir/ritonavir (Kaletra[®]) (Klein et al., 2007).

pH 4 was chosen as a realistic value based on studies from human aspirates (Litou et al., 2017). Therefore, SGF was adjusted to this pH and concentrations of drug dissolved were again measured in a non-sink dissolution setup as well as in the transfer model (Fig. 3). The solubility of crystalline KTZ at pH 4 is strongly decreased compared to pH 2 (4.3 mg/mL vs. 0.13 mg/mL, (Jede et al., 2019)) but was still significantly higher compared to the thermodynamic solubility of KTZ in FaSSIF pH 6.5 (0.02 mg/mL, (Auch et al., 2018)). Employing a pH of 4 for simulating the fasted stomach, the SDD with HPMCAS LF,

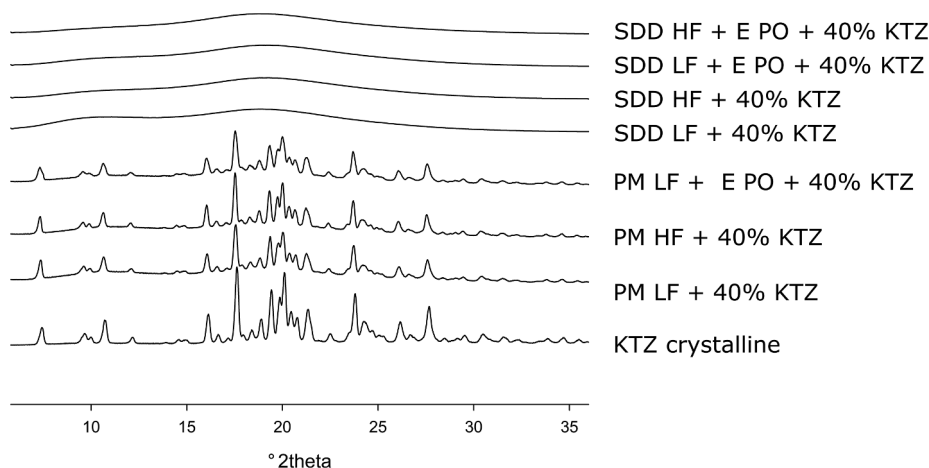


Fig. 1. XRD of neat crystalline KTZ, crystalline PM and amorphous SDD formulations.

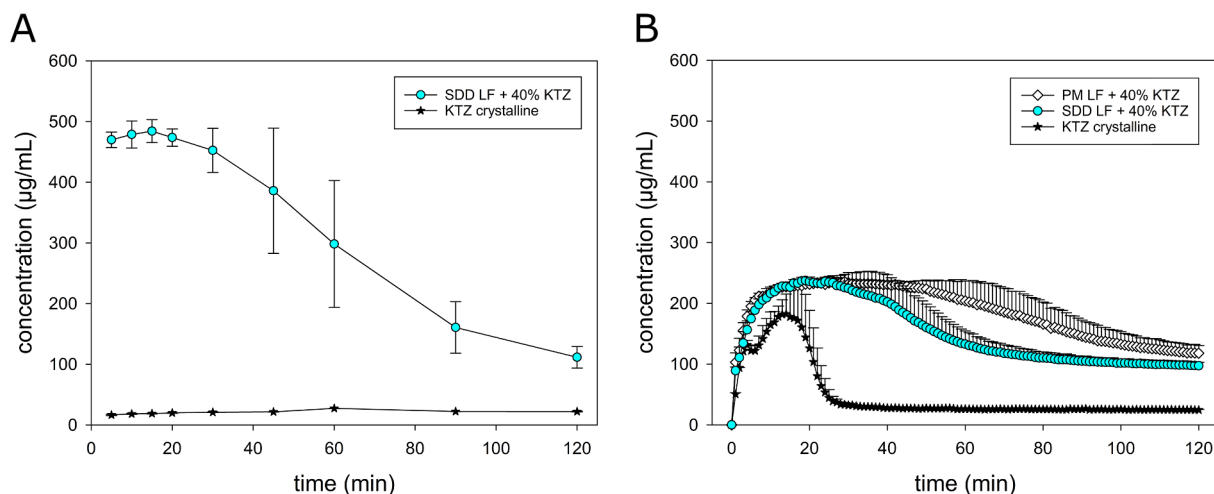


Fig. 2. (A) Non-sink dissolution testing of crystalline KTZ and SDD with HPMCAS LF and 40% DL KTZ in FaSSiF pH 6.5. Arithmetic means of $n = 3 \pm$ S.D. (B) Transfer of PM and SDD with HPMCAS LF and 40% DL KTZ from SGF pH 2 into FaSSiF-V1 pH 6.5. Arithmetic means of $n = 3 +$ S.D.

containing amorphous KTZ, showed a pronounced increase of apparent solubility compared to crystalline API (Fig. 3A). This was also well reflected by the transfer model results, where the PM containing crystalline KTZ did not provide any benefit in comparison to neat API. However, the amorphous SDD showed a strong solubility-enhancing effect on both supersaturation and AUC (2.9-fold in c_{max} and 1.7-fold in AUC) which is depicted Fig. 3B. These results support the usage of amorphous formulations to reduce variability and still increase bio-availability (although the AUC of the SDD was also decreased at pH 4 compared to pH 2). This finding was in contrast to the results for the drug nevirapine by Monschke and Wagner (2019). In this study, the usage of enteric polymers was claimed to avoid solubility variations due to variability (increase) of GI pH. An explanation might be a considerably less pronounced pH-dependent solubility profile of nevirapine compared to KTZ.

3.5. Transfer model of formulations with HPMCAS LF vs. HPMCAS HF

The comparison between HF and LF was drawn to examine stabilizing drug-polymer interactions. The HPMCAS HF grade contains a different composition of acetyl and succinoyl groups compared to HPMCAS LF (Table 4) and therefore only dissolves at pH values > 6.8 . While HPMCAS is in general amphiphilic in nature, HPMCAS HF is more hydrophobic than LF due to the different chemical composition

(Ueda et al., 2014; Wang et al., 2018).

SDD formulations containing 40% DL KTZ were again compared using the non-sink dissolution and the transfer model (Fig. 4). In both cases, the maximum concentration of drug dissolved was higher employing HPMCAS LF as matrix. In the non-sink setup (Fig. 4A), HPMCAS HF maintained the supersaturation without precipitation which was not achieved with HPMCAS LF. The same effect was observed in the transfer model (Fig. 4B). However, the drug concentration at the time where a stable plateau was reached (approx. after 60 min) was nearly the same resulting in sum in a higher AUC for the HPMCAS LF formulation.

In terms of drug-polymer interactions, the predominant ones often are ionic forces which should be in theory more distinct for the more acidic HPMCAS LF grade thus enabling better stabilization of supersaturation. However, these statements cannot be added as an explanation for the difference in stabilization of the supersaturation of the ASD in the single compartment FaSSiF buffer (Fig. 4A) where HPMCAS HF performed significantly better.

To explain such effects, Wang and co-workers investigated the aggregation behavior of HPMCAS under different pH values in PBS buffer via static and dynamic light scattering (Wang et al., 2018). The competition between polymer-solvent and intermolecular interactions was closer evaluated. On the one hand, an aggregation of polymer coils was found which was reflected in higher values for the radius of gyration as

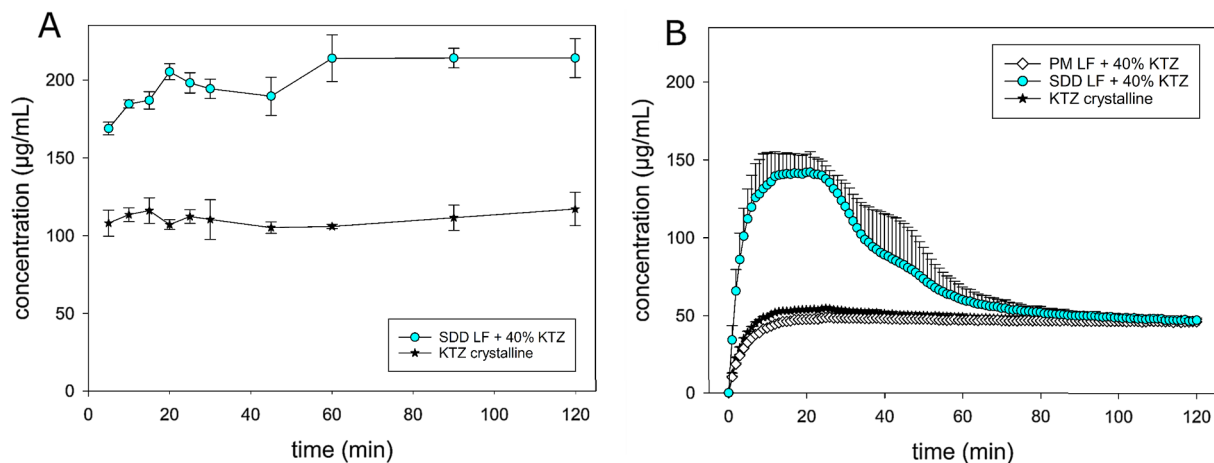


Fig. 3. (A) Non-sink dissolution testing of SDD HPMCAS LF vs. crystalline KTZ in SGF pH 4. Arithmetic means of $n = 3 \pm$ S.D. (B) Transfer model of PM HPMCAS LF compared to SDD HPMCAS LF with 40% DL each. Transfer was conducted from SGF pH 4 into FaSSiF-V1 pH 6.5. Arithmetic means of $n = 3 +$ S.D.

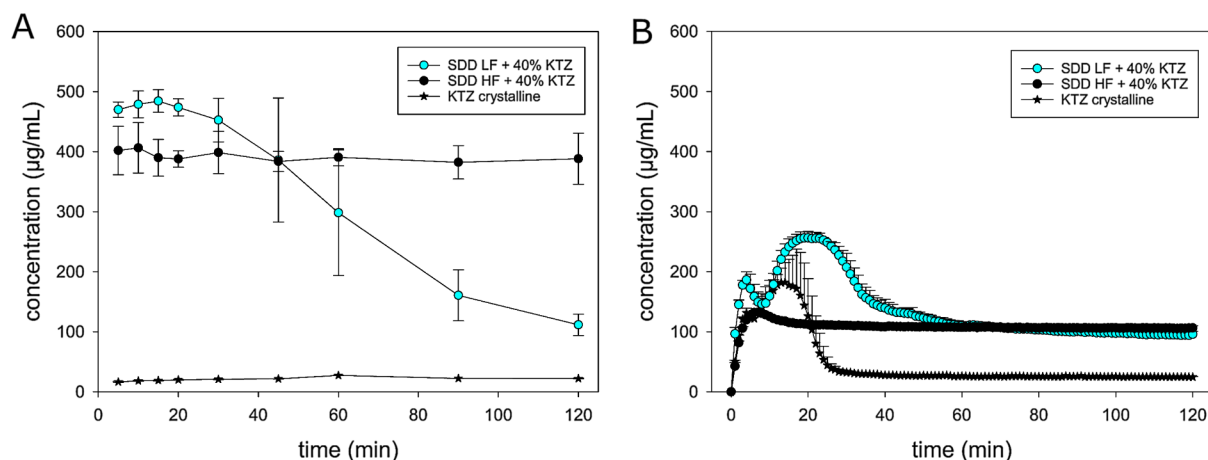


Fig. 4. (A) Non-sink dissolution testing of SDD HPMCAS LF vs. SDD HPMCAS HF with 40% DL each in FaSSiF-V1. Arithmetic means of $n = 3 \pm$ S.D. (B) Transfer model of SDD with HPMCAS LF compared to SDD HPMCAS HF with 40% DL each. Transfer was conducted from SGF pH 2 into FaSSiF-V1 pH 6.5. Arithmetic means of $n = 3 +$ S.D.

aggregates up to 113 nm were formed. This aggregation was also expressed as the aggregation number (N_{agg}) as the quotient between molecular weight of the colloids by the absolute molecular weight of HPMCAS. The maximum N_{agg} was 19 for HPMCAS LF and 23 for the HF grade and decreased with increasing pH dependent on the dissolving pH of HPMCAS.

HPMCAS HF dissolves under highest pH, maintaining high aggregation up to pH 7 in contrast to LF which only showed high N_{agg} up to pH 5.5. The authors could correlate this aggregation with drug affinity. If the pH is fixed as in case of the non-sink dissolution testing (Fig. 4A) to pH 6.5, HPMCAS HF forms the most drug-rich colloids, enabling hydrophobic interactions with the drug and therefore provided better stabilization of KTZ. This ranking of HPMCAS grades was also observed in other studies (Ueda et al., 2014).

In the transfer model, the status-quo is changed. Both HPMCAS grades are insoluble at pH 2 and form large colloids with interactions with the drug. In the transfer experiment though, the pH suddenly changes to 6.5 where N_{agg} of HPMCAS LF is strongly reduced. The stabilization mechanism, namely formation of polymer aggregates and drug-polymer colloids discussed beforehand, is not present anymore though the API (in free form) shows high supersaturation with quick precipitation. This might well explain why the LF grade outperforms HPMCAS HF during the first 60 min in c_{max} and AUC. The N_{agg} of HPMCAS HF is still not affected at pH 6.5. Hence, the API is still incorporated in drug-rich colloids and therefore not quickly released. At

the same time, the stabilizing mechanism is maintained.

The results acquired in this study supported the hypotheses by Wang and coworkers on a pH-dependent stabilization mechanism which gets even more difficult to be predicted when not only PBS buffer is used but bile salts and micelle-forming components of the FaSSiF buffer are being added like in this study.

3.6. Transfer model of formulations with HPMCAS grades w/wo E PO

The results from DSC testing and the comparison between HPMCAS LF and HF indicated different drug-polymer interactions and therefore stabilization of KTZ. As there were two main hypotheses on stabilizing interactions (ionic interactions as well as hydrophobic interactions and polymer colloids), the acid-base interactions should be tackled by a competitive basic component. As several studies examine polymer combinations to improve processability or stability of ASD or to tailor the drug's release (Baghel et al., 2018; Davis et al., 2017; Kalivoda et al., 2012; Liu et al., 2013; Six et al., 2004), it was decided to include Eudragit® E PO as a basic polymer. In this study, the main focus was to saturate interaction sites of the two HPMCAS grades and to investigate, whether the usage of polymer combinations might also be disadvantageous in terms of stability. The transfer was started from SGF pH 4, as this was found to be the discriminating condition between PM and SDD.

The dissolution profiles of the transfer model are depicted in Fig. 5.

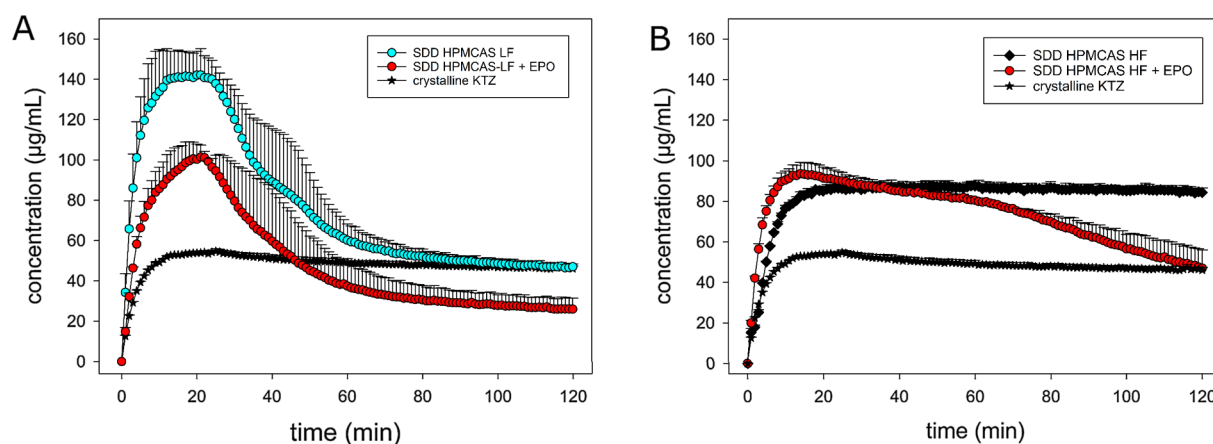


Fig. 5. Transfer model of (A) SDD with HPMCAS LF \pm E PO compared to (B) SDD HPMCAS HF \pm E PO with 40% DL each. Transfer was conducted from SGF pH 4 into FaSSiF-V1 pH 6.5. Arithmetic means of $n = 3 +$ S.D.

The AUC of the SDD with HPMCAS LF and E PO decreased to 63% compared to HPMCAS LF without using E PO. In contrast, the AUC of the SDD with HPMCAS HF in combination with E PO was only reduced to 89% compared to neat HPMCAS HF just as it was hypothesized before based on the strength of ionic interactions. This supports the hypothesis, that stabilization of KTZ by HPMCAS LF might be more related to ionic interactions whereas HPMCAS HF expresses hydrophobic interactions with the API which are less affected by E PO addition.

These results indicate the importance of interactions in the stabilization of supersaturation and underline the complexity of multi-component ASD as there are multiple effects to be considered.

4. Conclusion

This study demonstrated the importance of advanced dissolution testing for the selection of polymeric carriers for weakly basic drugs. By applying the GI transfer model in early development phases, it is possible to select an appropriate formulation strategy as well as the most promising polymeric precipitation inhibitor. Therefore, only small sample amounts are needed which does perfectly fit the demands for preclinical development.

First, it could be shown that the strong pH-dependent dissolution behavior of weakly basic and poorly soluble drugs adds the necessity of comparing the supersaturation induced by GI transfer in comparison to supersaturation due to amorphization. Since the supersaturation of KTZ under elevated gastric pH conditions was solely improved using the amorphous formulation and not by using the physical drug polymer combination, GI variability in human individuals should also be considered. In the second part, drug-polymer interactions were investigated under simulated physiological conditions. The high complexity of the stabilizing mechanisms must not be considered in an isolated manner but under physiologically relevant conditions to aid selection of a polymeric precipitation inhibitor (combination) which is likewise true for PM as well as for ASD.

CRedit authorship contribution statement

Carolin Auch: Writing - original draft, Conceptualization, Data curation, Investigation. **Christian Jede:** Writing - review & editing, Data curation, Investigation. **Meike Harms:** Conceptualization, Investigation, Writing - review & editing. **Christian Wagner:** Conceptualization, Investigation, Methodology, Writing - review & editing. **Karsten Mäder:** Conceptualization, Data curation, Writing - review & editing, Supervision.

Declaration of Competing Interest

The authors declare that they have no known competing financial interests or personal relationships that could have appeared to influence the work reported in this paper.

Acknowledgements

The authors gratefully acknowledge Holger Kubas, Mirko Koziolok and Markus Riehl for the scientific discussion of this manuscript.

Appendix A. Supplementary material

Supplementary data to this article can be found online at <https://doi.org/10.1016/j.ijpharm.2019.118917>.

References

Abuhelwa, A.Y., Williams, D.B., Upton, R.N., Foster, D.J., 2017. Food, gastrointestinal pH, and models of oral drug absorption. *Eur. J. Pharm. Biopharm.* 112, 234–248.
Amidon, G.L., L.H., Shah, V.P., Crison, J.R., 1995. A theoretical basis for a

biopharmaceutic drug classification: the correlation of in vitro drug product dissolution and in vivo bioavailability. *Pharmaceut. Res.*, vol. 12, pp. 413–420.
Auch, C., Harms, M., Mäder, K., 2018. Melt-based screening method with improved predictability regarding polymer selection for amorphous solid dispersions. *Eur. J. Pharm. Sci.* 124, 339–348.
Auch, C., Harms, M., Mäder, K., 2019. How changes in molecular weight and PDI of a polymer in amorphous solid dispersions impact dissolution performance. *Int. J. Pharm.* 556, 372–382.
Baghel, S., Cathcart, H., O'Reilly, N.J., 2018. Investigation into the solid-state properties and dissolution profile of spray-dried ternary amorphous solid dispersions: a rational step toward the design and development of a multicomponent amorphous system. *Mol. Pharm.* 15, 3796–3812.
Brouwers, J., Brewster, M.E., Augustijns, P., 2009. Supersaturating drug delivery systems: the answer to solubility-limited oral bioavailability? *J. Pharm. Sci.* 98, 2549–2572.
Buckley, S.T., Frank, K.J., Fricker, G., Brandl, M., 2013. Biopharmaceutical classification of poorly soluble drugs with respect to “enabling formulations”. *Eur. J. Pharm. Sci.* 50, 8–16.
Budha, N.R., Frymoyer, A., Smelick, G.S., Jin, J.Y., Yago, M.R., Dresser, M.J., Holden, S.N., Benet, L.Z., Ware, J.A., 2012. Drug absorption interactions between oral targeted anticancer agents and PPIs: is pH-dependent solubility the Achilles heel of targeted therapy? *Clin. Pharmacol. Ther.* 92, 203–213.
Davis, M.T., Potter, C.B., Mohammadpour, M., Albadarin, A.B., Walker, G.M., 2017. Design of spray dried ternary solid dispersions comprising itraconazole, soluplus and HPMCP: effect of constituent compositions. *Int. J. Pharm.* 519, 365–372.
Dressman, J.B., Reppas, C., 2000. In vitro–in vivo correlations for lipophilic, poorly water-soluble drugs. *Eur. J. Pharm. Sci.* 11, S73–S80.
Grimm, M., Koziolok, M., Kühn, J.-P., Weitschies, W., 2018. Interindividual and intraindividual variability of fasted state gastric fluid volume and gastric emptying of water. *Eur. J. Pharm. Biopharm.* 127, 309–317.
Hancock, B.C., Zografi, G., 1994. The relationship between the glass transition temperature and the water content of amorphous pharmaceutical solids. *Pharm. Res.* 11, 471–477.
Ishikawa, M., Hashimoto, Y., 2011. Improvement in aqueous solubility in small molecule drug discovery programs by disruption of molecular planarity and symmetry. *J. Med. Chem.* 54, 1539–1554.
Jankovic, S., O'Dwyer, P.J., Box, K.J., Imanidis, G., Reppas, C., Kuentz, M., 2019. Biphasic drug release testing coupled with diffusing wave spectroscopy for mechanistic understanding of solid dispersion performance. *Eur. J. Pharm. Sci.* 137, 105001.
Jede, C., Wagner, C., Kubas, H., Weber, C., Weigandt, M., Koziolok, M., Weitschies, W., 2019. Automated small-scale in vitro transfer model as screening tool for the prediction of in vivo-dissolution and precipitation of poorly solubles. *Int. J. Pharm.* 556, 150–158.
Jede, C., Wagner, C., Kubas, H., Weber, C., Weitschies, W., 2018. In-line derivative spectroscopy as a promising application to a small-scale in vitro transfer model in biorelevant supersaturation and precipitation testing. *J. Pharm. Pharmacol.*
Kalivoda, A., Fischbach, M., Kleinebudde, P., 2012. Application of mixtures of polymeric carriers for dissolution enhancement of omeprazole using hot-melt extrusion. *Int. J. Pharm.* 439, 145–156.
Klein, C.E., Chiu, Y.-L., Awni, W., Zhu, T., Heuser, R.S., Doan, T., Breitenbach, J., Morris, J.B., Brun, S.C., Hanna, G.J., 2007. The tablet formulation of lopinavir/ritonavir provides similar bioavailability to the soft-gelatin capsule formulation with less pharmacokinetic variability and diminished food effect. *JAIDS J. Acquir. Immune Deficien. Syndr.* 44, 401–410.
Kostewicz, E.S., Wunderlich, M., Brauns, U., Becker, R., Bock, T., Dressman, J.B., 2004. Predicting the precipitation of poorly soluble weak bases upon entry in the small intestine. *J. Pharm. Pharmacol.* 56, 43–51.
Leuner, C., Dressman, J., 2000. Improving drug solubility for oral delivery using solid dispersions. *Eur. J. Pharm. Biopharm.* 50, 47–60.
Litou, C., Vertzoni, M., Xu, W., Kesisisoglou, F., Reppas, C., 2017. The impact of reduced gastric acid secretion on dissolution of salts of weak bases in the fasted upper gastrointestinal lumen: data in biorelevant media and in human aspirates. *Eur. J. Pharm. Biopharm.* 115, 94–101.
Liu, J., Cao, F., Zhang, C., Ping, Q., 2013. Use of polymer combinations in the preparation of solid dispersions of a thermally unstable drug by hot-melt extrusion. *Acta Pharmaceutica Sinica B* 3, 263–272.
Manallack, D.T., 2009. The acid–base profile of a contemporary set of drugs: implications for drug discovery. *SAR QSAR Environ. Res.* 20, 611–655.
Manallack, D.T., Prankerd, R.J., Yuriev, E., Oprea, T.L., Chalmers, D.K., 2013. The significance of acid/base properties in drug discovery. *Chem. Soc. Rev.* 42, 485–496.
Monschke, M., Wagner, K.G., 2019. Amorphous solid dispersions of weak bases with pH-dependent soluble polymers to overcome limited bioavailability due to gastric pH variability – an in-vitro approach. *Int. J. Pharmaceut.*
Patel, S., Zhu, W., Xia, B., Sharma, N., Hermans, A., Ehrick, J.D., Kesisisoglou, F., Pennington, J., 2019. Integration of precipitation kinetics from an in vitro, multi-compartment transfer system and mechanistic oral absorption modeling for pharmacokinetic prediction of weakly basic drugs. *J. Pharm. Sci.* 108, 574–583.
Psachoulas, D., Vertzoni, M., Goumas, K., Kalioras, V., Beato, S., Butler, J., Reppas, C., 2011. Precipitation in and supersaturation of contents of the upper small intestine after administration of two weak bases to fasted adults. *Pharm. Res.* 28, 3145–3158.
Ruff, A., Fiolka, T., Kostewicz, E.S., 2017. Prediction of Ketoconazole absorption using an updated in vitro transfer model coupled to physiologically based pharmacokinetic modelling. *Eur. J. Pharm. Sci.* 100, 42–55.
Saal, W., Wyttenbach, N., Alsenz, J., Kuentz, M., 2018. Interactions of dimethylaminoethyl methacrylate copolymer with non-acidic drugs demonstrated high solubilization in vitro and pronounced sustained release in vivo. *Eur. J. Pharm. Biopharm.* 125, 68–75.

- Schneider, F., Grimm, M., Koziolok, M., Modess, C., Dokter, A., Roustom, T., Siegmund, W., Weitschies, W., 2016. Resolving the physiological conditions in bioavailability and bioequivalence studies: comparison of fasted and fed state. *Eur. J. Pharm. Biopharm.* 108, 214–219.
- Segregur, D., Flanagan, T., Mann, J., Moir, A., Karlsson, E.M., Hoch, M., Carlile, D., Sayah-Jeanne, S., Dressman, J., 2019. Impact of acid-reducing agents on gastrointestinal physiology and design of biorelevant dissolution tests to reflect these changes. *J. Pharm. Sci.* 108, 3461–3477.
- Shah, N.H.S., Choi, Duk Soon, Chokshi, Hitesh, Malick, Waseem A., 2014. *Amorphous Solid Dispersions*. Springer.
- Six, K., Verreck, G., Peeters, J., Brewster, M., Mooter, G.V.d., 2004. Increased physical stability and improved dissolution properties of itraconazole, a class II drug, by solid dispersions that combine fast- and slow-dissolving polymers. *J. Pharmaceut. Sci.*, vol. 93, pp. 124–131.
- Ting, J.M., Porter, W.W., Mecca, J.M., Bates, F.S., Reineke, T.M., 2018. Advances in polymer design for enhancing oral drug solubility and delivery. *Bioconjug. Chem.* 29, 939–952.
- Ueda, K., Higashi, K., Yamamoto, K., Moribe, K., 2014. The effect of HPMCAS functional groups on drug crystallization from the supersaturated state and dissolution improvement. *Int. J. Pharm.* 464, 205–213.
- Ullrich, A., Schiffter, H.A., 2018. The influence of polymer excipients on the dissolution and recrystallization behavior of ketoconazole: application, variation and practical aspects of a pH shift method. *Eur. J. Pharm. Biopharm.* 133, 20–30.
- Van Der Meer, J.W.M., Keuning, J.J., Scheijgrond, H.W., Heykants, J., Van Cutsem, J., Brugmans, J., 1980. The influence of gastric acidity on the bio-availability of ketoconazole. *J. Antimicrob. Chemother.* 6, 552–554.
- Vertzoni, M., Dressman, J., Butler, J., Hempenstall, J., Reppas, C., 2005. Simulation of fasting gastric conditions and its importance for the in vivo dissolution of lipophilic compounds. *Eur. J. Pharm. Biopharm.* 60, 413–417.
- Wagner, C., Jantratid, E., Kesisoglou, F., Vertzoni, M., Reppas, C., B. Dressman, J., 2012. Predicting the oral absorption of a poorly soluble, poorly permeable weak base using biorelevant dissolution and transfer model tests coupled with a physiologically based pharmacokinetic model. *Eur. J. Pharmaceut. Biopharmaceut.*, vol. 82, pp. 127–138.
- Wang, S., Liu, C., Chen, Y., Zhu, A., Qian, F., 2018. Aggregation of hydroxypropyl methylcellulose acetate succinate under its dissolving pH and the impact on drug supersaturation. *Mol. Pharmaceut.*
- Yalkowsky, S.H., Valvani, S.C., 1980. Solubility and partitioning I: solubility of nonelectrolytes in water. *J. Pharm. Sci.* 69, 912–922.
- Yoshioka, M., Hancock, B.C., Zografi, G., 1994. Crystallization of indomethacin from the amorphous state below and above its glass transition temperature. *J. Pharm. Sci.* 83, 1700–1705.
- Zhao, M., Barker, S.A., Belton, P.S., McGregor, C., Craig, D.Q.M., 2012. Development of fully amorphous dispersions of a low Tg drug via co-spray drying with hydrophilic polymers. *Eur. J. Pharm. Biopharm.* 82, 572–579.